



**HAL**  
open science

# Design, Modeling and Control of a Multi-Drone System for Aerial Manipulation

José de Jesús Castillo Zamora

► **To cite this version:**

José de Jesús Castillo Zamora. Design, Modeling and Control of a Multi-Drone System for Aerial Manipulation. Automatic Control Engineering. Université Paris-Saclay, 2021. English. NNT : 2021UP-ASG051 . tel-03778595

**HAL Id: tel-03778595**

**<https://theses.hal.science/tel-03778595>**

Submitted on 16 Sep 2022

**HAL** is a multi-disciplinary open access archive for the deposit and dissemination of scientific research documents, whether they are published or not. The documents may come from teaching and research institutions in France or abroad, or from public or private research centers.

L'archive ouverte pluridisciplinaire **HAL**, est destinée au dépôt et à la diffusion de documents scientifiques de niveau recherche, publiés ou non, émanant des établissements d'enseignement et de recherche français ou étrangers, des laboratoires publics ou privés.

Conception, Modélisation et Contrôle d'un  
System Multi-Drone pour la Manipulation  
Aérienne  
*Design, Modeling and Control of a Multi-Drone  
System for Aerial Manipulation*

**Thèse de doctorat de l'Université Paris-Saclay**

École doctorale n°580 : Science et Technologies de l'Information et de la  
Communication STIC  
Spécialité de doctorat: Automotique  
Unité de recherche : Université Paris-Saclay, CNRS, CentraleSupélec, Laboratoire des  
signaux et systèmes, 91190, Gif-sur-Yvette, France  
Réfèrent : Faculté des Sciences d'Orsay

**Thèse présentée et soutenue à Paris-Saclay,  
le 17/09/2021, par**

**José de Jesús CASTILLO ZAMORA**

**Composition du Jury**

<b>Catherine BONNET</b> Directrice de recherche, L2S-CentraleSupélec	Presidente du jury
<b>Paolo ROBUFFO GIORDANO</b> Directeur de recherche, IRISA, INRIA Rennes – Bretagne Atlantique	Rapporteur & Examineur
<b>Pedro CASTILLO</b> Chargé de recherche, CNRS Université de Technologie de Compiègne	Rapporteur & Examineur
<b>Elisa CAPELLO</b> Associate Professor, Politecnico di Torino	Examinatrice
<b>Franck RUFFIER</b> Directeur de recherche, Aix Marseille Université	Examineur
<b>Sami TLIBA</b> Maître de conférences, L2S-CentraleSupélec	Examineur
<b>Karim-Liviu TRABELSI</b> Enseignant-chercheur, IPSA	Invité

**Direction de la thèse**

<b>Islam BOUSSAADA</b> Professeur, HDR, IPSA and L2S-CentraleSupélec	Directeur de thèse
<b>Juan-Antonio ESCARENO</b> Maître de conférences, Université de Limoges	Co-encadrant & Examineur



# Résumé étendu

Un sujet récent et passionnant dans le domaine des véhicules aériens autonomes est l'interaction avec le milieu environnant via la manipulation en vol (récupération, transport, placement). Un tel profil opérationnel dévoile un énorme potentiel d'applications industrielles et de services. La nouvelle génération de robots aériens permet de disposer d'un actionneur robotique tridimensionnel capable d'exercer des forces et/ou des couples sur un ou plusieurs points spécifiques pour des opérations d'acquisition/déploiement, d'outillage ou de perchage.

Des recherches antérieures ont été menées sur ce type de véhicules en ce qui concerne les stratégies de contrôle, la conception et la modélisation, le transport de charges multi-drones complété par des stratégies de détection visuelle pour la navigation et la détection d'objets, entre autres.

Les opérations aériennes de prélèvement, de transport et de mise en place ont attiré l'attention des chercheurs car elles interviennent dans la plupart des applications réelles telles que la livraison de kits de survie, les opérations de sauvetage, le déploiement et l'acquisition de capteurs, etc. Des telles capacités peuvent être améliorées par la conjonction de plusieurs véhicules aériens, ce qui implique, en outre, la conception et les études de différents domaines technologiques. À cet égard, l'idée de la manipulation de charges utiles lourdes par un groupe d'aéronefs autonomes est prometteuse dans des conditions environnementales difficiles [71, 129, 112, 171, 17, 4].

Dans le cadre de la solution aux tâches susmentionnées, et en ayant à l'esprit la mise en œuvre d'un ensemble de véhicules aériens, les drones ont été physiquement connectés et étudiés comme une seule chaîne cinématique multiliée volante avec une morphologie et une structure similaires à celles des robots manipulateurs que l'on peut trouver dans le domaine industriel et manufacturier [156, 9, 175, 176].

Néanmoins, il est facile de relier cette solution à une structure de véhicule équivalente au sol: les trains. Un train est défini comme une série de voitures ou de wagons de chemin de fer déplacés en tant qu'unité par une locomotive ou par des moteurs intégrés. Pourtant, une définition générale peut faire référence à un certain nombre de véhicules ou d'animaux guidés se déplaçant dans une formation en ligne ou en courbe [154].

Les systèmes naturels fonctionnent souvent selon un principe de transport coopératif comme dans le cas de la colonie de fourmis [80] ou des abeilles [162]. Néanmoins, des êtres vivants comme les mille-pattes ou les serpents peuvent présenter une morphologie qui fait que l'on associe les systèmes multiliés de robotique et de transport à des telles formes. L'anatomie complexe du mille-pattes a inspiré les chercheurs à développer de nouvelles structures

robotiques ainsi que de nouvelles stratégies et méthodologies de contrôle pour surmonter le problème du suivi de trajectoire et de l'évitement d'obstacles dans des environnements complexes [84, 69, 70].

Il est donc logique de jeter son dévolu sur les systèmes naturels multi-écrans pour résoudre les problèmes complexes de locomotion et de transpiration.

L'objectif général de ce doctorat est de proposer une configuration multi-drones innovante destinée à réaliser des tâches de manipulation (récupération/déploiement/transport) dans des environnements complexes via des méthodes robotiques avancées. Trois approches complémentaires sont étudiées:

1. La première étape consiste à modéliser un nouveau système aérien interactif capable d'effectuer une manipulation collective en vol, où le resserrement définit la configuration du réseau de robots aériens.
2. La deuxième phase de la thèse se concentre sur les aspects de contrôle, notamment pour réaliser différentes formations avec le système multi-drones proposé, ainsi que sur la dextérité de manipulation de la charge utile pendant les opérations de transport et de manipulation.
3. La troisième étape est consacrée à l'étude des effets des retards dans le système aérien effectuant les tâches environnementales interactives comme celles mentionnées précédemment.

Les principaux aspects impliqués dans ce projet sont présentés afin d'établir un cadre de référence pour une lecture ultérieure.

Les drones, ou officiellement appelés véhicules aériens sans pilote, sont définis comme des véhicules de transport spatial qui volent sans équipage humain à bord et qui peuvent être contrôlés à distance ou voler de manière autonome. Ces véhicules ont récemment atteint des niveaux de croissance sans précédent dans divers domaines d'application militaires et civils [123, 166].

Les drones ont été introduits pour la première fois pendant la première guerre mondiale, enregistrant une longue implication des militaires. Des études telles que celles rassemblées dans [123, 166], affirment que les drones continueront à être le secteur de croissance le plus dynamique de l'industrie aérospatiale et que la tendance se tournera vers des drones plus petits, plus flexibles et plus polyvalents [106].

Il a été établi que la première contribution majeure aux mécanismes autonomes s'est produite à l'époque de Pythagore. Néanmoins, en Chine, vers 400 avant J.-C., a eu lieu la première idée documentée d'un aéronef à vol vertical ; et en 1483, Léonard de Vinci a conçu un aéronef capable de planer. Une machine de vol vertical à base de chaudière a également été conçue dans les années 1840 par Horatio Phillips. Cependant, c'est Ponton d'Amecourt qui, dans les années 1860, a fait voler de petits modèles d'hélicoptères propulsés à la vapeur. Thomas Alva Edison présente l'un des véhicules aériens les plus remarquables dans les années 1880. Pourtant, la principale avancée des temps modernes dans l'histoire des hélicoptères est l'hélicoptère jamais volé d'Igor Ivanovitch Sikorsky (1909) [166].

Parallèlement à la construction de machines à vol vertical et d'hélicoptères, les aéronefs à voilure fixe ont

commencé à évoluer au cours des 100 dernières années, avec le premier vol démontré par les frères Wright en 1903 [122].

L'entrée des drones à petite échelle dans la communauté universitaire a posé des défis dans une variété de domaines de recherche tels que l'aérodynamique et la modélisation de la dynamique de vol, le contrôle du vol, la vision par ordinateur, etc. Dans le même temps, elle offre également une excellente occasion de développer des méthodologies de conception et d'évaluer plus avant leurs performances pratiques.

Il convient de noter qu'à des fins de recherche scientifique, les petits drones sont de préférence classés en fonction de leur principe de fonctionnement, à savoir les giravions, les avions et les avions à ailes battantes.

Ces dernières années, l'amélioration des capacités des véhicules aériens sans pilote, en termes de manipulation aérienne, est un domaine d'intérêt pour les scientifiques du monde entier. Dans ce sens, la solution la plus adoptée a été d'attacher des bras manipulateurs robotiques aux drones, néanmoins, l'auto-conception inhérente implique une limitation en termes de performance et de dextérité [114].

Afin de surmonter le problème de dextérité susmentionné, de nouvelles configurations de systèmes et de véhicules aériens sont conçues. Parmi ces plateformes, les manipulateurs aériens "Snake" se distinguent. Ces véhicules sont définis, selon [114], comme *un type de manipulateur aérien couplé, reconfigurable en fonction des tâches et se transformant en forme, doté de capacités de manipulation robotique bidimensionnelles ou tridimensionnelles grâce à l'interaction de multicoptères ou d'hélices qui constituent deux ou plusieurs chaînes cinématiques bifurquées*. Il convient de mentionner que le travail dans [114] offre une vaste et complète enquête sur cette question, à cet égard, le texte ici peut être une interprétation compacte de l'information disponible, mais avec quelques commentaires complémentaires que l'auteur a considéré pour être enrichir la discussion.

Malgré l'essor technologique actuel, l'application de ces systèmes aériens multi-corps reste limitée en raison des problèmes de consommation d'énergie et d'onmidirectionnalité, mais ils permettent d'explorer de nouvelles méthodologies et techniques dans les domaines de la robotique reconfigurable, de la robotique continue et des humanoïdes volants, entre autres.

Néanmoins, selon les perspectives abordées dans la littérature, aucune des références consultées ne prend en considération les effets secondaires possibles qui peuvent être produits par les délais de communication, de détection, de traitement de l'information.

Les systèmes retardés représentent une classe de systèmes à dimension infinie souvent utilisés pour décrire les phénomènes de propagation, la dynamique des populations ou les systèmes d'ingénierie. Une caractéristique distincte de ces systèmes est que leur taux d'évolution est décrit par des équations différentielles qui incluent des informations sur l'histoire passée, pour cette raison, les systèmes retardés sont également connus sous le nom de systèmes héréditaires, systèmes avec effets secondaires, ou systèmes avec décalage temporel [58].

L'effet du retard sur la stabilité des systèmes avec des retards dans l'état et/ou l'entrée, est un problème d'intérêt récurrent puisque la présence d'un retard temporel peut induire des comportements complexes pour les schémas en

boucle fermée ou, pour certains grands retards temporels, le système peut être stabilisé. À cet égard, on dit que les systèmes de contrôle fonctionnent en présence de retards, principalement en raison du temps nécessaire pour acquérir les informations permettant de créer des décisions de contrôle et de les exécuter.

Une stratégie de contrôle efficace possible consiste à induire correctement des délais. Par exemple, l'augmentation ou l'extension du délai dans la boucle de rétroaction peut stabiliser un système qui est autrement instable. Pourtant, l'intérêt pour l'étude et la compréhension des effets des retards augmente rapidement comme une conséquence inhérente à l'évolution de la complexité des systèmes de contrôle. En ce sens, le délai est un opérateur de décalage qui retarde un signal d'entrée d'une quantité constante de temps.

L'objectif principal de l'étude de la stabilité des systèmes soumis à des retards est de déterminer les conditions nécessaires et suffisantes pour le système en boucle fermée alors que dans l'espace des paramètres de retard de l'espace des paramètres du contrôleur. En la matière, un système retardé est dit stable en fonction du retard s'il est stable pour seulement certaines valeurs dans l'espace des paramètres de retard, par contre, si la stabilité tient indépendamment du retard, le système est dit stable indépendamment du retard. Il peut exister plusieurs régions de retard disjointes, de sorte que le système est stable à l'intérieur de chaque région, mais devient instable à l'extérieur. Ces régions, appelées régions de stabilité, deviennent des intervalles de stabilité dans un système à retard unique. Les intervalles de stabilité peuvent être étendus à une carte bidimensionnelle, appelée carte de stabilité [127, 155].

Le contenu de cette thèse est divisé en deux parties: Partie I qui est consacrée à la modélisation et à l'étude dynamique de la proposition de système aérien sans pilote multiliason, y compris l'estimation des perturbations et les questions de contrôle robuste (chapitres 2, 3 et 4); et la Partie II qui se concentre sur l'étude des effets des délais dans les opérations des drones (chapitres 5, 6 et 7). En même temps, et comme indiqué, chacune de ces parties est divisée en chapitres qui correspondent au champ d'application correspondant. Une brève description du contenu de chaque chapitre composant cette thèse est fournie ci-dessous. En outre, les annexes A, B, C et D complètent la description des activités réalisées lors de la préparation de ce travail.

Dans les pages suivantes, une brève description de chaque chapitre et annexe, ainsi que les résultats obtenus, sont brièvement présentés.

## **Part I: Multi-Link Unmanned Aerial System**

### **Chapter 2: Modeling and Control: Robust Acquiring and Transport Operations**

Dans ce chapitre, le concept d'un système aérien sans pilote à liaisons multiples, conçu pour des tâches de transport de cargaisons multiples, est présenté. Un tel système comporte trois liens qui sont actionnés par quatre robots volants. La procédure de modélisation dynamique basée sur la formulation Euler-Lagrange est présentée en détail. Un schéma de contrôle préliminaire basé sur un contrôle robuste par mode glissant intégral adaptatif (AISMIC) est

appliqué en tenant compte des incertitudes du modèle ML-UAS et des perturbations externes. L'objectif du contrôle est de suivre les modèles d'acquisition inspirés par les oiseaux. L'efficacité de la stratégie proposée est validée par des simulations numériques.

Dans la suite du chapitre, la modélisation longitudinale et la commande robuste du nouveau système interactif aérien multi-link sont décrites en détail. La chaîne cinématique de vol inspirée par les capacités des véhicules aériens, la dextérité des manipulateurs de bras et une opération de transport de type train, est ainsi introduite.

Sur la base des résultats obtenus à partir des simulations et de l'analyse de stabilité de Lyapunov, le contrôleur AISM garantit la stabilité du système et la tolérance aux perturbations afin d'accomplir les opérations de prélèvement et de transport. Une amélioration de la stratégie de prélèvement sera proposée en se basant sur un objectif mobile, de plus le mouvement des charges utiles et la vitesse de l'opération seront analysés afin de concevoir une stratégie pour une transition douce des liens. La dynamique des actionneurs joue un rôle important dans la performance du système, ce qui suggère la mise en œuvre d'une loi de contrôle robuste pour les aéronefs. L'extension à un espace tridimensionnel et les expériences concernant la proposition sont laissées pour des travaux futurs.

### **Chapter 3: Disturbances and Coupling Compensation for Trajectory Tracking**

Comme dans le chapitre précédent, celui-ci se concentre sur un système aérien sans pilote à liaisons multiples mais le système est composé de trois hélicoptères attachés par deux liaisons en forme de barre. Le modèle mathématique est obtenu par la méthodologie d'Euler-Lagrange, tandis que le contrôleur repose sur un schéma linéaire classique. Comme le système est fortement couplé, en raison de sa dynamique inhérente et des influences de la cargaison, une extension dynamique des équations du mouvement pour appliquer un filtre Kalman linéaire est proposée pour répondre à la spécification de suivi de trajectoire. L'observateur d'état proposé est validé par des simulations numériques.

Dans ce chapitre, le modèle dynamique d'un système aérien à liaisons multiples, basé sur le formalisme Euler-Lagrange, est présenté. Même si le nombre de liens et de véhicules aériens est restreint à 2 et 3 respectivement, comme travail futur, l'étude du système avec  $n$  liens et  $n + 1$  aéronefs sera abordée.

La représentation linéaire du système et l'ajout des couplages correspondants dans les termes de perturbation permettent de concevoir un filtre de Kalman linéaire à état augmenté pour estimer ces perturbations. Celui-ci s'avère avoir une performance acceptable selon les résultats obtenus lors de simulations numériques.

L'implémentation d'un filtre de Kalman étendu, la conception d'une loi de contrôle robuste ainsi que l'ajout de perturbations dues au vent restent à être inclus dans une version étendue. De plus, l'étude du système dans un espace tridimensionnel en utilisant différentes structures d'avion comme actionneurs est envisagée pour des projets futurs.

## Chapter 4: Nonlinear Control and ASEKF-Based Disturbances Compensation

Ce chapitre présente une extension de la stratégie de modélisation et de contrôle du ML-UAS introduit précédemment. À cet égard, le système susmentionné est soumis à des perturbations forfaitaires qui comprennent des perturbations externes et des incertitudes paramétriques. Un filtre de Kalman étendu à états augmentés destiné à estimer les incertitudes endogènes et exogènes est conçu et un contrôleur de suivi de trajectoire respectant la stabilité asymptotique de Lyapunov est synthétisé. Une étape de simulation est menée pour valider l'efficacité de la proposition.

Un système aérien composé de trois quadrotors reliés entre eux est abordé tout au long du chapitre. Le modèle dynamique de l'ensemble est décrit en détail. En termes de contrôle, un contrôleur non linéaire basé sur Lyapunov est utilisé conjointement avec un filtre de Kalman étendu à état augmenté (ASEKF) afin de suivre une trajectoire dépendante du temps tout en compensant les perturbations paramétriques et externes pendant une tâche de transport de charges multiples. Pour plus de détails, les contributions de ce chapitre sont les suivantes: (i) La proposition d'un nouveau concept alternatif de système aérien multilien capable de transporter des charges multiples. (ii) Une synthèse de contrôle détaillée et une analyse de stabilité prenant en compte la dynamique longitudinale et la présence d'incertitudes structurelles et non structurelles. (iii) Contrairement à la majorité des travaux traitant de la compensation des perturbations via un filtre de Kalman à état augmenté, la déduction de la matrice de covariance basée sur les incertitudes présentes dans le modèle non linéaire complet est introduite. (iv) Une étape de simulation approfondie est menée pour évaluer l'efficacité de la stratégie de contrôle-estimation proposée. De plus, un scénario du monde réel est considéré en utilisant les spécifications de capteurs réels concernant le bruit et les défauts.

La dynamique d'une configuration non conventionnelle du ML-UAS est obtenue par le formalisme d'Euler-Lagrange, mais on ne réussit pas seulement à regrouper les équations du mouvement dans une structure compacte bien connue, on vérifie également les propriétés utiles du modèle en ce qui concerne la conception de la commande. Il est intéressant de souligner que ce dernier permet de multiples possibilités de développer contrôleurs potentiels pour stabiliser ce type de robots aériens.

Le performance du système est dégradée en raison de la dynamique non linéaire fortement couplée ainsi que de la présence d'incertitudes paramétriques et de perturbations externes non modélisées. Une stratégie conjointe de contrôle et d'observation, utilisant un ASEKF en cascade avec un contrôle non linéaire basé sur Lyapunov, est mise en oeuvre, montrant une efficacité accrue en ce qui concerne la performance globale.

Dans la veine du contrôle, un contrôleur basé sur Lyapunov garantissant la stabilité asymptotique globale est mis en oeuvre pour remplir l'objectif de suivi de trajectoire. Le succès du contrôleur repose sur l'efficacité de l'estimation ASEKF. En ce qui concerne la couche d'estimation, la déduction de la matrice de covariance du processus d'un ASEKF ad hoc en tenant compte de la structure réelle des paramètres incertains est validée, puisque l'estimation des états est suffisamment précise pour surmonter les problèmes parasites et ainsi stabiliser le système.

En l'occurrence, et comme en témoignent les performances de suivi, la perturbation externe globale est estimée avec précision. De plus, lorsque des anomalies sensorielles se produisent, les états estimés maintiennent une performance opérationnelle acceptable en restant à proximité de la trajectoire cible.

Les recherches à venir comprennent: (i) le développement expérimental du robot aérien, (ii) des stratégies de navigation 3D résilientes pour englober des scénarios hautement dégradés, par exemple des perturbations variables en fréquence/amplitude (rafales de vent) ainsi que (iii) des contrôleurs/observateurs tolérants aux retards.

## **Part III: Time-Delays on Unmanned Aerial Systems**

### **Chapter 5: Parametric Analysis of PID Delay-Based Controllers for Quadrotor UAVs**

Ce chapitre fournit un ensemble de diagrammes de stabilité paramétriques pour un quadrotor effectuant des manœuvres de stabilisation en présence de délais de rétroaction et soumis à des contrôleurs PID. L'analyse prend en compte les couplages entre les mouvements de translation (dynamique lente) et de rotation (dynamique rapide). Les paramètres des contrôleurs, dans le schéma de contrôle global, sont calculés en utilisant la théorie bien connue des racines croisées de stabilité. Des résultats de simulation numérique, incluant le modèle dynamique complet et le modèle linéaire correspondant du véhicule, sont présentés pour valider la proposition.

D'un point de vue général, et en se basant sur les preuves fournies par la littérature, on peut conclure que l'analyse des influences des délais sur les drones est un sujet de recherche avec une croissance exponentielle. Dans ce sens, ce chapitre est consacré à l'étude d'un quadrotor unique piloté par des contrôleurs PID à base de retard. Il est supposé que la détection de la position est effectuée par un système de suivi par vision dont les caméras sont situées à distance, incorporant le retard dans le schéma de contrôle des états de translation comme une conséquence de la latence des caméras. Le chapitre fournit un ensemble de cartes de stabilité qui permettent de sélectionner le jeu approprié de gains de contrôle en fonction du délai, du critère de stabilité  $\sigma$  et du gain intégral du contrôleur. À cette fin, la méthodologie repose sur la disponibilité d'un modèle linéaire pour la conception du contrôle.

D'une manière générale, les travaux futurs envisagent la définition formelle et stricte de la dépendance paramétrique des régions de stabilité et une étude détaillée de la fragilité du système afin de fournir un outil permettant de mesurer la robustesse de l'approche de contrôle. De plus, l'extension de ce chapitre prend en compte la stabilité de l'avion lorsque des perturbations rotationnelles influencent sa dynamique. La comparaison entre cette approche linéaire et le traitement non-linéaire de la question est également proposée comme un travail à venir. Des efforts supplémentaires seront consacrés à valider et à compléter ces résultats au moyen d'une expérimentation réelle.

## Chapter 6: Time-Delay Control of Quadrotor UAVs: a MID-Based Approach

Ce chapitre traite des effets des retards sur la stabilité des systèmes aériens sans pilote (UAV). La proposition de la recherche actuelle repose sur l'application de l'approche MID (Multiplicity-Induced-Dominancy) au domaine du contrôle des véhicules aériens. L'approche MID est appliquée à deux des plateformes de robots aériens les plus représentatives: un véhicule quadrotor typique et un véhicule quadrotor doté de rotors basculants. L'approche conduit à un critère de réglage des gains de contrôle, permettant au système de satisfaire un comportement prescrit basé sur le placement de la racine la plus à droite de la fonction caractéristique en boucle fermée. Enfin, des simulations numériques détaillées, incluant la dynamique linéaire et non linéaire du véhicule, sont réalisées pour valider la proposition.

Parmi les nouvelles tendances dans le domaine des systèmes à retard, le suivi du comportement des racines de l'équation caractéristique comme dans [20], a conduit à l'émergence de la soi-disant approche Multiplicity-Induced-Dominancy (MID). L'efficacité de cette approche a été largement prouvée pour des phénomènes généraux décrits par des équations différentielles linéaires à retard [21, 24, 25, 26, 110], cependant, l'application de cette découverte dans le domaine de la commande des robots aériens, pour autant qu'elle concerne l'auteur, n'a pas été correctement abordée, de cette manière, la contribution principale du présent travail s'appuie sur ce fait.

Ce travail aborde, au moyen de l'approche MID, les effets d'un délai produit par un système de suivi basé sur la vision sur la stabilité des drones quadrotors dans le but d'améliorer leur taux de convergence, ce qui peut être traduit par le fait que le quadrotor atteint l'équilibre aussi rapidement que possible avec une réponse transitoire non oscillatoire.

Les résultats des simulations détaillées, y compris la dynamique linéarisée du véhicule et la représentation du modèle non linéaire, vérifient le bon fonctionnement de la proposition. Cependant, l'extension de la recherche à venir comprend (i) l'étude des contrôleurs PID basés sur le délai au moyen de l'approche MID, (ii) l'application de l'approche MID au cas du suivi de trajectoire, (iii) une analyse comparative détaillée du véhicule quadrotor lorsqu'il est manipulé par des contrôleurs linéaires basés sur MID et des approches non linéaires ainsi que (iv) la validation des propositions dans des environnements conditionnés réels.

## Chapter 7: Time-Delay Control of a VTOL Multi-Agent System Towards Transport Operations

Ce chapitre traite de la commande consensuelle d'un système multi-agents composé de mini-rotors à décollage et atterrissage verticaux (VTOL) au moyen d'un contrôleur basé sur la paramétrisation du temps et du retard. La modélisation du système VTOL est présentée en utilisant la paramétrisation des quaternions pour développer la loi de stabilisation de l'attitude des robots aériens. La dynamique de la position du véhicule est étendue au cas multi-agent où une commande PID à retardement est conçue afin d'obtenir un consensus général en termes de

commande de formation du système. Enfin, une étude de simulation détaillée est présentée pour valider l'efficacité de la stratégie de contrôle proposée, où une interaction collective est également considérée.

Le chapitre actuel présente une proposition concernant le contrôle coordonné d'un ensemble de mini-girouettes VTOL. En plus des travaux cités, il est inclus le problème du suivi de trajectoire du VTOL MAS en tenant compte du délai dans la communication et dans les capteurs tout en visant à effectuer une interaction collective simple (transport). Ainsi, un contrôleur à retardement est synthétisé pour remplir l'objectif de stabilisation en considérant l'interaction collective aérienne pendant l'opération de transport simulée. Des cartes de stabilité explicites dont la valeur du gain sont utilisées pour réaliser une étude de simulation détaillée.

La stratégie de contrôle consiste en un contrôleur PID tolérant au retard, qui garantit à la fois la stabilité de l'attitude et de la position d'un robot aérien individuel et le suivi de la trajectoire sous différentes perturbations permettant la consensualité du système multi-robot. Les résultats de la simulation valident l'efficacité de la méthodologie de contrôle multi-agent proposée pour un scénario de transport d'objets, qui induit différentes perturbations sur chaque robot du quartet. La simulation souligne également que, même lorsque les effets du délai sont présents sur le système, la consensabilité, la formation et le suivi de trajectoire sont réalisables en utilisant la méthodologie de contrôle proposée. Dans le cadre de travaux futurs, la présentation et l'explication explicites des points de contact de l'objet et le calcul des forces exercées par les robots sur l'objet seront envisagés et étudiés.

## Appendices

### Appendix **A**: Properties of the Multi-Link Unmanned Aerial System

Cette annexe définit les propriétés de la matrice et du vecteur qui composent le modèle dynamique du ML-UAS. Ces propriétés sont utilisées pour effectuer l'analyse de stabilité du véhicule au moyen des critères de stabilité de Lyapunov.

### Appendix **B**: ML-UAS Linearization for Observability

Dans le cadre de la conception du filtre de Kalman étendu dans le **Chapitre 4**, la linéarisation du modèle dynamique non linéaire des systèmes est obligatoire. La procédure pour accomplir cette tâche est décrite dans cette annexe.

### Appendix **C**: A Pedagogical Approach to Data Fusion and Kalman Filter

Cette annexe expose, de manière pédagogique, le filtre de Kalman pour la fusion de données et son utilisation dans les systèmes mécaniques. Les équations du filtre de Kalman et du processus de fusion de données sont expliquées de manière intuitive et appliquées sur deux plates-formes pédagogiques utilisées à l'IPSA comme partie du matériel

de laboratoire pour introduire les étudiants au contrôle des systèmes et aux principes de navigation dans le domaine de la robotique mobile terrestre et aérienne. Enfin, les outils pour simuler de tels systèmes dans des conditions réelles d'exploitation dans Matlab et Simulink sont donnés et les résultats sont discutés.

## **Appendix D: Teaching Activities**

Un récapitulatif des activités pédagogiques menées pendant la formation doctorale, dans le cadre du contrat doctoral, est présenté dans cette dernière annexe. Le contenu de cette section de la thèse comprend une liste détaillée des cours, une liste des étudiants encadrés et les plateformes pédagogiques développées pour ces buts.

# Declaration of Authorship

I, José de Jesús Castillo Zamora, declare that this thesis, titled "*Design, Modeling and Control of a Multi-Drone System for Aerial Manipulation*", and the work introduced herein are of my own authorship, thus I confirm that:

- The current work was elaborated during the pre-established time corresponding to the Ph. D. formation at the corresponding institution/university.
- The publications where the (partial) results of this work have been presented are properly mentioned.
- Citations to the corresponding manuscripts and/or works are properly done.
- Any source of help has been included in the acknowledgements of this work.
- The work done in conjunction with others is clearly declared, highlighting the contributions of mine.

José de Jesús Castillo Zamora

Signed at **Gif-sur-Yvette, France** on **September 17th, 2021**

Copyright © of the papers may go to the corresponding publication institution



*"If you know the enemy and know yourself, you need not fear the result of a hundred battles. If you know yourself but not the enemy, for every victory gained you will also suffer a defeat. If you know neither the enemy nor yourself, you will succumb in every battle."*

Sun Tzu

*To my mother, my father, my brother and my sister*

# Acknowledgements

Firstly and shortly, I thank God, and above everything and everyone, I do thank to the two persons I will always love the most and to whom I will be forever thankful to, my parents, José Luz and María, you have always been there for me and I will always be there for you as well. For all your support and your love, thank you brother and sister, Ulises and Diana, I love you both.

All my gratitude and admiration to both of my advisors, Juan Escareño and Islam Boussaada. I am grateful specially to Juan Escareño, from who I have learned a lot of things, including non scientific experiences, for supporting me not only during my 3 years of doctoral formation but since the end of my Master thesis back in 2016. Thank you, Doc, for giving me the opportunity to develop this work and all the trust you have shown to me. I am equally thankful to my advisor at the L2S and IPSA, Islam Boussaada, who always showed his support during my stay and gave me the opportunity to carry out my research activities with independence and constant motivation not to mention that he always showed himself at my disposal for administrative tasks regarding the enrollment procedures and the teaching activities.

For the warm welcome and all the support from the very first day I arrived to France, I thank to Juan Escareño and his lovely family. God bless you and keep you always safe and sound. In the same way, I am grateful to the Álvarez Cote family that made me feel home and who showed an unconditional support but specially to Jonatan for the additional discussions on my thesis. To Guillermo Alcántara for the friendship and support, I have nothing but words of gratitude and admiration. I must do an special mention to all those people I met in France and that have been there during this time as Assia Belbachir, Kike, Johvany, Maksym, Tocayé, Amina and the list may go on, thank you.

I do not forget my mexican friends and colleagues that have been by my side, during this journey, yet there are few of them who deserve an honorific mention: Annecy, Yayis, Monsi and Claudia, you all have a place in my heart. To Los Oscuros, you all rock. Al Jefe, Alejandro Astudillo, gracias por los constantes saludos y ánimos. To the Mechatronics Engineering Department of the Instituto Tecnológico de Celaya. To Karla Camarillo and Gerardo Pérez, the ones that have guided me in my scientific journey and inspired me to become the professional I am today.

Last but not least, I thank to l'IPSA and all its people for the financial support during my thesis and the opportunity to introduce myself to teach at a french institution. In this same regard, I thank to all the staff of the L2S, CNRS-CentraleSupélec, that always showed its disposal and support.

Sincerely yours,

José de Jesús Castillo Zamora

Gif-sur-Yvette, France, September 2021



# Publications List

## Journals

1. **J. J. Castillo-Zamora**, J. Escareno, I. Boussaada, J. Stéphant, and O. Labbani, “Nonlinear Control of a Multi-Link Aerial System and ASEKF-based Disturbances Compensation”, *IEEE Transactions on Aerospace and Electronic Systems*, 57(2), 907-918, 2021.
- **J. J. Castillo-Zamora**, I. Boussaada, A. Benarab, and J. Escareno, “Time-Delay Control of Quadrotor Unmanned Aerial Vehicles: a Multiplicity-Induced-Dominancy-Based Approach”, *submitted to Journal of Vibration and Control*. 2021

## Conferences

1. **J. J. Castillo-Zamora**, J. Escareno, J. Alvarez, J. Stéphant, and I. Boussaada, “Disturbances and Coupling Compensation for Trajectory Tracking of a Multi-link Aerial Robot”, 6th International Conference on Control, Decision and Information Technologies (CoDIT), April 2019, pp. 738–743.
2. **J. J. Castillo-Zamora**, J. Escareno, I. Boussaada, O. Labbani, and K. Camarillo, “Modeling and Control of an Aerial Multi-cargo System: Robust acquiring and transport operations”, 18th European Control Conference (ECC). IEEE, 2019, pp. 1708–1713.
3. J. Alvarez-Muñoz, **J. J. Castillo-Zamora**, J. Escareno, I. Boussaada, F. Méndez -Barrios, and O. Labbani-Igbida, “Time-delay control of a multi-rotor VTOL multi-agent system towards transport operations”, International Conference on Unmanned Aircraft Systems (ICUAS). IEEE, 2019, pp. 276–283.
4. **J.J. Castillo-Zamora**, J.P. Aguilera-Alvarez, J. Escareno, I. Boussaada, J.J. Martinez-Nolasco, A.A. Jimenez-Garibay, “A pedagogical approach to data fusion and Kalman Filter”, *Pistas Educativas*, Vol. 32, No. 137, 2020.
5. **J. J. Castillo-Zamora**, J. E. Hernández-Díez, I. Boussaada and J. Escareno, “A Preliminary Parametric Analysis of PID Delay-Based Controllers for Quadrotor UAVs”, *accepted at the International Conference on Unmanned Aircraft Systems (ICUAS 2021)*.



# Scientific Animation

## Workshops

1. Modeling and Control of a Multi-link Convertible Drone for Manipulation Operations at Journée Technique: Drones et Manipulation, Aug 2018, 2RM in collaboration with GT UAV and GT3 Manipulation Multi-échelles de GDR Robotique at the HEUDIASYC laboratory, Compiègne, Oise, France.
2. 2D Dynamics of an Aerial Multi-cargo System at Seminaires of the ENSIL-ENSCI of the Université de Limoges and the XLIM ReMIX Research Institute, Sep 2018, Limoges, Haute-Vienne, France.
3. Modeling and Control of an Aerial Multi-cargo System: Robust Acquiring and Transport Operations at Seminaires of the ENSIL-ENSCI of the Université de Limoges and the XLIM ReMIX Research Institute, Jun 2019, Limoges, Haute-Vienne, France.
4. Design, Modeling and Control of a Multi-Drone System for Aerial Manipulation at Journée des Doctorants, Sep 2020, Université Paris Saclay, Université Paris Sud-CNRS-CentraleSupélec, Gif-sur-Yvette, Île-de-France, France.
5. Introducción al Control de Sistemas con Retardos (Introduction to Time-delay Systems Control) at Congreso Internacional en Sistemas Mecatrónicos (CISMe), Oct 2020, Tecnológico Nacional de México, Instituto Tecnológico de Celaya, Celaya, Guanajuato, México.
6. Modeling and Control of Multi-link Aerial Vehicles at Seminaires of the ENSIL-ENSCI of the Université de Limoges and the XLIM ReMIX Research Institute, Nov 2020, Limoges, Haute-Vienne, France.
7. Time-Delay Control of Quadrotor Unmanned Aerial Vehicles: a Multiplicity-Induced-Dominancy-based Approach at Journée des Doctorants, Mai 2021, Institut Polytechnique des Sciences Avancées (IPSA), Ivry-sur-Seine, Île-de-France, France.

## Contests

1. Aplicación Móvil de Enseñanza y Reconocimiento Gestual de Lengua de Señas Mexicanas (Mobile App for Teaching and Gestural Recognition of Mexican Sign Language) at the Third Meeting of Innovation and Creativity for Internationalization at Home, Oct 2019, Secretariat of Innovation, Science and Higher Education, Guanajuato, México



# Contents

<b>1 Introduction</b>	<b>5</b>
1.1 Thesis Framework	5
1.1.1 Thesis Description	5
1.1.2 Inspiration	6
1.1.3 Mission	7
1.2 Unmanned Aerial Vehicles (UAVs): An Overview	7
1.2.1 Early Designs	7
1.2.2 Small-size UAVs	8
1.2.3 Typical UAV System	9
1.3 Multi-Link Unmanned Aerial Systems (ML-UASs): State of the Art	11
1.3.1 Mechanical Elements and Classification	12
1.3.2 Flight Dynamics Consideration	14
1.3.3 Design Considerations of Energy and Power	14
1.3.4 Considerations on Electronics and Control	15
1.4 An Abstract on Time Delays Effects in Systems Stability	16
1.4.1 Examples of Systems with Time Delays	16
1.5 Thesis Outline	19
<b>I Multi-Link Unmanned Aerial System</b>	<b>23</b>
<b>2 Modeling and Control: Robust Acquiring and Transport Operations</b>	<b>25</b>
2.1 Introduction	25
2.2 Mathematical Modeling	26
2.3 Control Strategy	30
2.3.1 Trajectory Planning and Picking Strategy	33
2.4 Numerical Simulations and Results	34

<b>3 Disturbances and Coupling Compensation for Trajectory Tracking</b>	<b>39</b>
3.1 Introduction	39
3.2 Mathematical Modeling	40
3.2.1 Dynamics	41
3.2.2 Disturbed System Representation	42
3.3 Disturbances Estimation and Control	42
3.3.1 Augmented-State Kalman Filter Design	42
3.3.2 Control Strategy	44
3.4 Numerical Simulations and Results	45
<b>4 Nonlinear Control and ASEKF-Based Disturbances Compensation</b>	<b>51</b>
4.1 Introduction	51
4.2 Mathematical Modeling	52
4.2.1 Dynamics	53
4.2.2 Augmented State Representation	56
4.3 Uncertainties Estimation and Control	57
4.3.1 ASEKF Estimation Strategy	59
4.3.2 Control	60
4.4 Numerical Simulations and Results	65
<b>II Time-Delays on Unmanned Aerial Systems</b>	<b>71</b>
<b>5 Parametric Analysis of PID Delay-Based Controllers for Quadrotor UAVs</b>	<b>73</b>
5.1 Introduction	73
5.2 Quadrotor Modelling	75
5.3 Control Scheme Design	77
5.3.1 Rotational Dynamics Stability	79
5.3.2 Time-Delay Theoretical Definitions	79
5.3.3 PID Controllers Analysis	80
5.4 Results	83
5.4.1 Stability Charts	84
5.4.2 Control Simulations	84
<b>6 Time-Delay Control of Quadrotor UAVs: a MID-based Approach</b>	<b>91</b>
6.1 Introduction	91
6.2 MID Approach Fundamentals	92
6.3 Quadrotor Model	94
6.4 UAV Control: The Typical Quadrotor Case	96

6.4.1	MID-Property-Based Controllers Analysis	98
6.4.2	Symbolic/Numeric Analysis of the MID-Based Controller	100
6.5	UAV Control: The Tilting-Rotors Case	105
6.6	Simulation Results	107
6.6.1	Simulation results: The Typical Quadrotor Case	108
6.6.2	Simulation results: The Tilting-Rotors Case	109
<b>7</b>	<b>Time-delay Control of a VTOL Multi-Agent System</b>	<b>111</b>
7.1	Introduction	111
7.2	Theoretical Prerequisites	112
7.2.1	Graph Theory	112
7.2.2	Unit Quaternion and Attitude Kinematics	113
7.3	Attitude and Position Dynamics of the VTOL Multi-Agent System	114
7.4	Attitude and Position Control for the VTOL MAS	115
7.4.1	Attitude Stabilization Method	115
7.4.2	Position Control Strategy for the VTOL Multi-Agent System	116
7.4.3	VTOL Multi-agent Formation Control	119
7.5	Numerical Simulations and Results	120
<b>8</b>	<b>Concluding Remarks</b>	<b>125</b>
8.1	Part I: Multi-Link Unmanned Aerial System	125
8.1.1	Chapter 2: Modeling and Control: Robust Acquiring and Transport Operations	125
8.1.2	Chapter 3: Disturbances and Coupling Compensation for Trajectory Tracking	125
8.1.3	Chapter 4: Nonlinear Control and ASEKF-Based Disturbances Compensation	126
8.2	Part II: Time-Delays on Unmanned Aerial Systems	126
8.2.1	Chapter 5: Parametric Analysis of PID Delay-Based Controllers for Quadrotor UAVs	126
8.2.2	Chapter 6: Time-Delay Control of Quadrotor UAVs: a MID-based Approach	127
8.2.3	Chapter 7: Time-Delay Control of a VTOL Multi-Agent System Towards Transport Operations	127
8.3	General Conclusions	128
<b>A</b>	<b>Properties of the Multi-Link Unmanned Aerial System</b>	<b>129</b>
<b>B</b>	<b>ML-UAS Linearization for Observability</b>	<b>131</b>
<b>C</b>	<b>A Pedagogical Approach to Data Fusion and Kalman Filter</b>	<b>133</b>
C.1	Introduction	133
C.2	Methodology	134
C.3	Pedagogical Examples	136
C.3.1	Mini Car Robot	136

<b>C.3.2 Mini Bi-rotor Platform</b> . . . . .	137
<b>C.3.3 Sensors Characterization</b> . . . . .	138
<b>C.4 Simulation Results</b> . . . . .	139
<b>C.5 Conclusions</b> . . . . .	144
<b>D Teaching Activities</b>	<b>145</b>
<b>D.1 IPSA Courses</b> . . . . .	145
<b>D.2 Pedagogical Platforms</b> . . . . .	146
<b>D.3 Internships Mentoring</b> . . . . .	149

# List of Figures

1.1 Cooperative transport operations	6
1.2 Natural "multi-link" morphologies	6
1.3 Leonardo Da Vinci's air gyroscope	8
1.4 Examples of small tactical UAVs	9
1.5 Examples of miniature UAVs	9
1.6 Examples of micro UAVs	9
1.7 Typical UAV system	10
1.8 Aerial manipulators configuration [114]	12
1.9 Flexible ML-UAS [109]	13
1.10 Rigid ML-UASs	14
1.11 Constant delay model	16
1.12 Stability chart example	17
1.13 Variable pitch milling process	17
1.14 Control diagram for quiet-standing	18
1.15 Delays in a supply chain	19
2.1 Multi-linked Unmanned Aerial System description	26
2.2 Control strategy for the ML-UAS	32
2.3 Desired $\Theta$ angles relations	33
2.4 Translational behavior of the ML-UAS comparison	35
2.5 Rotational links behavior of the ML-UAS comparison	36
2.6 Payloads motion comparison	36
2.7 Translational motion disturbances	37
2.8 Rotational links motion disturbances	37
2.9 MAVs behaviour comparison	38
3.1 Multi-linked Unmanned Aerial System description	40
3.2 Desired trajectory and performance comparison	45

3.3 Performance comparison of the controllers in $x$	46
3.4 Performance comparison of the system in $z$	47
3.5 Performance comparison of the system in $\Theta_1$	47
3.6 Performance comparison of the system in $\Theta_2$	48
3.7 Trajectory errors comparison	48
3.8 Disturbances vs. Estimated disturbances	49
3.9 Estimation errors	49
4.1 3D CAD scheme of the multi-link system	53
4.2 ML-UAS longitudinal simplified scheme	54
4.3 Control blocks diagram	61
4.4 Position and orientation of the ML-UAS	66
4.5 Velocities of the ML-UAS	67
4.6 Disturbances estimation	67
4.7 Estimation errors	68
4.8 Controller response	68
4.9 Aircrafts performance	69
5.1 Quadrotor UAV and vision-based tracking system	74
5.2 Quadrotor block diagrams	78
5.3 Stability regions	81
5.4 Sigma stability regions	83
5.5 controllers' gains within the stability regions	85
5.6 Translational motion for constant reference inputs	86
5.7 Rotational motion for constant reference inputs in position	87
5.8 Translational motion for ramp reference inputs	88
5.9 Rotational motion for ramp reference inputs in position	89
5.10 Quadrotor velocities and control signals for constant reference inputs, $k_{i_{x,y,z}} = 0$ and $\tau = 0.13$ [s]	90
5.11 Quadrotor velocities and control signals for ramp reference inputs, $k_{i_{x,y,z}} = 1$ and $\tau = 0.08$ [s]	90
6.1 Quadrotor vehicle and vision-based tracking system (scheme conceived from figures available at <a href="http://freepik.com">freepik.com</a> )	94
6.2 Block diagram representation of the typical quadrotor closed-loop system	98
6.3 (left) Behavior of $R_{3,x}^*(\zeta; v)$ within the interval $0 < v < 1$ . Numerical evidence of the dominance of the root $s_{0_x}$ within the intervals in Eqns. (6.67)-(6.69) with $\tau = 0.1$ [s]: (Center) Spectral distribution of the roots. (Right) Time-domain solution.	105
6.4 Block diagram representation of the quadrotor with tilting-rotors closed-loop system	107
6.5 Motion of the typical quadrotor vehicle: Left) Translational states. Right) Rotational states.	109
6.6 Motion of the quadrotor vehicle endowed with tilting-rotors: Left) Translational states. Right) Rotational states.	110

7.1 Schematic configuration of a VTOL vehicle in the 3d space.	115
7.2 Multi-VTOL system and the communication flow.	120
7.3 Behavior of the multi-agent VTOL system in the 3d space.	122
7.4 Angular ( $\psi_i$ ) and linear positions for the multi-agent system featuring communication and sensor delay	123
7.5 Attitude ( $\phi_i, \theta_i$ ) behavior of the different aerial vehicles during the simulation	124
C.1 The mini car robot: Left) Real mini car robot. Right) Mini car free body diagram	136
C.2 The bi-rotor platform: Left) Real Bi-rotor platform. Right) Bi-rotor free body diagram	138
C.3 Matlab code: Systems properties and conditions	140
C.4 Matlab code: Kalman filter elements	140
C.5 Simulink environment: up left corner: ideal performance of the sensors; up right corner: usage of the ultrasonic sensor only; bottom left corner: usage of the accelerometer only, and, bottom right corner: data fusion by the Kalman Filter	141
C.6 Mini car simulation results	142
C.7 Accelerometer noise and offset blocks	142
C.8 Ultrasonic sensor noise block	143
C.9 Mini car simulation results	143
C.10 Mini car simulation results	144
C.11 Bi-rotor simulation results	144
D.1 Edu-copter pedagogical platform	146
D.2 Mini-car vehicle platforms	146
D.3 1(2)-DOF(s) Bi-rotor platform	147
D.4 Home-made visual tracking system	147
D.5 Edu-wing conception	147
D.6 Aerial mechanical gripper	148
D.7 Quadrotor tuning platform	148



# List of Tables

1.1 Small-size UAVs specifications	10
2.1 Simulation parameters	34
2.2 Simulation motion phases	34
3.1 Parameters of the system for simulations	45
4.1 Desired trajectories	65
4.2 Simulation parameters	65
5.1 Simulation parameters	84
5.2 Translational controllers gains	85
6.1 Definition of the vehicle's parameters and control gains	107
7.1 Physical parameters for the VTOL vehicle	120
7.2 Initial conditions for the system	121
C.1 Simulation parameters and conditions	139
D.1 Courses list	145



# Résumé & Abstract

## Résumé

Un sujet récent et passionnant dans le domaine des véhicules aériens autonomes (UAVs) est l'interaction avec l'environnement via la manipulation en vol (récupération, transport, placement). Ce profil opérationnel dévoile un énorme potentiel vis-à-vis des applications industrielles et de service. La nouvelle génération de robots aériens permet de disposer d'un actionneur robotique tridimensionnel capable d'exercer des forces et / ou des couples sur des points spécifiques pour des opérations d'acquisition / déploiement, d'outillage ou de perchoir. De nos jours, les drones de petite taille sont remarquables en raison de leur polyvalence, portabilité et maintenance facile, mais leur performance est limitée en raison de problèmes technologiques concernant la consommation d'énergie, l'efficacité du temps de vol, etc.

Il est donc évident que les opérations de prélèvement aérien, de transport et de placement ont capté l'attention des chercheurs car elles participent à la plupart des applications réelles telles que la livraison de kits de survie, les opérations de sauvetage, le déploiement / l'acquisition de capteurs, etc. Ces capacités peuvent être améliorées par la conjonction de plusieurs véhicules aériens ce qui implique la conception et les études sur différents domaines technologiques. À cet égard, l'idée d'une manipulation de charges lourdes par un groupe d'UAVs est prometteuse dans des conditions environnementales difficiles.

Dans le cadre de la solution aux tâches susmentionnées, et en ayant à l'esprit la mise en œuvre d'un ensemble de véhicules aériens, des drones ont été physiquement connectés et étudiés comme une seule chaîne cinématique volante avec une morphologie et une structure similaires à celles du robots manipulateurs. Néanmoins, il est simple d'associer cette solution à une structure de véhicule équivalente au sol: les trains. Une définition générale du train peut se référer à un certain nombre de véhicules guidés ou d'animaux se déplaçant dans une formation en ligne ou en courbe.

Ainsi, des nouveaux systèmes et configurations aériens sont en cours de conception. Parmi ces plates-formes, les manipulateurs aériens Snake se démarquent. Ces véhicules sont définis comme une sorte de manipulateur aérien reconfigurable et à morphing couplée avec des compétences de manipulation robotique bidimensionnelles ou tridimensionnelles grâce à l'interaction de multi-hélices ou d'hélices qui constituent deux chaînes cinématiques bifurquées ou plus.

L'application de ces systèmes aériens multi-corps est encore limitée en raison de problèmes de consommation d'énergie et de médiation, mais ils permettent d'explorer de nouvelles méthodologies et techniques dans les domaines de la robotique reconfigurable, de la robotique continue, des humanoïdes volants, entre autres.

L'objectif général du doctorat est de proposer une configuration multi-drone innovante destinée à effectuer des tâches de manipulation (récupération/déploiement/transport) dans des environnements complexes via des méthodes robotiques avancées

incluant l'étude des effets des retards dans le système aérien. La présence de retards au niveau du l'état et/ou des entrées d'un système affectent sa stabilité de telle sorte qu'un délai peut induire des comportements complexes pour les schémas en boucle fermée ou, pour certains délais importants, le système peut être stabilisé. De plus, il a été démontré que pour les systèmes interconnectés ou à grande échelle, les retards sont critiques.

Le contenu principal de cette thèse est divisé en: la partie 1 qui est consacrée à la modélisation et à l'étude dynamique du système aérien autonome à liaisons multiples; et la partie 2 qui se concentre sur l'étude des effets des retards dans les opérations d'UAV. Egalement, chacune de ces parties est divisée en chapitres qui correspondent à la portée correspondante. Enfin, les remarques finales sont fournies. De plus, 4 annexes complètent la description des activités réalisées.

## **Abstract**

A recent and exciting topic within the field of unmanned aerial vehicles (UAVs) is the interaction with the surrounding environment via in-flight manipulation (retrieving, transport, placing). Such operational profile unveils an enormous potential vis-a-vis industrial and service applications. The new generation of aerial robots allows to have three-dimensional robotic actuator capable of exerting forces and/or torques on specific point(s) for acquisition/deployment, tooling or perching operations. Nowadays, the small size UAVs are noteworthy because of their versatile, portable, and easy maintenance yet, their operational performance is restricted as a matter of technological issues regarding the power consumption, flight time efficiency, etc.

It is thus evident that the aerial picking, transporting and placing operations have captured the eye of researchers as these take part in most of real applications as survival-kit delivering, rescue operation, sensor deployment/acquiring and so on. Such capabilities can be improved by the conjunction of several aerial vehicles which implies, in addition, the conception and the studies on different technological domains. In this regard, the idea of heavy payloads manipulation by a group of autonomous aircrafts is promising in harsh environmental conditions.

As a part of the solution to the aforementioned tasks, and having in mind the implementation of a set of aerial vehicles, UAVs have been physically connected and studied as a single flying kinematic multi-link chain with a morphology and structure similar to those of the manipulator robots. Nevertheless, it is straightforward to relate such solution to a ground-equivalent vehicle structure: trains. A general definition of train may refer to a number of guided vehicles or animals moving in a line- or curve-like formation.

Thus, new aerial systems and vehicles configurations are being conceived. Amid such platforms, Snake Aerial Manipulators stand out. These vehicles are defined as a kind of coupled task re-configurable and shape-morphing aerial manipulator with bi-dimensional or three-dimensional robotic handling skills through the interaction of multi-copters or propellers that constitute two or more bifurcated kinematic chains.

The application of these multi-body aerial systems is still restricted due to power consumption and onmidirectionality issues, yet, they allow to explore new methodologies and techniques in the fields of re-configurable robotics, continuum robotics, flying humanoids, among others.

The general objective of the Ph.D. is to propose an innovative multi-drone configuration meant to perform manipulation tasks (retrieving/deployment/transport) within complex environments via advanced robotics methods including the study of the effects of time-delays in aerial system since the presence of time-delays at the state and/or inputs of a given system affects its stability such that a time-delay may induce complex behaviors for the closed-loop schemes or, for some large time-delays, the system may be

stabilized. Additionally, it has been shown that for interconnected or large-scale systems time-delays are thus critical.

Thus, the main content of this thesis is divided into: Part 1 which is devoted to the modelling and dynamical study of the Multi-Link Unmanned Aerial System proposal; and Part 2 that focuses on the study of the effects of time delays in UAV operations. At the same time, each of these parts is divided into chapters that fit the corresponding scope. At last, the concluding remarks are provided. In addition, 4 appendices complement the description of the activities carried out.



# Chapter 1

## Introduction

This chapter provides a brief description of the project, in this sense, the state of the art, regarding the different fields of knowledge addressed during the development of the thesis, is equally included.

The current chapter is outlined as follows. At [Section 1.1](#), a short description of the project is provided. [Section 1.2](#) reveals some appreciable introductory information on the domain of Unmanned Aerial Vehicles (UAVs) as well as some definitions commonly adopted in this research field. On the other hand, [Section 1.3](#) reports the advances and current developments on matters of Multi-Link Unmanned Aerial Systems (ML-UAS). [Section 1.4](#) exposes a brief summary of the effects of time-delays in the stability of dynamical systems and, lastly, [Section 1.5](#) establishes the general outline of the thesis.

### 1.1 Thesis Framework

**Keywords:** Multi-drone Manipulation, Dynamic System Modeling, Nonlinear Control, In-flight Inter-drone Docking, Aerial Pick-transportation-and-place, Time-Delay Effects.

#### 1.1.1 Thesis Description

A recent and exciting topic within the field of autonomous aerial vehicles is the interaction with the surrounding environment via in-flight manipulation (retrieving, transport, placing). Such operational profile unveils an enormous potential *vis-a-vis* industrial and service applications. The new generation of aerial robots allows to have three-dimensional robotic actuator capable of exerting forces and/or torques on specific point(s) for acquisition/deployment, tooling or perching operations.

Based on the multi-disciplinary nature of the actual project, it lies within the framework of a joint research collaboration between the “Laboratoire de Signaux et de Systèmes (L2S)” and the “Institut Polytechnique de Science Avancées (IPSA)” whose aim is to develop an interactive multi-drone autonomous aerial system.

Previous research has been conducted on such kind of vehicles regarding the control strategies, the design and modeling, multi-drone load transportation complemented by visual sensing strategies for navigation and object detection, among others. A further discussion on these regards is provided in the upcoming sections of the chapter.



(a) "El chepe" train



(b) Working ants

Figure 1.1: Cooperative transport operations

(a) *Scolopendra gigantea*

(b) Snake in motion

Figure 1.2: Natural "multi-link" morphologies

### 1.1.2 Inspiration

The aerial picking, transporting and placing operations have captured the eye of researchers as these take part in most of real applications as survival-kit delivering, rescue operation, sensor deployment/acquiring and so on. Such capabilities can be improved by the conjunction of several aerial vehicles which implies, in addition, the conception and the studies on different technological domains. In this regard, the idea of heavy payloads manipulation by a group of autonomous aircrafts is promising in harsh environmental conditions [71, 129, 112, 171, 17, 4].

As a part of the solution to the aforementioned tasks, and having in mind the implementation of a set of aerial vehicles, UAVs have been physically connected and studied as a single flying kinematic multi-link chain with a morphology and structure similar to those of the manipulator robots that can be found in the industrial and manufacturing field [156, 9, 175, 176].

Nevertheless, it is straightforward to relate such solution to a ground-equivalent vehicle structure: trains. A train is defined to be a series of railway carriages or wagons moved as a unit by a locomotive or by integral motors (Fig. 1.1a). Yet, a general definition may refer to a number of guided vehicles or animals moving in a line- or curve-like formation (Fig. 1.1b) [154]. However, one of the main differences may be the limitation in matters of mobility due to the railroads which are necessary for the trains to reach a specific location.

Natural systems often operate under a cooperative transportation principle as in the case of ants colony [80] or bees [162]. Nevertheless, live beings as the centipedes (Fig. 1.2a) or snakes (Fig. 1.2b) may present a morphology which makes one relate the robotic and transportation multi-link systems to such shapes. Centipedes possess body segments and legs, thus they generate body oscillations during terrestrial locomotion. Centipede locomotion has the characteristic that body oscillations are absent at low

speeds but appear at faster speeds; furthermore, their amplitude and wavelength increase as speed does, leading to its study and dynamical approach with more emphasis [110]. The complex anatomy of the centipede has inspired researchers to develop new robotic structures as well as new control strategies and methodologies to overcome the problem of trajectory tracking and obstacle avoidance in complex environments [84, 69, 70].

It is thus logical to place one's sight on natural multi-link systems to solve complex locomotion and transpiration issues.

### 1.1.3 Mission

The general objective of the Ph. D. is to propose an innovative multi-drone configuration meant to perform manipulation tasks (retrieving/deployment/transport) within complex environments via advanced robotics methods. Three complementary approaches are investigated:

1. The first stage consists in modeling a novel interactive aerial system capable of performing in-flight collective manipulation, where tightening define the configuration of the aerial robot array.
2. The second phase of the thesis focuses on the control aspects especially to achieve different formations with the proposed multi-drone system as well as the manipulation dexterity of the payload during the transportation and manipulation operations.
3. The third stage is devoted to study the effects of time-delays in aerial system performing the interactive environmental tasks as the ones previously mentioned.

The main aspects involved in this project are introduced in the following sections to establish a reference framework for ulterior analysis.

## 1.2 Unmanned Aerial Vehicles (UAVs): An Overview

UAVs, or formally called Unmanned Aerial Vehicles are defined as space-traversing vehicles that fly without a human crew on board and that can be remotely controlled or can fly autonomously. Such vehicles have recently reached unprecedented levels of growth in diverse military and civilian application domains [123, 166].

UAVs were first introduced during World War I, registering a long involvement of the military. In 1997, the total income of the UAV global market, including the Vertical Take-Off and Landing (VTOL) vehicles, reached \$2.27 billion dollars and for the middle 1990's, the demand for VTOL vehicles was limited, but since then, commercially available products started to increase [166]. Studies as the ones gathered in [123, 166], claim that UAVs will continue to be the most dynamic growth sector of the aerospace industry and the tendency will shift to smaller, more flexible and versatile UAVs [106].

### 1.2.1 Early Designs

It has been documented that the first major breakthrough contribution to autonomous mechanisms occurred during the era of Pythagoras. Nonetheless, in China, at about 400 B.C., took place the first documented idea of a vertical flight aircraft; and by 1483, Leonardo Da Vinci designed an aircraft hovering capable (Fig. 1.3) [166].

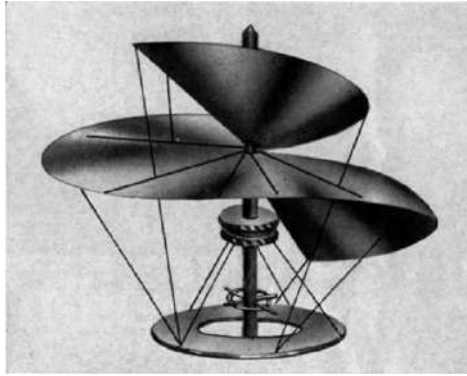


Figure 1.3: Leonardo Da Vinci's air gyroscope

A boiler-based vertical flight machine was also designed in the 1840's by Horatio Phillips. However, it was Ponton d'Amecourt in the 1860's who flew small helicopter models powered by steam. Thomas Alva Edison introduces one of the most remarkable aerial vehicles in the 1880's; he experimented with different rotor configurations and electric motors. Yet, the major breakthrough of modern times in helicopter history was the never-flown helicopter of Igor Ivanovitch Sikorsky (1909). UAVs entered the military applications arena during the First World War, nevertheless, as previously mentioned, the field of rotary-wing aviation owes its success almost entirely to Sikorsky, who built in 1939 the classical modern helicopter.

In parallel with building vertically flying machines and helicopters, fixed wing aircraft started to evolve over the last 100 years, with the first flight demonstrated by the Wright brothers in 1903 [122].

Nowadays, the small size UAVs noteworthy because of their versatile, portable, and easy maintenance; are employed for the same applications as larger UAVs on a smaller scale and at a lower cost.

## 1.2.2 Small-size UAVs

Among different types of UAVs, small-size or small-scale UAVs are gaining top interest and popularity because [29, 50]:

- They represent a powerful tool for scientific research due to characteristics such as low cost, high maneuverability, and easy maintenance.
- Their civil application range is wide and continue to increase.
- The role of small-scale UAVs in warfare and defense regards is still unique.

To date, and to the best of the author's knowledge, there is no common method that standardizes the classification of UAVs. The most essential UAV characteristics such as size, speed, reached altitude, operational range, flight endurance, amidst others, are often used to classify these vehicles [152, 153]. In general terms, and with base their size, small-scale UAVs are found to fall into three main categories:

- Small tactical UAVs (Fig. 1.4): the top performance UAVs. Small tactical UAVs are mainly deployed to army serving military operations, yet, some civil missions can be executed by these. Besides the conventional fixed-wing and single-rotor types, several are the UAV models that have been conceived, aiming to optimize the aerodynamics and flight endurance.

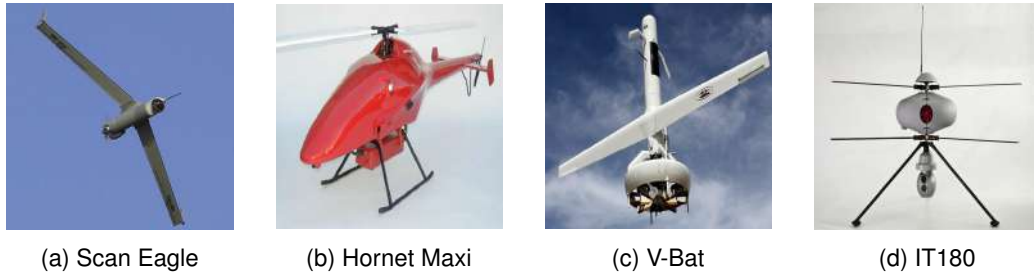


Figure 1.4: Examples of small tactical UAVs

- Miniature UAVs (Fig. 1.5): compared with the aforementioned type, these travel at slower speeds with less flight endurance, possess reduced payload manipulation capability, and operate in a more confined space. Most of these feature a detachable design. Miniature UAVs can be conveniently integrated into various civil applications.

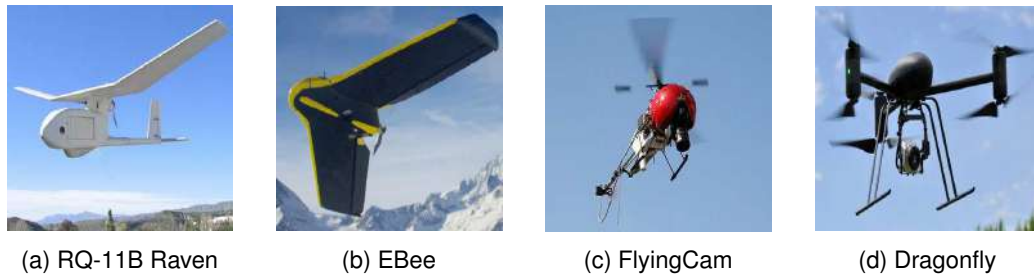


Figure 1.5: Examples of miniature UAVs

- Micro UAVs (Fig. 1.6): the primary aim was to develop a UAV prototype that had a wing- or rotor-span no greater than 15 cm and able fly up to 2 hrs. Such specifications may define the vehicles into this category. The recent technology boosting has shrunk many hobby models into the category.

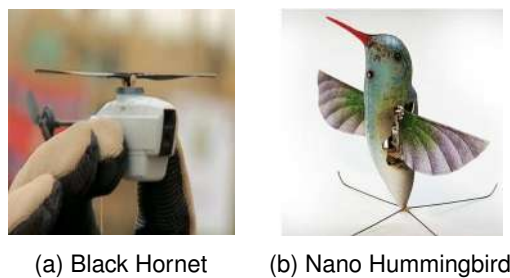


Figure 1.6: Examples of micro UAVs

Lastly, in order to resume the information above, Table 1.1 provides the detailed specifications of small-scale UAVs [29].

### 1.2.3 Typical UAV System

Prior to ulterior discussions, an overview of the general configuration of a UAV is shown in Fig. 1.7. Basically, a complete Unmanned Aerial System (UAS) consists of four parts: (1) a baseline aircraft, (2) manual control backup, (3) a Ground Control Station (GCS) for remotely monitoring the UAV's in-flight status and manipulation; and (4) an on-board Flight Control System

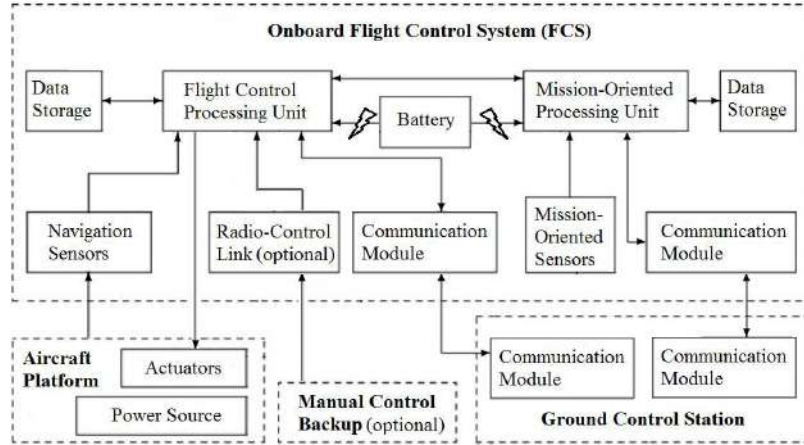


Figure 1.7: Typical UAV system

(FCS) [29, 152, 153].

As depicted in Fig. 1.7 and briefly introduced, a Flight Control System can be considered as an integration of seven main elements which are listed below.

- On-board processing units consist of two types: flight control processing unit and mission-oriented processing unit. Its technological evolution is mainly reflected by the transition from single board computer stacks to all-in-one board integration.
- Navigation sensors provide measurements of the in-flight status of the UAV. Mainly, there are five types of sensors belonging to this category: (1) accelerometer, (2) gyroscope, (3) magnetometer, (4) GNSS (Global Navigation Satellite System) receiver, and (5) peripheral sensors (e.g. barometer, odometer, airspeed sensor). Most of the time, several of these sensors can be found in one of the following elements: (1) Inertial Measurement Unit (IMU), (2) Attitude and Heading Reference System (AHRS), and (3) GPS-aided AHRS. The evolution of the navigation sensors can be attributed to the development of MEMS sensors and data fusion techniques.
- Mission-oriented sensors are the companion to the navigation sensors, providing additional information. These can be classified into two categories: passive and active sensors. Passive sensors may primarily refer to (1) electro-optical cameras, (2) low-light-level (LLL) cameras, and (3) thermal imagers. On the other hand, active sensors are mainly miniature laser devices for detection and ranging.
- Communication modules are the rover side of the wireless communication links between the UAV and the GCS. The only

Table 1.1: Small-size UAVs specifications

Specification	Small tactical	Miniature	Micro
Maximal size	10 m	5 m	15 cm
Gross Take-off Weight	10 to 25 kg	< 10 kg	< 0.1 kg
Speed	Up to 130 m/s	Up to 50 m/s	Up to 15 m/s
Maximal altitude (above ground)	3500 m	1200 m	100 m
Operation range	Up to 50 km	Up to 25 km	Up to 10 km
Flight endurance	Up to 48 hrs	Up to 48 hrs	Up to 20 mins

system known in practical operation is radio-based communication. Small-scale UAVs generally operate in a frequency range of 425 MHz to 5.8 GHz.

A GCS for small-scale UAVs is commonly portable. Its main responsibilities include: displaying and monitoring real-time in-flight status data, displaying navigation view, displaying received images, decision making, mission planning, sending real-time commands, facilitating the control for ground users, etc. The most obvious advance of GCS development may be the increasing prevalence of the open-source GCS software toolkits.

- Power source provides electricity to the UAV system in air.
- Data storage is for on-board in-flight or image data storage.
- Optional Radio Control link is the on-board terminal of the RC communication to realize piloted control backup.

Small-scale UAVs' entrance to the academic community has posed challenges in a variety of research fields such as aerodynamics and flight dynamics modeling, flight control, computer vision, and so on. In the meantime, it also brings an excellent opportunity of developing design methodologies and further evaluating their practical performances.

It should be noted that for scientific research purposes, small-scale UAVs are preferably classified in terms of operation principle, that is, rotorcraft, fixed-wing, and flapping-wing. The process of developing a fully autonomous small-scale UAV mainly consists of five steps:

1. Platform design and construction
2. Dynamics modeling
3. Flight control
4. Navigation algorithms design and implementation
5. Guidance algorithms design and implementation

For a further discussion on the matter, and in order to witness the popularity growth of these vehicles among the scientific community, refer to [29, 152, 153, 50, 123, 166] which are the main sources from where the presented information was taken.

### 1.3 Multi-Link Unmanned Aerial Systems (ML-UASs): State of the Art

In recent years, the improvement of Unmanned Aerial Vehicles (UAVs) capabilities, in terms of aerial manipulation, is an area of interest for scientist around the globe, as previously introduced in Section 1.2. In this sense, the most adopted solution had been to attach robotic manipulator arms to UAVs, nonetheless, the inherent self conception implies a limitation in terms of performance and dexterity [114].

In order to overcome the aforementioned dexterity issue, new aerial systems and vehicles configurations are being conceived. Amid such platforms, Snake Aerial Manipulators stand out. These vehicles are defined, according to [114], as *a kind of coupled task re-configurable and shape-morphing aerial manipulator with bi-dimensional or three-dimensional robotic handling skills through the interaction of multi-copters or propellers that constitute two or more bifurcated kinematic chains*. It is worth mentioning that the work in [114] offers a vast and complete survey on this matter, in this regard, the text herein may be a compact interpretation of the available information yet with some complementary comments that the author considered to be enrich the discussion.

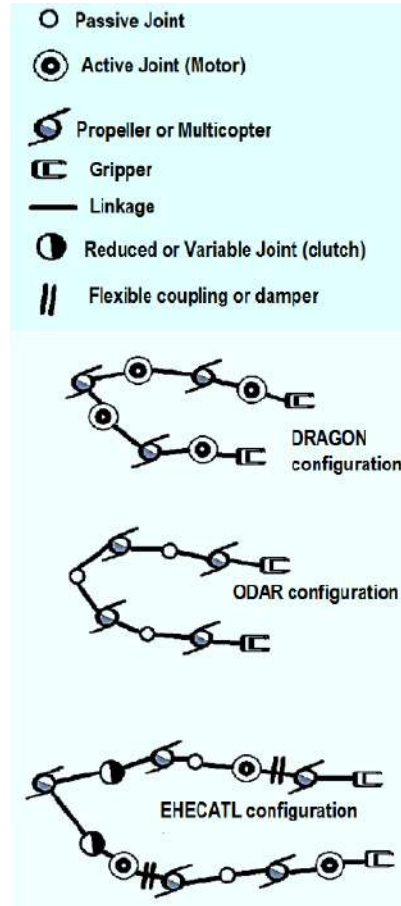


Figure 1.8: Aerial manipulators configuration [114]

Even with the actual technological surge, the application of these multi-body aerial systems is still restricted due to power consumption and onmidirectionality issues, yet, they allow to explore new methodologies and techniques in the fields of re-configurable robotics, continuum robotics, flying humanoids, among others.

Some of the most representative and significant works in the literature that address the conception and development of this kind of vehicles may be:

- The DRAGON, characterized by using propellers as hovering elements and servomotors for manipulation [176].
- The ODAR FAMILY, where multi-rotors are used as elements of hovering, dexterity and manipulation [132].
- The EHECATL, in which, as in the case of the ODAR FAMILY, the multi-rotors are used as elements of hovering, dexterity and manipulation yet it includes selective servomotors assistance [113].

Fig. 1.8 depicts the configuration of the cited reference works. A further discussion on the different aspects regarding the conception, modeling and control of this new aerial vehicle configuration is provided next.

### 1.3.1 Mechanical Elements and Classification

The main components of these robotic systems have been identified and defined by [114], in this regard, one may divide the elements in eight major categories as follows:

- Branching element: the reference point from which at least two kinematic chains fork.
- Kinematic chain: successive union of engine elements with movement transmission elements (usually bar linkages), by joints.
- Engine elements: the set of multi-copter aircrafts or individual propellers which serve as the main actuators of the system for hovering, translation and rotation.
- Transmission elements: bar linkages that connect one engine element to other and allow the chained transmission of their rotations and translations.
- Joint elements: these allow the general mobility and the propagation of relative movements. They could be any type of bearing or even auxiliary motors.
- Damping elements: components used to control or suppress undesired movements, vibrations or misalignment between elements.
- Power elements: components that provides the energy to the aircraft and the auxiliary engine elements.
- Elements of sensing and control: on-board electronic and electro-mechanical devices that allow to measure, store and regulate the states of the robot.

Additionally, according to the linkages material and behavior, the Snake Aerial Manipulators may fall into one of the following categories [129, 163]:

- Flexible Systems (Fig. 1.9): are based on the use of cables and ropes as linking elements, however, flexible materials can be used to built the linkages.

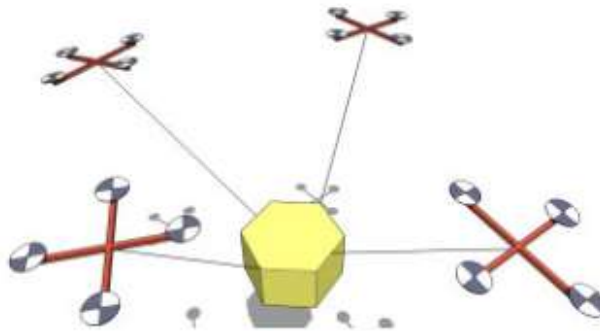
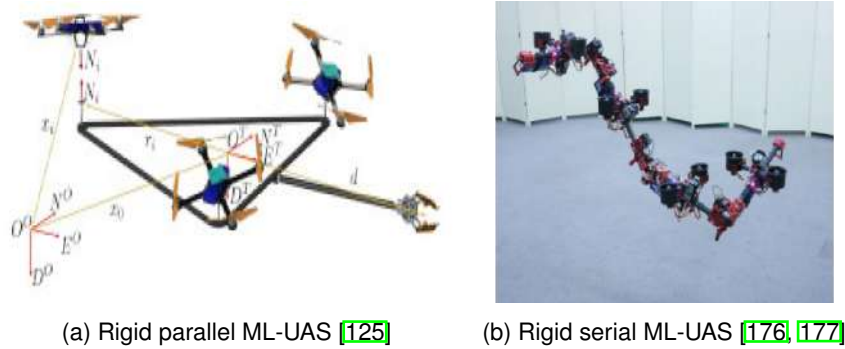


Figure 1.9: Flexible ML-UAS [109]

- Rigid Systems (Fig. 1.10): Consist of a set of UAVs or independent propellers mounted on rigid links. Based on the kinematic chain that the airships or propellers conform, a sub-classification arises:
  - Rigid Parallel ML-UAS (Fig. 1.10a): In this classification, the movement and force of the end-effector is determined by the coordinated operation of each individual engine element in a closed kinematic chain.
  - Rigid Serial ML-UAS (Fig. 1.10b): In this case, the movement and force applied to the point of interest follows an open kinematic chain.



(a) Rigid parallel ML-UAS [125]

(b) Rigid serial ML-UAS [176, 177]

Figure 1.10: Rigid ML-UASs

### 1.3.2 Flight Dynamics Consideration

Concerning the aerodynamics of the vehicle and its flight mode, a ML-UAS is subjected to be categorized within one of the following classifications [114]:

- On the flight: this is a dynamic operation mode, requires standard aerodynamic design, which corresponds, mainly, to wind-related phenomena acting on regular aircrafts [7, 88].
- In situ: this is a quasi-static operation as hovering is required in order to manipulate objects or to do miscellaneous tasks. The in situ tasks are related to hovering power consumption, the distance between propellers, the distance among manipulated objects and the operation altitude [78, 47].
- Transformation: is needed in order to change between on the flight and in situ modes. Such change also requires a smooth motion of the elements [158, 140].

A power source is still necessary in order to enable the motion of the system thus some remarks on the matter are addressed next.

### 1.3.3 Design Considerations of Energy and Power

The multi-link aerial manipulators are feasible by the implementation of propellers, valves and turbines; however, they all require a power source, and according to the options available nowadays in the market, there exist four alternatives: fuel-based sources, solar energies, batteries and direct wired connections. It is evident that the energy source of an aerial vehicle whereas it is a single drone or a multi link system, depends on its size and its weight. In this regard, small scale structures are preferred as there is a vast variety of batteries that satisfy the flight time demanded for the operations [63, 168, 148].

The degree of mobility of the entire aerial structure is highly dependent on the thrust (and on the power source). In this regard, the ML-UASs are observed to perform at three different optional regimes:

- Planar operation: the roll and pitch angles of each element of the system tend to zero. The only feasible independent movements are three-dimensional translations and yaw rotations. The execution of three-dimensional angular motion is exclusive of the gripper [113, 175].
- Omnidirectional operation: in this case, the aerial manipulator has total mobility or beyond the planar configuration [131, 79].

- Convertible operation: as the vehicles translates to the work area, it commonly keeps its entire structure as some sort of long-distance aircraft and once in the workplace it transforms itself to a shape-morphing aerial vehicle.

As the last observation to be mentioned on the mechanical regard, when designing ML-UASSs, the thruster autonomy is a consideration of critical importance as the autonomous manipulation task highly depends on this, nevertheless, assisted manipulation has been studied as a possible solution to extend the performance capability of the vehicles [175].

### 1.3.4 Considerations on Electronics and Control

As in most of the Snake Aerial Manipulator conception procedures, UAVs are used as the actuators of the system thus, the inherent problems of these vehicles appear equally on the dynamics of the flying chain. In this vein, some general implications related to a single vehicle and its control, as well as the implementation of a real time operating system, must be tackled. Some literature findings [114] establish that the aircraft's flight mode defines the approach to be followed in order to generate the motion of the overall kinematic chain, such that:

- Almost pure translational approaches: they focus on bringing the aircraft angles and their respective angular velocities to a zero reference (except for the yaw angles). The main objective is to achieve smooth translational movements.
- Kinodynamic approaches: they are based on back-stepping techniques, and the idea is to disengage translational and rotational models, providing a dynamic behavior to the translation and quasi-static character to the orientation.
- Geometric approaches: fully dynamical approaches in which the aircraft orientation is designed to achieve complex, aggressive and acrobatic movements.

In summary, the operation of a collaborative aerial manipulator depends on the operation of the rotorcrafts that serve as the actuators. In this manner, the operation of a single vehicle implies specific actions as: reading and control of orientation and position, propellers command, image processing, internal data communication and storage, signal filtering, among others [50, 152, 153].

The transformation sequence and the translation to the working area imply several difficulties which include: the coordination and parallel programming in physically restricted flight, the online disturbances and inertial parameters estimation, the conception and execution of a transformation/transition method (similar to those of convertible UAVs). The take-off and landing represent two of the simplest yet dangerous operations, consisting on gradually turning off the motors but taking care that they stay in their mode of thrust support. For these ends, orientation control takes higher priority in both modes of operation and in consequence it is crucial to keep the sensors and actuators working in precise times. Additionally, once in aerial manipulation operation, the restriction on the rotation of the propellers, online hierarchical control and over-actuation optimization must be considered during the design procedure of the controllers and the command strategy [114].

Nevertheless, according to the perspectives addressed in the current section, none of the consulted references takes into consideration the possible secondary effects that may be produced by communication, sensing, processing information time-delays.

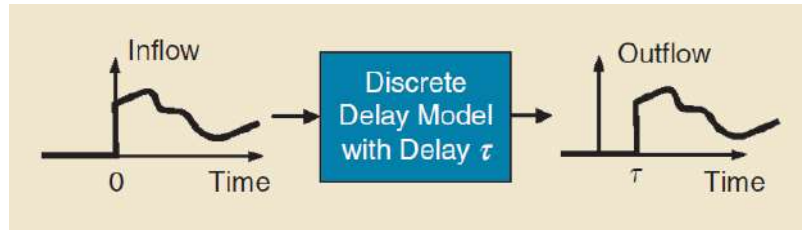


Figure 1.11: Constant delay model

## 1.4 An Abstract on Time Delays Effects in Systems Stability

Delayed systems represent a class of infinite-dimensional systems often used to describe propagation phenomena, population dynamics or engineering systems. A distinct feature of such systems is that their evolution rate is described by differential equations which include information on the past history, for such reason, time-delay systems are also known as hereditary systems, systems with aftereffects, or systems with time lags [58].

The delay effect on the stability of systems with delays in the state and/or input, is a problem of recurring interest since the presence of a time-delay may induce complex behaviors for the closed-loop schemes or, for some large time-delays, the system may be stabilized. In this regard, it is said that control systems operate in the presence of time-delays, mainly due to the time it takes to acquire the information to create control decisions and to execute these [87, 127].

One possible effective control strategy consists in the properly induction of time-delays. For instance, enlarging or extending the time delay in the feedback loop may stabilize a system that otherwise is unstable. Yet, the interest in studying and understanding the effects of delays is rapidly increasing as an inherent consequence of the evolution of control systems complexity. In this sense, the time-delay is a shift operator that lags an input signal by a constant amount of time as depicted in Fig. 1.11 [11].

The main objective of studying the stability of systems subjected to time-delays is to determine necessary and sufficient conditions for the closed-loop system whereas in the delay-parameter space of the controller-parameter space. In this matter, a delayed systems is said to be delay-dependent stable if it is stable for only some values in the delay parameter space, on the other hand, if the stability holds independently of the delay, the system is called delay-independent stable. Multiple disjoint delay regions may exist, such that the system is stable within each region, while becoming unstable outside. These regions, which are known as stability regions, become stability intervals in a system with a single delay. Stability intervals can be extended to a two-dimensional map, known as a stability chart (see Fig. 1.12) [127, 155].

### 1.4.1 Examples of Systems with Time Delays

The following examples are provided by [155], thus for further and detailed discussions on the matter, one may refer to the cited reference. For the purpose of this work, the examples are limited only to show and describe briefly the corresponding cases and how the time-delay is considered within the overall system dynamics and control.

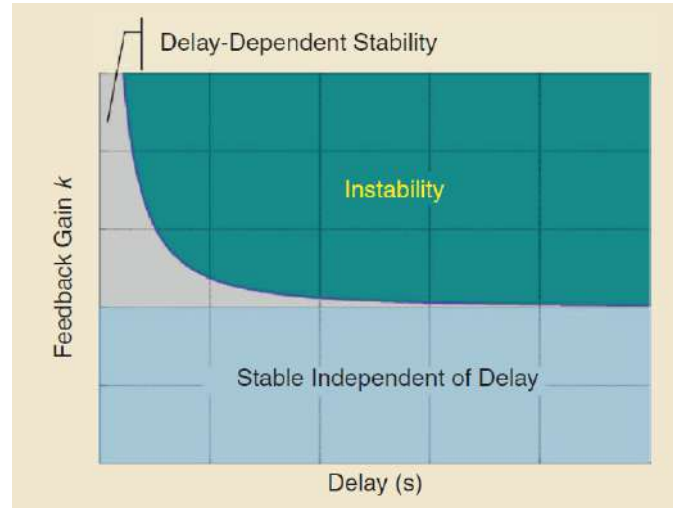


Figure 1.12: Stability chart example

### Delays in Vehicular Traffic Flow

The reaction of human drivers produces time delays, that is, drivers need a minimal amount of time to become aware of external events regarding the environment and the vehicle conditions. Vehicular traffic is thus affected by delays which, sometimes, invite collisions yet, delays can also cause traffic jams and stop-and-go waves, making traffic prone to slinky-type instabilities.

### Variable-Pitch Milling Dynamics

In the milling process shown in Fig. 1.13, the clamped metal piece is machined by a rotating cutting toothed tool. Since the cutting tool and the work-piece are deformable, uncut material is left by each tooth which then requires an additional force of the following tooth. Thus, a past event affects the evolution of the cutting dynamics. The delay in this context is defined by the tooth-passing period.

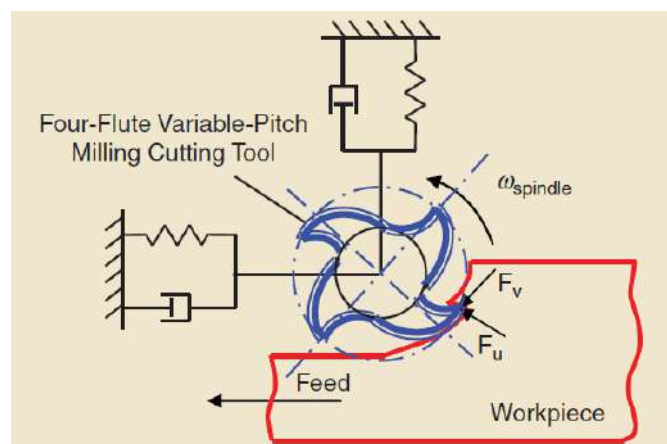


Figure 1.13: Variable pitch milling process

**Delays in Biology**

Experiments haven been designed and conducted, alongside the implementation of analytical tools, to analyze the effects of neuromusculoskeletal torque generation on quiet-standing stability. Such experiments involve the study of the muscle activity at the ankles. The torque due to the neuromusculoskeletal system is modeled by a critically damped system governed by a neural controller that exerts corrective actions after a time lag (about 80 ms). A block diagram of the closed-loop quiet-standing system is depicted in Fig. 1.14

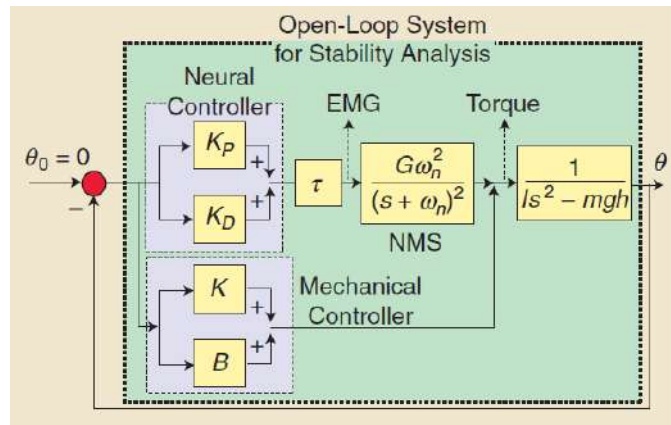


Figure 1.14: Control diagram for quiet-standing

**Epidemics**

Understanding the underlying mechanisms of biological processes and epidemics represents a challenge for health enthusiasts. These mechanisms can be revealed by considering epidemics and diseases as dynamical processes, generally, of the form:

$$\dot{x}(t) = -\lambda x(t) + G(x(t - \tau)) \tag{1.1}$$

which formulates the circulating cell populations, where  $x$  stands for the circulating cell population,  $\lambda$  is the cell-loss rate, and the monotone function  $G$  describes a feedback mechanism denoting the flux of cells from previous compartments. This model is also adopted to describe the dynamics of a given population, where the delay represents a maturation period.

As an additional example, in the case of chronic myelogenous leukemia, some models have multiple delays such that the stability is affected by large (one to eight days) and small (1 to 5 min) delays.

**Delays in Operations Research**

Among the main components of a supply chain model, the transportation, decision-making, and production are primary sources of delay as shown in Fig. 1.15. In this context, one of the objectives is to maintain a constant inventory as a safety stock, while responding to a dynamically changing customer demand, and receiving additional supplies that are not instantaneously available (transportation delays).

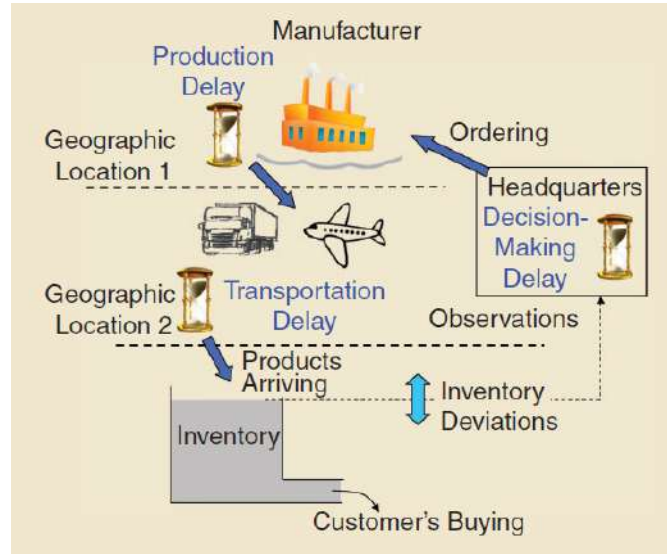


Figure 1.15: Delays in a supply chain

## 1.5 Thesis Outline

The main content of this thesis is divided in two parts: **Part I** which is devoted to the modelling and dynamical study of the Multi-Link Unmanned Aerial System proposal including the disturbances estimation and robust control matters; and **Part II** that focuses on the study of the effects of time delays in UAV operations. At the same time, each of these parts is divided into chapters that fit the corresponding scope. A brief description about the content of each chapter composing this thesis is provided next. In addition, the appendices complement the description of the activities carried out during the preparation of this work.

### Part I: Multi-Link Unmanned Aerial System

#### Chapter 2: Modeling and Control: Robust Acquiring and Transport Operations

In this chapter, the concept of a Multi-Link Unmanned Aerial System, designed for multi-cargo transportation tasks, is introduced. Such system features three links who are actuated by four flying robots. It is presented in detail the dynamics modeling procedure based on the Euler-Lagrange formulation. A preliminary control scheme based on robust Adaptive Integral Sliding Mode Control (AISMC) is applied considering the ML-UAS model uncertainties and the external disturbances. The control objective is to follow/track avian-inspired acquiring patterns for such operations. The effectiveness of the proposed strategy is validated by numerical simulations.

#### Chapter 3: Disturbances and Coupling Compensation for Trajectory Tracking

As in the previous chapter, this one focuses on a Multi-Link Unmanned Aerial System yet, the system is composed of three rotorcrafts attached by two bar like links. The mathematical model is obtained through the Euler-Lagrange energy-based methodology while the controller relies on a classical linear scheme. As the system is highly coupled, due to its inherent dynamics

and cargo influences, a dynamic extension of the equations of motion to apply a Linear Kalman filter is proposed to meet the trajectory tracking specification. The suggested state observer is validated via close-to-reality numerical simulations.

#### **Chapter 4: Nonlinear Control and ASEKF-Based Disturbances Compensation**

The chapter presents an extension on the previously introduced modeling and control strategy of the ML-UAS. In this regard, the aforementioned system is subjected to lumped disturbances which comprise external disturbances and parametric uncertainties. An Augmented-State Extended Kalman Filter intended to estimate endogenous and exogenous uncertainties is conceived and a trajectory-tracking controller fulfilling Lyapunov asymptotic stability is synthesized. A simulation stage is conducted to validate the effectiveness of the proposal.

### **Part III: Time-Delays on Unmanned Aerial Systems**

#### **Chapter 5: Parametric Analysis of PID Delay-Based Controllers for Quadrotor UAVs**

The chapter provides a set of parametric stability charts considering a quadrotor rotorcraft performing stabilizing maneuvers under the presence of feedback time-delays and subjected to PID controllers. The analysis considers the couplings between the translational (slow dynamics) and the rotational (fast dynamics) motions. The parameters of the controllers, within the overall control scheme, are computed using the well-known stability crossing roots theory. Numerical simulation results, including the full dynamic model and the corresponding linear model of the vehicle, are presented to validate the proposal.

#### **Chapter 6: Time-Delay Control of Quadrotor UAVs: a MID-Based Approach**

This chapter exploits the effects of time-delays on the stability of Unmanned Aerial Vehicles (UAVs). In this regard, the main contribution relies on the symbolic/numeric application of the Multiplicity-Induced-Dominancy (MID) property to the control of UAVs rotorcrafts featuring time-delays. The MID property is considered to address two of the most representative aerial robotic platforms: a classical quadrotor vehicle and a quadrotor vehicle endowed with tilting-rotors. The aforementioned property leads to proper control gains (MID tuning criteria), allowing the system to meet prescribed behavior conditions based on the placement of the characteristic function/polynomial closed-loop rightmost root. Lastly, the results of detailed numerical simulations, including the linear and non-linear dynamics of the vehicle, are presented and discussed to validate the proposal.

#### **Chapter 7: Time-Delay Control of a VTOL Multi-Agent System Towards Transport Operations**

The present chapter deals with a consensus control for a multi-agent system composed by a mini Vertical Take-off and Landing (VTOL) rotorcrafts by means of a controller based on time-delay parametrization. The VTOL system modeling is presented using the quaternion parametrization to develop the attitude-stabilizing law of the aerial robots. The vehicle position dynamics is extended to the multi-agent case where a time-delayed PID control is designed in order to achieve general consensus in terms of

formation control of the system. Finally, a detailed simulation study is presented to validate the effectiveness of the proposed control strategy, where a collective interaction is also considered.

## Appendices

### Appendix A: Properties of the Multi-Link Unmanned Aerial System

This appendix defines the properties of the matrix and vector which compose the dynamical model of the ML-UAS. These properties are used to perform the stability analysis of the vehicle by means of the Lyapunov stability criteria.

### Appendix B: ML-UAS Linearization for Observability

As a part of the conception of the Extended Kalman Filter in Chapter 4, the linearization of the dynamical non-linear model of the systems is mandatory. The procedure to accomplish such task is described in this appendix.

### Appendix C: A Pedagogical Approach to Data Fusion and Kalman Filter

This appendix exposes, in a pedagogical manner, the Kalman Filter for data fusion and its usage in mechanical systems. The equations conforming the Kalman Filter and the data fusion process are explained in an intuitive form and applied over two pedagogical platforms used at the IPSA as a part of the laboratory material to introduce the students to systems control and the principles of navigation in the domain of terrestrial and aerial mobile robotics. Lastly, the tools to simulate such systems under real operating conditions in Matlab and Simulink are given and the results are discussed.

### Appendix D: Teaching Activities

A recapitulate of the pedagogical activities conducted during the Ph. D. formation, as a part of the doctoral contract, is presented in this last appendix. The content of this thesis section comprehends a detailed list of courses, a list of the supervised students and the pedagogical platforms developed for these means.



## **Part I**

# **Multi-Link Unmanned Aerial System**



## Chapter 2

# Modeling and Control: Robust Acquiring and Transport Operations

This chapter is organized as follows: [Section 2.1](#) corresponds to the general description of the paper. [Section 2.2](#) comprises the equations describing the dynamics of the chain. In [Section 2.3](#), a robust Adaptive Integral Slide Mode (AISM) control law is designed and the trajectory generation is fully described. The proposal is validated by numerical simulations whose results are given in [Section 2.4](#). The corresponding conclusions are available at [Subsection 8.1.1](#).

## 2.1 Introduction

Unmanned Aerial Vehicles (UAVs) have been used for different tasks in the industrial or the scientific field, specially in those involving aerial environment-interactivity, it is also the case for swarm-based cooperation which demands a high degree of dexterity [\[71\]](#).

Aerial robots have been extensively used for natural disaster assessment. In this mission context, the contribution of micro aerial vehicles (MAVs) remains restricted to the collection of images. Thus, the vehicles capable of picking, transporting and placing represent an ideal solution for several emergency tasks. The impact of these capabilities might be amplified whether one multiplies the aerial robots and develops efficient interaction algorithms.

There exist different approaches and strategies as well as a vast variety of configurations to address the multi-vehicles interaction problem. Inspired by parallel manipulators, [\[156\]](#) presents a flying robot composed of three off-the-shelf quadcopters rigidly attached via an articulated structure yielding to interesting results showing the system's dexterity as well as enhanced cargo capacity.

The necessity to increase efficiency flight raises the interest in transformable/morphing flying robots. In [\[9\]](#) the problems of flight stability and center of gravity shifting, due to the payloads motion, are studied. In this regard, [\[175\]](#) exposes a multi-rotor aerial vehicle with two-dimensional multi-links and demonstrates stable aerial transformation for high mobility in three-dimensional environments. The DRAGON aerial robot is introduced in [\[176\]](#) and it has the ability of multi-degree of freedom aerial transformation

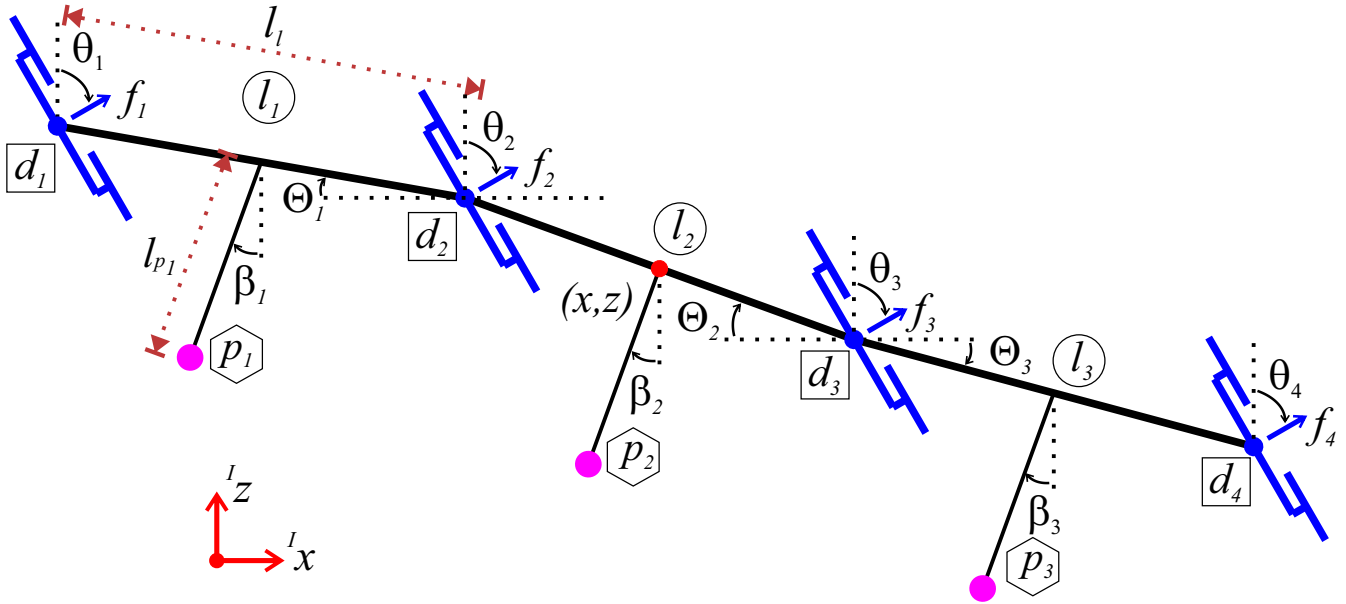


Figure 2.1: Multi-linked Unmanned Aerial System description

and full pose control regarding the center of gravity of multi-links.

The task of manipulating several cargos implies the understanding of the phenomena presents in transporting a single object which is a case widely studied in the literature. Hereof, the implementation of the Kalman Filter to estimate the payloads disturbances [48] and the trajectory path picking generation in windy environments [49] can be cited along with the use of learning automatas [27] and of fuzzy logic for computing the effects of the cargos in several quadrotors [17].

Nonetheless, the  $H_\infty$  control theory has been adopted due to its robustness [74]. By combining the  $H_2$  and  $H_\infty$  controls, [136] solves the trajectory tracking problem of a tilt-rotor UAV when transporting a suspended load. Sliding Mode Control (SMC) is another robust control strategy applied to aerial vehicles as in [49, 73, 130].

It is thus that the sequel of this chapter presents the longitudinal modeling and robust control of a novel multi-link aerial interactive system that is studied for multi-object acquisition and transport tasks while tracking an avian-inspired trajectory [49] with links-dependant trajectory dynamics. A Sliding Mode Controller alongside an adaptive gain with an integral term of the tracking error added to the sliding surface is designed [130, 176]. The flying kinematic chain inspired by the capabilities of aerial vehicles, the dexterity of arm manipulators and a train-like transporting operation is introduced herein to overcome the established problematic.

## 2.2 Mathematical Modeling

Let a system of 3 links interconnecting 4 rotorcrafts be considered as a flying kinematic chain and only its longitudinal dynamics as shown in Fig. 2.1 where the links are attached to the center of gravity of the corresponding vehicles and have frictionless angular motion [156, 74, 130]. In addition, the links are assume to have the same length  $l_l \in \mathbb{R}$  and mass  $m_l \in \mathbb{R}$  and, as a consequence, the same moment of inertia  $I_l \in \mathbb{R}$ . The attitude of the links is described by  $\Theta_j \in \mathbb{R}$  with  $j = 1, 2, 3$ .

The attitude of the  $i$ -th rotorcraft (with  $i = 1, 2, 3, 4$ ) is given by  $\theta_i \in \mathbb{R}$ . The masses and moments of inertia of the vehicles

are  $m_r \in \mathbb{R}$  and  $I_r \in \mathbb{R}$ , respectively. The pose of  $j$ -th pendulum-like load is described by  $\beta_j \in \mathbb{R}$ . Furthermore, their masses and lengths are defined by  $m_{p_j} \in \mathbb{R}$  and  $l_{p_j} \in \mathbb{R}$ , correspondingly.

The position of the chain  $\xi = [x \ z]^T \in \mathbb{R}^2$  is related to that of the center of gravity of the middle link, in this sense, the angles  $\Theta_j$  and  $\beta_j$  define the positions of the rotorcrafts  $\xi_{r_i}$ , the links  $\xi_{l_j}$  and the pendulums  $\xi_{p_j}$  w.r.t. the inertial frame as follows:

$$\xi_{r_i} = \begin{bmatrix} x_{r_i} \\ z_{r_i} \end{bmatrix} = \xi + \frac{Q_i l_i}{2} \begin{bmatrix} C_{\Theta_2} + V_i C_{\Theta_{D_i}} \\ -S_{\Theta_2} - V_i S_{\Theta_{D_i}} \end{bmatrix}, \quad \xi_{l_j} = \begin{bmatrix} x_{l_j} \\ z_{l_j} \end{bmatrix} = \xi + \frac{E_i l_j}{2} \begin{bmatrix} C_{\Theta_2} + C_{\Theta_j} \\ -S_{\Theta_2} - S_{\Theta_j} \end{bmatrix}, \quad \xi_{p_j} = \begin{bmatrix} x_{p_j} \\ z_{p_j} \end{bmatrix} = \xi_{l_j} - l_{p_j} \begin{bmatrix} S_{\beta_j} \\ C_{\beta_j} \end{bmatrix} \in \mathbb{R}^2 \quad (2.1)$$

where  $S_\bullet = \sin(\bullet)$ ,  $C_\bullet = \cos(\bullet)$ ,  $Q_k = \text{sign}(k - 2.5)$ ,  $D_k = (2k + 1)/3$ ,  $E_k = k - 2$  and  $V_k = k^2 - 5k + 6$ . Such functions are defined based on the established convention to measure the angles and the position of the element w.r.t the reference point in the structure.

By time differentiating Eqn. (2.1), the velocity of each component is obtained, hence:

$$\dot{\xi}_{r_i} = \dot{\xi} - \frac{Q_i l_i}{2} \begin{bmatrix} S_{\Theta_2} \dot{\Theta}_2 + V_i S_{\Theta_{D_i}} \dot{\Theta}_{D_i} \\ C_{\Theta_2} \dot{\Theta}_2 + V_i C_{\Theta_{D_i}} \dot{\Theta}_{D_i} \end{bmatrix}, \quad \dot{\xi}_{l_j} = \dot{\xi} - \frac{E_i l_j}{2} \begin{bmatrix} S_{\Theta_2} \dot{\Theta}_2 + S_{\Theta_j} \dot{\Theta}_j \\ C_{\Theta_2} \dot{\Theta}_2 + C_{\Theta_j} \dot{\Theta}_j \end{bmatrix}, \quad \dot{\xi}_{p_j} = \dot{\xi}_{l_j} - l_{p_j} \begin{bmatrix} C_{\beta_j} \dot{\beta}_j \\ -S_{\beta_j} \dot{\beta}_j \end{bmatrix} \in \mathbb{R}^2 \quad (2.2)$$

The dynamics of the flying multi-link robot is thus modelled by means of the Euler–Lagrange formalism.

The Lagrangian of the system is expressed as  $L = K - U \in \mathbb{R}$  such that  $K = K_r + K_l + K_p$  and  $U = U_r + U_l + U_p$  stand for the total kinetic and potential energies, respectively. Both terms are defined by the energies of the quadrotors ( $K_r$  and  $U_r$ ), the links ( $K_l$  and  $U_l$ ) and the pendulums ( $K_p$  and  $U_p$ ), given as

$$K_r = \sum_{k=1}^4 \left[ \frac{m_r}{2} (\dot{x}_{r_k}^2 + \dot{z}_{r_k}^2) + \frac{I_r}{2} \dot{\theta}_k^2 \right], \quad K_l = \sum_{k=1}^3 \left[ \frac{m_l}{2} (\dot{x}_{l_k}^2 + \dot{z}_{l_k}^2) + \frac{I_l}{2} \dot{\theta}_k^2 \right], \quad K_p = \sum_{k=1}^3 \frac{m_{p_k}}{2} (\dot{x}_{p_k}^2 + \dot{z}_{p_k}^2) \quad (2.3)$$

$$U_r = g m_r \sum_{k=1}^4 z_{r_k}, \quad U_l = g m_l \sum_{k=1}^3 z_{l_k}, \quad U_p = g \sum_{k=1}^3 m_{p_k} z_{p_k} \quad (2.4)$$

where  $g \in \mathbb{R}^+$  is the constant of gravity acceleration.

Let the vector of generalized coordinates be defined as  $q = [q_1 \ q_2 \ \dots \ q_5]^T = [x \ z \ \Theta_1 \ \Theta_2 \ \Theta_3]^T \in \mathbb{R}^5$ . By applying the equation provided by the Euler–Lagrange formalism, i.e.:

$$\frac{d}{dt} \frac{\partial}{\partial \dot{q}_a} L - \frac{\partial}{\partial q_a} L = \tau_a \quad \text{with } a = 1, 2, \dots, 5 \quad (2.5)$$

to the Lagrangian of the system, the dynamics of the ML-UAS is provided. It must be noticed that the attitudes of the vehicles are not considered as generalized coordinates since these are used as control inputs instead.

The equations of motion for the translation of the chain can be expressed as

$$\mu \ddot{x} - \sum_{k=1}^3 \left[ R_k \alpha_k \left( S_{\Theta_k} \ddot{\Theta}_k + C_{\Theta_k} \dot{\Theta}_k^2 \right) - m_{p_k} l_{p_k} \left( C_{\beta_k} \ddot{\beta}_k - S_{\beta_k} \dot{\beta}_k^2 \right) \right] = \tau_x \quad (2.6)$$

$$\mu (\ddot{z} + g) - \sum_{k=1}^3 \left[ R_k \alpha_k \left( C_{\Theta_k} \ddot{\Theta}_k - S_{\Theta_k} \dot{\Theta}_k^2 \right) + m_{p_k} l_{p_k} \left( S_{\beta_k} \ddot{\beta}_k + C_{\beta_k} \dot{\beta}_k^2 \right) \right] = \tau_z \quad (2.7)$$

where  $R_k = k^2 - 3k + 1$  and  $\mu$ ,  $\alpha_1$ ,  $\alpha_2$  and  $\alpha_3 \in \mathbb{R}$  are constants defined as

$$\mu = 4m_r + 3m_l + \sum_{j=1}^3 m_{p_j}; \quad \alpha_1 = l_l [m_r + (m_l + m_{p_1}) / 2]; \quad \alpha_2 = l_l (m_{p_1} - m_{p_3}) / 2; \quad \alpha_3 = l_l [m_r + (m_l + m_{p_3}) / 2] \quad (2.8)$$

Meanwhile, the equations of motion of the links follow the general form:

$$I_j \ddot{\Theta}_j - R_j \alpha_j \left[ S_{\Theta_j} \ddot{x} + C_{\Theta_j} (\ddot{z} + g) \right] + E_j^2 \frac{l_l \alpha_j}{2} \left( C_{\Theta_j - \Theta_2} \ddot{\Theta}_2 + S_{\Theta_j - \Theta_2} \dot{\Theta}_2^2 \right) + E_j \eta_j \left( S_{\Theta_j - \beta_j} \ddot{\beta}_j - C_{\Theta_j - \beta_j} \dot{\beta}_j^2 \right) + \quad (2.9)$$

$$\left( 1 - E_j^2 \right) \sum_{k=1}^3 \left[ E_k \eta_k \left( S_{\Theta_2 - \beta_k} \ddot{\beta}_k - C_{\Theta_2 - \beta_k} \dot{\beta}_k^2 \right) + \frac{l_l \alpha_k}{2} \left( C_{\Theta_k - \Theta_2} \ddot{\Theta}_k - S_{\Theta_k - \Theta_2} \dot{\Theta}_k^2 \right) \right] = \tau_{I_j} \quad (2.10)$$

By applying Eqn. (2.5) and considering  $\beta_j$  instead of the generalized coordinates  $q_a$ , the dynamics of the payloads can be represented in the general form:

$$m_{p_j} l_{p_j}^2 \ddot{\beta}_j - m_{p_j} l_{p_j} \left[ C_{\beta_j} \ddot{x} - S_{\beta_j} (\ddot{z} + g) \right] + E_j \eta_j \left( S_{\Theta_2 - \beta_j} \ddot{\Theta}_2 + C_{\Theta_2 - \beta_j} \dot{\Theta}_2^2 + S_{\Theta_j - \beta_j} \ddot{\Theta}_j + C_{\Theta_j - \beta_j} \dot{\Theta}_j^2 \right) = \tau_{p_j} \quad (2.11)$$

Along Eqns. (2.10) and (2.11), new constants were introduced to reduce the expression, such that these are:

$$\eta_j = m_{p_j} l_{p_j} l_l / 2; \quad \iota_1 = l_l^2 [m_r + (m_l + m_{p_1}) / 4] + I_l \in \mathbb{R}; \quad (2.12)$$

$$\iota_2 = l_l^2 [m_r + (2m_l + m_{p_1} + m_{p_3}) / 4] + I_l; \quad \iota_3 = l_l^2 [m_r + (m_l + m_{p_3}) / 4] + I_l \in \mathbb{R} \quad (2.13)$$

As previously mentioned, the aerial vehicles are considered as the actuator elements of the system, thus, their thrust and rotational dynamics are taken into consideration. The control input of the rotational motion,  $u_{d_i} \in \mathbb{R}$ , closes the corresponding loop as:

$$I_r \ddot{\theta}_i = u_{d_i} \quad (2.14)$$

The corresponding thrust and desired angles are computed as explained in the upcoming sections of the chapter. For instance, let one consider the system itself to be composed by the actuators (MAVs) and the rigid links, in this regard, the effects of the payloads can be treated as disturbances, which leads to a non-linear representation of the dynamics in the form:

$$\mathbf{M}(q)\ddot{q} + \mathbf{C}(q, \dot{q})\dot{q} + G(q) = u + \rho \quad (2.15)$$

such that

$$\mathbf{M}(q) = \begin{bmatrix} m_{11} & 0 & \alpha S_{\Theta_1} & 0 & -\alpha S_{\Theta_3} \\ 0 & m_{22} & \alpha C_{\Theta_1} & 0 & -\alpha C_{\Theta_3} \\ \alpha S_{\Theta_1} & \alpha C_{\Theta_1} & m_{33} & m_{34} & 0 \\ 0 & 0 & m_{43} & m_{44} & m_{45} \\ -\alpha S_{\Theta_3} & -\alpha C_{\Theta_3} & 0 & m_{54} & m_{55} \end{bmatrix} \in \mathbb{R}^{5 \times 5} \quad (2.16)$$

with the elements of the matrix being defined as  $m_{11} = m_{22} = 4m_r + 3m_l$ ,  $m_{33} = m_{55} = l_1^2(m_r + 0.25m_l) + I_1$ ,  $m_{34} = m_{43} = 0.5l_1\alpha_c C_{\Theta_1 - \Theta_2}$ ,  $m_{44} = l_1^2(m_r + 0.5m_l) + I_1$ ,  $m_{45} = m_{54} = 0.5l_1\alpha_c C_{\Theta_2 - \Theta_3}$  and  $\alpha = l_1(m_r + 0.5m_l)$ .

The term  $\mathbf{C}(q, \dot{q})\dot{q}$  in Eqn. (2.15) corresponds to the Coriolis and centripetal effects and it is given as:

$$\mathbf{C}(q, \dot{q})\dot{q} = \begin{bmatrix} \alpha (C_{\Theta_1} \dot{\Theta}_1^2 - C_{\Theta_3} \dot{\Theta}_3^2) \\ -\alpha (S_{\Theta_1} \dot{\Theta}_1^2 - S_{\Theta_3} \dot{\Theta}_3^2) \\ \frac{l_1}{2} \alpha S_{\Theta_1 - \Theta_2} \dot{\Theta}_2^2 \\ -\frac{l_1}{2} \alpha (S_{\Theta_1 - \Theta_2} \dot{\Theta}_1^2 - S_{\Theta_2 - \Theta_3} \dot{\Theta}_3^2) \\ -\frac{l_1}{2} \alpha S_{\Theta_2 - \Theta_3} \dot{\Theta}_2^2 \end{bmatrix} \in \mathbb{R}^5 \quad (2.17)$$

The gravitational effects are comprised in the vector

$$G(q) = \begin{bmatrix} 0 & m_{22}g & \alpha g C_{\Theta_1} & 0 & -\alpha g C_{\Theta_3} \end{bmatrix}^T \in \mathbb{R}^5 \quad (2.18)$$

Finally, the terms at the right part of Eqn. (2.15), correspond to the control input vector  $u = [u_x \ u_z \ u_{\Theta_1} \ u_{\Theta_2} \ u_{\Theta_3}]^T \in \mathbb{R}^5$  and the disturbances vector  $\rho \in \mathbb{R}^5$ .

Recalling the fact that the effects of the payloads are assumed as perturbations, the translational disturbances are established, with base on Eqns. (2.6) and (2.7), as

$$\rho_x = \sum_{k=1}^3 \left[ -m_{p_k} \ddot{x} + m_{p_k} l_{p_k} \left( C_{\beta_k} \ddot{\beta}_k - S_{\beta_k} \dot{\beta}_k^2 \right) \right] \quad (2.19)$$

$$\rho_z = \sum_{k=1}^3 \left[ -m_{p_k} (\ddot{z} + g) - m_{p_k} l_{p_k} \left( S_{\beta_k} \ddot{\beta}_k + C_{\beta_k} \dot{\beta}_k^2 \right) \right] \quad (2.20)$$

For each disturbance affecting the motion of the links, the friction between the corresponding linking element and the pendulous

payload is considered by the addition of the term  $\gamma_j (\dot{\beta}_j - \dot{\Theta}_j)$  where  $\gamma_j \in \mathbb{R}$  is the friction coefficient which implies that the friction effect must be equally considered in the dynamics of the cargos (Eqn. (2.11)) in the term  $\tau_{p_j}$ . The aforementioned consideration leads to the following definitions of the disturbances:

$$\rho_{\Theta_1} = -\frac{l_1 m_{p_1}}{2} \left[ \frac{l_1}{2} (\ddot{\Theta}_1 + C_{\Theta_1-\Theta_2} \ddot{\Theta}_2 + S_{\Theta_1-\Theta_2} \dot{\Theta}_2^2) + S_{\Theta_1} \ddot{x} + C_{\Theta_1} (\ddot{z} + g) - l_{p_1} (S_{\Theta_1-\beta_1} \ddot{\beta}_1 - C_{\Theta_1-\beta_1} \dot{\beta}_1^2) \right] + \gamma_1 (\dot{\beta}_1 - \dot{\Theta}_1) \quad (2.21)$$

$$\rho_{\Theta_2} = -\frac{l_1}{2} \left\{ (m_{p_1} - m_{p_3}) [S_{\Theta_2} \ddot{x} + C_{\Theta_2} (\ddot{z} + g)] + l_1 \frac{m_{p_1}}{2} [\ddot{\Theta}_2 + C_{\Theta_1-\Theta_2} \dot{\Theta}_1 - S_{\Theta_1-\Theta_2} \dot{\Theta}_1^2 - l_{p_1} (S_{\Theta_2-\beta_1} \ddot{\beta}_1 - C_{\Theta_2-\beta_1} \dot{\beta}_1^2)] + l_1 \frac{m_{p_3}}{2} [\ddot{\Theta}_2 + C_{\Theta_3-\Theta_2} \dot{\Theta}_3 - S_{\Theta_3-\Theta_2} \dot{\Theta}_3^2 + l_{p_3} (S_{\Theta_2-\beta_3} \ddot{\beta}_3 - C_{\Theta_2-\beta_3} \dot{\beta}_3^2)] \right\} + \gamma_2 (\dot{\beta}_2 - \dot{\Theta}_2) \quad (2.22)$$

$$\rho_{\Theta_3} = -\frac{l_1 m_{p_3}}{2} \left[ \frac{l_1}{2} (\ddot{\Theta}_3 + C_{\Theta_3-\Theta_2} \ddot{\Theta}_2 + S_{\Theta_3-\Theta_2} \dot{\Theta}_2^2) - S_{\Theta_3} \ddot{x} - C_{\Theta_3} (\ddot{z} + g) + l_{p_3} (S_{\Theta_3-\beta_3} \ddot{\beta}_3 - C_{\Theta_3-\beta_3} \dot{\beta}_3^2) \right] + \gamma_3 (\dot{\beta}_3 - \dot{\Theta}_3) \quad (2.23)$$

The well-defined model in Eqn. (2.15) is used in the upcoming section in order to design the AISM controller.

## 2.3 Control Strategy

For control purposes, let the dynamics of the system provided in Eqn. (2.15) be expressed as:

$$\ddot{q} = f(q, \dot{q}) + \mathbf{B}(q)u + w \quad (2.24)$$

where  $f(q, \dot{q}) = f_o(q, \dot{q}) + \Delta f$  is the dynamic state-dependent function of the system defined by the nominal dynamics  $f_o(q, \dot{q}) = -\mathbf{M}^{-1}(q)(\mathbf{C}(q, \dot{q})\dot{q} + \mathbf{G}(q))$  and the unmodeled uncertainties  $\Delta f \in \mathbb{R}^5$ . The control matrix  $\mathbf{B}(q) \in \mathbb{R}^{5 \times 5}$  is conformed by the nominal control matrix  $\mathbf{B}_o(q) = \mathbf{M}^{-1}(q)$  and the uncertainties in the control matrix  $\Delta \mathbf{B} \in \mathbb{R}^{5 \times 5}$  resulting in  $\mathbf{B}(q) = \mathbf{B}_o(q) + \Delta \mathbf{B}$ . The term  $w = \mathbf{M}^{-1}(q)\rho \in \mathbb{R}^5$  comprises the external disturbances [73].

One must provide a control input  $u = u_o + u_w \in \mathbb{R}^5$  such that  $u_o$  mitigates the nominal dynamics and  $u_w$  compensates the parametric and environmental uncertainties [73, 130].

Defining the tracking error vector as  $e = q - q^d \in \mathbb{R}^5$  where the vector  $q^d$  defines the desired trajectories, the sliding surface is proposed as follows:

$$\sigma = \dot{e} + \Lambda e + \varepsilon \in \mathbb{R}^5 \quad (2.25)$$

where  $\varepsilon$  is a vector containing the integral terms of the error [49] and  $\Lambda = \text{diag}(\lambda_x, \lambda_z, \lambda_{\Theta_1}, \lambda_{\Theta_2}, \lambda_{\Theta_3}) \in \mathbb{R}^{5 \times 5}$  is a diagonal matrix of control gains such that each  $\lambda$ -gain satisfies  $\lambda > 0$ .

The control input must approach  $\sigma$  to zero and sustain it there ( $\sigma \dot{\sigma} < 0$ ). The nominal control input shall provide stability once the system has reached  $\sigma$ , i. e.  $\dot{\sigma} = \mathbf{0} = \ddot{e} + \Lambda \dot{e} + \varepsilon \in \mathbb{R}^5$ .

By the substitution of the error and its time derivatives, it is obtained that

$$u_o = \mathbf{C}(q, \dot{q})\dot{q} + G(q) + \mathbf{M}(q) \left( \ddot{q}^d - \Lambda \dot{e} - e \right) \quad (2.26)$$

To mitigate the plant parameters variation and the external disturbances, a viable solution is to consider  $u_w$  as:

$$u_w = -\mathbf{M}(q) \mathbf{H} T(\sigma) \quad (2.27)$$

such that  $\mathbf{H} = \text{diag}(\eta_x, \eta_z, \eta_{\theta_1}, \eta_{\theta_2}, \eta_{\theta_3}) \in \mathbb{R}^{5 \times 5}$  corresponds to a matrix of adaptive control gains, all subjected to the restriction  $\eta > 0 \in \mathbb{R}$  and  $T = [\text{sign } \sigma_x \text{ sign } \sigma_z \dots \text{sign } \sigma_{\theta_3}]^T \in \mathbb{R}^5$ .

Recalling Eqn. (2.25) and the model in Eqn. (2.24), the time derivative of the sliding surface reads as:

$$\dot{\sigma} = f_o(q, \dot{q}) + \mathbf{B}_o(q)u - \ddot{q}^d + \Lambda \dot{e} + e + W_L \quad (2.28)$$

where the term  $W_L = \Delta f + \Delta \mathbf{B}u + w \in \mathbb{R}^5$  is the Lumped uncertainties vector, bounded in the manner:

$$\|W_L\| < \|\mathbf{H}^d\| \quad (2.29)$$

with  $\mathbf{H}^d = \text{diag}(\eta_x^d, \eta_z^d, \eta_{\theta_1}^d, \eta_{\theta_2}^d, \eta_{\theta_3}^d) \in \mathbb{R}^{5 \times 5}$  being the terminal value of  $\mathbf{H}$ .

In order to achieve  $\mathbf{H}^d$ , the dynamics of  $\mathbf{H}$  is defined as

$$\dot{\mathbf{H}} = \mathbf{A}^{-1} \mathbf{S}_A \in \mathbb{R}^{5 \times 5} \quad (2.30)$$

with  $\mathbf{S}_A = \text{diag}(|\sigma_x|, |\sigma_z|, |\sigma_{\theta_1}|, |\sigma_{\theta_2}|, |\sigma_{\theta_3}|) \in \mathbb{R}^{5 \times 5}$ ; and  $\mathbf{A} = \text{diag}(\alpha_x, \alpha_z, \alpha_{\theta_1}, \alpha_{\theta_2}, \alpha_{\theta_3}) \in \mathbb{R}^{5 \times 5}$  which defines the adaptation rate of the  $\eta$ -gains. To prove the closed-loop stability, let one consider the following Lyapunov candidate function:

$$V = \frac{1}{2} \sigma^T \sigma + \frac{1}{2} \mathbf{1}^T \tilde{\mathbf{H}}^T \mathbf{A} \tilde{\mathbf{H}} \mathbf{1} \in \mathbb{R} \quad (2.31)$$

with  $\tilde{\mathbf{H}} = \mathbf{H} - \mathbf{H}^d$  being the adaptation error and  $\mathbf{1} \in \mathbb{R}^5$  the ones vector.

By time differentiating Eqn. (2.31) and considering Eqns. (2.26), (2.27) and (2.28), the time derivative of the Lyapunov candidate function can be expressed as

$$\dot{V} = \sigma^T \left( W_L - \mathbf{H}^d T(\sigma) \right) \quad (2.32)$$

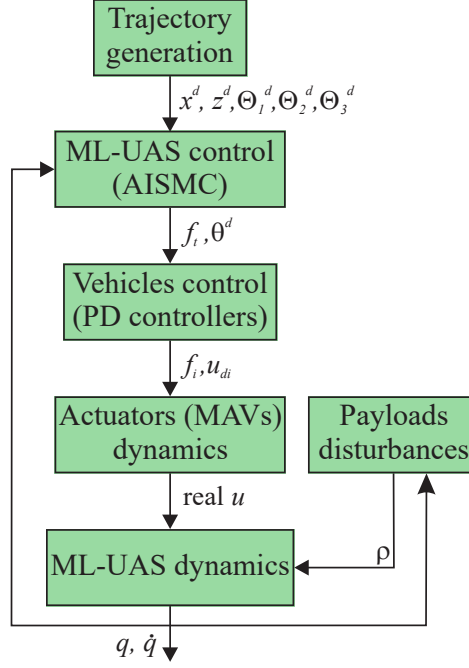


Figure 2.2: Control strategy for the ML-UAS

and since  $\sigma^T \mathbf{H}^d T(\sigma) \geq 0$  by definition, and considering the boundness property of  $W_L$  established in Eqn. (2.29), it follows that  $\dot{V} \leq 0 \forall t > 0$  which ensures the asymptotic stability of the system subjected to the proposed control law.

In order to control the attitude of the vehicles, a PD controller given as  $u_{di} = -K_{p_i} e_{p_i} - K_{v_i} e_{v_i}$  is chosen. The constants  $K_{p_i}, K_{v_i} \in \mathbb{R}$  correspond to the proportional and derivative gains, respectively, the position and velocity errors are defined as  $e_{p_i} = \theta_i - \theta_i^d \in \mathbb{R}$  and  $e_{v_i} = \dot{\theta}_i - \dot{\theta}_i^d \in \mathbb{R}$  in which the index  $d$  stands for the references. The stability analysis for this well-known controller can be found in [35].

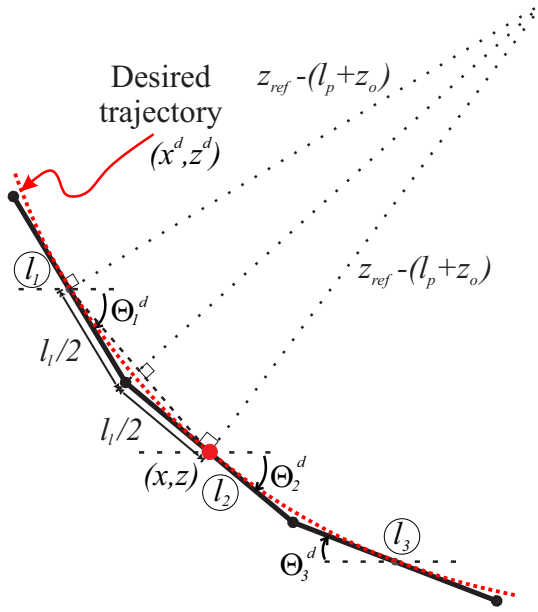
The desired orientation of the vehicles and the forces to be exerted by each aerial vehicle are computed with base on the control inputs generated by the AISM controller.

Let one recall the control input vector in Eqn. (2.15) and the description of the system in Fig. 2.1, thus

$$\begin{bmatrix} u_x \\ u_z \\ u_{\Theta_1} \\ u_{\Theta_2} \\ u_{\Theta_3} \end{bmatrix} = \begin{bmatrix} S_{\theta_1} f_1 + S_{\theta_2} f_2 + S_{\theta_3} f_3 + S_{\theta_4} f_4 \\ C_{\theta_1} f_1 + C_{\theta_2} f_2 + C_{\theta_3} f_3 + C_{\theta_4} f_4 \\ \frac{l_i}{2} (C_{\Theta_1 - \theta_1} f_1 - C_{\Theta_1 - \theta_2} f_2) \\ \frac{l_i}{2} (C_{\Theta_2 - \theta_2} f_2 - C_{\Theta_2 - \theta_3} f_3) \\ \frac{l_i}{2} (C_{\Theta_3 - \theta_3} f_3 - C_{\Theta_3 - \theta_4} f_4) \end{bmatrix} \quad (2.33)$$

As  $q \in \mathbb{R}^5$  and 8 possible control inputs (the force and attitude of each the vehicle) are available, the ML-UAS is considered to be an over-actuated system thus, to avoid this issue, let one establish  $\forall t > 0 \theta^d = \theta_1^d = \theta_2^d = \theta_3^d = \theta_4^d \in \mathbb{R}$  which leads to

$$\theta^d = \tan^{-1} \left( \frac{u_x}{u_z} \right) \quad (2.34)$$

Figure 2.3: Desired  $\Theta$  angles relations

Therefore, the force that each MAV should exert over the system can be computed according to the expression:

$$\begin{bmatrix} f_1 \\ f_2 \\ f_3 \\ f_4 \end{bmatrix} = \frac{1}{4} \begin{bmatrix} 1 & 3 & 2 & 1 \\ 1 & -1 & 2 & 1 \\ 1 & -1 & -2 & 1 \\ 1 & -1 & -2 & -3 \end{bmatrix} \begin{bmatrix} \sqrt{u_x^2 + u_z^2} \\ (2u_{\Theta_1}) / (l_1 C_{\Theta_1 - \theta^d}) \\ (2u_{\Theta_2}) / (l_1 C_{\Theta_2 - \theta^d}) \\ (2u_{\Theta_3}) / (l_1 C_{\Theta_3 - \theta^d}) \end{bmatrix} \quad (2.35)$$

The control section is summarized in Fig. 2.2 which shows the control algorithm in a graphical representation for a better understanding. The trajectory planning block, as can be appreciated, is described in the following subsection.

### 2.3.1 Trajectory Planning and Picking Strategy

The altitude trajectory of the overall system is based on a co-sinusoidal function whose parameters (frequency and amplitude) are updated according to the object location  $(x_o, z_o)$  [49].

The desired trajectory in  $^I x$  is established in order to keep a constant velocity  $v_h \in \mathbb{R}$ , i.e.  $x^d(t) = v_h t \in \mathbb{R}$  and to reach the grasping at the time  $t_g = v_h / x_o \in \mathbb{R}$ .

For the motion along  $^I z$ , the desired trajectory is defined by  $t_g$ , the altitude of the chain during the operation  $z_{ref} \in \mathbb{R}$ , the length of the pendulums  $l_p = l_{p_1} = l_{p_2} = l_{p_3}$  and the position of the object in the corresponding axis  $z_o \in \mathbb{R}$ , as:

$$z^d(t) = z_{ref} + \{z_{ref} - (l_p + z_o)\} \cos(\pi t / t_g) \quad (2.36)$$

The desired attitude of the links is computed with base on a tangent relation with respect to the translational pattern. By time

differentiation of Eqn. (2.36) and adopting a sign change in the sin function due to the measurement convention, one can compute  $\Theta_2^d \in \mathbb{R}$  which, alongside the geometric relations described in Fig. 2.3, defines  $\Theta_1^d, \Theta_3^d \in \mathbb{R}$  as follows:

$$\Theta_2^d = \tan^{-1} (\pi \{z_{ref} - (l_p + z_o)\} \sin(\pi t / t_g) / t_g) \tag{2.37}$$

$$\Theta_1^d = \pi - 2 \tan^{-1} (2 \{z_{ref} - (l_p + z_o)\} / l_l) + \Theta_2^d \tag{2.38}$$

$$\Theta_3^d = 2 \tan^{-1} (2 \{z_{ref} - (l_p + z_o)\} / l_l) + \Theta_2^d - \pi \tag{2.39}$$

## 2.4 Numerical Simulations and Results

To validate the control strategy proposal, a numerical simulation was performed, such study considered the parameters introduced in Table 2.1 additionally, the initial conditions of the flying chain were all set to zero as well as the initial attitude of the vehicles. A comparison between the system under the command of a PD controller and the AISM controller was equally addressed, in this regard, the PD control (PDC) law was defined as

$$u = -\mathbf{K}_P e - \mathbf{K}_V \dot{e} + \mathbf{M}(\dot{q}^d) \ddot{q}^d + \mathbf{C}(\dot{q}^d, q^d) \dot{q}^d + G(q^d) \tag{2.40}$$

where  $\mathbf{K}_P, \mathbf{K}_V \in \mathbb{R}^{5 \times 5}$  are the diagonal control gain matrices of the PD controller to command the overall system.

The results of the simulation are exposed throughout Figs. 2.4-2.9 where the vertical dashed lines in black represents the time marks described in Table 2.2. The three different colors at the background indicate the moment when a payload is picked.

Table 2.1: Simulation parameters

Parameter	Value	Parameter	Value
$m_r$	0.62 kg	$A_z$	7 m
$I_r$	0.253 kg m <sup>2</sup>	$t_g$	40 s
$m_l$	0.1 kg	$v_h$	0.25 m/s
$I_l$	0.0125 kg m <sup>2</sup>	$x_o$	12.5 m
$l_l$	1 m	$z_o$	0.5 m
$m_{p1}$	0.3 kg	$\gamma_j$	0.035
$m_{p2}$	0.3 kg	$g$	9.81 m/s <sup>2</sup>
$m_{p3}$	0.4 kg	$l_p$	0.5 m

Table 2.2: Simulation motion phases

Phase	Time marks (s)
$A_z$ and $v_h$ reaching phase	$0 \leq t < 30$
Avian inspired trajectory and picking	$30 \leq t < 70$
Stabilization and $A_z$ reaching phase	$70 \leq t$

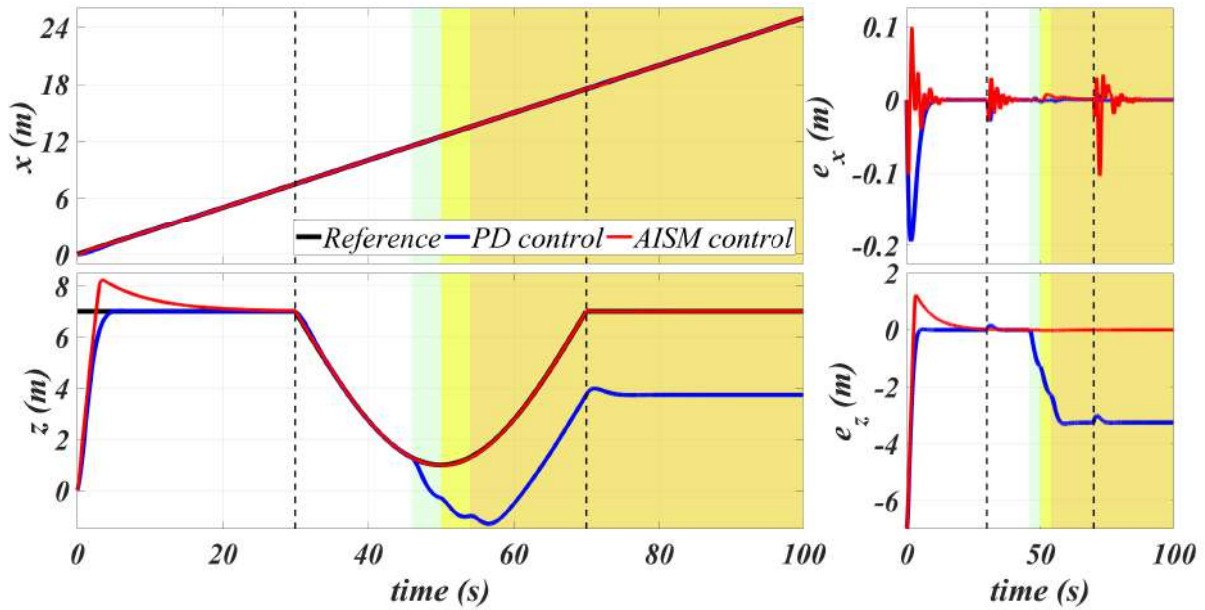


Figure 2.4: Translational behavior of the ML-UAS comparison

Fig. 2.4 shows the translational motion of the flying kinematic chain and the corresponding errors. One can infer from the  $^1x$  plot that both controllers drive the system to the desired horizontal velocity. The motion in  $^1z$  is successfully tracked by the two controllers until the picking operation starts.

The motion of the payloads is described in Fig. 2.6 where the amplitude of the oscillation reaches a larger value in the case of the AISM controller than in the PD controller.

The movement of the cargos influences directly the dynamics of the overall system, Fig. 2.7 shows the magnitude and the behavior of the disturbances produced by the motion of each payload, altering the translation of the chain.

As depicted by Fig. 2.8, the rotational disturbances follow the same behavior for both cases, differing only in the peak at  $t = 70$  s when applying the AISMC implying that the transition is suddenly done and that a modification in the transition strategy needs to be considered in order to have a smoother disturbances influence.

It can be inferred from Fig. 2.9 that the perturbations are mitigated by the MAVs rotational motion. When implementing the AISMC, the magnitude of the disturbances rises nevertheless, the picking pattern is successfully tracked due to the actuators response. In the case of the PD control, no considerable oscillations are present in the motion of the aerial vehicles though the picking trajectory is not followed.

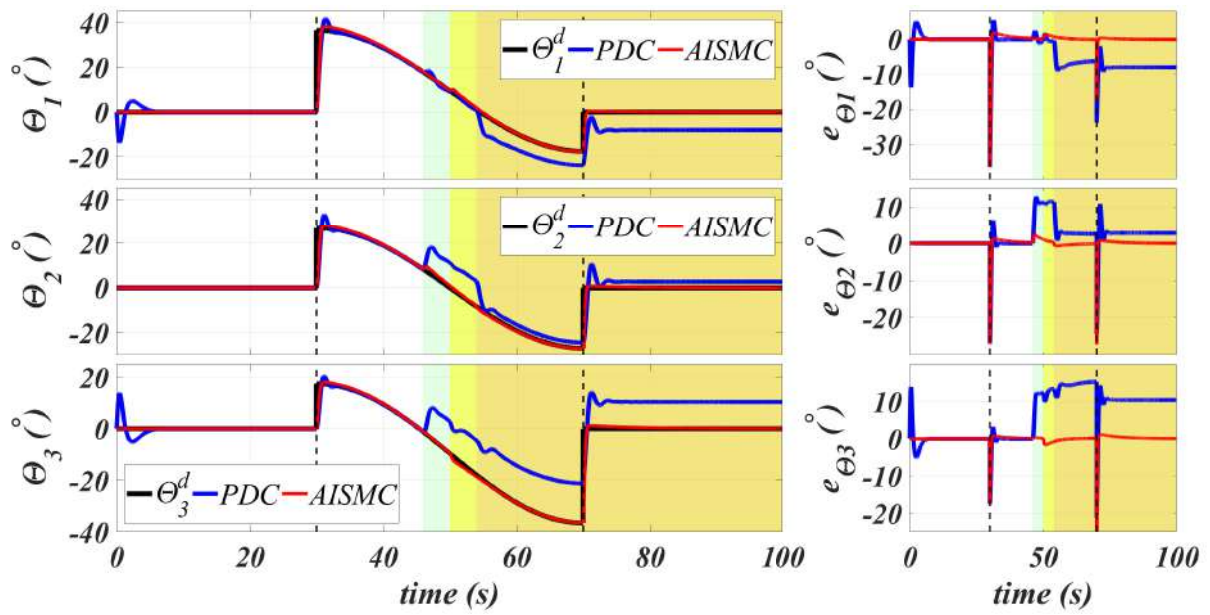


Figure 2.5: Rotational links behavior of the ML-UAS comparison

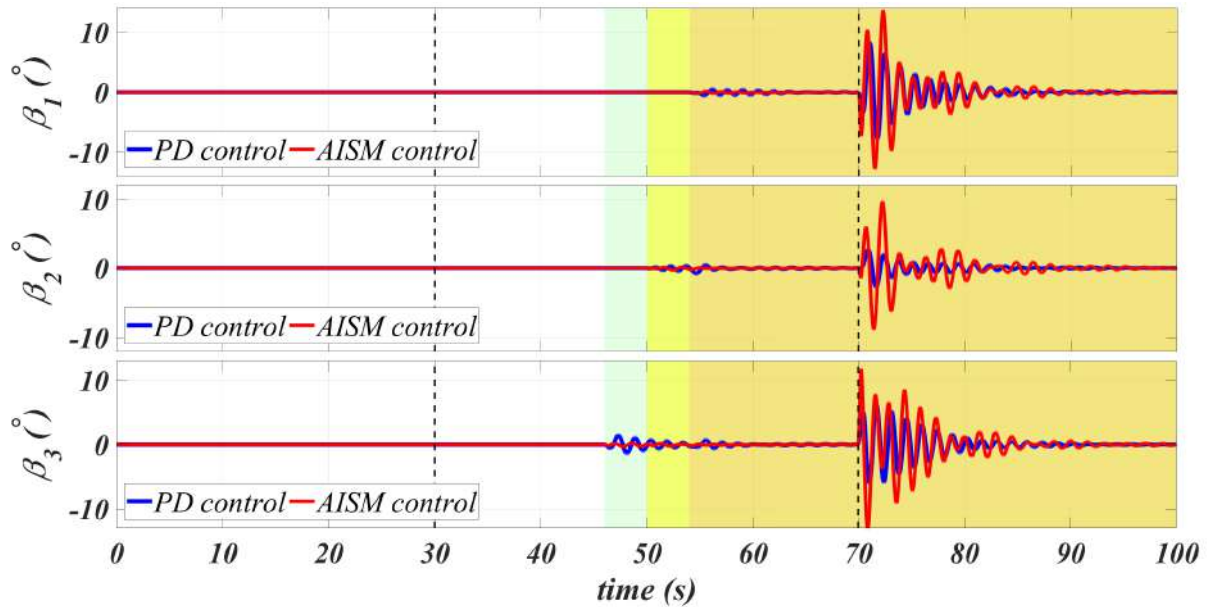


Figure 2.6: Payloads motion comparison

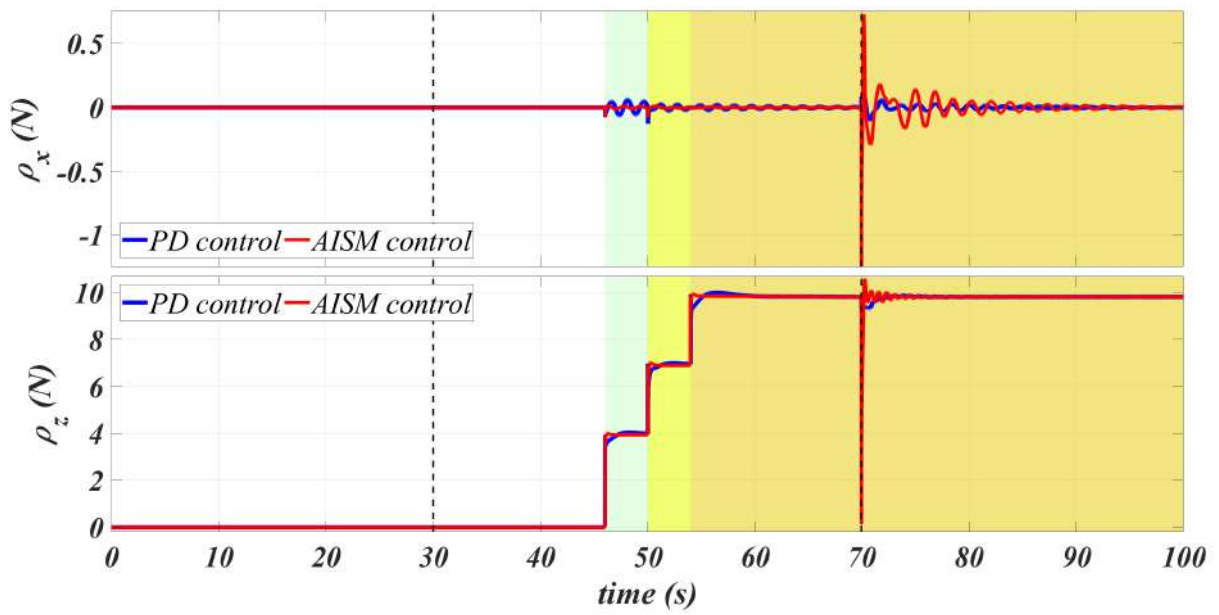


Figure 2.7: Translational motion disturbances

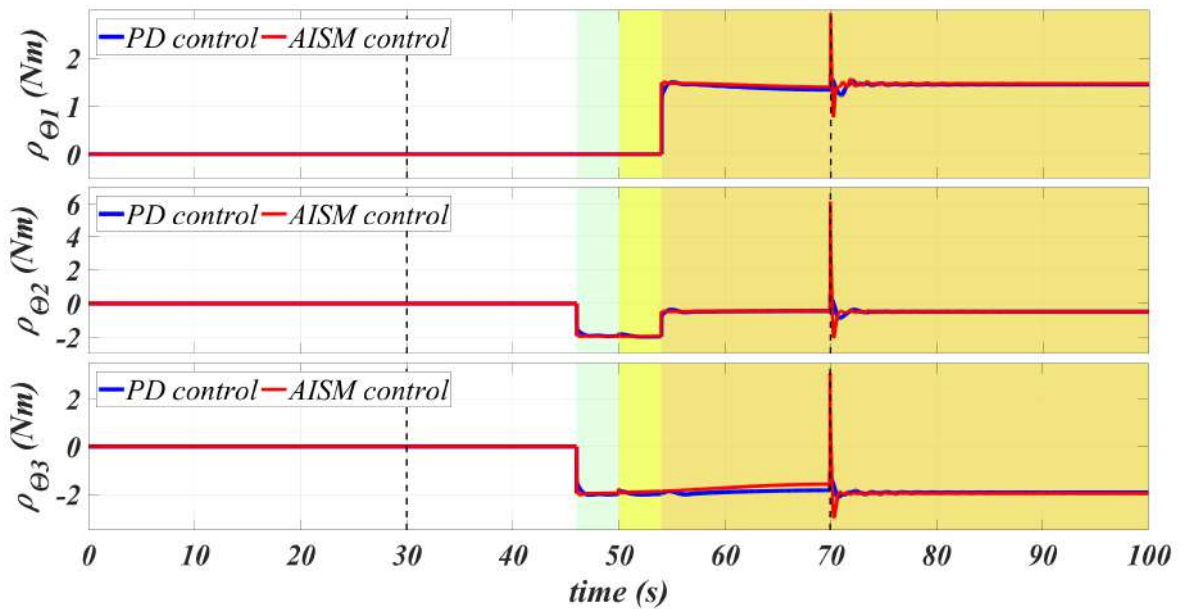


Figure 2.8: Rotational links motion disturbances

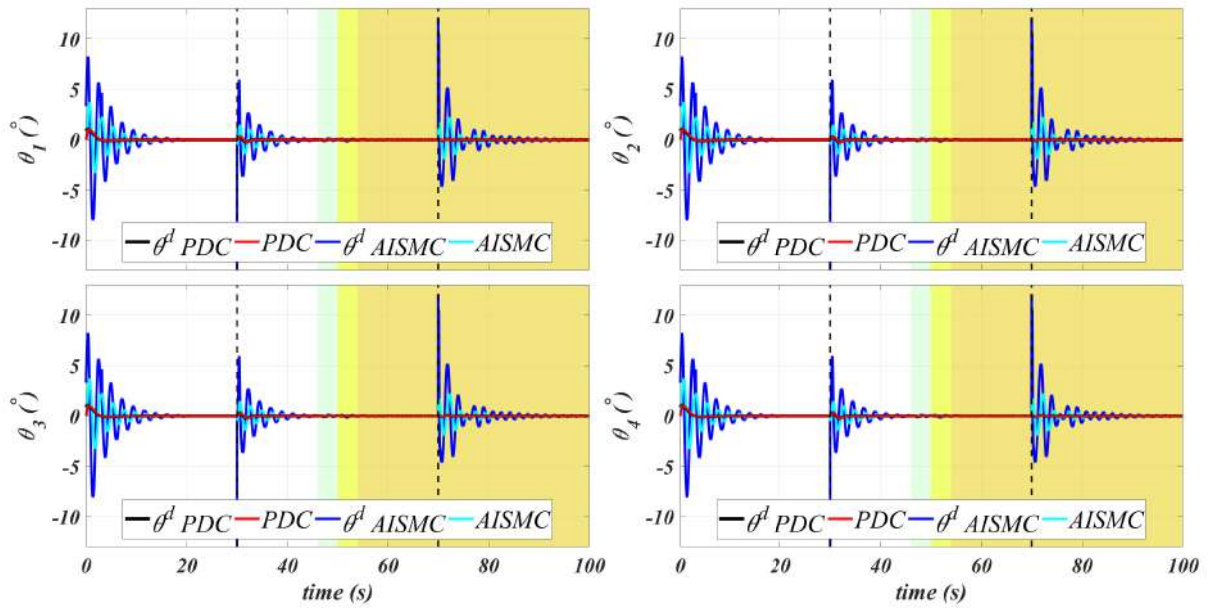


Figure 2.9: MAVs behaviour comparison

## Chapter 3

# Disturbances and Coupling Compensation for Trajectory Tracking

The current chapter is distributed as follows: [Section 3.1](#) provides an introduction to the addressed problem. The mathematical model of the system as well as the disturbed system representation are given in [Section 3.2](#). The results of the aforementioned section leads to [Section 3.3](#), where the Kalman Filter estimator and the control strategy are explained in detail. The proposal is validated by numerical simulations whose results are presented in [Section 3.4](#). Finally, the conclusions and future works are written in [Subsection 8.1.2](#).

### 3.1 Introduction

Nowadays, the implementation of Unmanned Aerial Vehicles (UAVs) in the industrial and scientific fields has increased due to its potential and yet unexploited capability to carry out aerial environment-interactivity activities like manipulation, assembling, picking and transporting [\[71\]](#).

The vehicles capable of picking, transporting and placing represent an ideal solution for tasks such as survival-kit delivering, rescue operation, sensor deployment/acquiring and so on. The impact of these capabilities might be amplified whether one multiplies the aerial robots and develop efficient interaction algorithms.

There exist different approaches and strategies which are address the multi-vehicles interaction problem. [\[156\]](#) introduces a dexterous flying parallel robot composed of three quadrotors rigidly attached via an articulated structure.

Increasing the flight efficiency raises the interest in transformable/morphing flying robots. In [\[9\]](#), the problems of flight stability and center of gravity shifting due to the payloads motion are studied. In addition, [\[175\]](#) exposes a multi rotor aerial vehicle with two-dimensional multi-links and demonstrates stable aerial transformation. The DRAGON transformable aerial robot is introduced in [\[176\]](#). This flying machine is a dual-rotor-embedded multi-link robot with the ability of multi degree of freedom aerial transformation and the full pose control regarding the center of gravity of multi-links.

In order to manipulate several cargos at the same time, the phenomena of transporting a single object must be understood,



where one may recall that  $S_\bullet = \sin(\bullet)$ ,  $C_\bullet = \cos(\bullet)$ .

By time differentiating the Eqns. (3.1) and (3.2), it is straightforward to compute the velocity of each component. These velocities are described in the inertial frame and represented by the vectors  $\dot{\xi}_{r_i}$ ,  $\dot{\xi}_{l_j}$  and  $\dot{\xi}_{p_j}$ , respectively.

The dynamics of the flying multi link system is then modelled by the means of the Euler–Lagrange formalism.

### 3.2.1 Dynamics

The definition of the Lagrangian of the system has already been introduced in Section 2.2 yet, for the corresponding case of study, the total kinetic and potential energies are respectively defined as:

$$K = \sum_{k=1}^3 \left\{ \frac{m_r}{2} (\dot{x}_{r_k}^2 + \dot{z}_{r_k}^2) + \frac{I_r}{2} \dot{\theta}_k^2 \right\} + \sum_{k=1}^2 \left\{ \frac{m_l}{2} (\dot{x}_{l_k}^2 + \dot{z}_{l_k}^2) + \frac{I_l}{2} \dot{\Theta}_k^2 + \frac{m_{p_k}}{2} (\dot{x}_{p_k}^2 + \dot{z}_{p_k}^2) \right\} \quad (3.3)$$

$$U = g \left( m_r \sum_{k=1}^3 z_{r_k} + \sum_{k=1}^2 (m_l z_{l_k} + m_{p_k} z_{p_k}) \right) \quad (3.4)$$

The vector of generalized coordinates corresponds to  $\mathbf{q} = [q_1 \ q_2 \ q_3 \ q_4]^T = [x \ z \ \Theta_1 \ \Theta_2]^T \in \mathbb{R}^4$ . Then, by applying the equation provided by the Euler–Lagrange formalism to the Lagrangian, the dynamics of the multi-link system can be established.

The equations of motion for the translation of the chain can be expressed as

$$\mu \ddot{x} + \sum_{k=1}^2 \left\{ (3-2k) \alpha_k (S_{\Theta_k} \ddot{\Theta}_k + C_{\Theta_k} \dot{\Theta}_k^2) - m_{p_k} l_{p_k} (C_{\beta_k} \ddot{\beta}_k - S_{\beta_k} \dot{\beta}_k^2) \right\} = u_x \quad (3.5)$$

$$\mu (\ddot{z} + g) + \sum_{k=1}^2 \left\{ (3-2k) \alpha_k (C_{\Theta_k} \ddot{\Theta}_k - S_{\Theta_k} \dot{\Theta}_k^2) + m_{p_k} l_{p_k} (S_{\beta_k} \ddot{\beta}_k + C_{\beta_k} \dot{\beta}_k^2) \right\} = u_z \quad (3.6)$$

where  $\mu = 3m_r + 2m_l + m_{p_1} + m_{p_2} \in \mathbb{R}$ ,  $\alpha_k = l_l(m_r + 0.5(m_l + m_{p_k})) \in \mathbb{R}$ . Meanwhile, the equations of motion of the links are described by the expression:

$$l_j \ddot{\Theta}_j + (3-2j) \left\{ \alpha_j (S_{\Theta_j} \ddot{x} + C_{\Theta_j} (\ddot{z} + g)) - 0.5 m_{p_j} l_l l_{p_j} (S_{(\Theta_j - \beta_j)} \ddot{\beta}_j - C_{(\Theta_j - \beta_j)} \dot{\beta}_j^2) \right\} = u_{\Theta_j} \quad (3.7)$$

with  $l_j = l_l^2(m_r + 0.25(m_l + m_{p_j})) + I_l$ .

The dynamics of the payloads can be found by following the Euler–Lagrange equation and considering the  $\beta_j$  angle instead of the generalized coordinates, resulting in:

$$m_{p_j} l_{p_j} \left\{ l_{p_j} \ddot{\beta}_j - C_{\beta_j} \ddot{x} + S_{\beta_j} (\ddot{z} + g) - 0.5(3-2j) l_l (S_{(\Theta_j - \beta_j)} \ddot{\Theta}_j + C_{(\Theta_j - \beta_j)} \dot{\Theta}_j^2) \right\} = \tau_{p_j} \quad (3.8)$$

As in Section 2.2, the aerial vehicles are considered as the actuators of the system, thus, one may refer to such section.

### 3.2.2 Disturbed System Representation

The system itself is composed by the actuators (MAVs) and the rigid links. In this regard, the effects of the payloads can be treated as disturbances and, furthermore, the couplings of the system can also be treated as perturbations, leading to a representation of the system of the form:

$$\ddot{q}_a = \frac{1}{b_{q_a}} (u_{q_a} + \rho_{q_a} - g_{q_a}) \quad (3.9)$$

which is a suitable linear representation for the implementation of Linear Kalman Filter [176, 48]; with  $a = 1, 2, 3, 4$  and

- $\ddot{q}_1 = \ddot{x}$ ,  $\ddot{q}_2 = \ddot{z}$ ,  $\ddot{q}_3 = \ddot{\Theta}_1$  and  $\ddot{q}_4 = \ddot{\Theta}_2$
- $b_x = b_z = 3m_r + 2m_l$  and  $b_{\Theta_1} = b_{\Theta_2} = I_l^2 (m_r + 0.25m_l) + I_l$
- $g_x = 0$ ,  $g_z = (3m_r + 2m_l)g$ ,  $g_{\Theta_1} = (m_r + 0.5m_l)gl_l$  and  $g_{\Theta_2} = -(m_r + 0.5m_l)gl_l$

In Eqn. (3.9),  $u_{q_a} \in \mathbb{R}$  represents the control input and  $\rho_{q_a} \in \mathbb{R}$  stands for the disturbance of the corresponding degree of freedom. These disturbing terms are defined as

$$\rho_x = \sum_{k=1}^2 \left[ -m_{p_k} \ddot{x} + (2k-3) \alpha_k \left( S_{\Theta_k} \ddot{\Theta}_k + C_{\Theta_k} \dot{\Theta}_k^2 \right) + m_{p_k} l_{p_k} \left( C_{\beta_k} \ddot{\beta}_k - S_{\beta_k} \dot{\beta}_k^2 \right) \right] \quad (3.10)$$

$$\rho_z = \sum_{k=1}^2 \left[ -m_{p_k} (\ddot{z} + g) + (2k-3) \alpha_k \left( C_{\Theta_k} \ddot{\Theta}_k - S_{\Theta_k} \dot{\Theta}_k^2 \right) - m_{p_k} l_{p_k} \left( S_{\beta_k} \ddot{\beta}_k + C_{\beta_k} \dot{\beta}_k^2 \right) \right] \quad (3.11)$$

$$\rho_{\Theta_j} = -0.25l_l^2 m_{p_j} + (2j-3) \left\{ \alpha_j \left[ S_{\Theta_j} \ddot{x} + C_{\Theta_j} (\ddot{z} + g) \right] - 0.5m_{p_j} l_l l_{p_j} \left( S_{\Theta_j - \beta_j} \ddot{\beta}_j - C_{\Theta_j - \beta_j} \dot{\beta}_j^2 \right) \right\} \quad (3.12)$$

With the given rearrangement of the equations of motion of the system, the estimation process and control strategy can be conceived, as explained next.

## 3.3 Disturbances Estimation and Control

The current section describes the procedure to design an Augmented-State Linear Kalman Filter (ASLKM) to estimate the disturbances due to the couplings and the payloads previously introduced. The control strategy proposal is described right after.

### 3.3.1 Augmented-State Kalman Filter Design

An Augmented-State Discrete Linear Kalman filter is designed regarding the estimation of the couplings and disturbances arising during the motion of the overall system. The Linear Kalman Filter (LKF) is derived from a continuous system:

$$\dot{x}(t) = \mathbf{A}x(t) + \mathbf{B}u(t) + \mathbf{M}\zeta(t) \quad (3.13)$$

$$y(t) = \mathbf{C}x(t) + \gamma(t) \quad (3.14)$$

that considers that the pair AC verifies the observability property. Additionally, the signals  $\zeta$  and  $\gamma$  stand for a white Gaussian random process with zero-mean ( $E[\zeta(t)] = 0$  and  $E[\gamma(t)] = 0$ ) with constant power spectral density (PSD)  $W(t)$  and  $V(t)$  defining respectively:

- The process covariance matrix

$$Q = E \left[ \zeta(t) \zeta(t+t_c)^T \right] = W \Delta(t_c) \quad (3.15)$$

- The sensor covariance matrix

$$R = E \left[ \gamma(t) \gamma(t+t_c)^T \right] = V \Delta(t_c) \quad (3.16)$$

It is also assumed that both stochastic processes are not correlated. Thus, let one rewrite the system in Eqn. (3.9) in a state space representation with the state  $X(t) = [q_a \dot{q}_a]^T$  and the output  $Y(t) = [q_a \dot{q}_a]^T = X(t)$  (implying that the translational and rotational positions and velocities are available), as:

$$\begin{cases} \dot{X} &= AX + B(u_{q_a} - g_{q_a}) + P\rho_{q_a} \\ Y &= CX \\ X(0) &= X_0 \end{cases} \quad (3.17)$$

The matrices of the system in Eqn. (3.17) are:

$$A = \begin{bmatrix} 0 & 1 \\ 0 & 0 \end{bmatrix}; B = \frac{1}{b_{q_a}} \begin{bmatrix} 0 \\ 1 \end{bmatrix}; P = \frac{1}{b_{q_a}} \begin{bmatrix} 0 \\ 1 \end{bmatrix}; C = \begin{bmatrix} 1 & 0 \\ 0 & 1 \end{bmatrix} \quad (3.18)$$

By assuming that the disturbance has a slow time-varying dynamics that can be modeled by a random walk process  $\dot{\rho}_{q_a} = 0 + \zeta_{q_a}(t)$ , the extended state-space vector can be introduced as:

$$X^e(t) = [q_a \dot{q}_a \rho_{q_a}]^T \in \mathbb{R}^3 \quad (3.19)$$

and its associated state-space model:

$$\begin{cases} \dot{X}^e &= A^e X^e + B^e(u_{q_a} - g_{q_a}) + M^e \zeta_{q_a} \\ Y^e &= C^e X^e + \gamma^e \\ X^e(0) &= X_0^e \end{cases} \quad (3.20)$$

where

$$A^e = \begin{bmatrix} 0 & 1 & 0 \\ 0 & 0 & 1/b_{q_a} \\ 0 & 0 & 0 \end{bmatrix}; B^e = \frac{1}{b_{q_a}} \begin{bmatrix} 0 \\ 1 \\ 0 \end{bmatrix}; M^e = \begin{bmatrix} 0 \\ 0 \\ 1 \end{bmatrix}; C^e = \begin{bmatrix} 1 & 0 & 0 \\ 0 & 1 & 0 \end{bmatrix} \quad (3.21)$$

Finally, the classical Kalman Filter is applied to the system in Eqn. (3.20) [49, 3].

### 3.3.2 Control Strategy

The trajectory tracking control is given by a PD controller in which the estimation of the disturbances  $\hat{\rho}_{q_a}$ , provided by the LKF, and a gravity compensation term, are considered, i.e.

$$u_{q_a} = -b_{q_a} (K_{P_{q_a}} e_{q_a} + K_{V_{q_a}} \dot{e}_{q_a}) - \hat{\rho}_{q_a} + g_{q_a} \quad (3.22)$$

where  $K_{P_{q_a}}, K_{V_{q_a}} > 0 \in \mathbb{R}$  are the proportional and derivative gains of the PD controller, respectively, and  $e_{q_a} = q_a - q_a^d$  and  $\dot{e}_{q_a} = \dot{q}_a - \dot{q}_a^d$  define the position and velocity tracking errors in which the index  $d$  stands for the desired positions and velocities.

The control of the rotational states of the vehicles follows the guidelines in Section 2.3. Nevertheless, the desired rotational dynamics of the aircrafts must be rewritten as in the current case of analysis the number of elements, conforming the flying chain, differs from the system in Chapter 2; in this regard, it follows that:

$$\begin{bmatrix} u_x \\ u_z \\ u_{\Theta_1} \\ u_{\Theta_2} \end{bmatrix} = \begin{bmatrix} S_{\theta_1} f_1 + S_{\theta_2} f_2 + S_{\theta_3} f_3 \\ C_{\theta_1} f_1 + C_{\theta_2} f_2 + C_{\theta_3} f_3 \\ \frac{l_1}{2} (C_{\Theta_1 - \theta_1} f_1 - C_{\Theta_1 - \theta_2} f_2) \\ \frac{l_1}{2} (C_{\Theta_2 - \theta_2} f_2 - C_{\Theta_2 - \theta_3} f_3) \end{bmatrix} \quad (3.23)$$

To avoid the over actuation of the system, recalling Section 2.3, the attitude reference for the vehicles is defined as:

$$\theta^d = \tan^{-1} \left( \frac{u_x}{u_z} \right) \quad (3.24)$$

Therefore the force that each Micro Aerial Vehicle should exert over the flying chain is computed according to the expression:

$$\begin{bmatrix} f_1 \\ f_2 \\ f_3 \end{bmatrix} = \frac{1}{3} \begin{bmatrix} 1 & 2 & 1 \\ 1 & -1 & 1 \\ 1 & -1 & -2 \end{bmatrix} \begin{bmatrix} \sqrt{u_x^2 + u_z^2} \\ (2u_{\Theta_1}) / (l_1 C_{\Theta_1 - \theta^d}) \\ (2u_{\Theta_2}) / (l_1 C_{\Theta_2 - \theta^d}) \end{bmatrix} \quad (3.25)$$

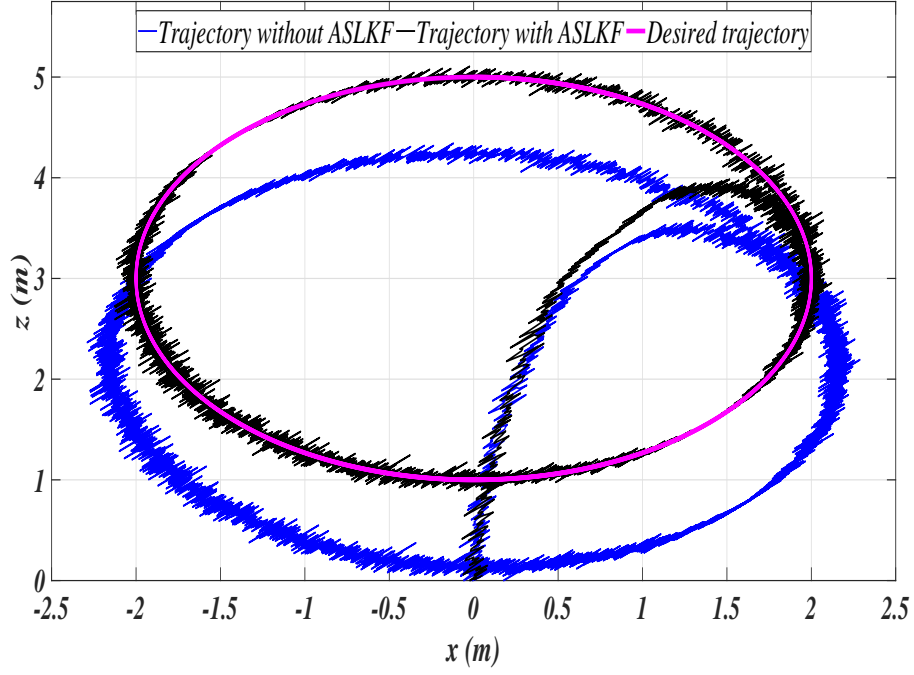


Figure 3.2: Desired trajectory and performance comparison

### 3.4 Numerical Simulations and Results

To validate the control strategy proposal, a numerical simulation was conducted and it considered a system with the parameters presented in Table 3.1 in addition, the initial conditions of the flying chain were all set to zero as well as the initial attitude of the vehicles.

In such simulation, the comparison of the behaviour of the system under the same PD control law is shown, yet, the only difference is the addition of the estimated disturbances computed by the ASLKM. To prove the performance of the estimator the desired trajectories are described by:

$$x^d = 2 \sin\left(\frac{t}{5}\right) ; z^d = 3 + 2 \cos\left(\frac{t}{5}\right) ; \Theta_1^d = \frac{\pi}{8} \cos\left(\frac{t}{7}\right) ; \Theta_2^d = -\frac{\pi}{8} \sin\left(\frac{t}{7}\right) \quad (3.26)$$

The desired velocities and accelerations were computed by time differentiation of the desired trajectories, as it is a straightforward procedure, the corresponding expressions are omitted.

Table 3.1: Parameters of the system for simulations

Parameter	Value	Parameter	Value
$m_r$	0.62 kg	$I_r$	0.253 kg m <sup>2</sup>
$m_l$	0.1 kg	$I_l$	0.125 kg m <sup>2</sup>
$l_l$	1 m	$g$	9.81 m/s <sup>2</sup>
$m_{p_1}$	0.15 kg	$l_{p_1}$	0.3 m
$m_{p_2}$	0.1 kg	$l_{p_2}$	0.4 m

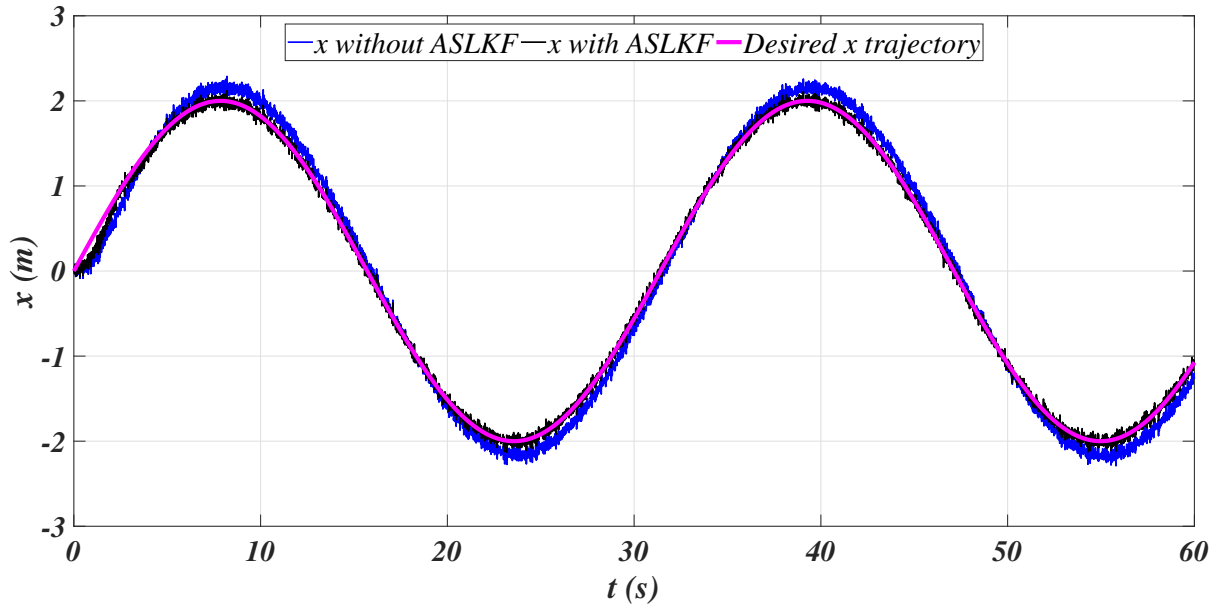


Figure 3.3: Performance comparison of the controllers in  $x$

The results of the simulation are exposed in Figs. 3.2 - 3.9 which are introduced and described next.

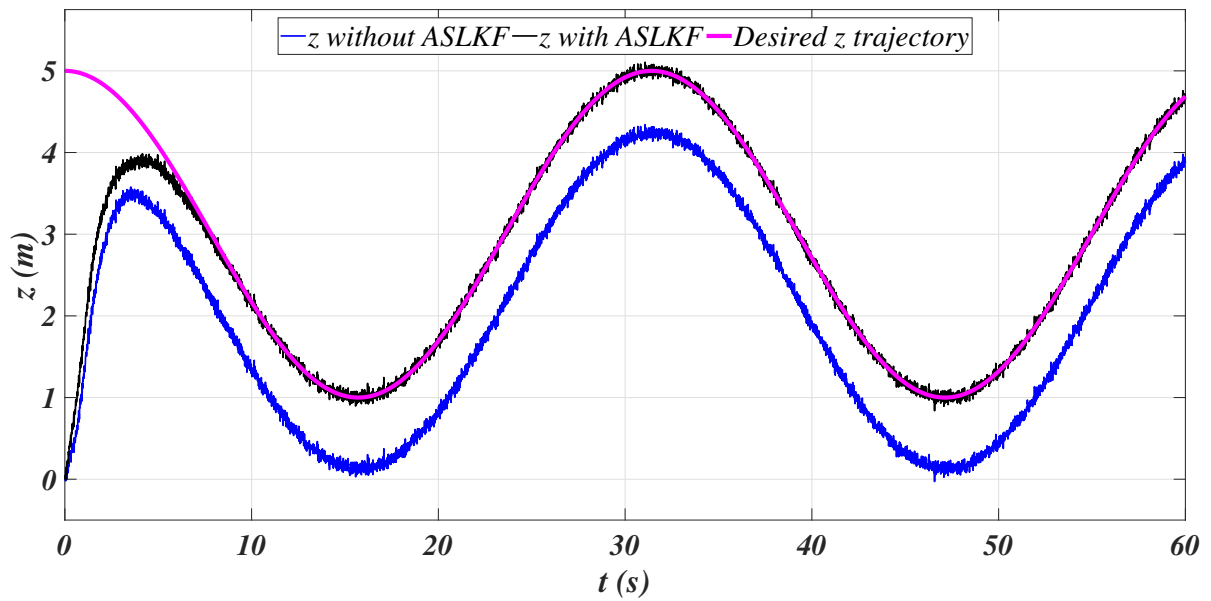
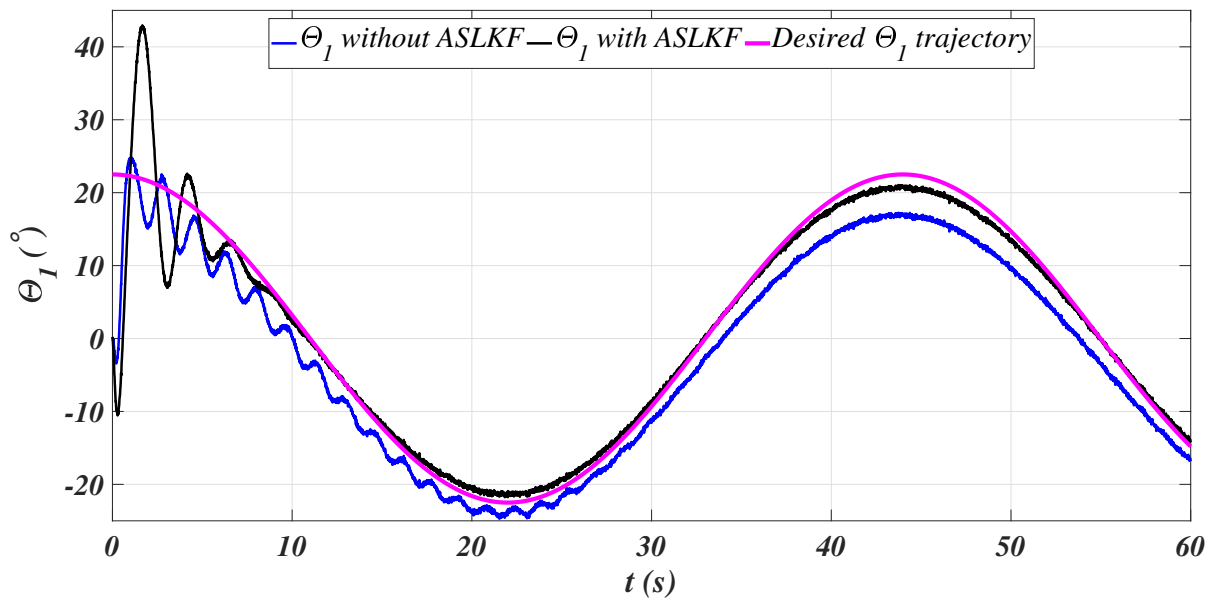
The desired trajectory in the plane is depicted by a magenta line in Fig. 3.2. The performance of the system without the estimated disturbances considered into the controller (blue) exposes the influence of the couplings and the pendulum-like payloads in the translational motion of the system, meanwhile, it can be established that the system performs a better tracking operation when considering the effects of the external disturbances into the control strategy, this asseveration can be made based on the motion described by the black noisy line.

Moreover, Figs. 3.3 and 3.4 present a comparison between the PD controller with and without disturbances estimation for the  $x$  and  $z$  degrees of freedom, respectively. In both cases the improvement of the system performance when considering the perturbations in the controller turns to be evident.

The rotational degree of freedom of each link follows a similar improvement behavior, and according to Figs. 3.5 and 3.6, the oscillations presented in the links are attenuated by the estimator leading to a rejection of the pendulums' motion effects since these depend on the overall dynamics of the system, as described in Section 3.3.

Fig. 3.7 reinforces what has been discussed in previous paragraphs. In this figure, a comparison of the errors, for a better appreciation and comprehension, is depicted.

However, the improvement in the trajectory tracking performance of the flying system is the result of a successful estimation process, to prove this fact, the Figs. 3.8 and 3.9 are presented. In Fig. 3.8 the disturbances of the system and those estimated by the Kalman Filter are shown. Fig. 3.9 correspond to the error of the estimation process, which leads to conclude that even when the estimation is not exact, the obtained approximation is close enough to improve the system performance.

Figure 3.4: Performance comparison of the system in  $z$ Figure 3.5: Performance comparison of the system in  $\theta_1$

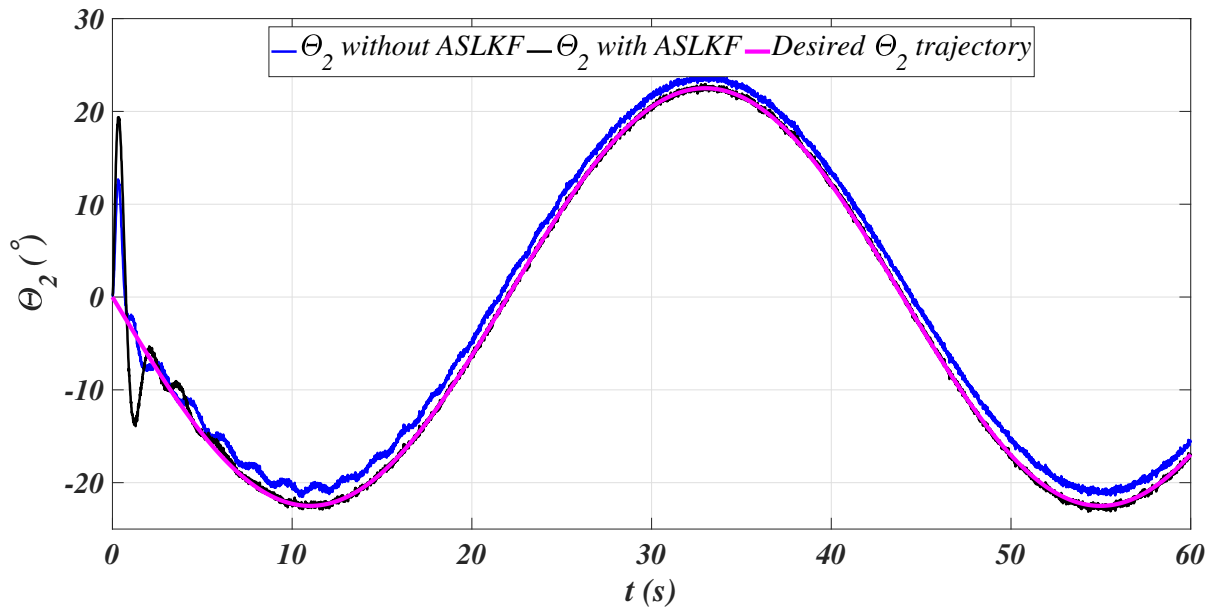


Figure 3.6: Performance comparison of the system in  $\Theta_2$

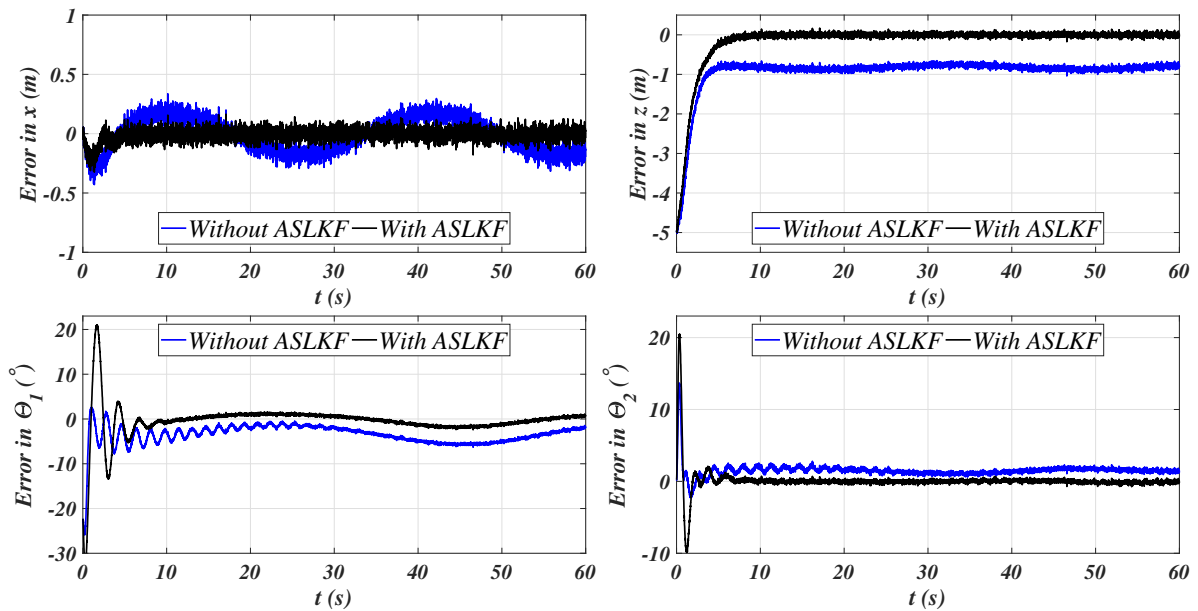


Figure 3.7: Trajectory errors comparison

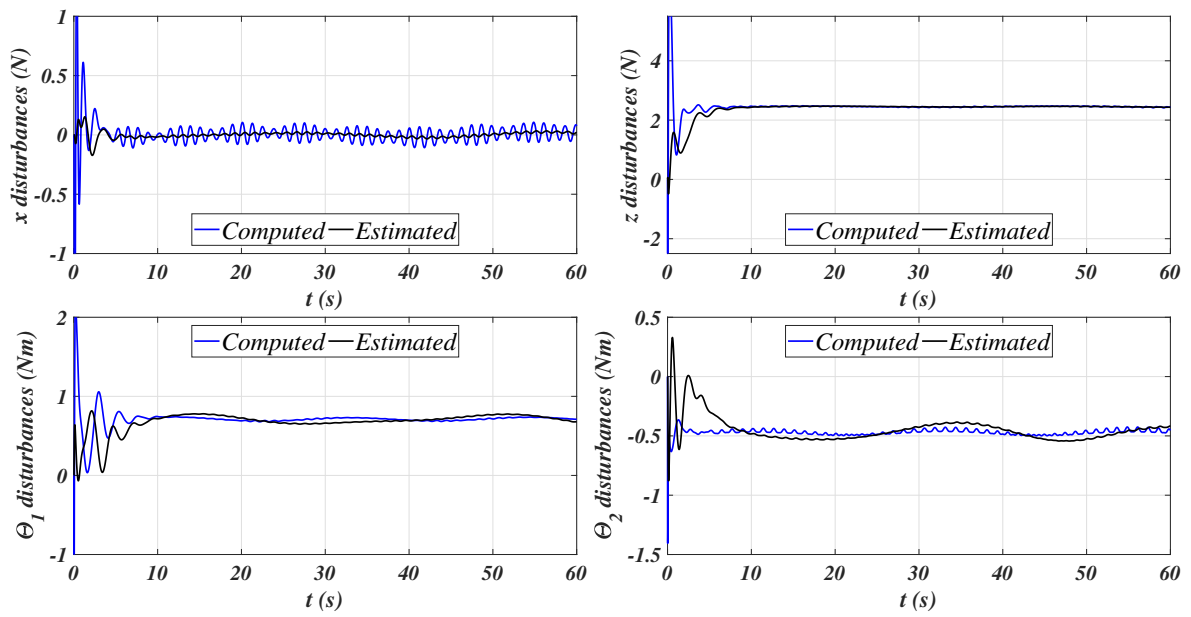


Figure 3.8: Disturbances vs. Estimated disturbances

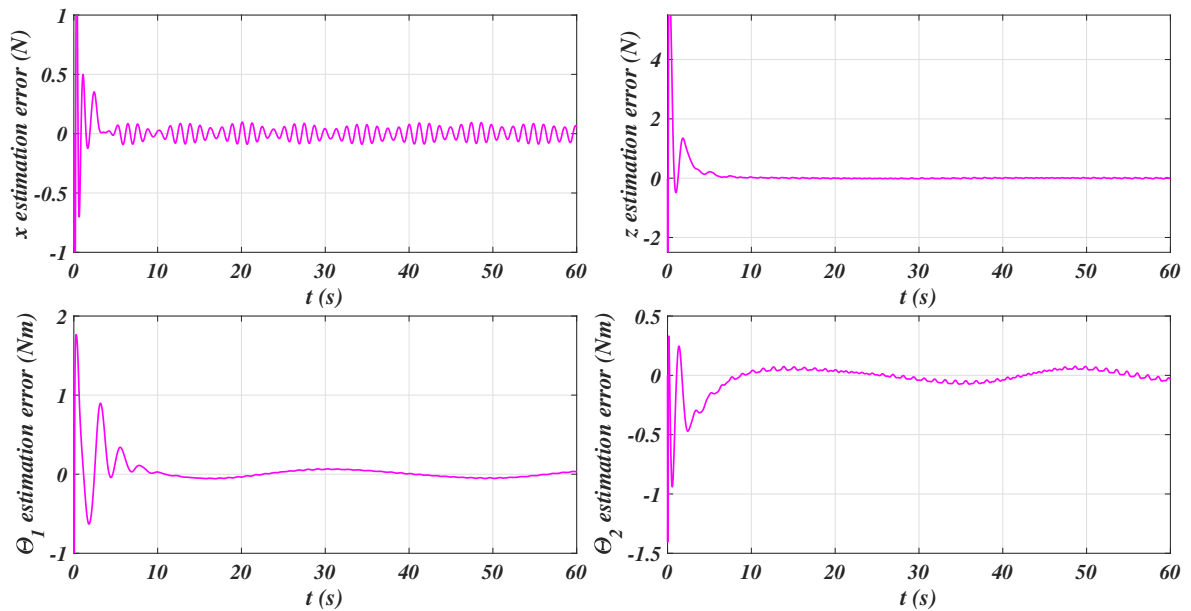


Figure 3.9: Estimation errors



## Chapter 4

# Nonlinear Control and ASEKF-Based Disturbances Compensation

The sequel of the chapter is outlined as follows: [Section 4.1](#) provides an introduction to the case of study and a brief revision of the literature. [Section 4.2](#) presents the description of the proposed aerial system. The dynamic model is explained alongside the mathematical model extension which defines the augmented state space representation. [Section 4.3](#) entails the model's uncertainties analysis that shapes the ASEKF estimation algorithm and the Lyapunov-based control strategy. The validation of the approach via numerical simulation is presented in [Section 4.4](#), the set of results is also discussed. Concluding remarks alongside forthcoming research are established in [Subsection 8.1.3](#).

### 4.1 Introduction

Amid the current technological surge, interactive Unmanned Aerial Systems (UAS) have enlarged their application spectrum including high-precision weather monitoring, swarm-based remote sensing, parcel transport and delivering, precision agriculture, disaster assessment and infrastructure inspection, among others [\[149, 71, 28\]](#).

Overcoming current operational limitations on aerial transport remains as the main motivation of the actual chapter. On one hand, it is well known the limited cargo capacity of a single rotorcraft [\[49, 136, 27\]](#). On the other hand, multi-rotorcraft systems imply complex control laws to achieve enhanced coordination (inter-agent/obstacle avoidance and formation flight) as well as inter-agent sensing and communication issues (delays and radio signal degradation) [\[17, 6\]](#). Inspired by the latter arguments, inter-linked rotorcrafts configurations can potentially surpass such issues. These appealing features combined with the aerial versatility are triggering the interest of the research community on such vehicles whose shape adaptability similar to that of snake-like amphibious robots [\[103, 161\]](#) or that of the serial manipulator robots [\[64, 138\]](#) represents a potential advantage to enhance the performance of multiple-cargo transportation within complex scenarios. Parallel robots configurations [\[101, 8\]](#) have also inspired several works nonetheless, the susceptibility to singularities remains as a challenging issue that dispels scientists attention [\[156\]](#).

To the best of the author's consideration, the vehicle proposal introduced in [175, 176, 9, 177] represents one of the most significant efforts to explore and to exploit the capabilities of these configurations as the authors have studied its behavior and performance in different scenarios including pure pose control, center of gravity (CoG) shifting due to couplings and payloads motion and the trajectory planning and navigation tasks. While the aforementioned vehicle is equipped with dual-rotors actuators, the herein proposed concept is endowed with quad-rotors actuators enlarging the flight envelope which reduces singularities and enhances self-reconfiguration maneuvers. Additionally, previous works [36, 37], have reported the treatment of the nonlinear dynamics with a robust control approach and a linear representation in which the couplings and non-linearities are estimated and compensated by a Linear Kalman Filter yet the uncertainties of the system parameters and the carried objects have not been considered.

As far as one is concerned, and according to [35], parametric uncertainties and external disturbance estimation refers to one of the main issues to solve in the conception of multi-link aerial systems and the performance of transport maneuvers.

In this regard, Kalman Filter-based estimation techniques have been designed and successfully implemented to ensure a smooth and reliable aerial transformation [133], to mitigate the wind effects [53] and to compensate the external phenomena influences on aerial multi-link robots [150]. The basis of the Kalman Filtering technique established in works as [141, 60, 147] has permitted this filter to evolve in such a manner that it is still a valuable resource in the scientific community nowadays [56, 83, 46, 13, 139, 134] even when literature gives evidence of the increasing tendency in studying and conceiving new state observation techniques [117, 118, 40].

A novel aerial system consisting of three linked rotorcrafts, referred as ML-UAS, is addressed throughout the chapter. The dynamic model of the ensemble is described in detail. In terms of control, a nonlinear Lyapunov-based controller is jointly utilised with an Augmented-State Extended Kalman Filter (ASEKF) aiming at tracking a time-parametrized trajectory while compensating parametric and external disturbances during a multiple-load transportation task. For the sake of detail, the contributions of the actual chapter are listed below:

- The proposition of a novel alternative concept of multi-link aerial system capable of transporting multiple cargo.
- A detailed control synthesis and stability analysis considering the longitudinal dynamics and the presence of structural and nonstructural uncertainties.
- Unlike the majority of works addressing disturbance compensation via an augmented-state Kalman filter, the deduction of the covariance matrix based on the uncertainties present in the full nonlinear model is introduced.
- An in-depth simulation stage is conducted to evaluate the effectiveness of the proposed control-estimation strategy. Moreover, a real-world scenario is considered using actual sensors specifications regarding noise and faults.

## 4.2 Mathematical Modeling

The system proposed herein consists of three quadrotors physically interlinked by two rods (Fig. 4.1), similar to that of Chapter 3 nevertheless, aerial transportation, manipulation and deployment are possible since controllable 1-DoF robotic manipulators are attached at the CoG of the rods. As in previous chapters, the analysis is restricted to the longitudinal dynamics as depicted in Fig. 4.2.



Figure 4.1: 3D CAD scheme of the multi-link system

In order to describe the system, let one adopt the notation established in Section 2.2 which was also used at Chapter 3. In this regard, the reference tracking point of the system with respect to the inertial frame corresponds to the CoG of the  $d_2$  rotorcraft whose position is denoted as  $\xi_{r_2} = [x \ z]^T \in \mathbb{R}^2$ , moreover, from Fig. 4.2 the positions of the UAVs,  $\xi_{r_i}$  (with  $i = 1, 2, 3$ ) and those of the rigid links,  $\xi_{l_j}$ , and the payloads,  $\xi_{p_j}$  (with  $j = 1, 2$ ), are defined as:

$$\xi_{r_1} = \begin{bmatrix} x - l_1 C_{\Theta_1} \\ z + l_1 S_{\Theta_1} \end{bmatrix}; \quad \xi_{r_3} = \begin{bmatrix} x + l_1 C_{\Theta_2} \\ z - l_1 S_{\Theta_2} \end{bmatrix}; \quad \xi_{l_1} = \begin{bmatrix} x - 0.5l_1 C_{\Theta_1} \\ z + 0.5l_1 S_{\Theta_1} \end{bmatrix}, \quad \xi_{l_2} = \begin{bmatrix} x + 0.5l_1 C_{\Theta_2} \\ z - 0.5l_1 S_{\Theta_2} \end{bmatrix}; \quad (4.1)$$

$$\xi_{p_1} = \xi_{l_1} - \begin{bmatrix} l_{p_1} S_{\beta_1} \\ l_{p_1} C_{\beta_1} \end{bmatrix}; \quad \xi_{p_2} = \xi_{l_2} - \begin{bmatrix} l_{p_2} S_{\beta_2} \\ l_{p_2} C_{\beta_2} \end{bmatrix} \quad (4.2)$$

By differentiating Eqns. (4.1) and (4.2) with respect to time and assuming the parameters of the system to be time-invariant, it is straightforward to compute the velocity of each component as well as the acceleration.

### 4.2.1 Dynamics

According to the Euler-Lagrange formalism, the total kinetic and potential energies must be established as these define the Lagrangian of the system as in Section 2.2, in this sense, it follows that:

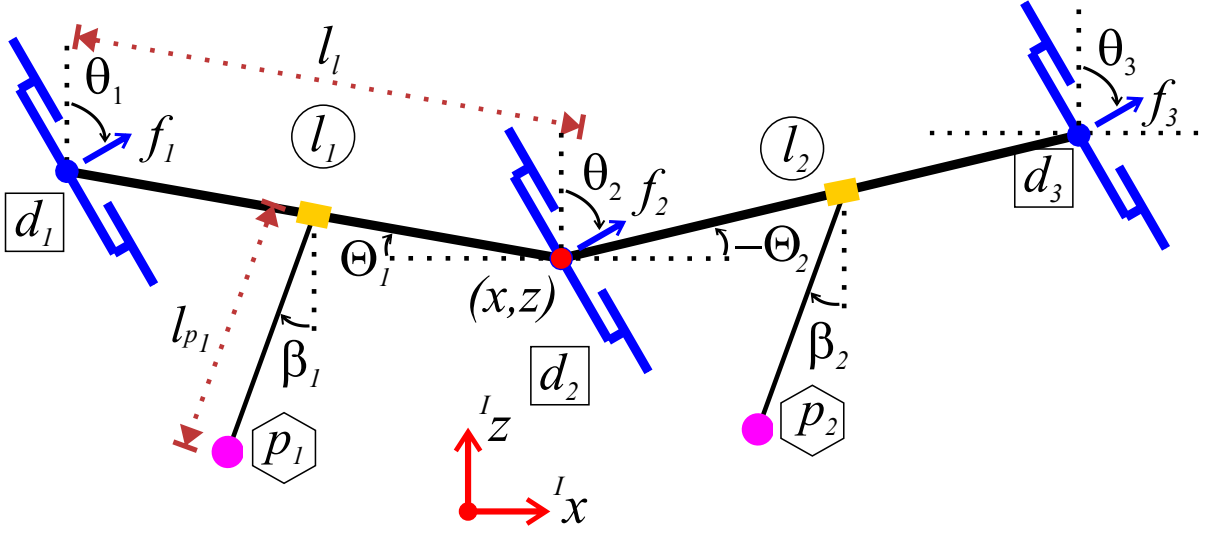


Figure 4.2: ML-UAS longitudinal simplified scheme

$$K = \sum_{i=1}^3 \left( \frac{m_r}{2} \dot{\xi}_{r_i}^2 + \frac{I_r}{2} \dot{\theta}_i^2 \right) + \sum_{j=1}^2 \left( \frac{m_{l_j}}{2} \dot{\xi}_{l_j}^2 + \frac{I_{l_j}}{2} \dot{\Theta}_j^2 + \frac{m_{p_j}}{2} \dot{\xi}_{p_j}^2 \right) \quad (4.3)$$

$$U = g \left[ m_r \sum_{i=1}^3 z_{r_i} + \sum_{j=1}^2 (m_{l_j} z_{l_j} + m_{p_j} z_{p_j}) \right] \quad (4.4)$$

where  $\dot{\xi}_{(*)}^2 = \dot{\xi}_{(*)}^T \dot{\xi}_{(*)}$ .

Recalling Eqn. (2.5), the Euler-Lagrange equation follows the form:

$$\frac{d}{dt} \frac{\partial}{\partial \dot{q}_k} L - \frac{\partial}{\partial q_k} L = \tau_{q_k} \quad (4.5)$$

which implies the definition of a vector  $\mathbf{q} \in \mathbb{R}^6$  of generalized coordinates  $q_k \in \mathbb{R}$  ( $k = 1, 2, \dots, 6$ ) which, for this specific case of study:  $q_1 = x$ ,  $q_2 = z$ ,  $q_3 = \Theta_1$ ,  $q_4 = \Theta_2$ ,  $q_5 = \beta_1$  and  $q_6 = \beta_2$ . The term  $\tau_{q_k} \in \mathbb{R}$  stands for the external forces/torques.

The equations of motion of the system are comprised in the expression:

$$M(\mathbf{q}) \ddot{\mathbf{q}} + C(\mathbf{q}, \dot{\mathbf{q}}) \dot{\mathbf{q}} + \mathbf{G}(\mathbf{q}) = \boldsymbol{\tau} \quad (4.6)$$

where the inertial matrix  $M(\mathbf{q}) \in \mathbb{R}^{6 \times 6}$  and the vector of gravitational terms  $\mathbf{G}(\mathbf{q}) \in \mathbb{R}^6$  are defined as:

$$M(\mathbf{q}) = \begin{bmatrix} m_{11} & 0 & m_{13} & m_{14} & m_{15} & m_{16} \\ 0 & m_{22} & m_{23} & m_{24} & m_{25} & m_{26} \\ m_{31} & m_{32} & m_{33} & 0 & m_{35} & 0 \\ m_{41} & m_{42} & 0 & m_{44} & 0 & m_{46} \\ m_{51} & m_{52} & m_{53} & 0 & m_{55} & 0 \\ m_{61} & m_{62} & 0 & m_{64} & 0 & m_{66} \end{bmatrix} \quad (4.7)$$

$$\mathbf{G}(\mathbf{q}) = g \begin{bmatrix} 0 & m_{22} & m_{23} & m_{24} & m_{25} & m_{26} \end{bmatrix}^T \quad (4.8)$$

and the Coriolis and centripetal effects matrix  $C(\mathbf{q}, \dot{\mathbf{q}}) \in \mathbb{R}^{6 \times 6}$  is computed such that it satisfies  $\dot{M}(\mathbf{q}) = C(\mathbf{q}, \dot{\mathbf{q}}) + C(\mathbf{q}, \dot{\mathbf{q}})^T$ . Due to the symmetry property of  $M(\mathbf{q})$ , it is sufficient to define the elements below, where  $\vartheta_j = \Theta_j - \beta_j$ .

$$m_{11} = m_{22} = 3m_r + 2m_l + m_{p_1} + m_{p_2}; \quad m_{13} = l_l [m_r + 0.5(m_l + m_{p_1})] S_{\Theta_1}; \quad m_{14} = -l_l [m_r + 0.5(m_l + m_{p_2})] S_{\Theta_2}; \quad (4.9)$$

$$m_{15} = -m_{p_1} l_{p_1} C_{\beta_1}; \quad m_{16} = -m_{p_2} l_{p_2} C_{\beta_2}; \quad m_{23} = l_l [m_r + 0.5(m_l + m_{p_1})] C_{\Theta_1}; \quad m_{24} = -l_l [m_r + 0.5(m_l + m_{p_2})] C_{\Theta_2}; \quad (4.10)$$

$$m_{25} = m_{p_1} l_{p_1} S_{\beta_1}; \quad m_{26} = m_{p_2} l_{p_2} S_{\beta_2}; \quad m_{33} = l_l^2 [m_r + 0.25(m_l + m_{p_1})] + I_l; \quad m_{35} = -0.5m_{p_1} l_l l_{p_1} S_{\Theta_1}; \quad (4.11)$$

$$m_{44} = l_l^2 [m_r + 0.25(m_l + m_{p_2})] + I_l; \quad m_{46} = 0.5m_{p_2} l_l l_{p_2} S_{\Theta_2}; \quad m_{55} = m_{p_1} l_{p_1}^2; \quad m_{66} = m_{p_2} l_{p_2}^2 \quad (4.12)$$

The vector  $\boldsymbol{\tau} = [\tau_x \ \tau_z \ \tau_{\Theta_1} \ \tau_{\Theta_2} \ \tau_{\beta_1} \ \tau_{\beta_2}]^T \in \mathbb{R}^6$  in Eqn. (4.6) comprises the control inputs produced by the UAVs and the manipulator arm actuators,  $\mathbf{u}_\tau \in \mathbb{R}^6$ , and the disturbances  $\boldsymbol{\rho} = [\rho_x \ \rho_z \ \rho_{\Theta_1} \ \rho_{\Theta_2} \ \rho_{\beta_1} \ \rho_{\beta_2}]^T \in \mathbb{R}^6$  caused by external unmodeled phenomena, in this sense  $\boldsymbol{\tau} = \mathbf{u}_\tau + \boldsymbol{\rho}$  where the vector of control inputs  $\mathbf{u}_\tau$  depends on the geometry of the system, the thrusts  $f_1, f_2, f_3$  exerted by the vehicles, the orientation of the aircrafts  $\theta_1, \theta_2, \theta_3$  and the torques  $\tau_{s_1}, \tau_{s_2} \in \mathbb{R}$  produced by the servomotors to manipulate the robotic arms, moreover, we assume that the dynamics of the servomotors is significantly faster than that of the overall system, thus it follows that:

$$\mathbf{u}_\tau = \begin{bmatrix} u_x \\ u_z \\ u_{\Theta_1} \\ u_{\Theta_2} \\ u_{\beta_1} \\ u_{\beta_2} \end{bmatrix} = \begin{bmatrix} \sum_{i=1}^3 f_i S_{\theta_i} \\ \sum_{i=1}^3 f_i C_{\theta_i} \\ \frac{l_l}{2} (f_1 C_{\Theta_1 - \theta_1} - f_2 C_{\Theta_1 - \theta_2}) \\ \frac{l_l}{2} (f_2 C_{\Theta_2 - \theta_2} - f_3 C_{\Theta_2 - \theta_3}) \\ \tau_{s_1} \\ \tau_{s_2} \end{bmatrix} \quad (4.13)$$

By following Eqn. (4.5) and taking into account  $\xi_{r_i}$  and  $\theta_i$  instead of  $q_k$ , and assuming no friction between the inter-connected elements, the translational and rotational equations of motion of the rotorcrafts are defined as:

$$m_r \ddot{x}_{r_i} = f_i S \theta_i \quad (4.14)$$

$$m_r (\ddot{z}_{r_i} + g) = f_i C \theta_i \quad (4.15)$$

$$I_r \ddot{\theta}_i = \tau_{r_i} \quad (4.16)$$

where  $\tau_{r_i} \in \mathbb{R}$  is the control torque of the  $i^{\text{th}}$  vehicle generated by the differential thrust of the quadrotor propellers. The roll and pitch motions are considered to be successfully stabilized separately [49, 36, 37, 104].

## 4.2.2 Augmented State Representation

Based on Eqn. (4.6), the dynamics of the multi-link system can be expressed as

$$\ddot{\mathbf{q}} = M(\mathbf{q})^{-1} [\mathbf{u}_\tau + \boldsymbol{\rho} - C(\mathbf{q}, \dot{\mathbf{q}}) \dot{\mathbf{q}} - \mathbf{G}(\mathbf{q})] \quad (4.17)$$

The latest yields to a state space representation of the system as follows:

$$\frac{d}{dt} \boldsymbol{\chi} = \begin{bmatrix} \dot{\mathbf{q}} \\ M(\mathbf{q})^{-1} [\mathbf{u}_\tau + \boldsymbol{\rho} - C(\mathbf{q}, \dot{\mathbf{q}}) \dot{\mathbf{q}} - \mathbf{G}(\mathbf{q})] \end{bmatrix} \quad (4.18)$$

where  $\boldsymbol{\chi} = [\mathbf{q}^T \dot{\mathbf{q}}^T]^T \in \mathbb{R}^{12}$ . Eqn. (4.18) can be extended to include the external disturbances in the states vector such that it becomes:

$$\frac{d}{dt} \boldsymbol{\chi}^e = \begin{bmatrix} \dot{\mathbf{q}} \\ M(\mathbf{q})^{-1} [\mathbf{u}_\tau + \boldsymbol{\rho} - C(\mathbf{q}, \dot{\mathbf{q}}) \dot{\mathbf{q}} - \mathbf{G}(\mathbf{q})] \\ \boldsymbol{\vartheta} \end{bmatrix} \quad (4.19)$$

with  $\boldsymbol{\chi}^e = [\mathbf{q}^T \dot{\mathbf{q}}^T \boldsymbol{\rho}^T]^T \in \mathbb{R}^{18}$ . Notice that  $\mathbf{q}$ ,  $\dot{\mathbf{q}}$  and  $\boldsymbol{\rho}$  are functions of time and that the dynamics of the disturbances is modeled as a random walk process with zero mean (Gaussian)  $\boldsymbol{\vartheta}(t) = [\vartheta_x \ \vartheta_z \ \vartheta_{\theta_1} \ \vartheta_{\theta_2} \ \vartheta_{\beta_1} \ \vartheta_{\beta_2}]^T \in \mathbb{R}^6$ . For instance, such system can be rewritten in the form:

$$\dot{\boldsymbol{\chi}}^e = \mathbf{F}(\boldsymbol{\chi}^e, \mathbf{U}) + \mathbf{J} \boldsymbol{\vartheta} \quad (4.20)$$

with

$$\mathbf{F}(\boldsymbol{\chi}^e, \mathbf{U}) = \begin{bmatrix} \dot{\mathbf{q}} \\ M(\mathbf{q})^{-1} [\mathbf{U} + \boldsymbol{\rho} - C(\mathbf{q}, \dot{\mathbf{q}}) \dot{\mathbf{q}}] \\ \mathbf{0}^* \end{bmatrix} \quad (4.21)$$

$$J = \begin{bmatrix} \mathbf{0} & \mathbf{0} & \mathbf{I} \end{bmatrix}^T \quad (4.22)$$

where  $\mathbf{0} \in \mathbb{R}^{6 \times 6}$  and  $\mathbf{I} \in \mathbb{R}^{6 \times 6}$  stands for the zero and the identity matrices, respectively,  $\mathbf{0}^* \in \mathbb{R}^6$  is the zero vector and  $\mathbf{U} = \mathbf{u}_\tau - \mathbf{G}(\mathbf{q}) \in \mathbb{R}^6$ .

### 4.3 Uncertainties Estimation and Control

Assuming that the parameters of the system in the vector  $\boldsymbol{\gamma} = [\gamma_1 \dots \gamma_9]^T = [m_r \ m_l \ m_{p_1} \ m_{p_2} \ l_l \ l_{p_1} \ l_{p_2} \ I_l \ g]^T \in \mathbb{R}^9$  are subjected to some degree of uncertainty, the performance of the system is degraded as a consequence. Even when the gravity acceleration is not a parameter of the system, a deviation from the nominal value is considered. The influence of parametric uncertainties is modeled as a noisy Gaussian signal with zero mean  $\boldsymbol{\alpha} = [\alpha_{m_r} \ \alpha_{m_l} \ \alpha_{m_{p_1}} \ \alpha_{m_{p_2}} \ \alpha_{l_l} \ \alpha_{l_{p_1}} \ \alpha_{l_{p_2}} \ \alpha_{I_l} \ \alpha_g]^T \in \mathbb{R}^9$  within the system dynamics in Eqn. (4.20) as follows:

$$\dot{\boldsymbol{\chi}}^e = \mathbf{F}(\boldsymbol{\chi}^e, \mathbf{U}) + J\boldsymbol{\vartheta} + Z\boldsymbol{\alpha} \quad (4.23)$$

The influence of the parametric deviation is weighted by  $Z \in \mathbb{R}^{18 \times 9}$  that contains the partial derivative of the function  $\mathbf{F}(\boldsymbol{\chi}^e, \mathbf{U})$  with respect to the corresponding parameter, such that:

$$Z = \left[ \begin{array}{cccc} \frac{\partial \mathbf{F}(\boldsymbol{\chi}^e, \mathbf{U})}{\partial m_r} & \frac{\partial \mathbf{F}(\boldsymbol{\chi}^e, \mathbf{U})}{\partial m_l} & \dots & \frac{\partial \mathbf{F}(\boldsymbol{\chi}^e, \mathbf{U})}{\partial g} \end{array} \right] \Bigg|_{\boldsymbol{\chi}^e, \mathbf{U}} \quad (4.24)$$

This definition implies the computation of the partial derivatives and their evaluation at each time step and at the current  $\boldsymbol{\chi}^e$  and  $\mathbf{U}$ . In this regard, the dynamics of  $\mathbf{q}$  and that of  $\boldsymbol{\rho}$ , as described in Eqn. (4.20), does not depend on  $\boldsymbol{\gamma}$  which leads to:

$$\frac{\partial \dot{\mathbf{q}}}{\partial \boldsymbol{\gamma}} = \frac{\partial \dot{\boldsymbol{\rho}}}{\partial \boldsymbol{\gamma}} = \mathbf{0}' \in \mathbb{R}^{6 \times 9} \quad (4.25)$$

On the other hand, the dynamics of  $\dot{\mathbf{q}}$  prevents to compute the partial derivatives with easiness. The definition of  $\dot{\mathbf{q}}$  established in Eqn. (4.17) implies the computation of  $M(\mathbf{q})^{-1}$  which is obtained considering its adjugate,  $A_M \in \mathbb{R}^{6 \times 6}$ , and its determinant  $d_M \in \mathbb{R}^+$ :

$$M(\mathbf{q})^{-1} = d_M^{-1} A_M^T \quad (4.26)$$

Thus, Eqn. (4.17) can be rewritten as follows:

$$\ddot{\mathbf{q}} = d_M^{-1} A_M^T \mathbf{v} \quad (4.27)$$

where  $\mathbf{v} = \mathbf{U} + \boldsymbol{\rho} - C(\mathbf{q}, \dot{\mathbf{q}}) \dot{\mathbf{q}}$ . Such substitutions ease the expression manipulation regarding the computation of  $M(\mathbf{q})^{-1}$  and the derivatives within the software used. Thus, the partial derivative of  $\ddot{\mathbf{q}}$  in Eqn. (4.27) can be computed as:

$$\frac{\partial \ddot{\mathbf{q}}}{\partial \boldsymbol{\gamma}} = \frac{\partial}{\partial \boldsymbol{\gamma}} \left( \frac{1}{d_M} A_M^T \mathbf{v} \right) = \frac{\partial}{\partial \boldsymbol{\gamma}} \left( \frac{1}{d_M} A_M^T \right) \mathbf{v} + \frac{1}{d_M} A_M^T \frac{\partial \mathbf{v}}{\partial \boldsymbol{\gamma}} \quad (4.28)$$

which can be expanded in such a manner that:

$$\ddot{q}_\gamma = \frac{\partial \ddot{\mathbf{q}}}{\partial \boldsymbol{\gamma}} = \frac{1}{d_M} \left[ \frac{\partial A_M^T}{\partial \boldsymbol{\gamma}} \mathbf{v} - \left( \frac{1}{d_M} A_M^T \mathbf{v} \right) \frac{\partial d_M}{\partial \boldsymbol{\gamma}} \right] + \frac{1}{d_M} A_M^T \mathbf{v}_\gamma \quad (4.29)$$

Considering Eqns. (4.26) and (4.27), one obtains:

$$\ddot{q}_\gamma = d_M^{-1} (A_{M_\gamma} - \ddot{\mathbf{q}} \mathbf{d}_{M_\gamma}) + M(\mathbf{q})^{-1} \mathbf{v}_\gamma \quad (4.30)$$

where

$$A_{M_\gamma} = \begin{bmatrix} \frac{\partial A_M^T}{\partial m_r} \mathbf{v} & \frac{\partial A_M^T}{\partial m_i} \mathbf{v} & \dots & \frac{\partial A_M^T}{\partial I_i} \mathbf{v} & \frac{\partial A_M^T}{\partial g} \mathbf{v} \end{bmatrix} \in \mathbb{R}^{6 \times 9} \quad (4.31)$$

$$\mathbf{d}_{M_\gamma} = \frac{\partial d_M}{\partial \boldsymbol{\gamma}} = \begin{bmatrix} \frac{\partial d_M}{\partial m_r} & \frac{\partial d_M}{\partial m_i} & \dots & \frac{\partial d_M}{\partial I_i} & \frac{\partial d_M}{\partial g} \end{bmatrix} \in \mathbb{R}^{1 \times 9} \quad (4.32)$$

$$\mathbf{v}_\gamma = \frac{\partial \mathbf{v}}{\partial \boldsymbol{\gamma}} = \begin{bmatrix} \frac{\partial \mathbf{v}}{\partial m_r} & \frac{\partial \mathbf{v}}{\partial m_i} & \dots & \frac{\partial \mathbf{v}}{\partial I_i} & \frac{\partial \mathbf{v}}{\partial g} \end{bmatrix} \in \mathbb{R}^{6 \times 9} \quad (4.33)$$

Redefining  $Z$  to be:

$$Z = \begin{bmatrix} \mathbf{0}^T & \ddot{q}_\gamma^T & \mathbf{0}^T \end{bmatrix}^T \Big|_{\mathbf{x}^e, \mathbf{U}} \quad (4.34)$$

Such definition of  $Z$  results advantageous in the computation of the partial derivatives in  $A_{M_\gamma}$ ,  $\mathbf{d}_{M_\gamma}$  and  $\mathbf{v}_\gamma$  as they result relatively ease to manipulate within the software environment. Thus, the most relative expensive computational task to be developed at

each loop is the computation of  $M(\mathbf{q})^{-1}$ . Moreover, one possible solution to this issue could be to implement the definition given in Eqn. (4.26) in a user-defined function for evaluation only.

The two noise signals in Eqn. (4.23) can be regrouped into one single vector  $\boldsymbol{\omega} = \begin{bmatrix} \boldsymbol{\alpha}^T & \boldsymbol{\vartheta}^T \end{bmatrix}^T \in \mathbb{R}^{15}$  therefore, Eqn. (4.23) can be rewritten as:

$$\dot{\boldsymbol{x}}^e = \mathbf{F}(\boldsymbol{x}^e, \mathbf{U}) + \mathcal{M}\boldsymbol{\omega} \quad (4.35)$$

with  $\mathcal{M} = \begin{bmatrix} Z & J \end{bmatrix} \in \mathbb{R}^{18 \times 15}$ . The observation model of the system is directly expressed in a discrete domain [53], [91] as:

$$\mathbf{Y}_k^e = C_k^e \boldsymbol{x}_k^e + \mathbf{V}_k \quad (4.36)$$

with  $\mathbf{Y}_k^e \in \mathbb{R}^{12}$ ,  $\mathbf{V}_k = [v_{x_k} \ v_{z_k} \ \dots \ v_{\beta_{2_k}}]^T \in \mathbb{R}^{12}$  and

$$C_k^e = \begin{bmatrix} \mathbf{I} & \mathbf{0} & \mathbf{0} \\ \mathbf{0} & \mathbf{I} & \mathbf{0} \end{bmatrix} \in \mathbb{R}^{12 \times 18} \quad (4.37)$$

implying that  $\mathbf{q}$  and  $\dot{\mathbf{q}}$  are available but noisy since the vector  $\mathbf{V}_k$  corresponds to the variance of the Gaussian noises affecting the sensors.

### 4.3.1 ASEKF Estimation Strategy

Due to the high non-linearity and couplings of the dynamics, the discretization process becomes complex and computationally expensive, thus, a continuous-discrete ASEKF is conceived. In this regard, the prediction phase is executed considering a continuous time representation of the system (Eqn. (4.35)) meanwhile, Eqn. (4.36) is used in the correction phase [134], [91]. Moreover, the system is considered to be observable at a given operation point (Appendix B).

The signals noises  $\boldsymbol{\omega}$  and  $\mathbf{V}_k$  previously introduced in Section 4.2.1 stand for uncorrelated white Gaussian random processes with zero mean, i.e.  $E[\boldsymbol{\omega}(t)\mathbf{V}_k(t)^T] = \mathbf{0}^* \in \mathbb{R}^{15 \times 12}$ ,  $E[\boldsymbol{\omega}(t)] = 0$  and  $E[\mathbf{V}_k(t)] = 0$ . The process covariance matrix  $Q \in \mathbb{R}^{15 \times 15}$  is characterized by  $\mathcal{M}$  as:

$$Q(t) = E[\boldsymbol{\omega}\boldsymbol{\omega}^T] = E[(\mathcal{M}\boldsymbol{\omega})(\mathcal{M}\boldsymbol{\omega})^T] = \mathcal{M}W\mathcal{M}^T \quad (4.38)$$

where  $W = E[\boldsymbol{\omega}\boldsymbol{\omega}^T] \in \mathbb{R}^{15 \times 15}$  is a diagonal matrix containing the variances of the process noise signals. The covariance matrix of the measurement noise  $R_k = \text{diag}(E[v_{x_k}] \ E[v_{z_k}] \ \dots \ E[v_{\beta_{1_k}}] \ E[v_{\beta_{2_k}}]) \in \mathbb{R}^{12 \times 12}$  is defined by the variances of the noisy signals of the sensors.

The prediction phase of the ASEKF is thus described by:

$$\dot{\hat{\boldsymbol{\chi}}^e}(t) = \mathbf{F}(\hat{\boldsymbol{\chi}}^e, \mathbf{U}) \quad (4.39)$$

$$\dot{P}(t) = F_{\mathcal{X}^e}(\hat{\boldsymbol{\chi}}^e, \mathbf{U})P(t) + P(t)F_{\mathcal{X}^e}^T(\hat{\boldsymbol{\chi}}^e, \mathbf{U}) + Q(t) \quad (4.40)$$

with

$$F_{\mathcal{X}^e}(\hat{\boldsymbol{\chi}}^e, \mathbf{U}) = \left. \frac{\partial \mathbf{F}(\boldsymbol{\chi}^e, \mathbf{U})}{\partial \boldsymbol{\chi}^e} \right|_{\boldsymbol{\chi}^e, \mathbf{U}} \in \mathbb{R}^{18 \times 18} \quad (4.41)$$

computed by the same procedure that defined  $\mathbf{Z}$ . It is worth highlighting that  $\hat{\boldsymbol{\chi}}^e = \hat{\boldsymbol{\chi}}^e(t)$  and  $\mathbf{U} = \mathbf{U}(t)$ .

The set of differential equations in Eqns. (4.39) and (4.40) is solved via numerical methods to find  $\hat{\boldsymbol{\chi}}^e(t)$  and  $P(t)$  [91]. For the first iteration, the initial values of  $\hat{\boldsymbol{\chi}}^e(t)$  and  $P(t)$  are given as  $\hat{\boldsymbol{\chi}}_0^e$  and  $P_0$ , respectively. In order to adopt the values obtained during the prediction phase  $\hat{\boldsymbol{\chi}}_{k|k-1}^e = \hat{\boldsymbol{\chi}}^e(t_k)$  and  $P_{k|k-1} = P(t_k)$  for ulterior computations.

The correction phase is given by the set of equations:

$$K_k = P_{k|k-1}C_k^{eT} \left( C_k^e P_{k|k-1} C_k^{eT} + R_k \right)^{-1} \quad (4.42)$$

$$\hat{\boldsymbol{\chi}}_{k|k}^e = \hat{\boldsymbol{\chi}}_{k|k-1}^e + K_k \left( \mathbf{Y}_k^e - C_k^e \hat{\boldsymbol{\chi}}_{k|k-1}^e \right) \quad (4.43)$$

$$P_{k|k} = (\mathbf{I}' - K_k C_k^e) P_{k|k-1} \quad (4.44)$$

where  $\mathbf{I}' \in \mathbb{R}^{18 \times 18}$  is the identity matrix. Thus, the estimation of the disturbances is taken from the state estimation:

$$\hat{\boldsymbol{\chi}}_{k|k}^e = \left[ \hat{\mathbf{q}}_{k|k}^T \quad \hat{\dot{\mathbf{q}}}_{k|k}^T \quad \hat{\boldsymbol{\rho}}_{k|k}^T \right]^T \quad (4.45)$$

The sub-index  $k|k$  is omitted from now-on for sake of simplicity.

Further information concerning the parameters of the filter and the influence of each of these in the estimation efficiency can be found at [141, 60, 147, 13, 124].

## 4.3.2 Control

The control of the overall ML-UAS features a nested control architecture: an external loop related to the flying chain and an inner loop referred to the control of the rotorcrafts. For a proper identification, a blocks schema is exhibited on Fig. 4.3 where the control algorithm is built up with the disturbances estimation and  $\hat{\mathbf{q}}$ ,  $\hat{\dot{\mathbf{q}}}$  and  $\hat{\boldsymbol{\rho}}$  closing the control loop.

A PD control law with disturbances compensation:



The constants  $k_g$ ,  $k_M$  and  $k_{C_1}$  are defined in the Appendix A. To perform the stability analysis, let it exist a constant  $\varepsilon \in \mathbb{R}^+$  such that it defines the matrices  $K_V$  and  $K_P$  as follows:

$$\lambda_{Max}(K_V) \geq \lambda_{min}(K_V) > k_{h_1} + \varepsilon b \quad (4.49)$$

$$\lambda_{Max}(K_P) \geq \lambda_{min}(K_P) > \frac{(2\varepsilon a + k_{h_2})^2}{4\varepsilon [\lambda_{min}(K_V) - k_{h_1} - \varepsilon b]} + k_{h_2} \quad (4.50)$$

$$\lambda_{Max}(K_P) \geq \lambda_{min}(K_P) > \varepsilon^2 \frac{\lambda_{Max}^2[M(\mathbf{q})]}{\lambda_{min}[M(\mathbf{q})]} \quad (4.51)$$

with  $k_{h_1}$  and  $k_{h_2}$  introduced in Appendix A and

$$a = \frac{1}{2} [\lambda_{Max}(K_V) + k_{C_1} \|\dot{\mathbf{q}}_d\|_{max} + k_{h_1}] \in \mathbb{R}^+ \quad (4.52)$$

$$b = \lambda_{Max}[M(\mathbf{q})] + \sqrt{6} k_{C_1} \in \mathbb{R}^+ \quad (4.53)$$

Let the Lyapunov candidate function  $V(t, \mathbf{e}, \dot{\mathbf{e}}) \in \mathbb{R}$  be

$$V = \frac{1}{2} \dot{\mathbf{e}}^T M(\mathbf{q}) \dot{\mathbf{e}} + \frac{1}{2} \mathbf{e}^T K_P \mathbf{e} + \varepsilon \mathbf{f}_{th}(\mathbf{e})^T M(\mathbf{q}) \dot{\mathbf{e}} \quad (4.54)$$

with  $\mathbf{f}_{th}(\mathbf{e})$  the hyperbolic tangent function in Appendix A

Since  $M(\mathbf{q})$  and  $K_P$  are positive definite matrices by definition and as  $K_P$  satisfies Eqn. (4.51), it is trivial to conclude that

$$\dot{\mathbf{e}}^T M(\mathbf{q}) \dot{\mathbf{e}} \geq \lambda_{min}[M(\mathbf{q})] \|\dot{\mathbf{e}}\|^2 \quad (4.55)$$

$$\mathbf{e}^T K_P \mathbf{e} \geq \lambda_{min}(K_P) \|\mathbf{e}\|^2 \quad (4.56)$$

$\forall \mathbf{q}, \mathbf{e}, \dot{\mathbf{e}} \in \mathbb{R}^6$ . Moreover, given the properties of the system, it is possible to find that:

$$\varepsilon \mathbf{f}_{th}(\mathbf{e})^T M(\mathbf{q}) \dot{\mathbf{e}} \geq -\varepsilon \lambda_{Max}[M(\mathbf{q})] \|\mathbf{e}\| \|\dot{\mathbf{e}}\| \quad (4.57)$$

Thus,  $V(t, \mathbf{e}, \dot{\mathbf{e}})$  is a radially unbounded positive definite function as it satisfies:

$$V \geq \frac{1}{2} \begin{bmatrix} \|\mathbf{e}\| \\ \|\dot{\mathbf{e}}\| \end{bmatrix}^T \begin{bmatrix} \lambda_{min}(K_P) & -\varepsilon \lambda_{Max}[M(\mathbf{q})] \\ -\varepsilon \lambda_{Max}[M(\mathbf{q})] & \lambda_{min}[M(\mathbf{q})] \end{bmatrix} \begin{bmatrix} \|\mathbf{e}\| \\ \|\dot{\mathbf{e}}\| \end{bmatrix} \quad (4.58)$$

The time derivative of the Lyapunov candidate function  $\dot{V}(t, \mathbf{e}, \dot{\mathbf{e}}) \in \mathbb{R}$  in Eqn. (4.54) is expressed as:

$$\dot{V} = -\dot{\mathbf{e}}^T K_V \dot{\mathbf{e}} - \varepsilon \mathbf{f}_{th}(\mathbf{e})^T K_P \mathbf{e} + \varepsilon \mathbf{f}_{th}(\mathbf{e})^T [C(\mathbf{q}, \dot{\mathbf{q}}) - K_V] \dot{\mathbf{e}} - \dot{\mathbf{e}}^T \mathbf{h}(\mathbf{e}, \dot{\mathbf{e}}) - \varepsilon \mathbf{f}_{th}(\mathbf{e})^T \mathbf{h}(\mathbf{e}, \dot{\mathbf{e}}) + \varepsilon \dot{\mathbf{f}}_{th}(\mathbf{e})^T M(\mathbf{q}) \dot{\mathbf{e}} \quad (4.59)$$

From Appendix A it follows that:

$$-\dot{\mathbf{e}}^T K_V \dot{\mathbf{e}} \leq -\lambda_{\min}(K_V) \|\dot{\mathbf{e}}\|^2 \quad (4.60)$$

$$\varepsilon \dot{\mathbf{f}}_{th}(\mathbf{e})^T M(\mathbf{q}) \dot{\mathbf{e}} \leq \varepsilon \lambda_{\max}[M(\mathbf{q})] \|\dot{\mathbf{e}}\|^2 \quad (4.61)$$

$$-\varepsilon \mathbf{f}_{th}(\mathbf{e})^T K_P \mathbf{e} \leq -\varepsilon \lambda_{\min}(K_P) \|\mathbf{f}_{th}(\mathbf{e})\|^2 \quad (4.62)$$

$$\varepsilon \mathbf{f}_{th}(\mathbf{e})^T K_V \dot{\mathbf{e}} \leq \varepsilon \lambda_{\max}(K_V) \|\dot{\mathbf{e}}\| \|\mathbf{f}_{th}(\mathbf{e})\| \quad (4.63)$$

$$\varepsilon \mathbf{f}_{th}(\mathbf{e})^T C(\mathbf{q}, \dot{\mathbf{q}})^T \dot{\mathbf{e}} \leq \varepsilon k_{C_1} \left( \|\dot{\mathbf{q}}_d\|_{\max} \|\dot{\mathbf{e}}\| \|\mathbf{f}_{th}(\mathbf{e})\| + \sqrt{6} \|\dot{\mathbf{e}}\|^2 \right) \quad (4.64)$$

$$-\dot{\mathbf{e}}^T \mathbf{h}(\mathbf{e}, \dot{\mathbf{e}}) \leq k_{h_1} \|\dot{\mathbf{e}}\|^2 + k_{h_2} \|\dot{\mathbf{e}}\| \|\mathbf{f}_{th}(\mathbf{e})\| \quad (4.65)$$

$$-\varepsilon \mathbf{f}_{th}(\mathbf{e})^T \mathbf{h}(\mathbf{e}, \dot{\mathbf{e}}) \leq \varepsilon k_{h_1} \|\dot{\mathbf{e}}\| \|\mathbf{f}_{th}(\mathbf{e})\| + \varepsilon k_{h_2} \|\mathbf{f}_{th}(\mathbf{e})\|^2 \quad (4.66)$$

$\dot{V}(t, \mathbf{e}, \dot{\mathbf{e}})$  in Eqn. (4.59) satisfies the inequality

$$\dot{V} \leq -\varepsilon \begin{bmatrix} \|\mathbf{f}_{th}(\mathbf{e})\| \\ \|\mathbf{e}\| \end{bmatrix}^T R_M(\varepsilon) \begin{bmatrix} \|\mathbf{f}_{th}(\mathbf{e})\| \\ \|\mathbf{e}\| \end{bmatrix} \quad (4.67)$$

with  $R_M(\varepsilon) \in \mathbb{R}^{2 \times 2}$  being

$$R_M(\varepsilon) = \begin{bmatrix} \lambda_{\min}(K_P) - k_{h_2} & -\left(a + \frac{k_{h_2}}{2\varepsilon}\right) \\ -\left(a + \frac{k_{h_2}}{2\varepsilon}\right) & \frac{1}{\varepsilon} [\lambda_{\min}(K_V) - k_{h_1}] - b \end{bmatrix} \quad (4.68)$$

thus  $\dot{V}(t, \mathbf{e}, \dot{\mathbf{e}})$  is a global definite negative function if the matrix  $R_M(\varepsilon)$  is definite positive which is guaranteed if the first element of the matrix and its determinant are strictly greater than zero. In this regard, it is sufficient and enough that:

$$\lambda_{\min}(K_P) > \frac{(2\varepsilon a + k_{h_2})^2}{4\varepsilon [\lambda_{\min}(K_V) - k_{h_1} - \varepsilon b]} + k_{h_2} \quad (4.69)$$

$$\lambda_{\min}(K_V) > k_{h_1} + \varepsilon b \quad (4.70)$$

With a proper selection of  $\varepsilon$ , the matrices  $K_P$  and  $K_V$  can be computed such that  $V(t, \mathbf{e}, \dot{\mathbf{e}})$  is a radially unbounded positive definite function and  $\dot{V}(t, \mathbf{e}, \dot{\mathbf{e}})$  is a globally negative definite function, thus the  $V(t, \mathbf{e}, \dot{\mathbf{e}})$  is a strict Lyapunov function and the system possesses globally asymptotically stability [82].

### Inner-Loop Control

The desired thrust and attitude of the vehicles are computed according to Eqns. (4.13) and (4.46). Taking into consideration the ML-UAS redundant actuation (6 DOFs and 8 actual control inputs, i.e.  $f_i$ ,  $\theta_{i,d}$  and  $t_{\beta_j}$ ), the desired orientation angle of the virtual actuators (rotorcrafts) is established to be  $\theta_{1,d} = \theta_{2,d} = \theta_{3,d} = \theta_d$  to avoid the prescribed condition. This assumption can be considered in Eqn. (4.13), leading to:

$$\mathbf{u}_\tau = \begin{bmatrix} u_x \\ u_z \\ u_{\Theta_1} \\ u_{\Theta_2} \\ u_{\beta_1} \\ u_{\beta_2} \end{bmatrix} = \begin{bmatrix} (f_1 + f_2 + f_3) S_{\theta_d} \\ (f_1 + f_2 + f_3) C_{\theta_d} \\ \frac{l_i}{2} (f_1 - f_2) C_{\Theta_1 - \theta_d} \\ \frac{l_i}{2} (f_2 - f_3) C_{\Theta_2 - \theta_d} \\ t_{\beta_1} \\ t_{\beta_2} \end{bmatrix} \quad (4.71)$$

Thus, the desired orientation of the UAVs is defined as:

$$\theta_d = \tan^{-1} \left( \frac{u_x}{u_z} \right) \quad (4.72)$$

Notice that  $u_z > 0$  as it tends to the total desired thrust.

The  $i^{th}$  vehicle is driven to  $\theta_d$  via a PD controller of the form:

$$u_{\theta_i} = K_{p_\theta} e_{\theta_i} + K_{v_\theta} \dot{e}_{\theta_i} \quad (4.73)$$

with  $K_{p_\theta}, K_{v_\theta} > 0 \in \mathbb{R}$  the proportional and derivative gains and  $e_{\theta_i}, \dot{e}_{\theta_i} \in \mathbb{R}$  the position and velocity errors of the  $i^{th}$  vehicle.

The stability proof and a detailed treatment of the controller are available at [82, 35].

The total thrust exerted by the vehicles is computed such that:

$$\mathbf{f}_d = \begin{bmatrix} f_1 \\ f_2 \\ f_3 \end{bmatrix} = \frac{1}{3} \begin{bmatrix} 1 & 2 & 1 \\ 1 & -1 & 1 \\ 1 & -1 & -2 \end{bmatrix} \begin{bmatrix} \sqrt{u_x^2 + u_z^2} \\ \frac{2}{l_i C_{\Theta_1 - \theta_d}} u_{\Theta_1} \\ \frac{2}{l_i C_{\Theta_2 - \theta_d}} u_{\Theta_2} \end{bmatrix} \in \mathbb{R}^3 \quad (4.74)$$

A detailed simulation was carried out in the next section considering close-to-reality scenarios.

## 4.4 Numerical Simulations and Results

In this track, three different operational conditions (labeled as  $c_1$ ,  $c_2$  and  $c_3$ ) were addressed via numerical simulations conducted in MATLAB/Simulink<sup>®</sup> 2018b (using an equipment with an 8GB RAM and an Inter<sup>®</sup> Core™ i5-8250 CPU @ 1.60 GHz & 1.80 GHz processor).

The aerial robotic system was intended to reach and track a trajectory  $\mathbf{q}_{d_{c_{1,2,3}}}$  provided in Table 4.1 (where  $t_a = t \in [0, 48]$ ,  $t_b = t \in [48, 72]$  and  $t_c = t \in [72, 120]$  stand for time intervals [s] and given in [m] and [deg], correspondingly. The simulation time and the sampling rate were set as  $t_{sim} = 120$  s and  $dt = 0.01$  s, respectively. The disturbances vector, given in the corresponding units ([N] and [Nm]), was defined, for each case, as  $\boldsymbol{\rho}_{c_1, c_2} = [1.5 \ 2 \cos(\frac{t\pi}{55}) \ -0.55 \cos(\frac{t\pi}{35}) \ -0.5 \sin(\frac{t\pi}{45}) \ 0.75]^T$  and

Table 4.1: Desired trajectories

$\mathbf{q}_{d_{c_1}}$	$\mathbf{q}_{d_{c_2}}$	$\mathbf{q}_{d_{c_3}}$
$-\sin\left(\frac{4\pi t}{t_{sim}}\right)$	$-1_{t_a}, 1_{t_b}, 2.5_{t_c}$	$0.05t$
$3 + \cos\left(\frac{4\pi t}{t_{sim}}\right)$	$2_{t_a}, 3_{t_b}, 1.5_{t_c}$	$3.5 + (2.75 - l_p) \cos\left(\frac{2\pi t}{t_{sim}}\right)$
$15 + 14.3 \cos\left(\frac{4\pi t}{t_{sim}}\right)$	30	$14.3 \cos\left(\frac{4\pi t}{t_{sim}}\right)$
-37	-45	$14.3 \cos\left(\frac{4\pi t}{t_{sim}}\right)$
25	0	15
$-28.6 \sin\left(\frac{4\pi t}{t_{sim}}\right)$	0	10

Table 4.2: Simulation parameters

Parameter	Parameters properties		
	Nominal value	Variance	
$m_r$	0.653 kg	0.00111111 kg <sup>2</sup>	
$m_l$	0.10 kg	0.0000693 kg <sup>2</sup>	
$m_{p_1}$	0.272 kg	0.0002775 kg <sup>2</sup>	
$m_{p_2}$	0.383 kg	0.0002775 kg <sup>2</sup>	
$l_l$	1.25 m	0.000544 m <sup>2</sup>	
$l_{p_1}, l_{p_2}$	0.5 m	0.0002775 m <sup>2</sup>	
$I_l$	0.172 kg m <sup>2</sup>	0.000100 kg <sup>2</sup> m <sup>4</sup>	
$g$	9.81 m s <sup>-2</sup>	0.004900 m <sup>2</sup> s <sup>-4</sup>	
Sensors parameters			
Sensor	Variance	Sensor	Variance
$x$	$2.3 \times 10^{-4} \text{ m}^2$	$\dot{x}$	$5 \times 10^{-4} \text{ m}^2 \text{ s}^{-2}$
$z$	$3.5 \times 10^{-4} \text{ m}^2$	$\dot{z}$	$6.5 \times 10^{-4} \text{ m}^2 \text{ s}^{-2}$
$\Theta_1, \Theta_2$	$2.6 \times 10^{-4} \text{ rad}^2$	$\dot{\Theta}_1, \dot{\Theta}_2$	$1.7 \times 10^{-4} \text{ rad}^2 \text{ s}^{-2}$
$\beta_1, \beta_2$	$2.3 \times 10^{-4} \text{ rad}^2$	$\dot{\beta}_1, \dot{\beta}_2$	$5.1 \times 10^{-5} \text{ rad}^2 \text{ s}^{-2}$
Disturbances parameters			
Disturbance		Variance	
$\rho_x, \rho_z$		$3 \times 10^{-4} \text{ N}^2$	
$\rho_{\Theta_1}, \rho_{\Theta_2}$		$1 \times 10^{-4} \text{ N}^2 \text{ m}^2$	
$\rho_{\beta_1}, \rho_{\beta_2}$		$7 \times 10^{-5} \text{ N}^2 \text{ m}^2$	



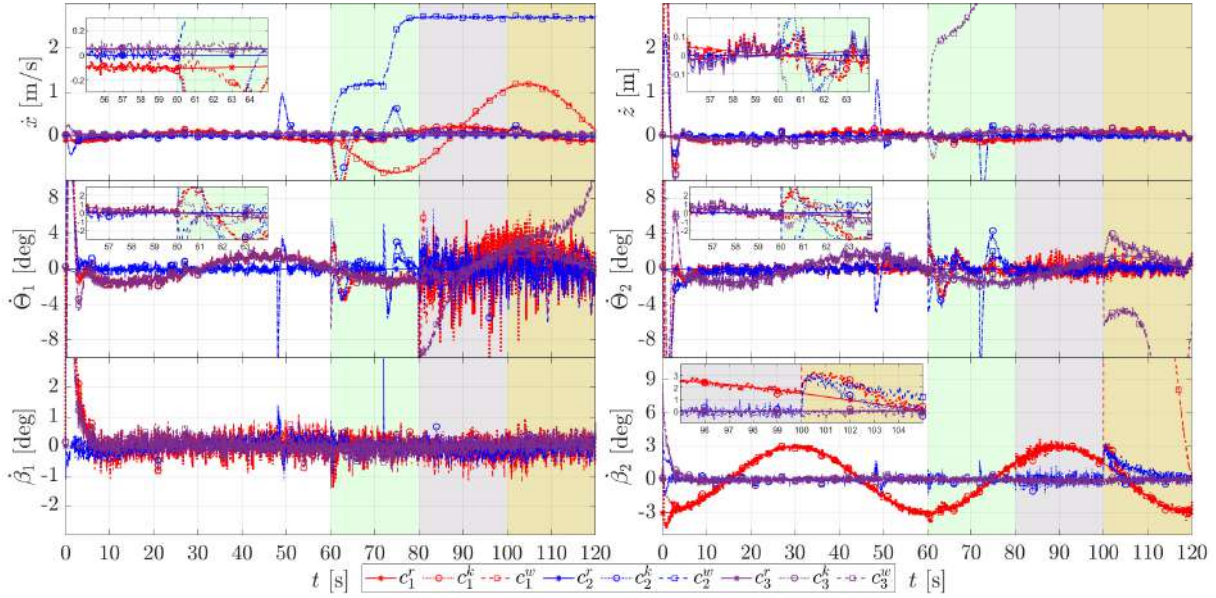


Figure 4.5: Velocities of the ML-UAS

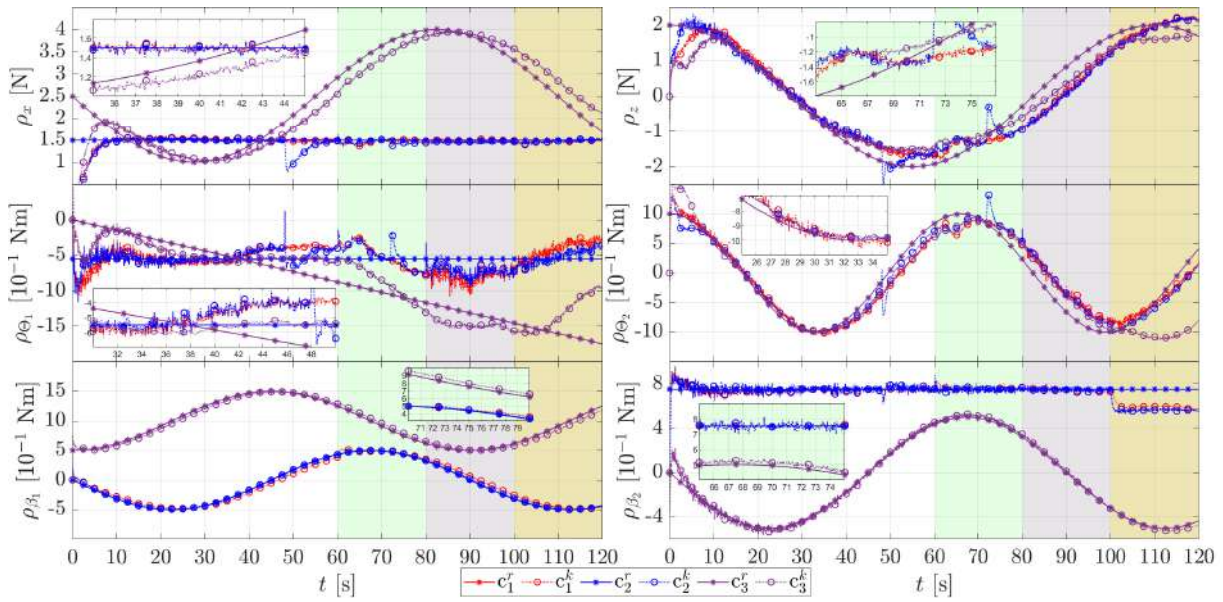


Figure 4.6: Disturbances estimation

performance is the product of an adequate estimation process which is further addressed and reinforced by the evidences provided in Figs. 4.6 and 4.7 where the disturbances estimation and the corresponding estimation errors are depicted, respectively.

Regarding the performance of the system in the presence of sensors faults, which clearly deteriorate the behavior of the flying chain, closing the loop with the states estimation tends to mitigate the adverse effects thus the states estimation could be used as a last safety measure to prevent a worst system response as long as reliable sensors data is still available as it is evident that the estimation tends to diverge in the absence of sensors information.

The response of the ASEKF provides a reliable estimation of the disturbances, even under the assumption of relative slow time varying dynamics  $\rho$ , within an acceptable margin [13, 147, 36] which is evidenced by the enhanced performance of the

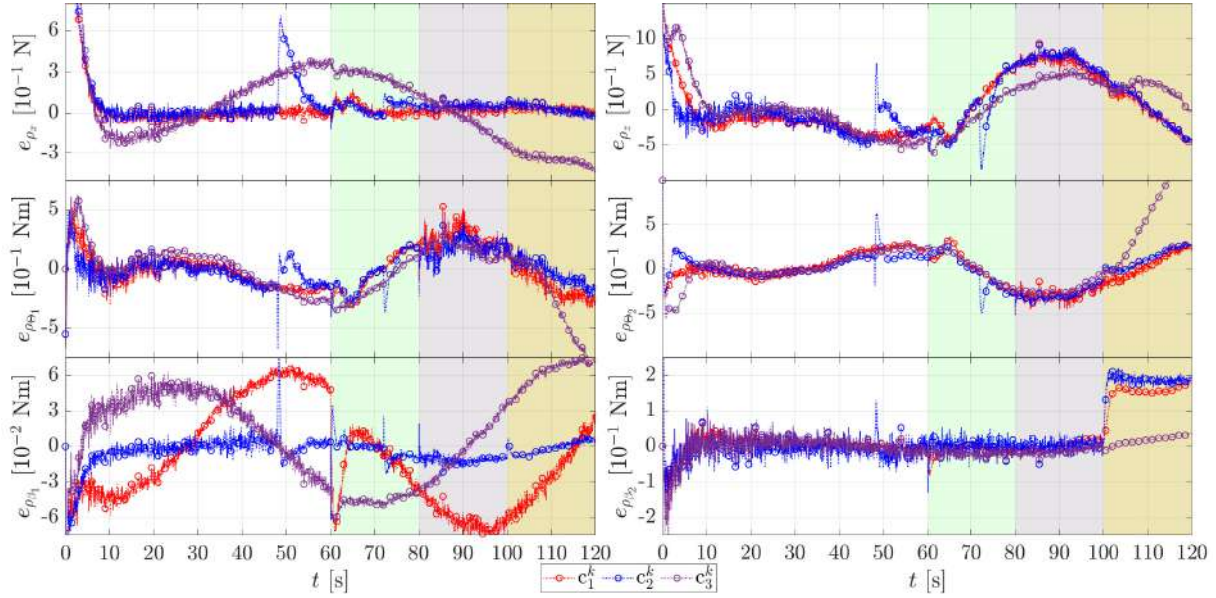


Figure 4.7: Estimation errors

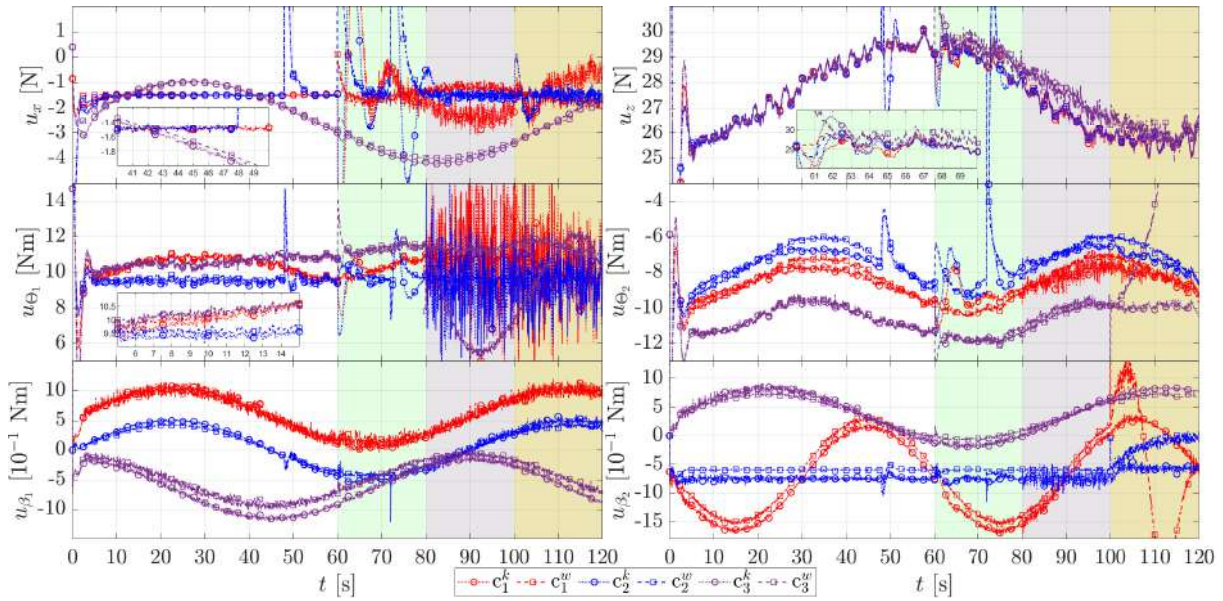


Figure 4.8: Controller response

ML-UAS, notwithstanding a phase change occurs due to the delayed action of the filter at considering the previous state and the computation time yet it still improves the performance of the system.

According to Eqns. (4.39)-(4.44), the estimated states depend on the process and sensors noises so do the controller response and the aircrafts as a consequence which can be appreciated in Figs. 4.8 and 4.9 respectively. The signals provided by the control law in Eqn. (4.46) slightly differ due to the disturbances compensation nevertheless, such difference impacts the overall performance of the chain as previously discussed. The presence of noise increases as less sensor data is available, in this regard, the loss of the  $\Theta_1$  and  $\Theta_2$  sensors seems to have a more prominent influence. These effects are translated to the vehicles in terms of thrust and orientation. The results suggest that the disturbances compensation affects mainly the attitude of

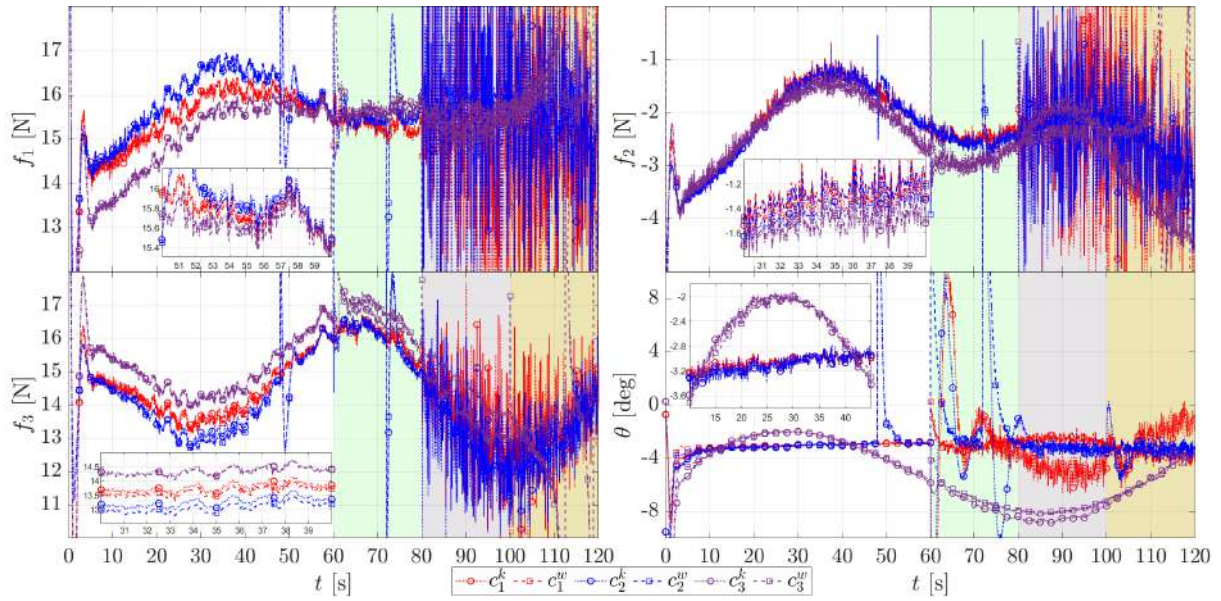


Figure 4.9: Aircrafts performance

the vehicles as the thrust is observed to act within the same operational range in all cases as similarly concluded in [36].



## **Part II**

# **Time-Delays on Unmanned Aerial Systems**



## Chapter 5

# Parametric Analysis of PID Delay-Based Controllers for Quadrotor UAVs

The structure of this chapter consists of 6 Sections which are outlined as follows. As it may have been noticed, [Section 5.1](#) provides a brief study of the literature and establishes the main contribution of the chapter. The description of the vehicle and the linearized representation of its dynamics are provided in [Section 5.2](#). The control scheme conceived for the aerial vehicle is described in [Section 5.3](#) where, the stability of the system subjected to the proposed time-delay control law is also studied. The stability charts as well as the results of numerical simulations are exposed in [Section 5.4](#); and, lastly, the concluding remarks are given in [Subsection 8.2.1](#).

### 5.1 Introduction

Unmanned Aerial Vehicles (UAVs) have witnessed the enlargement of their application spectrum in the last decades within several scientific and industrial fields. The technological surge has enabled such vehicles to be implemented in order to develop tasks as photography, surveillance, high-precision weather monitoring, parcel transport and delivering, precision agriculture and disaster assessment, among others.

To accomplish the aforementioned tasks, whereas these are performed by a single quadrotor or several of them, control theory has a critical role. In this vein, the literature gives evidence of the implementation of different control techniques as PD, PID and Sliding Mode to drive only one vehicle [\[49, 35\]](#) or a set of these [\[37, 36, 6, 38\]](#) during diverse operations. Yet, it is known that such feedback control schemes experience time-delays caused by the sensors intrinsic implementation, the remote communication process, the control scheme computation, the vision-based tracking systems, among others. In most of the cases, these time-delays tend to deteriorate the system's performance [\[155\]](#).

The stability of aerial vehicles operating under the influence of time-delays, as suggested by [\[159, 102\]](#), has been a matter of study in recent years. Particularly, UAVs affected by feedback time-delays caused by the sensing process or the image acquisition and treatment, has been addressed by different approaches which include transient response analysis by means of

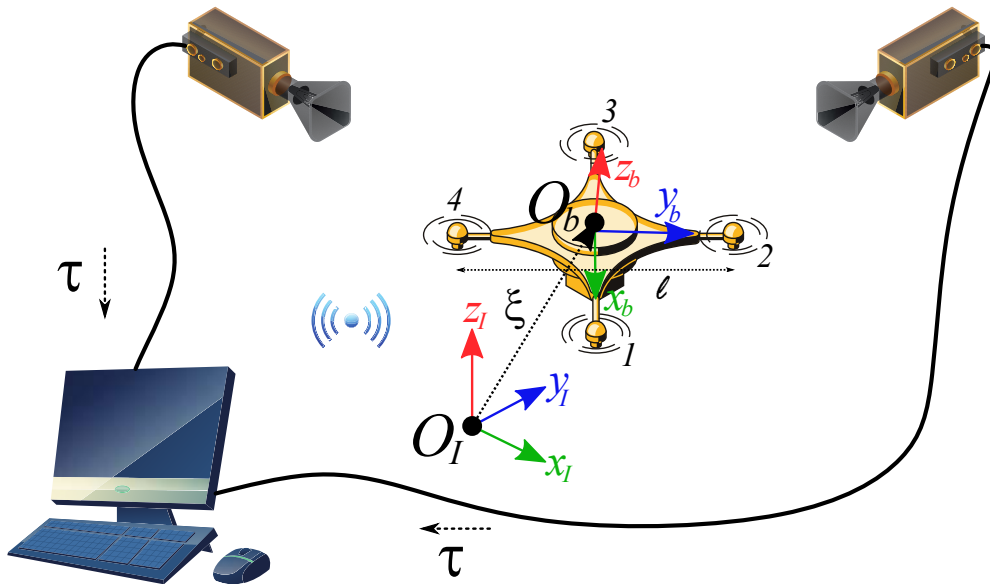


Figure 5.1: Quadrotor UAV and vision-based tracking system

Lambert W-functions [11] or LQI linear optimal control [151]. Even when such results are firmly grounded on experimentation, the implementation of linear controllers still restricts the range of operations in which aerial vehicles could be potentially used. In addition, the linear-based approach may lead to a slightly distinct behavior of the system when translated to real conditions and environments. Having such constraints in mind, the problem has also been treated by means of non-linear approaches as in [39, 174].

Time-delays in the communication channel that affect directly the generation and processing of control commands, have also been subjected to analysis, however, less attention has been focused on this subject [1, 98, 99]. On the other hand, the effects of time-delays in multi-agent UAVs systems have caught the attention of scientists worldwide. In [31], the impact of communication delays on a reliable flock of UAVs is studied, establishing the constraints over the time-delay communication. In this same regard, a consensus time-delay parametrization control scheme is presented and validated via numerical simulations in [6] meanwhile, the authors of [170] deal with this issue from a different perspective, they combine a nonlinear delayed controller with a model prediction control to maintain the formation with respect to the leader.

From a general perspective, and with base upon the evidence provided by the literature, one may conclude that the analysis of time-delays influences over UAVs is a research topic with exponential growth. In this sense, the actual chapter is devoted to the study of a single quadrotor driven by PID delay-based controllers. It is assumed that the position sensing is performed by a vision-tracking system whose cameras are located remotely, incorporating the time-delay in the control scheme of the translational states as a consequence of the cameras' latency. The chapter provides a set of stability charts which permits to select the proper set of control gains depending on the time-delay, the  $\sigma$ -stability criteria and the integral gain of the controller. To this end, the methodology relies on the availability of a linear model for control design purposes.

## 5.2 Quadrotor Modelling

In this section, the equations of motion of the quadrotor system in Fig. 5.1 (created from images available at *freepik.com*) are discussed. The dynamics of the system is described with respect to two reference frames: (i) the inertial frame  $O_I \{x_I, y_I, z_I\}$ , and (ii) the body frame  $O_b \{x_b, y_b, z_b\}$  whose origin matches the center of gravity (CoG) of the vehicle. Furthermore,  $x_b, y_b, z_b$  define to the roll, pitch and yaw axis which are aligned to the corresponding principal axis of inertia. The motion of a rigid body with 6 degrees of freedom (DoFs), which occurs to be the case of the aerial vehicle, can be fully described by the equations provided by the well-known Newton Euler formulation [35] as follows:

$$m\ddot{\boldsymbol{\xi}} + m\mathbf{g} = \boldsymbol{\tau}_\xi + \boldsymbol{\rho}_\xi \quad (5.1)$$

$$I\dot{\boldsymbol{\omega}} + \boldsymbol{\omega} \times (I\boldsymbol{\omega}) = \boldsymbol{\tau}_\omega \quad (5.2)$$

where  $m > 0$  is the mass of the vehicle and  $\mathbf{g} = [0 \ 0 \ g]^T$  comprises the constant of gravity acceleration  $g > 0$ . These equations are discussed in detail in the following lines.

The translational motion is described by Eqn. (5.1). Thus,  $\boldsymbol{\xi} = [x \ y \ z]^T \in \mathbb{R}^3$  denotes the position of the vehicle with respect to the inertial frame, and its first and second time derivatives stand for the velocity and acceleration, respectively.  $\boldsymbol{\tau}_\xi \in \mathbb{R}^3$  is the vector of external forces defined as:

$$\boldsymbol{\tau}_\xi = R_\eta \begin{bmatrix} 0 & 0 & T \end{bmatrix}^T \quad (5.3)$$

where the forces provided by the propellers  $f_i$  (with  $i = 1, 2, 3, 4$ ) conform the total thrust  $T$  in a sense that:

$$T = \sum_{i=1}^4 f_i \geq 0 \quad (5.4)$$

Furthermore, the rotation matrix  $R_\eta \in \mathbb{R}^{3 \times 3}$  provides a vector mapping from the body reference frame to the inertial reference frame. This matrix depends on the attitude of the vehicle described by the Euler angles  $\boldsymbol{\eta} = [\phi \ \theta \ \psi]^T \in \mathbb{R}^3$  (or roll, pitch and yaw angles, respectively) such that:

$$R_\eta = \begin{bmatrix} C_\theta C_\psi & S_\phi S_\theta C_\psi - C_\phi S_\psi & C_\phi S_\theta C_\psi + S_\phi S_\psi \\ C_\theta S_\psi & S_\phi S_\theta S_\psi + C_\phi C_\psi & C_\phi S_\theta S_\psi - S_\phi C_\psi \\ -S_\theta & S_\phi C_\theta & C_\phi C_\theta \end{bmatrix} \quad (5.5)$$

where  $C_{(\bullet)} = \cos(\bullet)$  and  $S_{(\bullet)} = \sin(\bullet)$ . Such an abuse of this notation is considered throughout the sequel of the chapter unless other is specified. Lastly, the vector  $\boldsymbol{\rho}_\xi = [\rho_x \ \rho_y \ \rho_z]^T \in \mathbb{R}^3$  represents the external unmodeled forces acting over the vehicle's CoG and that disturb its translational motion.

On the other hand, Eqn. (5.2) describes the rotational motion of the quadrotor in the body reference frame. The diagonal matrix  $I = \text{diag}\{I_x, I_y, I_z\} \in \mathbb{R}^{3 \times 3}$  contains the moments of inertia about the roll, pitch and yaw axis, respectively. The angular velocity vector  $\boldsymbol{\omega} = [p \ q \ r]^T \in \mathbb{R}^3$  is related to the Euler rates  $\boldsymbol{\eta} = [\dot{\phi} \ \dot{\theta} \ \dot{\psi}]^T \in \mathbb{R}^3$  in the sense that:

$$\boldsymbol{\omega} = W_{\boldsymbol{\eta}} \boldsymbol{\eta} \quad ; \quad W_{\boldsymbol{\eta}} = \begin{bmatrix} 1 & 0 & -S_{\theta} \\ 0 & C_{\phi} & S_{\phi} C_{\theta} \\ 0 & -S_{\phi} & C_{\phi} C_{\theta} \end{bmatrix} \in \mathbb{R}^{3 \times 3} \quad (5.6)$$

Finally, the vector  $\boldsymbol{\tau}_{\boldsymbol{\omega}} \in \mathbb{R}^3$  gathers the torques exerted by the propellers over the vehicle and it reads as:

$$\boldsymbol{\tau}_{\boldsymbol{\omega}} = \begin{bmatrix} \tau_x \\ \tau_y \\ \tau_z \end{bmatrix} = \begin{bmatrix} \ell(f_2 - f_4)/2 \\ \ell(f_3 - f_1)/2 \\ \alpha(f_1 - f_2 + f_3 - f_4) \end{bmatrix} \quad (5.7)$$

where  $\ell > 0$  denotes the diagonal motor-to-motor distance and  $\alpha > 0$  is a proportionality constant that relates the force produced by the propeller to the corresponding free moment in such a manner that  $\tau_i = \alpha f_i$ .

As mentioned in Section 5.1, the here-in studied approach addresses the influence of time-delays in the control system and relies on the availability of a linear model which can be obtained by recalling Eqns. (5.1) and (5.2) and considering the following assumptions [49, 35, 159, 102, 67]:

1. The vehicle does not perform acrobatic maneuvers. Thus, it operates in a quasi-hover state which implies that  $\phi \approx 0$  and  $\theta \approx 0$ .
2. Small-angle approximation leads to the definitions:  $S_{\phi} \approx \phi$  and  $C_{\phi} \approx 1$  which are equally valid for  $\theta$ .
3. For sake of simplicity and without loss of generality  $\forall t \geq 0$ ,  $\psi = 0$  (being  $t$  the time).
4. The Coriolis and Centripetal effects are neglected as the angular velocities are small enough such that the corresponding terms are smaller in comparison with the inertial ones.

Under these assumptions, Eqns. (5.1) and (5.2) are simplified and rewritten. Consequently, the motion of each DoF can be described by the following set of linear differential equations:

$$m\ddot{x} = \theta T \quad ; \quad I_x \ddot{\phi} = \tau_x; \quad (5.8)$$

$$m\ddot{y} = -\phi T \quad ; \quad I_y \ddot{\theta} = \tau_y; \quad (5.9)$$

$$m\ddot{z} + mg = T \quad ; \quad I_z \ddot{\psi} = \tau_z \quad (5.10)$$

The following section describes in detail the control scheme design using the linear formulation of the vehicle dynamics. Particularly, this analysis considers the frequential form of these equations. In other words, it uses the Laplace transform (with initials conditions set to zero) to obtain the frequency domain representation:

$$X(s) = \frac{1}{ms^2} \theta(s) T(s) ; \phi(s) = \frac{1}{I_x s^2} \tau_x(s); \quad (5.11)$$

$$Y(s) = -\frac{1}{ms^2} \phi(s) T(s) ; \theta(s) = \frac{1}{I_y s^2} \tau_y(s); \quad (5.12)$$

$$Z(s) = \frac{1}{ms^2} (T(s) - mg) ; \psi(s) = \frac{1}{I_z s^2} \tau_z(s) \quad (5.13)$$

where  $s = \sigma + j\omega$  is a complex variable with  $\sigma, \omega \in \mathbb{R}$ .

## 5.3 Control Scheme Design

The content of this section provides a discussion concerning the overall closed-loop control scheme proposal, it is also at this step where the influence of time-delays on the system is taken into account. It is worthy recalling that this relies as one of the main contributions of this chapter. In this regard, and as depicted in Fig. 5.1, the feedback time-delay is considered and thus, denoted by a positive fixed value  $\tau \in \mathbb{R}$ . The time-delay  $\tau$  is the time taken by the position-sensing process to treat and send the information back to the external workstation [42].

Considering the frequency domain representation provided in Eqn. (5.13), it is straightforward to conclude that the dynamics of  $z$  and that of  $\psi$  are decoupled. In this regard, the thrust  $T(s)$  is used as a control input to drive the system to a desired height  $z_d \in \mathbb{R}$ , and the torque  $\tau_z(s)$  is intended to keep the vehicle yaw angle at  $\psi_d = 0$ . Both control inputs are respectively defined by linear controllers as follows:

$$T(s) = m(C_z(s) + g) \quad (5.14)$$

$$\tau_z(s) = I_z C_\psi(s) \quad (5.15)$$

Since the translational dynamics of the aircraft is considered to be disturbed by external unmodeled phenomena, the widely studied PD controller does not ensure to drive and keep the vehicle at the desired position [159, 102, 35, 128] thus, the linear controller  $C_v(s)$  (with  $v \in \xi$ ) is selected to be a PID controller of the form:

$$C_v(s) = k_{p_v} + k_{d_v} s + k_{i_v} s^{-1} \quad (5.16)$$

where  $k_{p_v}, k_{d_v}, k_{i_v} \in \mathbb{R}$  stand for the corresponding proportional, derivative and integral gains whose definition is provided in the upcoming sections of the chapter.

Since the rotational motion is assumed undisturbed, the controller of the  $\psi$  motion is defined as a PD controller of the form  $C_\psi(s) = k_{p_\psi} + k_{d_\psi} s$ , equally adopted for all the controllers regarding the orientation of the vehicle.

Due to its under-actuated nature, the system features a rotational-translational nested control structure. The inner-loop, corresponding to the rotational dynamics, is thus faster than the outer-loop driving the translation; in practice, most of the inner-loop controllers (based on embedded/on-board inertial sensory modules) are considered time-delay-free [102, 159] nevertheless, the

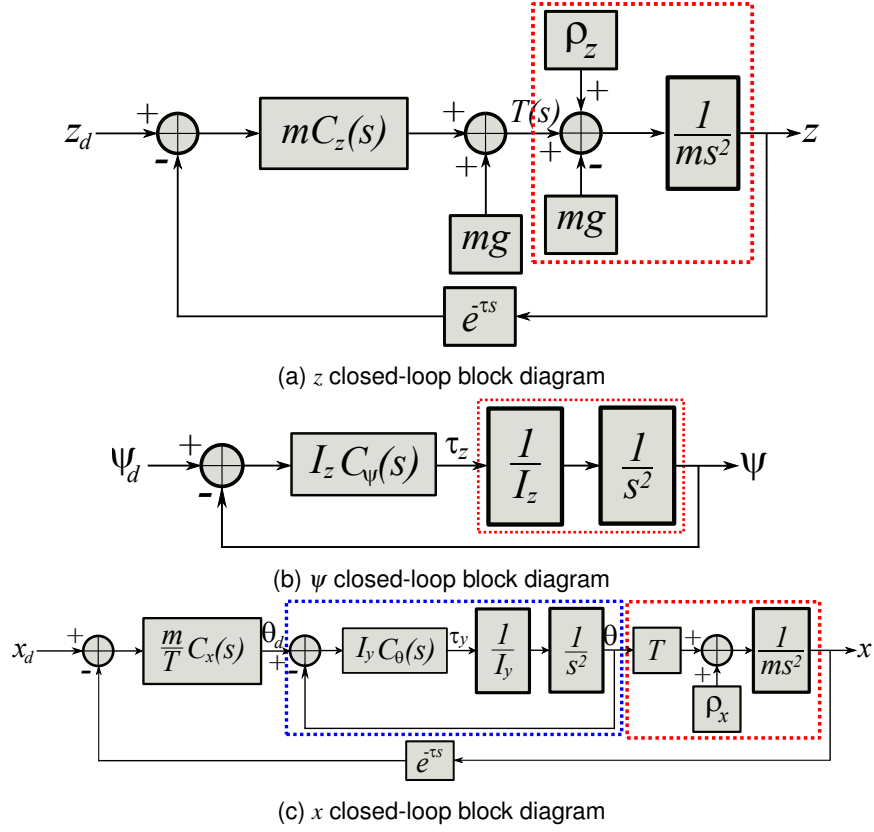


Figure 5.2: Quadrotor block diagrams

translational dynamics is subjected to time-delays as previously explained. In this vein, Figs. 5.2a and 5.2b respectively describe the closed-loop dynamics of the  $z$  and  $\psi$  DoFs where the time-delay is introduced and the plant dynamics is highlighted by a red dashed box.

From Figs. 5.2a and 5.2b, and considering a proper selection of the control gains, it can be concluded that, for a large enough time,  $T(s) \rightarrow mg$  and  $\tau_z(s) \rightarrow 0$  [159, 102]. On the other hand, Eqns. (5.11) and (5.12) give evidence of the existing couplings between the  $x$  and  $\theta$  motions and the  $y$  and  $\phi$  dynamics. In this regard,  $\theta(s)T(s)$  and  $-\phi(s)T(s)$  are considered to be the control inputs for the  $x$  and  $y$  degrees of freedom, respectively, which reads as follows:

$$\theta(s)T(s) = mC_x(s) \quad ; \quad -\phi(s)T(s) = mC_y(s) \quad (5.17)$$

Thus, from Eqn. (5.17), the reference values  $\theta_d \in \mathbb{R}$  and  $\phi_d \in \mathbb{R}$  are computed as a function of the controller in Eqn. (5.16) and the prescribed assumptions, in such a manner that:

$$\phi_d(s) = -\frac{mC_y(s)}{T} \quad ; \quad \theta_d(s) = \frac{mC_x(s)}{T} \quad (5.18)$$

The previous reference values are achieved by the action of the linear controllers  $C_\phi(s)$  and  $C_\theta(s)$  whose gains can be properly selected such that the corresponding (inner) rotational dynamics is faster than that of translation.

Assuming the existence of the time-delay  $\tau$  due to the position sensing process as previously explained, the diagram block of

the translational DoF  $x$  is depicted in Fig. 5.2c (the  $y$  dynamics is omitted as it follows the same structure with the corresponding adaptations) where it is possible to appreciate the inner rotational dynamics (blue dashed box) and the respective translational motion dynamics (red dashed box).

For instance, let the inner (rotational) dynamics as depicted in Fig. 5.2c be expressed as a single transfer function block of the form:

$$H_{\phi,\theta}(s) = \frac{P_{\phi,\theta}(s)}{Q_{\phi,\theta}(s)} = \frac{k_{d_{\phi,\theta}}s + k_{p_{\phi,\theta}}}{s^2 + P_{\phi,\theta}(s)} \quad (5.19)$$

The stability analysis of the quadrotor UAV as well as the definitions of the control gains are provided in the upcoming section.

For a suitable analysis, the rotational dynamics is treated separately from the translational dynamics as it does not depend on the time-delay. The main goal of the current section is to define the control gains of the translational linear controllers such that the system stability is guaranteed for a given time-delay.

### 5.3.1 Rotational Dynamics Stability

From the system described by Eqn. (5.15) and Fig. 5.2b, it is possible to find the control gains that ensure the stability of the system in matters of rotation. In this regard, the analysis of the  $\psi$  dynamics is presented only.

Recalling Eqn. (5.15), it is enough and sufficient that the roots of the characteristic closed-loop function:

$$\Delta_{\psi}(s) = s^2 + k_{d_{\psi}}s + k_{p_{\psi}} \quad (5.20)$$

be on the left-side plane of the complex space. For the PD controller, it is sufficient to define the control gains as  $k_{p_{\psi}}, k_{d_{\psi}} \in \mathbb{R}^+$  to ensure the stability of the system.

The previous results can be translated to the  $\phi$  and  $\theta$  dynamics to ensure the stability of the inner dynamics block exemplified in Fig. 5.2c. Thus, for a given set of control gains regarding the rotational motion of the body and a predefined time-delay, the stability analysis of the translational DoFs is presented next.

### 5.3.2 Time-Delay Theoretical Definitions

As this dynamics includes the effects of a time-delay, some definitions (established at [68]) are cited and adapted to the current case of study in order to perform the stability analysis afterwards.

1. For a given time-delay  $\tau > 0$ , and a linear controller with gains  $k_1, k_2 \in \mathbb{R}$ , the *frequency crossing set*  $\Omega \subset \mathbb{R}$  is the set of all frequencies  $\omega$  such that there exists at least a triplet  $(k_1, k_2, \tau)$  for which the closed-loop characteristic function  $\Delta(s; k_1, k_2, \tau)$  satisfies:

$$\Delta(s; k_1, k_2, \tau) = 0 \quad (5.21)$$

2. The *stability crossing curves*  $T$  is the set of all parameters  $(k_1, k_2, \tau) \in \mathbb{R}^2 \times \mathbb{R}^+$  for which there exists at least one  $\omega \geq 0$  such that  $\Delta(s; k_1, k_2, \tau) = 0$ . For a fixed time-delay value  $\tau^* > 0$ , any point  $\mathbf{k} = [k_1 \ k_2]^T \in T$  is known as a *crossing point*.

3. The *sigma stability* problem can be described as the task of determining the controller gains  $k_1, k_2$  for which the real part of the rightmost roots of the characteristic function of the closed-loop system, is smaller than  $\sigma < 0$ .

In this regard, the stability regions for the translational motion of the vehicle are provided, yet, let the closed-loop transfer functions for the  $x$  and  $z$  motion,  $G_{x,z}(s)$ , be defined. From Figs. 5.2a and 5.2c, the transfer functions of the  $z$  and  $x$  dynamics are found such that:

$$G_z(s) = \frac{C_z(s)}{s^2 + e^{-\tau s} C_z(s)} \quad (5.22)$$

$$G_x(s) = \frac{C_x(s) P_\theta(s)}{Q_\theta(s) s^2 + e^{-\tau s} C_x(s) P_\theta(s)} \quad (5.23)$$

For the transfer function in Eqn. (5.23), it is assumed that the control gains of the rotational motion have been already selected and fixed with base on the result of Subsection 5.3.1 thus, the main goal of the analysis is to define the gains of the controllers  $C_x(s)$  and  $C_z(s)$ .

### 5.3.3 PID Controllers Analysis

The main issue emerging at analyzing time-delay systems subjected to the action of a PID controller, is the fact that there exist more gains to determine than equations to solve. In this regard, [92] suggest to establish a proportional relation between two of these gains such as  $k_d = k_i / \gamma$  where  $\gamma > 0$  is the constant of proportionality. The latest limits the spectra of possible gains to be selected nonetheless, the proposal of this work is to choose a fixed value for  $k_i$  and to find the corresponding  $k_p$  and  $k_d$  based on parametric stability charts ( $\tau$ ,  $k_i$  and  $\sigma$ ). Before proceeding, one must ensure that the tuning of the controllers of the rotational motion has been properly done (see Subsection 5.3.1).

Recalling Eqns. (5.22) and (5.23), and assuming that  $k_{i_{x,z}} > 0 \in \mathbb{R}$ , the characteristic functions of the corresponding DoFs under the influence of a PID controller can be written as:

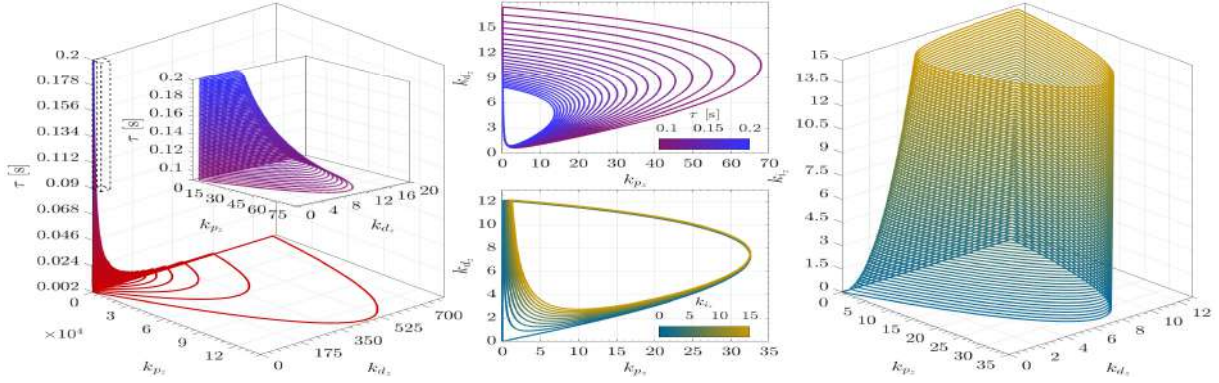
$$\Delta_z(s) = s^3 + e^{-\tau s} (k_{d_z} s^2 + k_{p_z} s + k_{i_z}) \quad (5.24)$$

$$\Delta_x(s) = (s^2 + P_\theta(s)) s^3 + e^{-\tau s} (k_{d_x} s^2 + k_{p_x} s + k_{i_x}) P_\theta(s) \quad (5.25)$$

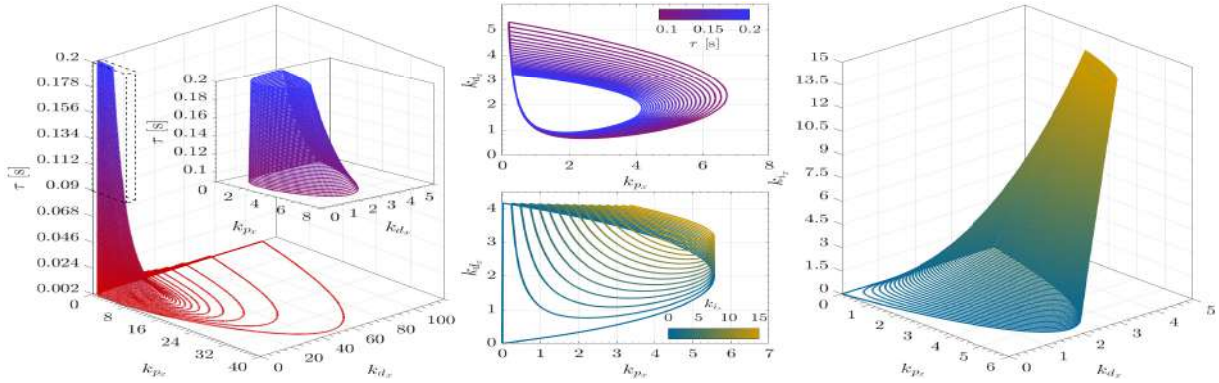
Considering  $s = j\omega$  with  $\omega > 0$  and solving  $\Delta_z(j\omega) = 0$  and  $\Delta_x(j\omega) = 0$ , respectively, the corresponding pairs of gains can be computed from:

$$\begin{bmatrix} 1 & 0 \\ 0 & \omega \end{bmatrix} \begin{bmatrix} k_{p_z} \\ k_{d_z} \end{bmatrix} = R_{\tau\omega} \begin{bmatrix} \omega^2 \\ 0 \end{bmatrix} + \mathfrak{K}_{i_z} \quad (5.26)$$

$$\begin{bmatrix} \mathfrak{A}_\theta & -\mathfrak{B}_\theta \omega \\ \mathfrak{B}_\theta & \mathfrak{A}_\theta \omega \end{bmatrix} \begin{bmatrix} k_{d_x} \\ k_{p_x} \end{bmatrix} = R_{\tau\omega} \begin{bmatrix} k_{p_\theta} \omega^2 - \omega^4 \\ k_{d_\theta} \omega^3 \end{bmatrix} + \mathfrak{K}_{i_x} \quad (5.27)$$



(a)  $z$  stability regions. Left: for  $k_{i_z} = 1$  and  $0.002 \leq \tau \leq 0.2$  [s]. Right: for  $0 \leq k_{i_z} \leq 15$  and  $\tau = 0.13$  [s]. Center:  $k_{p_x}$ - $k_{d_x}$  plane views.



(b)  $x$  stability regions. Left: for  $k_{i_x} = 1$  and  $0.002 \leq \tau \leq 0.2$  [s]. Right: for  $0 \leq k_{i_x} \leq 15$  and  $\tau = 0.13$  [s]. Center:  $k_{p_x}$ - $k_{d_x}$  plane views.

Figure 5.3: Stability regions

with:

$$R_{\tau\omega} = \begin{bmatrix} C_{\tau\omega} & -S_{\tau\omega} \\ S_{\tau\omega} & C_{\tau\omega} \end{bmatrix} \in \mathbb{R}^{2 \times 2} \quad (5.28)$$

$$\mathfrak{R}_{i_z} = \begin{bmatrix} 0 \\ k_{i_z}/\omega \end{bmatrix}; \mathfrak{R}_{i_x} = \begin{bmatrix} -k_{i_x}k_{d_\theta} \\ k_{i_x}k_{p_\theta}/\omega \end{bmatrix} \in \mathbb{R}^2 \quad (5.29)$$

$$\mathfrak{A}_\theta = k_{p_\theta}; \mathfrak{B}_\theta = k_{d_\theta}\omega \quad (5.30)$$

The analysis of the special case in which  $\omega = 0$  implies the definition and solution of the corresponding characteristic functions thus, one finds that:

$$\Delta_z(0) = k_{i_z} = 0 \quad (5.31)$$

$$\Delta_x(0) = k_{i_x}k_{p_\theta} = 0 \quad (5.32)$$

In this scenario, the only value of  $k_{i_x}$  that satisfies the previous equations is 0, since  $k_{p_\theta} > 0$ . It is worth highlighting the fact

that such value of  $k_{i_v}$  modifies the controller and turns it into a PD controller which has been widely treated in the literature [102, 159, 68] and whose stability curve for  $\omega = 0$  is defined by the gains:

$$\begin{bmatrix} k_{p_{z,x}} \\ k_{d_{z,x}} \end{bmatrix} = \begin{bmatrix} 0 \\ \in \mathbb{R} \end{bmatrix} \quad (5.33)$$

The sigma stability curves and regions can be obtained by considering  $s = \sigma + j\omega$  and solving Eqns. (5.24) and (5.25) to find the gains as previously discussed. In this regard, the corresponding gains pairs are defined according to the expressions:

$$\begin{bmatrix} 1 & \sigma \\ 0 & \omega \end{bmatrix} \begin{bmatrix} k_{p_z} \\ k_{d_z} \end{bmatrix} = e^{\tau\sigma} R_{\tau\omega} \begin{bmatrix} \mathfrak{R}_z \\ \mathfrak{I}_z \end{bmatrix} + \mathfrak{R}_\sigma^{i_z} \quad (5.34)$$

$$\begin{bmatrix} P_\theta(\sigma) & \mathfrak{A}_x \\ \mathfrak{B}_\theta & \mathfrak{B}_x \end{bmatrix} \begin{bmatrix} k_{p_x} \\ k_{d_x} \end{bmatrix} = e^{\tau\sigma} R_{\tau\omega} \begin{bmatrix} \mathfrak{R}_\theta \\ \mathfrak{I}_\theta \end{bmatrix} + \mathfrak{R}_\sigma^{i_x} \quad (5.35)$$

with

$$\mathfrak{R}_\sigma^{i_z} = \frac{k_{i_z}}{\sigma^2 + \omega^2} \begin{bmatrix} -\sigma \\ \omega \end{bmatrix} \in \mathbb{R}^2 \quad (5.36)$$

$$\mathfrak{R}_\sigma^{i_x} = \frac{k_{i_x}}{\sigma^2 + \omega^2} \begin{bmatrix} -P_\theta(\sigma)\sigma - \mathfrak{B}_\theta\omega \\ \mathfrak{A}_\theta\omega \end{bmatrix} \in \mathbb{R}^2 \quad (5.37)$$

$$\mathfrak{A}_x = P_\theta(\sigma)\sigma - \mathfrak{B}_\theta\omega \quad ; \quad \mathfrak{B}_x = P_\theta(\sigma)\omega + \mathfrak{B}_\theta\sigma \quad (5.38)$$

$$\mathfrak{R}_z = \omega^2 - \sigma^2 \quad ; \quad \mathfrak{I}_z = -2\sigma\omega \quad (5.39)$$

$$\mathfrak{R}_\theta = \mathfrak{R}_z(P_\theta(\sigma) - \mathfrak{R}_z) - \mathfrak{I}_z(\mathfrak{B}_\theta - \mathfrak{I}_z) \quad (5.40)$$

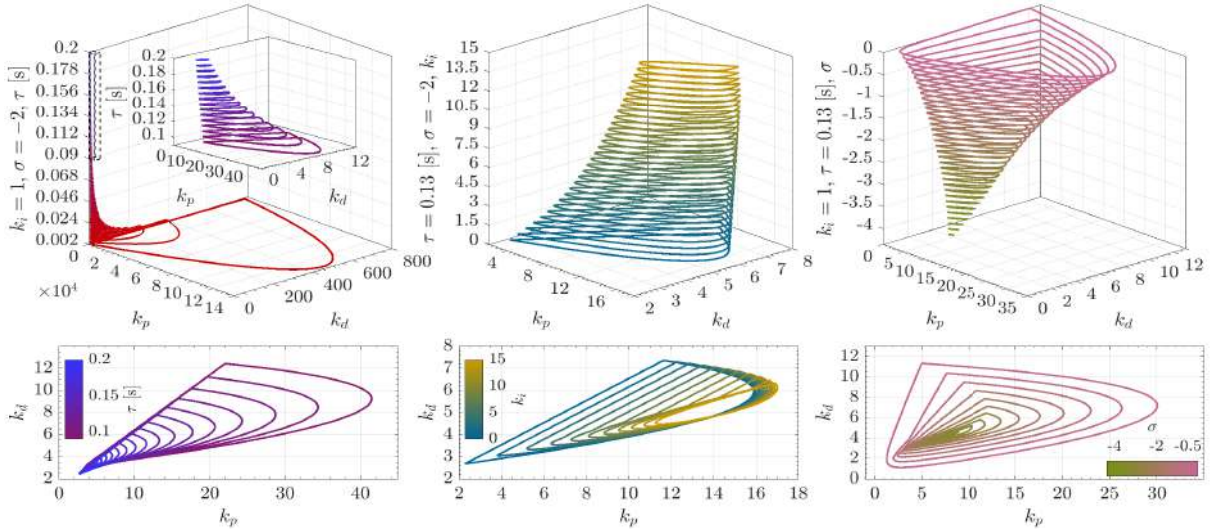
$$\mathfrak{I}_\theta = \mathfrak{R}_z(\mathfrak{B}_\theta - \mathfrak{I}_z) + \mathfrak{I}_z(P_\theta(\sigma) - \mathfrak{R}_z) \quad (5.41)$$

For the particular case where  $s = \sigma$ , i.e.  $\omega = 0$ , it follows that each control gains pair in  $\mathbb{R}^2$  defines a crossing curve if the expressions below are satisfied for the corresponding DoF.

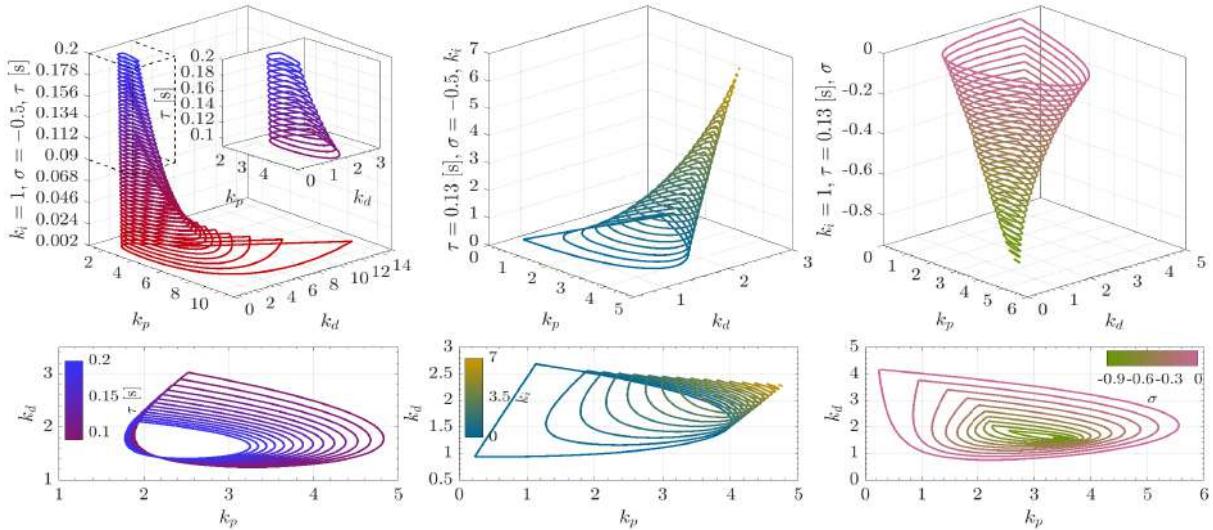
$$k_{d_z}\sigma + k_{p_z} = -e^{\tau\sigma}\sigma^2 - \frac{k_{i_z}}{\sigma} \quad (5.42)$$

$$k_{d_x}\sigma + k_{p_x} = -e^{\tau\sigma}\sigma^2 \left( \frac{\sigma^2}{P_\theta(\sigma)} + 1 \right) - \frac{k_{i_x}}{\sigma} \quad (5.43)$$

The stability regions and crossing curves are presented in the following section alongside the results of numerical control simulations.



(a) z sigma stability regions. Left: for  $k_{i_z} = 1, \sigma = -2$  and  $0.002 \leq \tau \leq 0.2$  [s]. Center: for  $0 \leq k_{i_z} \leq 15, \sigma = -2$  and  $\tau = 0.13$  [s]. Right: for  $k_{i_z} = 1, -4.2 \leq \sigma \leq 0$  and  $\tau = 0.13$  [s].



(b) x sigma stability regions. Left: for  $k_{i_x} = 1, \sigma = -0.5$  and  $0.002 \leq \tau \leq 0.2$  [s]. Center: for  $0 \leq k_{i_x} \leq 7, \sigma = -0.5$  and  $\tau = 0.13$  [s]. Right: for  $k_{i_x} = 1, -0.95 \leq \sigma \leq 0$  and  $\tau = 0.13$  [s].

Figure 5.4: Sigma stability regions

## 5.4 Results

The current section is intended to expose the stability charts of the quadrotor and the numerical validation of these by simulations which were performed taking into consideration the linearized model of the vehicle in Eqns. (5.11) - (5.13) and the 6 DoFs dynamic model provided by Eqns. (5.1) and (5.2).

Let one recall the results exposed in [159, 102] which concern the PD controller for quadrotor systems subjected to time-delays; in this regard, the results introduced in the aforementioned works, differ from the ones obtained herein in the  $\hat{\mathcal{R}}_{i_v}$  and  $\hat{\mathcal{R}}_{i_\sigma}^{iv}$  terms at the right part of Eqns. (5.26) - (5.43). Such terms are related to the corresponding integral gains and are discussed in the sequel of the section.

### 5.4.1 Stability Charts

Recalling Section 5.3 to obtain the stability charts of the vehicle regarding the motion along  $x_I$  and  $y_I$ , the gains of the controllers that stabilize the rotational dynamics should be defined first. In this sense, the gains of the rotational controllers were set as  $k_{p_{\phi, \theta, \psi}} = 20$  and  $k_{d_{\phi, \theta, \psi}} = 5$  [102].

With base on the definitions provided in Subsection 5.3 and the frequency sweeping technique for analyzing time-delay systems [95], the stability regions for the given systems can be found. Figs. 5.3a and 5.3b show, respectively, the stability regions for the  $z$  and  $x$  DoFs under the prescribed conditions. In such plots the red-to-blue color gradient represents the variation on  $\tau$  and the blue-to-yellow color gradient is used to indicate the behavior of the stability regions according to the corresponding gain  $k_i$ . For both controllers, it can be appreciated that the regions stretch as  $\tau$  or  $k_i$  increases. Due to the coupling between the rotational and the translational dynamics, the stability region of the  $x$  PID controller is significantly smaller than that of the  $z$  PID controller.

Regarding the  $\sigma$ -stability analysis; Figs. 5.4a and 5.4b show, correspondingly, the sigma stability regions for the  $z$  and  $x$  controllers. In such figures, the pink-to-green color gradient represents the  $\sigma$  variation. The introduction of the aforementioned figures permits to observe the parametric variation of the sigma stability regions. In this sense, the figures that depict the variation of the stability regions w.r.t.  $\sigma$  may lead to find the maximum  $\sigma$ -stability, that is the minimal value of  $\sigma$  at which the rightmost root of the quasi-polynomial can be placed; due to this fact, different intervals of sigma were defined for the controllers. In the same manner, one can observe that a great value of the  $k_i$  gain may cause that the  $\sigma$ -stability region stretches to the point of almost being empty (as depicted in Fig. 5.4b). Special attention may be payed also to the singularity of Eqn. (5.35) found at  $\sigma = -k_{p_{\theta}}/k_{d_{\theta}}$ , which for the current case of study corresponds to  $-4$  that is out of the boundary defined by the maximum *sigma*-stability.

### 5.4.2 Control Simulations

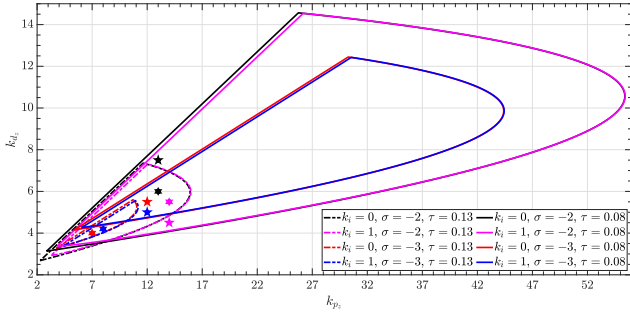
In order to validate the effectiveness of the previous results, numerical simulations<sup>1</sup> were conducted using an equipment with an 8GB RAM and an Intel<sup>®</sup> Core™ i5-8250 CPU @ 1.60 GHz & 1.80 GHz processor. In this regard, the simulations considered the set of parameters provided in Table 5.1.

Different scenarios were considered to perform the numerical simulations. In this regard, one scenario considered a constant fixed point in the space as a desired reference to be reached by the vehicle. In such simulation, the controllers gains were selected to satisfy the  $\sigma$ -stability criteria. For the  $z$  controller, the gains were tuned to ensure that the rightmost roots of the quasi-polynomial

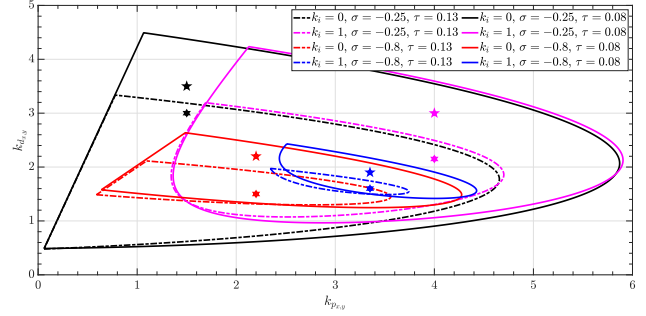
<sup>1</sup>MATLAB/Simulink<sup>®</sup> 2018b

Table 5.1: Simulation parameters

Parameter	Nominal value
$m$	0.675 kg
$I_x, I_y$	0.271 kg m <sup>2</sup>
$I_z$	0.133 kg m <sup>2</sup>
$\ell$	0.45 m
$g$	9.81 m/s <sup>2</sup>
$\alpha$	0.34 m



(a)  $z$  PID controllers' gains within the stability regions



(b)  $x(y)$  PID controllers' gains within the stability regions

Figure 5.5: controllers' gains within the stability regions

stay at the left side of the plane defined by  $\sigma = -3$  meanwhile, for the  $x$  and  $y$  controllers, the reference  $\sigma$  value was chosen to be  $-0.25$ . The second scenario considered a ramp signal as a reference input for the position of the aircraft. In this case, the controller of the  $z$  motion was tuned to guarantee that the rightmost roots of the corresponding quasi-polynomial lay at the left of the plane defined by  $\sigma = -2$ , in this same regard, the controllers of the  $x$  and  $y$  motions were conceived to ensure that the roots of the characteristic functions be found at the left of the plane  $\sigma = -0.8$ .

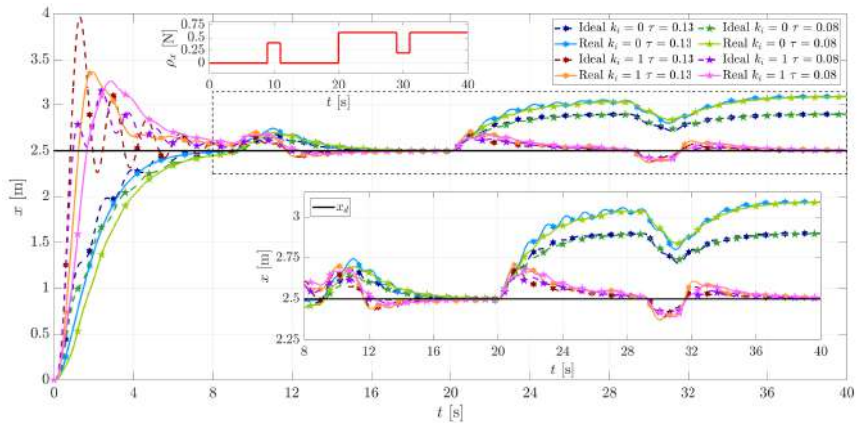
For both of the cases explained, the special case where  $k_{i_v} = 0$  was considered to observe the behavior of the system in the presence of external disturbances and compare it with the performance of the system driven by a PID controller in which  $k_{i_v} = 1$ . Additionally, two different values for the time-delay were taken into consideration, these values were set as 0.08 and 0.13 [s]. The overall information concerning the gains of the controllers is summarized in [Table 5.2](#)

In addition to what is exposed in [Table 5.2](#), [Figs. 5.5a](#) and [5.5b](#) depict the selected gains within the corresponding stability regions. In these plots, the points represented by a  $\star$  correspond to the gains chosen for the time-delay value of 0.08 [s] meanwhile, the rest of the points are referred to the gains of the controllers operating with a feedback time-delay of 0.13 [s].

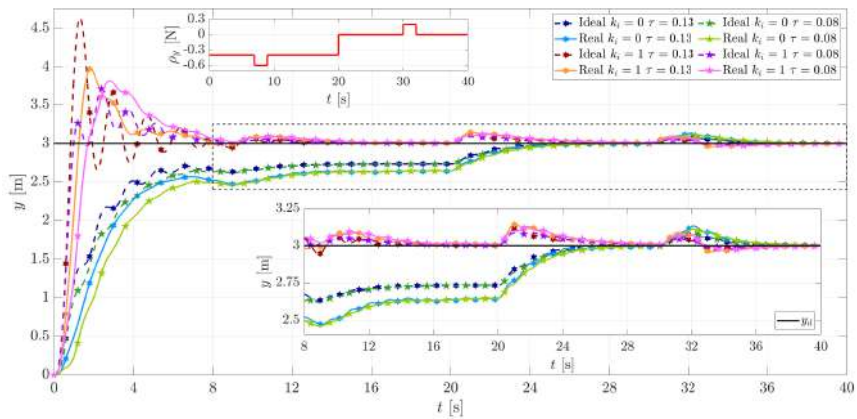
The performance of the vehicle, subjected to the first simulation conditions, is exposed throughout [Figs. 5.6a](#) - [5.7c](#). In this regard, one may find that some curves are referred to with the legend "Ideal" or "Real", such legends denote the dynamic model used to carry out the simulation; the "Ideal" responses represent those of the simulation where the linearized model was used, on the other hand, the word "Real" denotes the response of the non-linear quadrotor system.

Table 5.2: Translational controllers gains

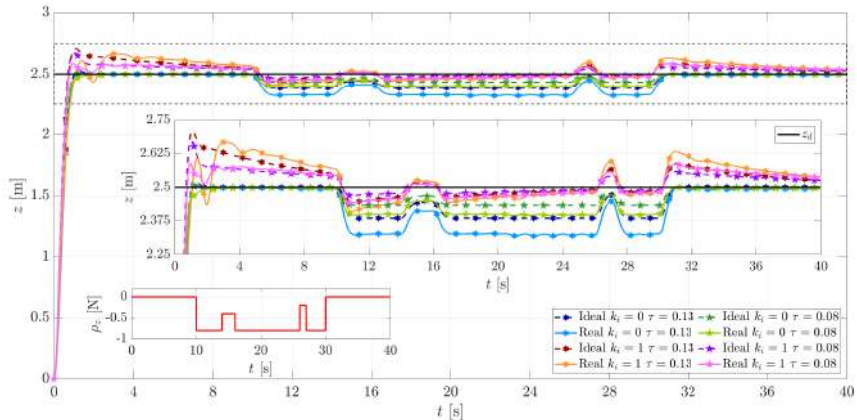
$\sigma$	Gain	$k_{i_v} = 0$		$k_{i_v} = 1$		Input
		$\tau = 0.08$	$\tau = 0.13$	$\tau = 0.08$	$\tau = 0.13$	
-3	$k_{p_z}$	12	7	12	8	Step
	$k_{d_z}$	5.5	4	5	4.2	
-0.25	$k_{p_{x,y}}$	1.5	1.5	4	4	Step
	$k_{d_{x,y}}$	3.5	3	3	2.15	
-2	$k_{p_z}$	13	13	14	14	Ramp
	$k_{d_z}$	7.5	6	4.5	5.5	
-0.8	$k_{p_{x,y}}$	2.2	2.2	3.35	3.35	Ramp
	$k_{d_{x,y}}$	2.2	1.5	1.9	1.6	



(a) Displacement along  $x_I$



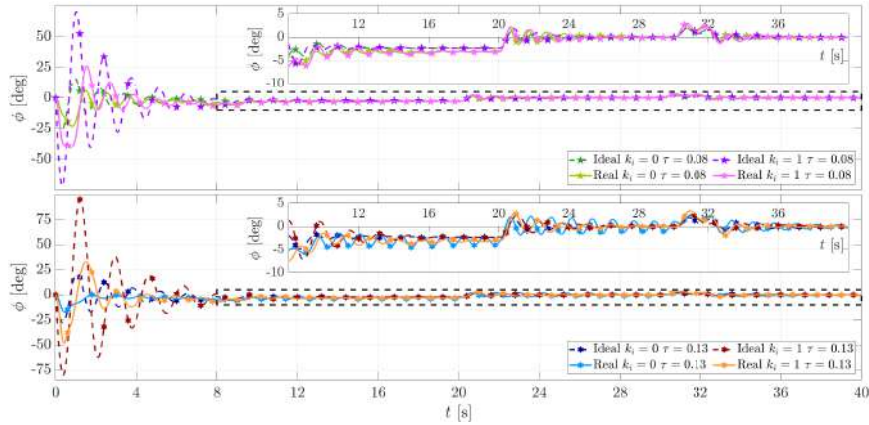
(b) Displacement along  $y_I$



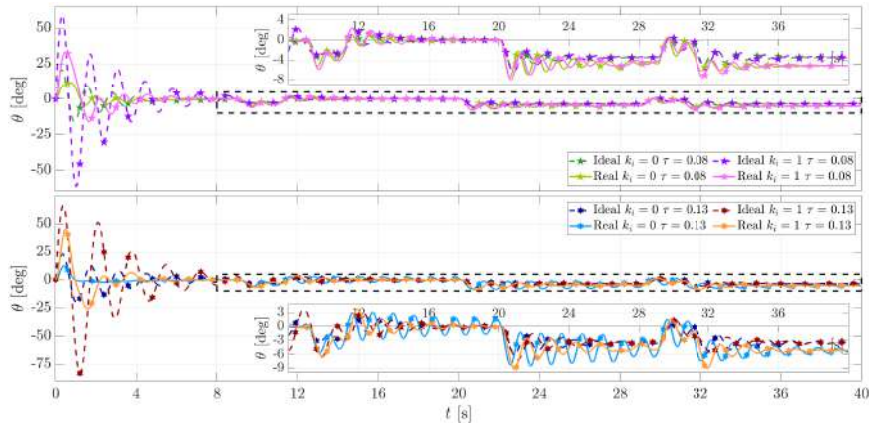
(c) Displacement along  $z_I$

Figure 5.6: Translational motion for constant reference inputs

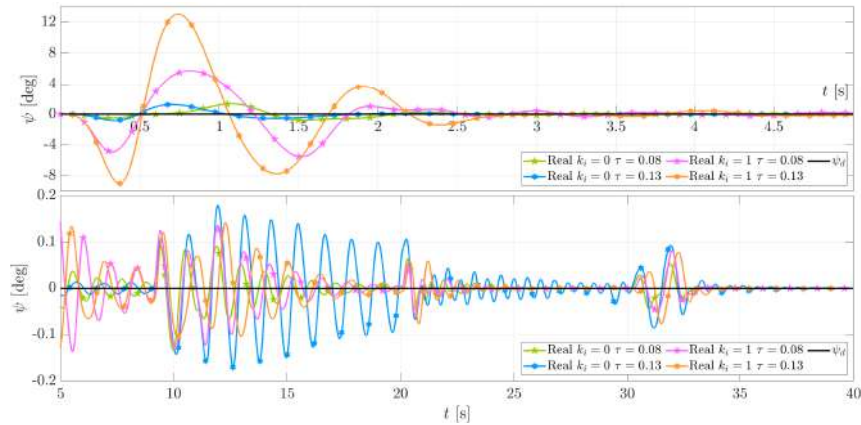
The translational behavior of the vehicle is depicted in Fig. 5.6 where the disturbances considered are equally plotted in a minor scale. From such figure, it is possible to appreciate that the system driven by the PID controllers successfully reaches the desired position even in the presence of external disturbances yet, the system operating under the influence of PD controllers presents an steady state error produced by the perturbations applied to the quadrotor. One may notice the overshoot on the response of the system actuating under the PID control law, nevertheless such overshoot can be reduced with the proper gains selection.



(a) Roll ( $\phi$ ) motion



(b) Pitch ( $\theta$ ) motion

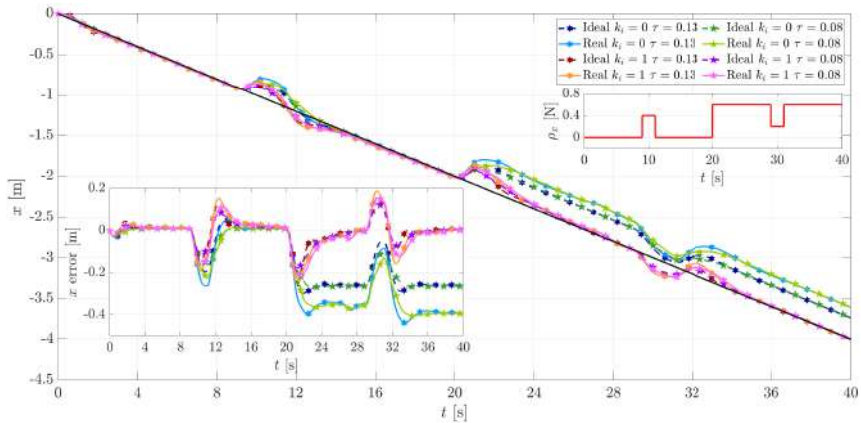


(c) Yaw ( $\psi$ ) motion

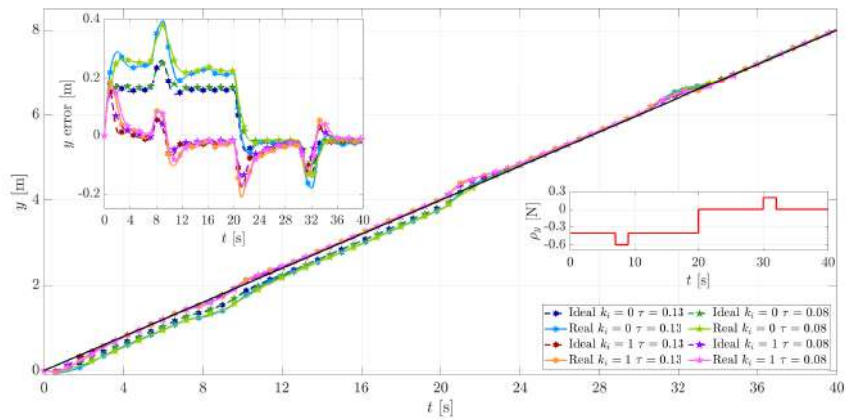
Figure 5.7: Rotational motion for constant reference inputs in position

Regarding the rotational performance of the vehicle for the current simulation case (see Fig. 5.7), one can clearly appreciate oscillations with a considerable magnitude at the transient phase as expected for step reference inputs. Notice that the results concerning the yaw motion of the vehicle correspond only to those obtained by the full dynamics simulation as, ideally, it is assumed that it remains always at 0 [deg].

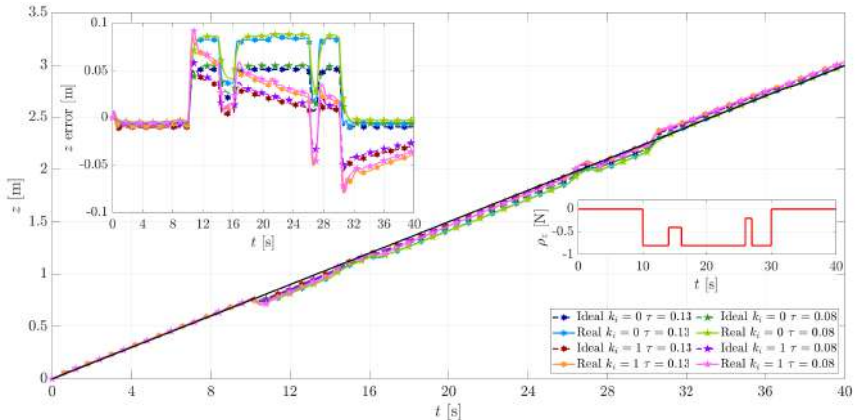
With base on the results exposed in Figs. 5.6 and 5.7, it is immediate to appreciate that the behavior of the linear quadrotor system differs from that of the vehicle with the full dynamics being considered. In this sense, the system simulated using the



(a) Displacement along  $x_I$



(b) Displacement along  $y_I$



(c) Displacement along  $z_I$

Figure 5.8: Translational motion for ramp reference inputs

full dynamic model possesses a smoother behavior in comparison with the linear system, i.e. no oscillations are appreciated in the translational response and the angular motion of the aircraft does not reach those peaks presented during the “ideal” vehicle simulation.

The results concerning the second simulation scenario (depicted in Figs. 5.8 and 5.9) reinforce the discussion of the results standing for the first case. Fig. 5.8 shows the evolution of the position of the vehicle in the space; plots of the corresponding error defined, for  $v \in \xi$ , as  $e_v(t, \tau) = v_d(t) - v(t - \tau)$  are also provided for a better appreciation of the performance. In this manner, and

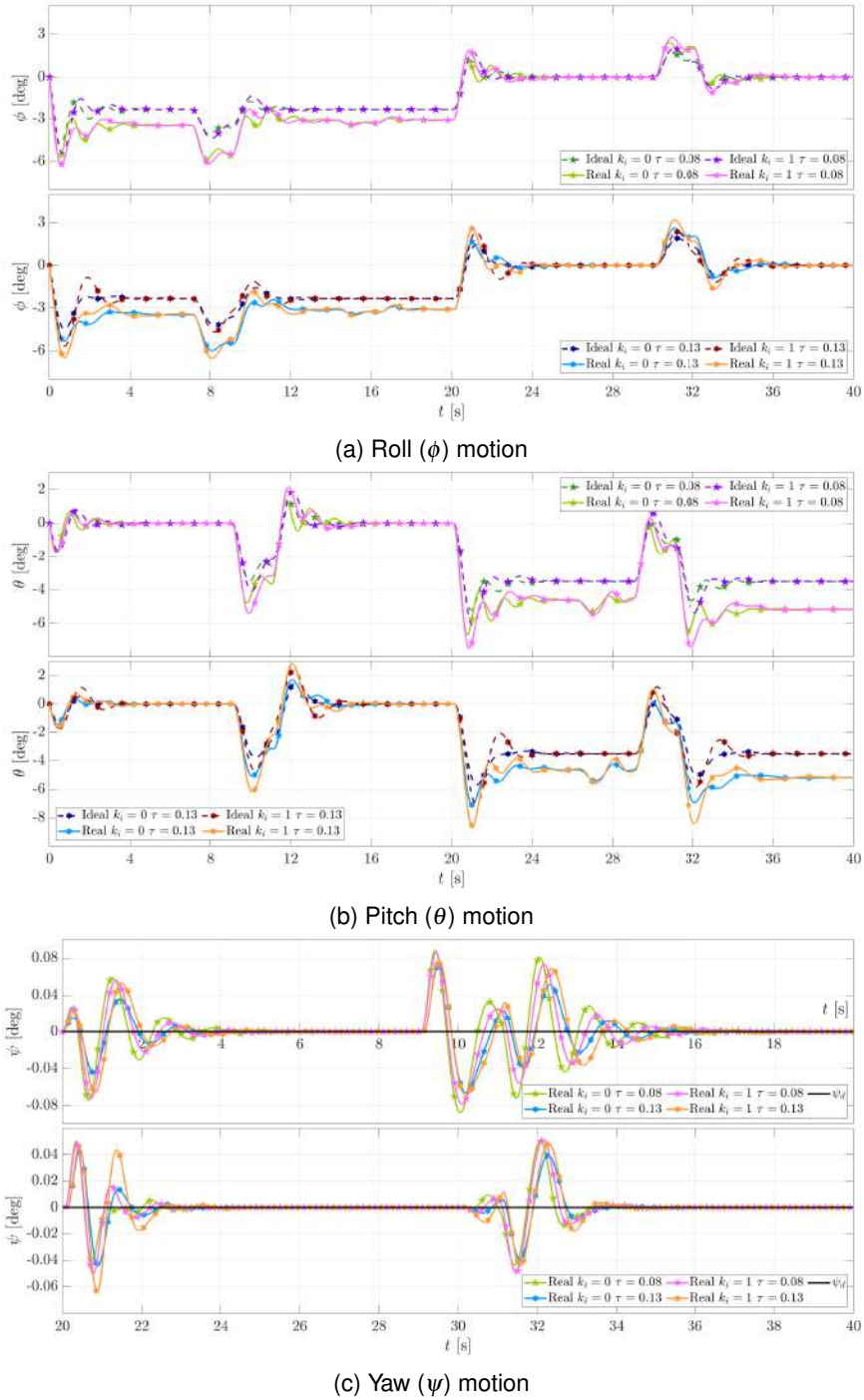
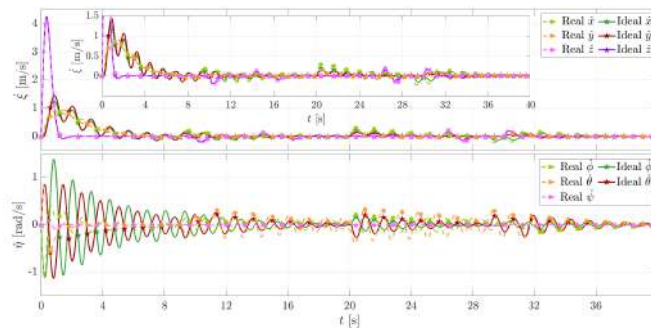


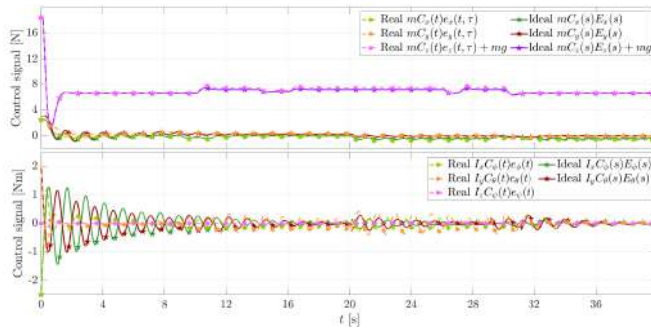
Figure 5.9: Rotational motion for ramp reference inputs in position

for the cases where PID controllers were implemented, one can appreciate that  $e_V(t, \tau) \rightarrow 0$  as  $t \rightarrow \infty$  even when in the presence of disturbances.

The absence of prominent and abrupt oscillation on the rotational response of the vehicle is clearly appreciated in Fig. 5.9. This behavior is produced as a consequence of the smoothness on the desired position input since it corresponds to ramp-like signal, yet, one can observe the reaction of the system to disturbances. One may find attractive Figs. 5.10 and 5.11 for supplementary information that supports the results discussion. In both figures, the velocities of the vehicle and the control signals are depicted.

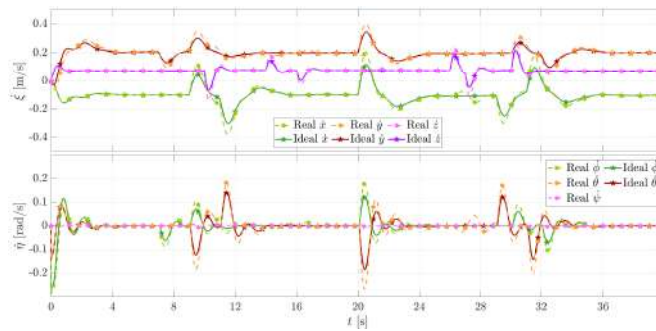


(a) Velocities

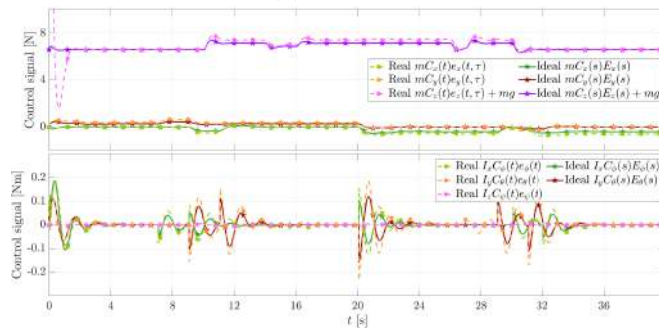


(b) Control signals

Figure 5.10: Quadrotor velocities and control signals for constant reference inputs,  $k_{i_{x,y,z}} = 0$  and  $\tau = 0.13$  [s]



(a) Velocities



(b) Control signals

Figure 5.11: Quadrotor velocities and control signals for ramp reference inputs,  $k_{i_{x,y,z}} = 1$  and  $\tau = 0.08$  [s]

## Chapter 6

# Time-Delay Control of Quadrotor UAVs: a MID-based Approach

The sequel of the chapter is outlined in the following manner: [Section 6.1](#) offers an introduction to the problematic. [Section 6.2](#) provides a brief introduction to time-delay differential equations and MID property fundamentals. In [Section 6.3](#), the dynamics of the quadrotor vehicles is described. [Section 6.4](#) is devoted to the conception of the controllers that stabilize the typical quadrotor vehicle. On the other hand, [Section 6.5](#) exposes the control strategy adopted to stabilize the UAV endowed with 1-DOF tilting-rotors. [Section 6.6](#) provides the results of the detailed numerical simulations carried out to validate the proposals. Lastly, concluding remarks are drawn in [Subsection 8.2.2](#).

### 6.1 Introduction

Among the actual technological surge, Unmanned Aerial Vehicles (UAVs), witnessed by their extensive applications spectrum, remain as a popular and challenging topic within the control systems and robotics scientific community. Such attractiveness relies on friendly design and controllability criteria which have lead to a wide application range such as high-precision weather monitoring, precision agriculture, swarm-based distributed perception, parcel transport and delivering, disaster assessment and infrastructure inspection, for instance [\[143, 149, 28\]](#).

The autonomy and capability of UAVs to perform accurate maneuvers are strongly dependent on the efficient synthesis and implementation of control-task-oriented algorithms. Several of these strategies take into consideration quaternion-based modeling approaches [\[5\]](#), image-aimed stabilization or the well-known proportional-derivative (PD) and proportional-integral-derivative (PID) controllers [\[169, 35\]](#) alongside robust control techniques [\[37, 75\]](#) and/or state estimations and observers [\[49, 36, 38\]](#).

Among the vast variety of issues undermining the aerial systems performance, and to the best of the author's knowledge, the study of time-delay effects remains relatively as an unexplored topic of interest which conceals an enormous potential regarding the stability of such vehicles. In practice, UAVs' control systems operate in presence of time-delays arising from perception processing for decision-making navigation, control commands and actuators' delayed dynamics. It has been proved that time-delays induce

oscillatory phenomena rendering the system unstable. Nevertheless, some stabilizing effects of time-delays can be exploited to improve the system's performance [126, 155].

The stability of aerial vehicles under the influence of time-delays has been conducted in [102, 34] providing a set of stability charts to describe the parametric behavior of the stability regions. Meanwhile, [94] considers the full non-linear dynamics to study the trajectory tracking problem. It is worthwhile highlighting that a considerable part of prior works focuses on the communication and information exchange processes as the main sources of time-delays [6, 120, 86]. In this regard, the range of solutions to overcome such issue goes from delay-optimization approaches [93] to Backstepping and non-linear control [43, 77] yet, a vast variety of different approaches can be found in the literature, see for instance [59, 172, 126, 115, 119].

Amid novel time-delay systems analysis, tracking the behavior of the roots of the characteristic equation, as in [20], has led to an increasing interest on studying and exploiting the Multiplicity-Induced-Dominancy (MID) property. This property refers to a special condition in which a given root of the characteristic function matches the spectral abscissa such that the corresponding spectral value is dominant.

The MID property has already been suggested for some low-order cases [66] and some other phenomena described by linear time-delay differential equations [21, 24, 25, 26, 110]. Recent results in this direction provide necessary and sufficient conditions for roots of maximal multiplicity in reduced-order time-delay systems and their extension to a general class of second-order differential equation and linear time-invariant single-delay equations, both of retarded type [25, 110]. These findings equally concern linear time-delay systems of neutral type. [107] extends the MID property in order to stabilize a second order time-delay neutral system by means of a PID controllers. In addition, in [18], necessary and sufficient conditions for the existence of a root of maximal multiplicity are provided. Nevertheless, the application of such findings on the domain of aerial robots control, as far as it is concerned by the author, has not been specifically considered.

The present chapter exploits the effects of the time-delay arising from generic perception vision-based tracking systems in order to stabilize two popular rotorcraft classes: (i) a classical "+" quadrotor and (ii) a "+" quadrotor endowing 1-Degree-Of-Freedom (DOF) tilting-rotors. The MID property leads to a tuning criteria of the controllers' gains such that the quadrotors reach the equilibrium state as fast as possible with a non-oscillatory transient response.

## 6.2 MID Approach Fundamentals

The MID property refers to a special condition in which multiple roots of the characteristic function match the spectral abscissa such that the corresponding spectral value is strictly dominant under some given constraints. Moreover, it is worth distinguishing two possible scenarios regarding the multiplicity of the roots; in this sense, the term Generic MID (GMID) property stands for the case where maximal multiplicity is reached. The property is simply named MID otherwise. The GMID property is completely characterized for the single delay case (in both delayed and neutral cases) in [18] permitting one to establish conditions over all the parameters of the system which is not feasible from a control point of view. A control oriented MID is however proposed in [25, 15, 16].

Extensive literature is available (see for instance [25, 111]) analysing the behavior of time-delayed linear systems whose equation structures are written in the form:

$$\mathcal{F}^{(n)}(t) + a_{n-1}\mathcal{F}^{(n-1)}(t) + \dots + a_0\mathcal{F}(t) + \varphi_{n-1}\mathcal{F}^{(n-1)}(t-\tau) + \dots + \varphi_0\mathcal{F}(t-\tau) = 0 \quad (6.1)$$

such that  $\mathcal{F}$  is an unknown real-valued function,  $n$  is a positive integer,  $a_k, \varphi_k \in \mathbb{R}$  for  $k \in \{0, \dots, n-1\}$  are constant coefficients, and  $\tau > 0$  is a time-delay. Thus, Eqn. (6.1) is named as a retarded delay differential equation due to the fact that the highest order derivative,  $\mathcal{F}^{(n)}(t)$ , is included only in the time-delay-independent term.

The analysis of Eqn. (6.1) occurs to be important as it represents linear control systems subjected a control input and a time-delay feedback  $u(t-\tau)$ , such that:

$$\mathcal{F}^{(n)}(t) + a_{n-1}\mathcal{F}^{(n-1)}(t) + \dots + a_0\mathcal{F}(t) = u(t-\tau) \quad (6.2)$$

In the time-delay-free scenario, the control input is often established as  $u(t) = -\varphi_{n-1}\mathcal{F}^{(n-1)}(t) - \dots - \varphi_0\mathcal{F}(t)$ , assuming that the measurement of  $\mathcal{F}(t)$  and its derivatives  $\mathcal{F}^{(n-1)}(t), \dots, \mathcal{F}'(t)$  are instantaneously available; thus the roots of the characteristic function can be strategically chosen, according to a desired exponential behavior, by a proper selection of the coefficients  $\varphi_0, \dots, \varphi_{n-1}$ .

Spectral methods are equally adopted to address systems with time-delays. In this regard, the asymptotic behavior of the solutions depends on the roots of the characteristic function which, for Eqn. (6.1) is defined as  $\Delta: \mathbb{C} \rightarrow \mathbb{C}$  for  $s \in \mathbb{C}$  such that:

$$\Delta(s) = s^n + \sum_{k=0}^{n-1} a_k s^k + e^{-s\tau} \sum_{k=0}^{n-1} \varphi_k s^k \quad (6.3)$$

Thus  $\sigma_0 = \sup\{\operatorname{Re}\{s\} | s \in \mathbb{C}, \Delta(s) = 0\}$  defines the exponential behavior of the solutions of Eqn. (6.1). Such real number  $\sigma_0$  is named the spectral abscissa of  $\Delta$  and it follows that for every  $\varepsilon > 0$ , there exists a  $\kappa < 0$  such that, for every solution  $\mathcal{F}$  of Eqn. (6.1), one has  $|\mathcal{F}(t)| \leq \kappa e^{(\sigma_0 + \varepsilon)t} \max_{\vartheta \in [-\tau, 0]} |\mathcal{F}(\vartheta)|$  [65]. In addition, to ensure the exponential convergence of the solutions to 0,  $\sigma < 0$  shall strictly hold. Nevertheless, the analysis of the (asymptotic) behavior of the solution of Eqn. (6.1) stands as a challenge since the corresponding characteristic function  $\Delta$  has infinitely many roots.

If  $\Delta$  possesses a dominant root with negative real part, then the exponential stability of Eqn. (6.1) is equivalent to it, additionally, it may often hold, for some characteristic quasipolynomials of time-delay systems, that the real roots of maximal multiplicity are dominant which gives name to the Multiplicity-Induced-Dominancy (MID) property, and it follows that a root  $s_0$  with multiplicity  $n \in \mathbb{N}$  satisfies:

$$\Delta(s_0) = \Delta'(s_0) = \dots = \Delta^{(n-2)}(s_0) = \Delta^{(n-1)}(s_0) = 0 \quad (6.4)$$

The formal definition of a *quasipolynomial* is provided below.

**Definition 6.2.1** A quasipolynomial  $\Lambda$  is an entire function  $\Lambda: \mathbb{C} \rightarrow \mathbb{C}$  which can be written under the form

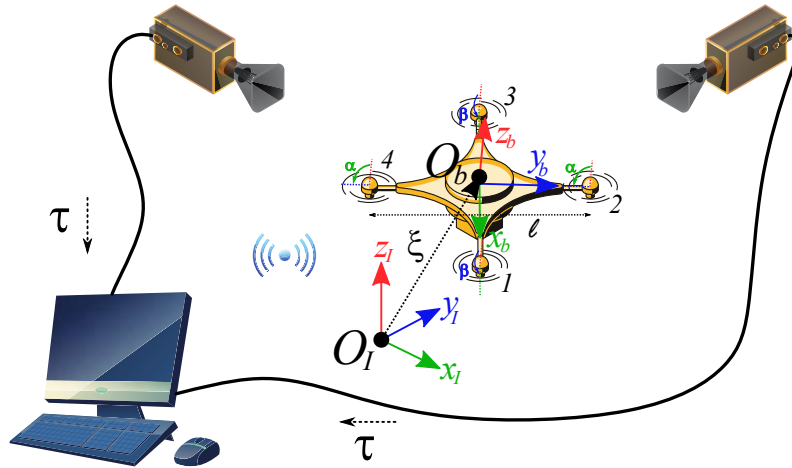


Figure 6.1: Quadrotor vehicle and vision-based tracking system (scheme conceived from figures available at [freepik.com](http://freepik.com))

$$\Lambda(s) = \sum_{k=0}^{\iota} \rho_k(s) e^{\lambda_k s} \quad (6.5)$$

where  $\iota$  is a nonnegative integer,  $\lambda_0, \dots, \lambda_{\iota}$  are pairwise distinct real numbers, and, for  $k \in \{0, \dots, \iota\}$ ,  $\rho_k$  is a nonzero polynomial with complex coefficients of degree  $\mu_k \geq 0$ . The integer  $D = \iota + \sum_{k=0}^{\iota} \mu_k$  is called the degree of  $\Lambda$ .

When  $\lambda_0 = 0$  and  $\lambda_k < 0$  for  $k \in \{1, \dots, \iota\}$  in Eqn. (6.5),  $\Lambda$  is the characteristic function of a linear time-delay system with delays  $-\lambda_1, \dots, -\lambda_{\iota}$ .

A set of necessary results and additional definitions on quasipolynomials for the understanding and analysis of these, are given next. For an extended and detailed treatment of these concerns, the reader is referred to [21, 25, 119, 15, 16, 111].

- The roots of a quasipolynomial do not change when its coefficients are all multiplied by the same nonzero number, and hence one may always assume, without loss of generality, that one nonzero coefficient of a quasipolynomial is normalized to 1, such as the coefficient of the term of highest degree in  $\rho_0$ .
- Let  $\Lambda$  be a quasipolynomial of degree  $D$  in the form of Eqn. (6.5). Then any root  $s_0 \in \mathbb{C}$  of  $\Lambda$  has multiplicity at most  $D$ .
- Let  $\Lambda : \mathbb{C} \rightarrow \mathbb{C}$  and  $s_0 \in \mathbb{C}$  be such that  $\Lambda(s_0) = 0$ . It is said that  $s_0$  is a dominant (respectively, strictly dominant) root of  $\Lambda$  if, for every  $s \in \mathbb{C} \setminus \{s_0\}$  such that  $\Lambda(s) = 0$ , one has  $\text{Re}\{s\} \leq \text{Re}\{s_0\}$  (respectively,  $\text{Re}\{s\} < \text{Re}\{s_0\}$ ).
- The roots of the quasipolynomial  $\Delta$  in Eqn. (6.3) with maximal multiplicity are necessarily dominant and such multiplicity can be attained only in the real axis.

### 6.3 Quadrotor Model

Let the quadrotor system be depicted in Fig. 6.1 where the vision-based tracking system permits to know the position of the vehicle,  $\xi = [x \ y \ z]^T \in \mathbb{R}^3$ , in a conditioned environment. Such sensing strategy often takes a fraction of time  $\tau > 0$  to be executed; this issue is translated to control terms as a feedback time-delay [67, 151].

The dynamics of the vehicle is described w.r.t. an inertial frame  $O_I \{x_I, y_I, z_I\}$  and a body frame  $O_b \{x_b, y_b, z_b\}$  whose origin matches the center of gravity (CoG) of the UAV.  $x_b, y_b, z_b$  define the roll, pitch and yaw axes and the corresponding principal axis of inertia which are associated to the Euler angles  $\boldsymbol{\eta} = [\phi \ \theta \ \psi]^T \in \mathbb{R}^3$ , respectively. The motion of the aerial vehicle can be described, according to the Newton Euler formulation [35], as:

$$m_r \ddot{\boldsymbol{\xi}} + m_r \mathbf{g} = \boldsymbol{\tau}_\xi \quad (6.6)$$

$$I \dot{\boldsymbol{\omega}} + \boldsymbol{\omega} \times (I \boldsymbol{\omega}) = \boldsymbol{\tau}_\omega \quad (6.7)$$

where  $m_r > 0$  stands for the mass of the UAV and  $\mathbf{g} = [0 \ 0 \ g]^T \in \mathbb{R}^3$  does for the vector containing the constant of gravity acceleration  $g > 0$ ;  $I = \text{diag}([I_x \ I_y \ I_z]^T) \in \mathbb{R}^{3 \times 3}$ , the inertia matrix, is respectively defined by the moments of inertia about the roll, pitch and yaw axis, and the function  $\text{diag} : \mathbb{R}^n \rightarrow \mathbb{R}^{n \times n}$  such that, for a given  $\mathbf{v} \in \mathbb{R}^n$ , it stands as:

$$\text{diag}(\mathbf{v}) = \begin{bmatrix} v_1 & 0 & \dots & 0 \\ 0 & v_2 & \dots & 0 \\ \vdots & \vdots & \ddots & \vdots \\ 0 & 0 & \dots & v_n \end{bmatrix} \quad (6.8)$$

The angular velocity vector  $\boldsymbol{\omega} = [p \ q \ r]^T \in \mathbb{R}^3$  is related to the Euler rates  $\dot{\boldsymbol{\eta}}$  in a sense that:

$$\boldsymbol{\omega} = W_\eta \dot{\boldsymbol{\eta}} \quad ; \quad W_\eta = \begin{bmatrix} 1 & 0 & -S_\theta \\ 0 & C_\phi & S_\phi C_\theta \\ 0 & -S_\phi & C_\phi C_\theta \end{bmatrix} \in \mathbb{R}^{3 \times 3} \quad (6.9)$$

where  $C_{(\bullet)} = \cos(\bullet)$  and  $S_{(\bullet)} = \sin(\bullet)$ . Such an abuse of this notation is considered throughout the sequel of the chapter.

The translational motion described by Eqn. (6.6) is provided in terms of the inertial frame. On the other hand, Eqn. (6.7) describes the rotational motion of the quadrotor in the body reference frame.

The actuation of the system stands as the main difference between a typical quadrotor and a quadrotor endowed with tilting-rotors. In this sense, the translational motion of the aircraft is driven by the forces comprised in the vector  $\boldsymbol{\tau}_\xi \in \mathbb{R}^3$  which is defined, for the typical quadrotor, by the rotation matrix  $R_\eta \in \mathbb{R}^{3 \times 3}$  and the forces of the propellers  $f_i \geq 0$  (with  $i = 1, 2, 3, 4$ ), as:

$$\boldsymbol{\tau}_\xi = R_\eta \begin{bmatrix} 0 \\ 0 \\ T = f_1 + f_2 + f_3 + f_4 \end{bmatrix} \quad \text{and} \quad R_\eta = \begin{bmatrix} C_\theta C_\psi & S_\phi S_\theta C_\psi - C_\phi S_\psi & C_\phi S_\theta C_\psi + S_\phi S_\psi \\ C_\theta S_\psi & S_\phi S_\theta S_\psi + C_\phi C_\psi & C_\phi S_\theta S_\psi - S_\phi C_\psi \\ -S_\theta & S_\phi C_\theta & C_\phi C_\theta \end{bmatrix} \quad (6.10)$$

For the quadrotor endowed with 1-DOF tilting-rotors, the vector  $\boldsymbol{\tau}_\xi$  is rewritten in terms of  $R_\eta$ ,  $f_i$  and the tilt angles  $\alpha, \beta \in \mathbb{R}$  as:

$$\boldsymbol{\tau}_\xi = R\boldsymbol{\eta} \begin{bmatrix} (f_1 + f_3) \mathbf{S}_\beta \\ -(f_2 + f_4) \mathbf{S}_\alpha \\ (f_1 + f_3) \mathbf{C}_\beta + (f_2 + f_4) \mathbf{C}_\alpha \end{bmatrix} \quad (6.11)$$

The rotational states of the aircraft are governed by the torques in the vector  $\boldsymbol{\tau}_\omega \in \mathbb{R}^3$  which, for the typical quadrotor structure, is defined as:

$$\boldsymbol{\tau}_\omega = \begin{bmatrix} \tau_\phi = \ell(f_2 - f_4)/2 \\ \tau_\theta = \ell(f_3 - f_1)/2 \\ \tau_\psi = \varepsilon(f_1 - f_2 + f_3 - f_4) \end{bmatrix} \quad (6.12)$$

where  $\ell > 0$  denotes the diagonal motor-to-motor distance and  $\varepsilon > 0$  is a proportionality constant that relates the force  $f_i$  to the corresponding free moment  $\tau_i$  such that  $\tau_i = \varepsilon f_i$ .

For the quadrotor vehicle equipped with tilting-rotors,  $\boldsymbol{\tau}_\omega$  reads as:

$$\boldsymbol{\tau}_\omega = \begin{bmatrix} \ell(f_2 - f_4) \mathbf{C}_\alpha / 2 + \varepsilon(f_1 + f_3) \mathbf{S}_\beta \\ \ell(f_3 - f_1) \mathbf{C}_\beta / 2 - \varepsilon(f_2 + f_4) \mathbf{S}_\alpha \\ \varepsilon [(f_1 + f_3) \mathbf{C}_\beta - (f_2 + f_4) \mathbf{C}_\alpha] \end{bmatrix} \quad (6.13)$$

The non-linear description of the vehicles provided in the current section allows one to proceed to the conception of the controllers as exposed next.

## 6.4 UAV Control: The Typical Quadrotor Case

Let the quadrotor class be firstly addressed. As it can be found in the literature [67, 35, 34, 102], it is typically assumed that the vehicle operates at low speeds, such that The Coriolis and Centripetal effects are neglected, at quasi-hovering flight ( $\phi \approx 0$  and  $\theta \approx 0$ ) and ,without loss of generality,  $\psi = 0$  holds  $\forall t \geq 0$ . These considerations lead to a linear representation of Eqns. (6.6), (6.7), (6.10) and (6.12) of the form:

$$\begin{cases} X(s) = \frac{1}{m_r s^2} \theta(s) T(s), & Y(s) = -\frac{1}{m_r s^2} \phi(s) T(s), & Z(s) = \frac{1}{m_r s^2} (T(s) - m_r g), \\ \phi(s) = \frac{1}{I_x s^2} \tau_\phi(s), & \theta(s) = \frac{1}{I_y s^2} \tau_\theta(s), & \psi(s) = \frac{1}{I_z s^2} \tau_\psi(s) \end{cases} \quad (6.14)$$

which corresponds to a representation of the system in the frequency domain where  $s = \sigma + j\omega$  with  $\sigma, \omega \in \mathbb{R}$ .

From Eqn. (6.14), it is immediate to observe that the  $Z(s)$  and  $\psi(s)$  motions are decoupled, yet the  $X(s)$  dynamics is coupled to that of  $\theta(s)$  and the  $Y(s)$  motion is related to that of  $\phi(s)$ . In this regard, let the thrust  $T(s)$  be used as the control input to drive the system to a desired height  $Z_d(s)$  and  $\tau_\psi(s)$  does the proper to keep the yaw angle at 0. These control inputs are respectively

defined, as:

$$T(s) = m_r (\mathcal{C}_z(s) E_z(s) + g) \quad \text{and} \quad \tau_\psi(s) = I_z \mathcal{C}_\psi(s) E_\psi(s) \quad (6.15)$$

where the  $z$  error reads as  $E_z(s) = Z_d(s) - e^{-\tau s} Z(s)$  since the translational states of the quadrotor are subjected to a feedback time-delay  $\tau$  due to the inherent latency of the vision-based tracking system, and the  $\psi$  error stands as  $E_\psi(s) = -\psi(s)$  since  $\psi_d(s) = 0$ . The linear controllers  $\mathcal{C}_z(s)$  and  $\mathcal{C}_\psi(s)$  correspond to PD controllers of the form:

$$\mathcal{C}_z(s) = k_{p_z} + k_{d_z} s \quad \text{and} \quad \mathcal{C}_\psi(s) = k_{p_\psi} + k_{d_\psi} s \quad (6.16)$$

with  $k_{p_z}, k_{p_\psi} \in \mathbb{R}$  defined as the proportional gains and  $k_{d_z}, k_{d_\psi} \in \mathbb{R}$  standing as the derivative gains. The aforementioned control gains are tuned by means of the MID property in the case of time-delays presence. In the sequel of the chapter, the methodology is exposed.

Regarding the translational motion of the vehicle, let one consider that, for a large enough time,  $T(s) \rightarrow T_c = m_r g$  as  $Z(s) \rightarrow Z_d(s)$  [102, 159]. The latter allows one to rewrite the equations of motion for  $X(s)$  and  $Y(s)$  in Eqn. (6.14) respectively, as:

$$X(s) = \frac{1}{m_r s^2} \theta(s) T_c \quad \text{and} \quad Y(s) = -\frac{1}{m_r s^2} \phi(s) T_c \quad (6.17)$$

It is thus considered that  $\theta(s)$  and  $\phi(s)$  act as the control inputs for the corresponding DOF, such that the reference values are defined by linear PD controllers,  $\mathcal{C}_x(s)$  and  $\mathcal{C}_y(s)$ , as follows

$$\theta_d(s) = \frac{m_r}{T_c} \mathcal{C}_x(s) E_x(s) \quad \text{and} \quad \phi_d(s) = -\frac{m_r}{T_c} \mathcal{C}_y(s) E_y(s) \quad (6.18)$$

with

$$\mathcal{C}_x(s) = k_{p_x} + k_{d_x} s, \quad \mathcal{C}_y(s) = k_{p_y} + k_{d_y} s \quad (6.19)$$

$$E_x(s) = X_d(s) - e^{-\tau s} X(s), \quad E_y(s) = Y_d(s) - e^{-\tau s} Y(s) \quad (6.20)$$

where the proportional gains correspond to  $k_{p_x}, k_{p_y} \in \mathbb{R}$ , and the derivative gains are denoted by  $k_{d_x}, k_{d_y} \in \mathbb{R}$ . Nonetheless, the reference values in Eqn. (6.18) are achieved by the action of the linear PD controllers:

$$\mathcal{C}_\theta(s) = k_{p_\theta} + k_{d_\theta} s \quad \text{and} \quad \mathcal{C}_\phi(s) = k_{p_\phi} + k_{d_\phi} s \quad (6.21)$$

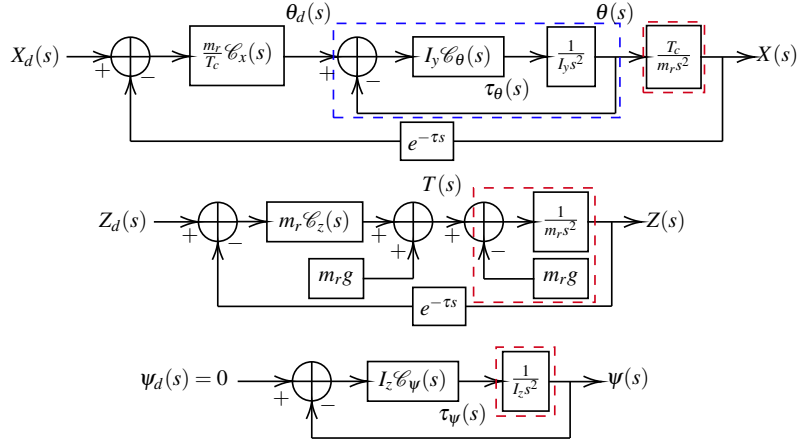


Figure 6.2: Block diagram representation of the typical quadrotor closed-loop system

such that:

$$\tau_{\theta}(s) = I_y \mathcal{C}_{\theta}(s) E_{\theta}(s) \quad \text{and} \quad \tau_{\phi}(s) = I_x \mathcal{C}_{\phi}(s) E_{\phi}(s) \quad (6.22)$$

with  $E_{\theta}(s) = \theta_d(s) - \theta(s)$  and  $E_{\phi}(s) = \phi_d(s) - \phi(s)$ . The proportional gains  $k_{p_{\theta}}, k_{p_{\phi}} \in \mathbb{R}$  as well as the derivative gains  $k_{d_{\theta}}, k_{d_{\phi}} \in \mathbb{R}$  are tuned in such a manner that the rotational dynamics is stable converging faster than that of translation [159]. To accomplish such task, spectral methods can be applied.

To synthesize the previous establishments, the  $X(s)$ ,  $Z(s)$  and  $\psi(s)$  closed-loop systems are depicted in Fig. 6.2 where the dynamics of the plant is highlighted in red and the inner dynamics is surrounded by a blue dashed box (if it occurs to be the case). Notice that the  $Y(s)$  dynamics is omitted since it follows the same structure as that of  $X(s)$ .

### 6.4.1 MID-Property-Based Controllers Analysis

According to Fig. 6.2, the closed-loop transfer functions of each DOF can be computed such that the characteristic functions correspond to:

$$\Delta_x(s) = s^2 \left[ s^2 + \mathcal{C}_{\theta}(s) \right] + e^{-\tau s} \mathcal{C}_x(s) \mathcal{C}_{\theta}(s) \quad (6.23)$$

$$\Delta_y(s) = s^2 \left[ s^2 + \mathcal{C}_{\phi}(s) \right] + e^{-\tau s} \mathcal{C}_y(s) \mathcal{C}_{\phi}(s) \quad (6.24)$$

$$\Delta_z(s) = s^2 + e^{-\tau s} \mathcal{C}_z(s) \quad (6.25)$$

$$\Delta_{\psi}(s) = s^2 + \mathcal{C}_{\psi}(s) \quad (6.26)$$

Regarding Eqn. (6.26), no time-delay effect is present thus, the exponential behavior of the solutions can be tuned by the proper placement of the roots of the polynomial. In this sense, it is enough that such roots are on the left-plane of the complex space, moreover, a non-oscillatory stable system's response is achieved if the roots are over the negative real axis [159]. The

latter is comprised in [Proposition 6.4.1](#) below.

**Proposition 6.4.1** *For the closed-loop dynamics described by [Eqn. \(6.26\)](#), a non-oscillatory stable system's response is achieved and guaranteed if the controller's gains satisfy:*

$$k_{d\psi} = s_{\psi,1} + s_{\psi,2} \quad \text{and} \quad k_{p\psi} = s_{\psi,1}s_{\psi,2} \quad (6.27)$$

with  $s_{\psi,2} > s_{\psi,1} > 0$  such that the system can be as fast as  $s_{\psi,1}$  is placed.

**Proof.** The proof is provided by the substitution of the gains given in [Eqn. \(6.27\)](#) into [Eqn. \(6.26\)](#) that is solved as:

$$s^2 + (s_{\psi,1} + s_{\psi,2})s + s_{\psi,1}s_{\psi,2} = (s + s_{\psi,1})(s + s_{\psi,2}) = 0 \quad (6.28)$$

such that the roots of the system are located at  $s = -s_{\psi,1}$  and  $s = -s_{\psi,2}$ . ■

It must be noticed that [Proposition 6.4.1](#) can be applied to stabilize the inner-loop dynamics highlighted in blue in [Fig. 6.2](#) as the existence of negative real roots of the characteristic function of the open-loop system is essential for the MID property to be exploited.

Regarding the translational dynamics where the time-delay effect is found, the analysis of the  $Z(s)$  dynamics is provided at first place, afterwards, the  $X(s)$  dynamics of the vehicle is studied.

The following result, which is a direct consequence of [\[25\]](#), allows to characterize an assignable spectral value guaranteeing  $\sigma$ -stability as well as the corresponding controller's gains.

**Proposition 6.4.2** *For the quasipolynomial in [Eqn. \(6.25\)](#), the following assertions hold:*

1. *The multiplicity of any given root of the quasipolynomial function is bounded by 4.*
2. *For a positive delay  $\tau$ , the quasipolynomial in [Eqn. \(6.25\)](#) admits a real spectral value at  $s = s_{0_z}$  with algebraic multiplicity 3 if and only if:*

$$s_{0_z} = \frac{-2 + \sqrt{2}}{\tau} \quad (6.29)$$

and the controller's gains satisfy:

$$k_{p_z} = e^{\tau s_{0_z}} s_{0_z}^2 (s_{0_z} \tau + 1) \quad \text{and} \quad k_{d_z} = -e^{\tau s_{0_z}} s_{0_z} (s_{0_z} \tau + 2) \quad (6.30)$$

**Proof.** The first statement of the proposition is a direct assimilation of the results presented at [\[21\]](#). On the other hand, if  $s_{0_z}$  is a root with multiplicity at least 2, it follows that  $\Delta_z(s_{0_z}) = 0$  and  $\Delta'_z(s_{0_z}) = 0$ .

By solving these equations for the control gains, the definitions in [Eqn. \(6.30\)](#) are obtained. The root  $s_{0_z}$  reaches a multiplicity 3 if and only if:

$$\Delta_z''(s_{0z}) = 2 + e^{-\tau s_{0z}} \left[ \tau^2 (k_{d_z} s_{0z} + k_{p_z}) - 2\tau k_{d_z} \right] = 0 \quad (6.31)$$

The substitution of Eqn. (6.30) into Eqn. (6.31) leads to Eqn. (6.29). To prove that  $s_{0z}$  is the dominant root, one may exploit the result from [25, Theorem 4.2].

■

Let one proceed to study the quasipolynomial in Eqn. (6.23). In this regard, and due to the complexity of the expressions, a useful proposition based on a symbolic/numerical analysis is provided next.

## 6.4.2 Symbolic/Numeric Analysis of the MID-Based Controller

Firstly, to study the behavior of the system whose characteristic function corresponds to the quasipolynomial provided in Eqn. (6.23), one must ensure that the delay-free part of the quasipolynomial has only real roots which occurs if and only if:

$$k_{d_\theta}^2 > 4k_{p_\theta} > 0 \quad (6.32)$$

One must notice that Eqn. (6.32) is equivalent to Proposition (6.4.1) furthermore, the relation in Eqn. (6.32) is given by the discriminant  $\delta_\theta \in \mathbb{R}$  of the characteristic function of the inner closed-loop ( $\theta(s)$  dynamics) such that its roots are computed as

$$s_{\theta,\{1,2\}} = \frac{-k_{d_\theta} \pm \sqrt{\delta_\theta}}{2} \quad \text{with} \quad \delta_\theta = k_{d_\theta}^2 - 4k_{p_\theta} \quad (6.33)$$

These conditions over the gains  $k_{p_\theta}$  and  $k_{d_\theta}$  are taken into consideration to exploit the MID property as numerically established next.

**Proposition 6.4.3** *For the quasipolynomial in Eqn. (6.23), the following assertions hold:*

1. *The multiplicity of any given root of the quasipolynomial function is bounded by 7.*
2. *For a given positive delay  $\tau$ , an arbitrary root  $s_{0_x}$  with algebraic multiplicity 4 is a dominant root of Eqn. (6.23) if  $s_{0_x} \in \mathbb{S}$ , where*

$$\mathbb{S} = \left\{ s_{0_x} : -\frac{3}{10\tau} < s_{0_x} < 0 \right\} \quad (6.34)$$

*and the controllers' gains  $k_{p_\theta}$ ,  $k_{d_\theta}$ ,  $k_{p_x}$  and  $k_{d_x}$  satisfy:*

$$k_{p_\theta} = \lambda s_{0_x}^2, \quad k_{d_\theta} = -\frac{s_{0_x}}{9} \left( \frac{n_2 \lambda^2 - n_1 \lambda + n_0}{d_2 \lambda^2 - d_1 \lambda + d_0} \right) \quad (6.35)$$

$$k_{p_x} = \frac{s_{0_x}^2 e^{\tau s_{0_x}}}{\mathcal{E}_\theta^2(s_{0_x})} \left\{ \mathcal{E}_\theta(s_{0_x}) (\tau s_{0_x} + 1) \left[ s_{0_x}^2 + \mathcal{E}_\theta(s_{0_x}) \right] + s_{0_x}^2 [\mathcal{E}_\theta(s_{0_x}) + k_{p_\theta}] \right\} \quad (6.36)$$

$$k_{d_x} = \frac{-s_{0_x} e^{\tau s_{0_x}}}{\mathcal{E}_\theta^2(s_{0_x})} \left\{ \mathcal{E}_\theta(s_{0_x}) (\tau s_{0_x} + 2) \left[ s_{0_x}^2 + \mathcal{E}_\theta(s_{0_x}) \right] + s_{0_x}^2 [\mathcal{E}_\theta(s_{0_x}) + k_{p_\theta}] \right\} \quad (6.37)$$

where  $\lambda$  is defined as the only positive real root of the following algebraic equation

$$p_3 \lambda^3 + p_2 \lambda^2 + p_1 \lambda + p_0 = 0 \quad (6.38)$$

with

$$p_3 = 27 \left( s_{0_x}^2 \tau^2 + 4s_{0_x} \tau + 2 \right)^4 \quad (6.39)$$

$$p_2 = -10s_{0_x}^9 \tau^9 - 243s_{0_x}^8 \tau^8 - 2352s_{0_x}^7 \tau^7 - 12090s_{0_x}^6 \tau^6 - 36360s_{0_x}^5 \tau^5 - 65916s_{0_x}^4 \tau^4 - 72288s_{0_x}^3 \tau^3 - 47736s_{0_x}^2 \tau^2 - 17280s_{0_x} \tau - 2592 \quad (6.40)$$

$$p_1 = \left( s_{0_x}^3 \tau^3 + 12s_{0_x}^2 \tau^2 + 36s_{0_x} \tau + 24 \right) \left( s_{0_x}^3 \tau^3 + 18s_{0_x}^2 \tau^2 + 54s_{0_x} \tau + 24 \right) \left( s_{0_x}^4 \tau^4 + 8s_{0_x}^3 \tau^3 + 24s_{0_x}^2 \tau^2 + 24s_{0_x} \tau + 12 \right) \quad (6.41)$$

$$p_0 = - \left( s_{0_x}^4 \tau^4 + 8s_{0_x}^3 \tau^3 + 24s_{0_x}^2 \tau^2 + 24s_{0_x} \tau + 12 \right) \left( s_{0_x}^3 \tau^3 + 12s_{0_x}^2 \tau^2 + 36s_{0_x} \tau + 24 \right)^2 \quad (6.42)$$

and

$$n_2 = 11s_{0_x}^{12} \tau^{12} + 309s_{0_x}^{11} \tau^{11} + 3738s_{0_x}^{10} \tau^{10} + 25938s_{0_x}^9 \tau^9 + 115452s_{0_x}^8 \tau^8 + 348192s_{0_x}^7 \tau^7 + 731016s_{0_x}^6 \tau^6 + 1077408s_{0_x}^5 \tau^5 + 1105920s_{0_x}^4 \tau^4 + 771120s_{0_x}^3 \tau^3 + 347328s_{0_x}^2 \tau^2 + 90720s_{0_x} \tau + 10368 \quad (6.43)$$

$$n_1 = \left( s_{0_x}^3 \tau^3 + 12s_{0_x}^2 \tau^2 + 36s_{0_x} \tau + 24 \right) \left( 2s_{0_x}^6 \tau^6 + 39s_{0_x}^5 \tau^5 + 249s_{0_x}^4 \tau^4 + 744s_{0_x}^3 \tau^3 + 1116s_{0_x}^2 \tau^2 + 756s_{0_x} \tau + 180 \right) \left( s_{0_x}^4 \tau^4 + 8s_{0_x}^3 \tau^3 + 24s_{0_x}^2 \tau^2 + 24s_{0_x} \tau + 12 \right) \quad (6.44)$$

$$n_0 = 2 \left( s_{0_x}^3 \tau^3 + 6s_{0_x}^2 \tau^2 + 12s_{0_x} \tau + 6 \right) \left( s_{0_x}^4 \tau^4 + 8s_{0_x}^3 \tau^3 + 24s_{0_x}^2 \tau^2 + 24s_{0_x} \tau + 12 \right) \left( s_{0_x}^3 \tau^3 + 12s_{0_x}^2 \tau^2 + 36s_{0_x} \tau + 24 \right)^2 \quad (6.45)$$

$$d_2 = 3 \left( 2s_{0_x}^3 \tau^3 + 9s_{0_x}^2 \tau^2 + 12s_{0_x} \tau + 6 \right) \left( s_{0_x}^2 \tau^2 + 4s_{0_x} \tau + 2 \right)^4 \quad (6.46)$$

$$d_1 = (s_{0_x}^4 \tau^4 + 16s_{0_x}^3 \tau^3 + 63s_{0_x}^2 \tau^2 + 84s_{0_x} \tau + 30) (s_{0_x}^4 \tau^4 + 8s_{0_x}^3 \tau^3 + 24s_{0_x}^2 \tau^2 + 24s_{0_x} \tau + 12) (s_{0_x}^2 \tau^2 + 4s_{0_x} \tau + 2)^2 \quad (6.47)$$

$$d_0 = (s_{0_x} \tau + 2) (s_{0_x}^3 \tau^3 + 12s_{0_x}^2 \tau^2 + 36s_{0_x} \tau + 24) (s_{0_x}^4 \tau^4 + 8s_{0_x}^3 \tau^3 + 24s_{0_x}^2 \tau^2 + 24s_{0_x} \tau + 12) (s_{0_x}^2 \tau^2 + 4s_{0_x} \tau + 2)^2 \quad (6.48)$$

**Proof.** The first statement of the proposition is a direct assimilation of the results presented at [21], see also [111]. Furthermore, Eqs. (6.35)-(6.37) are found as in Proposition 6.4.2. In this regard, if  $s_{0_x}$  is a root with multiplicity at least 2, it follows that:

$$\Delta_x(s_{0_x}) = s_{0_x}^2 (s_{0_x}^2 + k_{d_\theta} s_{0_x} + k_{p_\theta}) + e^{-\tau s_{0_x}} (k_{d_x} s_{0_x} + k_{p_x}) (k_{d_\theta} s_{0_x} + k_{p_\theta}) = 0 \quad (6.49)$$

$$\Delta'_x(s_{0_x}) = s_{0_x} (4s_{0_x}^2 + 3k_{d_\theta} s_{0_x} + 2k_{p_\theta}) - e^{-\tau s_{0_x}} [\tau (k_{d_x} s_{0_x} + k_{p_x}) (k_{d_\theta} s_{0_x} + k_{p_\theta}) - (2k_{d_\theta} k_{d_x} s_{0_x} + k_{p_x} k_{d_\theta} + k_{p_\theta} k_{d_x})] = 0 \quad (6.50)$$

By solving Eqns. (6.49) and (6.50) for the control gains  $k_{p_x}$  and  $k_{d_x}$ , the definitions in Eqns. (6.36) and (6.37) are obtained. Moreover, the root  $s_{0_x}$  reaches a multiplicity 4 if and only if:

$$\Delta''_x(s_{0_x}) = 2(6s_{0_x}^2 + 3k_{d_\theta} s_{0_x} + k_{p_\theta}) + e^{-\tau s_{0_x}} \left\{ \tau^2 (k_{d_x} s_{0_x} + k_{p_x}) (k_{d_\theta} s_{0_x} + k_{p_\theta}) - 2\tau (2k_{d_\theta} k_{d_x} s_{0_x} + k_{p_x} k_{d_\theta} + k_{p_\theta} k_{d_x}) + 2k_{d_x} k_{d_\theta} \right\} = 0 \quad (6.51)$$

$$\Delta'''_x(s_{0_x}) = 6(4s_{0_x} + k_{d_\theta}) - e^{-\tau s_{0_x}} \left\{ \tau^3 (k_{d_x} s_{0_x} + k_{p_x}) (k_{d_\theta} s_{0_x} + k_{p_\theta}) + 3\tau^2 (2k_{d_\theta} k_{d_x} s_{0_x} + k_{p_x} k_{d_\theta} + k_{p_\theta} k_{d_x}) - 6\tau k_{d_x} k_{d_\theta} \right\} = 0 \quad (6.52)$$

The substitution of Eqns. (6.36) and (6.37) into the equations  $\Delta''_x(s_{0_x}) = 0$  and  $\Delta'''_x(s_{0_x}) = 0$  leads to Eqn. (6.35) yet, one must analyse with detail the results concerning the definitions in Eqns. (6.35) and (6.38). For these ends, let one adopt the change of variable  $\zeta = s_{0_x} \tau$  throughout Eqns. (6.38)-(6.48) yielding to rewrite the expressions as follows:

$$p_3^* \lambda^3 + p_2^* \lambda^2 + p_1^* \lambda + p_0^* = 0 \quad (6.53)$$

$$p_3^* = 27(\zeta^2 + 4\zeta + 2)^4 \quad (6.54)$$

$$p_2^* = -10\zeta^9 - 243\zeta^8 - 2352\zeta^7 - 12090\zeta^6 - 36360\zeta^5 - 65916\zeta^4 - 72288\zeta^3 - 47736\zeta^2 - 17280\zeta - 2592 \quad (6.55)$$

$$p_1^* = (\zeta^3 + 12\zeta^2 + 36\zeta + 24)(\zeta^3 + 18\zeta^2 + 54\zeta + 24)(\zeta^4 + 8\zeta^3 + 24\zeta^2 + 24\zeta + 12) \quad (6.56)$$

$$p_0^* = -(\zeta^4 + 8\zeta^3 + 24\zeta^2 + 24\zeta + 12)(\zeta^3 + 12\zeta^2 + 36\zeta + 24)^2 \quad (6.57)$$

$$n_2^* = 11\zeta^{12} + 309\zeta^{11} + 3738\zeta^{10} + 25938\zeta^9 + 115452\zeta^8 + 348192\zeta^7 + 731016\zeta^6 + 1077408\zeta^5 + 1105920\zeta^4 + 771120\zeta^3 + 347328\zeta^2 + 90720\zeta + 10368 \quad (6.58)$$

$$n_1^* = (\zeta^3 + 12\zeta^2 + 36\zeta + 24)(2\zeta^6 + 39\zeta^5 + 249\zeta^4 + 744\zeta^3 + 1116\zeta^2 + 756\zeta + 180)(\zeta^4 + 8\zeta^3 + 24\zeta^2 + 24\zeta + 12) \quad (6.59)$$

$$n_0^* = 2(\zeta^3 + 6\zeta^2 + 12\zeta + 6)(\zeta^4 + 8\zeta^3 + 24\zeta^2 + 24\zeta + 12)(\zeta^3 + 12\zeta^2 + 36\zeta + 24)^2 \quad (6.60)$$

$$d_2^* = 3(2\zeta^3 + 9\zeta^2 + 12\zeta + 6)(\zeta^2 + 4\zeta + 2)^4 \quad (6.61)$$

$$d_1^* = (\zeta^4 + 16\zeta^3 + 63\zeta^2 + 84\zeta + 30)(\zeta^4 + 8\zeta^3 + 24\zeta^2 + 24\zeta + 12)(\zeta^2 + 4\zeta + 2)^2 \quad (6.62)$$

$$d_0^* = (\zeta + 2)(\zeta^3 + 12\zeta^2 + 36\zeta + 24)(\zeta^4 + 8\zeta^3 + 24\zeta^2 + 24\zeta + 12)(\zeta^2 + 4\zeta + 2)^2 \quad (6.63)$$

As previously mentioned, to exploit the results of [23, 16], the non-delayed part of the quasipolynomial must have only real roots which is guaranteed if Eqn. (6.32) holds, thus it follows that  $\lambda > 0$  as  $s_{0_x}^2 > 0$  and, from Eqns. (6.53)-(6.63), that

$$\frac{n_2^* \lambda^2 - n_1^* \lambda + n_0^*}{d_2^* \lambda^2 - d_1^* \lambda + d_0^*} > 18\sqrt{\lambda} \quad (6.64)$$

To ensure the existence of a given  $\lambda$  satisfying the condition above, some restrictions over  $\zeta$  (consequently over  $\tau$  and  $s_{0_i}$ ) must be established. In this regard, the analysis of the polynomial in Eqn. (6.53) can be performed in any mathematical software that allows the treatment of symbolic and numerical computations. In the current case of study, Maple and its package *RootFinding[Parametric]* were used.

The aforementioned maple package divides the space of parameters into two parts: the discriminant variety and its complement. The discriminant variety is referred as a generalization of the discriminant of a univariate polynomial and contains those parameter values leading to non-generic solutions, meanwhile, its complement can be expressed as a finite union of open cells such that the number of real solutions of the system is constant on each cell. In this manner, all parameter values leading to generic solutions of the system can be described. The underlying techniques used are Gröbner bases, polynomial real root finding, and cylindrical algebraic decomposition, see for instance [142, 89, 90, 121]. Further details of the package and its implementation are available at [55, 96]. Thus, the cell decomposition of Eqn. (6.53), assuming the condition in Eqn. (6.64) and that  $\lambda > 0$ , provides three  $\zeta$  intervals where the conditions holds. These intervals are defined by the projection polynomials:

$$\begin{aligned} \varphi_1(\zeta) = & \zeta^{12} - 78\zeta^{10} - 120\zeta^9 + 2772\zeta^8 + 13824\zeta^7 + 8208\zeta^6 - 105408\zeta^5 - 357696\zeta^4 - 546048\zeta^3 - \\ & 456192\zeta^2 - 207360\zeta - 41472 \end{aligned} \quad (6.65)$$

$$\varphi_2(\zeta) = \zeta^2 + 4\zeta + 2, \quad \varphi_3(\zeta) = \zeta^3 + 9\zeta^2 + 18\zeta + 6 \quad (6.66)$$

and their real roots, such that

$$\zeta_{\varphi_1,1} \approx -0.8478574488 < \zeta < \zeta_{\varphi_2,2} \approx -0.5857864376 \quad (6.67)$$

$$\zeta_{\varphi_2,2} \approx -0.5857864376 < \zeta < \zeta_{\varphi_3,3} \approx -0.4157745568 \quad (6.68)$$

$$\zeta_{\varphi_3,3} \approx -0.4157745568 < \zeta < 0 \quad (6.69)$$

where  $\zeta_{\varphi_i,j}$  denotes the  $j$ -th real root of the projection polynomial  $\varphi_i(\zeta)$  (considering that the real roots have been arranged in increasing order). For instance, only the conditions over  $\zeta$  that ensure the existence of a proper  $\lambda$  have been given thus, one shall investigate the dominance of the corresponding roots within the intervals.

Applying the integral factorization suggested in [21, 15, 16], if the quasipolynomial in Eqn. (6.23) possesses a root of multiplicity at least 4, an integral representation can be adopted. The computation of the control gains as previously performed, allows one to establish a negative real root of multiplicity 4 thus, the substitution of Eqns. (6.35)-(6.37) into Eqn. (6.23) yields to:

$$\Delta_x(s; s_{0_x}, \tau) = (s - s_{0_x})^4 \left( 1 + \int_0^1 e^{-(s-s_{0_x})\tau v} \frac{\tau R_{3,x}(s_{0_x}; \tau v)}{3!} dv \right) \quad (6.70)$$

such that:

$$R_{3,x}(s_{0_x}; \tau v) = s_{0_x} \left[ s_{0_x}^3 \tau^3 v^3 \left( 1 + \lambda - \frac{1}{9} \frac{n_2 \lambda^2 - n_1 \lambda + n_0}{d_2 \lambda^2 - d_1 \lambda + d_0} \right) + 6s_{0_x}^2 \tau^2 v^2 \left( 2 + \lambda - \frac{1}{6} \frac{n_2 \lambda^2 - n_1 \lambda + n_0}{d_2 \lambda^2 - d_1 \lambda + d_0} \right) + 6s_{0_x} \tau v \left( 6 + \lambda - \frac{1}{3} \frac{n_2 \lambda^2 - n_1 \lambda + n_0}{d_2 \lambda^2 - d_1 \lambda + d_0} \right) + 2 \left( 12 - \frac{1}{3} \frac{n_2 \lambda^2 - n_1 \lambda + n_0}{d_2 \lambda^2 - d_1 \lambda + d_0} \right) \right] \quad (6.71)$$

The results in [23] provide a necessary and sufficient condition for the dominance of a given multiple root (of maximal multiplicity) to hold in the first-order case. The main idea of the cited work is used in the current case of study to get sufficient conditions for the dominance of the quadruple root at  $s_{0_x}$ , such that if:

$$\left| \frac{\tau R_{3,x}(s_{0_x}; \tau v)}{3!} \right| \leq 1 \quad \forall 0 < v < 1 \quad (6.72)$$

holds,  $s_{0_x}$  is the dominant root of Eqn. (6.23). Nevertheless, to keep the consistency of the proof, one may rewrite Eqn. (6.72) in terms of  $\zeta$  as follows:

$$\left| R_{3,x}^*(\zeta; v) \right| \leq 1 \quad \forall 0 < v < 1 \quad (6.73)$$

with

$$R_{3,x}^*(\zeta; v) = \frac{1}{6} \left[ \zeta^4 v^3 \left( 1 + \lambda - \frac{1}{9} \frac{n_2^* \lambda^2 - n_1^* \lambda + n_0^*}{d_2^* \lambda^2 - d_1^* \lambda + d_0^*} \right) + 6\zeta^3 v^2 \left( 2 + \lambda - \frac{1}{6} \frac{n_2^* \lambda^2 - n_1^* \lambda + n_0^*}{d_2^* \lambda^2 - d_1^* \lambda + d_0^*} \right) + 6\zeta^2 v \left( 6 + \lambda - \frac{1}{3} \frac{n_2^* \lambda^2 - n_1^* \lambda + n_0^*}{d_2^* \lambda^2 - d_1^* \lambda + d_0^*} \right) + 2\zeta \left( 12 - \frac{1}{3} \frac{n_2^* \lambda^2 - n_1^* \lambda + n_0^*}{d_2^* \lambda^2 - d_1^* \lambda + d_0^*} \right) \right] \quad (6.74)$$

Due to the high order of the polynomials involved in the definition of  $R_{3,x}^*(\zeta; v)$ , an analytic analysis of its behavior results complex and computationally expensive, instead, a numerical analysis implies less computational resources and can provide enough and sufficient information to validate the proposal. In this regard, Fig. 6.3 exposes the plots of  $R_{3,x}^*(\zeta; v)$  for a given  $\zeta$  within each of the intervals in Eqns. (6.67)-(6.69) such that  $v$  varies from 0 to 1 in order to verify Eqn. (6.73).

The results depicted in Figs. 6.3 show that for a given  $\zeta$  within the intervals in Eqns. (6.67) and (6.68), respectively, the condition in Eqn. (6.73) does not hold. On the other hand, for a given  $\zeta$  within the interval in Eqn. (6.69), one can obtain a bound over  $\zeta$  such that Eqn. (6.73) holds. By solving  $R_{3,x}^*(\zeta; v = 0) = 1$ , one finds that the aforementioned condition is satisfied if  $0 > \zeta > -0.3109805570$  which ends the proof. ■

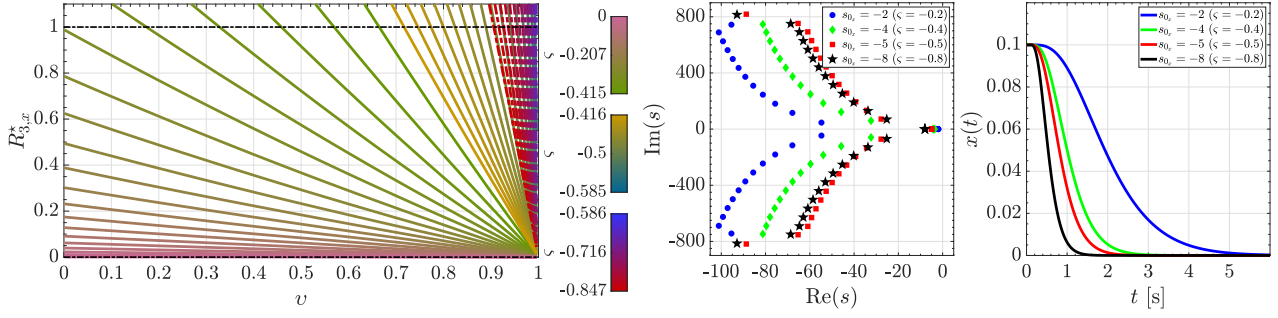


Figure 6.3: (left) Behavior of  $R_{3,x}^*(\zeta; \nu)$  within the interval  $0 < \nu < 1$ . Numerical evidence of the dominance of the root  $s_{0_x}$  within the intervals in Eqns. (6.67)-(6.69) with  $\tau = 0.1$  [s]: (Center) Spectral distribution of the roots. (Right) Time-domain solution.

Notice that the numerical study revealed that for any  $\zeta$  within the intervals in Eqns. (6.67)-(6.69), the dominance of  $s_{0_x}$  holds (as illustrated in Fig. 6.3) yet, the analytic extension of the validity of the proposition implies a further and more complex analysis that comprehends the definition of more inequalities and conditions over the integral.

## 6.5 UAV Control: The Tilting-Rotors Case

The analysis of the quadrotor endowed with tilting-rotors takes into consideration the prescribed linearized conditions established in Section 6.4 additionally, the small-angle approximation is extended to the tilt angle of the rotors  $\beta, \alpha$ , i.e.  $C_\beta \approx 1$ ,  $S_\beta \approx \beta$ ,  $C_\alpha \approx 1$  and  $S_\alpha \approx \alpha$ . In this regard, the dynamic model in Eqns. (6.6), (6.7), (6.11) and (6.13) is linearized such that the corresponding representation in the frequency domains reads as:

$$X(s) = \frac{1}{m_r s^2} ((F_{p_1}(s) + F_{p_3}(s)) \beta(s) + \theta(s) T(s)), \quad Y(s) = \frac{1}{m_r s^2} (-(F_{p_2}(s) + F_{p_4}(s)) \alpha(s) - \phi(s) T(s)) \quad (6.75)$$

$$Z(s) = \frac{1}{m_r s^2} (T(s) - m_r g), \quad \psi(s) = \frac{1}{I_z s^2} \tau_\psi(s) \quad (6.76)$$

$$\phi(s) = \frac{1}{I_x s^2} (\tau_\phi(s) + \rho_\phi(s)), \quad \theta(s) = \frac{1}{I_y s^2} (\tau_\theta(s) + \rho_\theta(s)) \quad (6.77)$$

Notice that, in Eqn. (6.75), the influence of the free-moments  $\varepsilon (F_{p_1}(s) + F_{p_3}(s)) \beta(s)$  and  $-\varepsilon (F_{p_2}(s) + F_{p_4}(s)) \alpha(s)$  is considered as a disturbance and denoted instead as  $\rho_\phi(s)$  and  $\rho_\theta(s)$ , respectively. In addition, it can be appreciated that the 6 DOFs of the current quadrotor vehicle are decoupled which permits a separate treatment nonetheless, for the linearization assertions to hold, the vehicle should operate at  $\phi, \theta, \psi \approx 0$ , as a consequence the controllers stabilizing the attitude of the vehicle are devoted to keep the vehicle at such operational point as described next.

As in Section 6.4, the  $Z(s)$  and  $\psi(s)$  dynamics is addressed firstly as they provide valuable information used in the sequel of the procedure. Thus, let  $T(s)$  and  $\tau_\psi(s)$  be used as the respective control inputs for  $Z(s)$  and  $\psi(s)$ , such that these are defined in Eqn. (6.76).

Regarding the  $\phi(s)$  and  $\theta(s)$  motions of the vehicle, the corresponding control inputs  $\tau_\phi(s)$  and  $\tau_\theta(s)$  are defined as

$$\tau_\phi(s) = I_x \mathcal{C}_\phi^*(s) E_\phi(s), \quad \tau_\theta(s) = I_y \mathcal{C}_\theta^*(s) E_\theta(s) \quad (6.78)$$

where

$$\mathcal{C}_\phi^*(s) = k_{d_\phi} s + k_{p_\phi} + \frac{k_{i_\phi}}{s}, \quad \mathcal{C}_\theta^*(s) = k_{d_\theta} s + k_{p_\theta} + \frac{k_{i_\theta}}{s} \quad (6.79)$$

correspond to linear PID controllers with gains  $k_{p_\phi}, k_{p_\theta}, k_{d_\phi}, k_{d_\theta}, k_{i_\phi}, k_{i_\theta} > 0$  since the presence of disturbances can be neutralized by the effects of the integral term. These controllers can be tuned by means of spectral methods.

To conceive the control strategy of the translational DOFs  $X(s)$  and  $Y(s)$ , one must keep in mind that the rotational dynamics is faster than that of translation, which let one assume that for a large enough time,  $\phi(s), \theta(s), \psi(s) \rightarrow 0$  and as a consequence  $\phi(s)T(s), \theta(s)T(s) \rightarrow 0$  which permits to rewrite Eqn. (6.75) as:

$$X(s) = \frac{1}{m_r s^2} ((F_{p_1}(s) + F_{p_3}(s)) \beta(s)), \quad Y(s) = \frac{1}{m_r s^2} (-(F_{p_2}(s) + F_{p_4}(s)) \alpha(s)) \quad (6.80)$$

Consequently, and as in Section 6.4 it is also considered that, for a large enough time,  $\tau_\psi(s) \rightarrow 0$  and  $T(s) \rightarrow T_c = m_r g$ , which in conjunction with the definition of  $T$  in Eqn. (6.10) and that of  $\tau_\psi$  in Eqn. (6.12), leads to conclude that  $F_{p_1}(s) + F_{p_3}(s) \rightarrow T_c/2$  and  $F_{p_2}(s) + F_{p_4}(s) \rightarrow T_c/2$ . The latter is translated to Eqn. (6.80) as follows:

$$X(s) = \frac{T_c}{2m_r s^2} \beta(s) \quad Y(s) = -\frac{T_c}{2m_r s^2} \alpha(s) \quad (6.81)$$

The set of assumptions leads to define  $\alpha(s)$  and  $\beta(s)$  as the only control inputs that drive the translational states of the system in a sense that:

$$\beta(s) = \frac{2m_r}{T_c} \mathcal{C}_x(s) E_x(s) \quad \alpha(s) = -\frac{2m_r}{T_c} \mathcal{C}_y(s) E_y(s) \quad (6.82)$$

with  $\mathcal{C}_x(s), \mathcal{C}_y(s), E_x(s)$  and  $E_y(s)$  being linear PD controllers and the error signals as defined by Eqns. (6.19)-(6.20).

The dynamics of the servomotors are neglected since, according to the results reported in the literature (see for instance [144, 145, 54, 2]), it is relatively much faster than that of the overall aircraft. Thus, the  $\alpha(s)$  and  $\beta(s)$  angles are assumed to be instantaneously tracked.

Lastly, the  $X(s)$  and  $\theta(s)$  closed-loop dynamics of the quadrotor with tilting-rotors are depicted as block diagrams in Fig. 6.4 for a suitable understanding of the current section. The diagram blocks regarding the  $Z(s)$  and  $\psi(s)$  dynamics coincide with those of the typical quadrotor vehicle shown in Fig. 6.2.

From the previous establishment of the control schemes, and recalling that the effect of the time-delay  $\tau$  affects only the

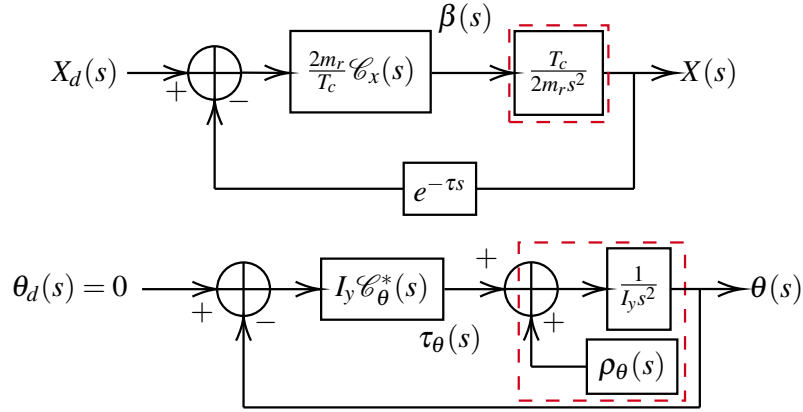


Figure 6.4: Block diagram representation of the quadrotor with tilting-rotors closed-loop system

translation of the system, one can find that the characteristic quasipolynomials of the concerned degrees of freedom are:

$$\Delta_x(s : k_{p_x}, k_{d_x}, \tau) = s^2 + e^{-\tau s} \mathcal{C}_x(s), \quad \Delta_y(s : k_{p_y}, k_{d_y}, \tau) = s^2 + e^{-\tau s} \mathcal{C}_y(s), \quad \Delta_z(s : k_{p_z}, k_{d_z}, \tau) = s^2 + e^{-\tau s} \mathcal{C}_z(s) \quad (6.83)$$

Since the three characteristic quasipolynomials above have the form of that in Eqn. (6.25), Proposition 6.4.2 is used to tune the controllers' gains.

## 6.6 Simulation Results

The actual section provides the results validating the proposed overall control scheme, i.e. a MID-Property-Based control tuning criteria. The latter is carried out through a set of detailed numerical simulations comprehending both the full non-linear model and the linearized versions, this latter part actually used to synthesize the control strategy and controllers' tuning. Both considered vehicles specification parameters are listed in Table 6.1a, while the translational references to be achieved and tracked were set as:

Table 6.1: Definition of the vehicle's parameters and control gains

(a) Parameters of the UAVs		(b) Control gains: Typical quadrotor		(c) Control gains: Quadrotor endowed with titling rotors				
Parameter	Nominal value	DOF	$k_p$	$k_d$	DOF	$k_p$	$k_d$	$k_i$
$m_r$	0.675 kg	$x, y$	1.658539	1.842677	$x, y, z$	7.91223	4.611587	
$I_x, I_y$	0.271 kg m <sup>2</sup>	$z$	7.91223	4.611587	$\phi, \theta$	10	15	0.5
$I_z$	0.133 kg m <sup>2</sup>	$\psi$	10	15	$\psi$	10	15	
$\ell$	0.45 m							
$g$	9.81 m/s <sup>2</sup>							
$\varepsilon$	0.34 m							

$$x_d(t) = \begin{cases} 0 & 0 \leq t < 20 \\ \frac{20-t}{10} & 20 < t < 30 \\ \frac{t-30}{5} - 1 & 30 < t < 40 \\ 1 - \frac{t-40}{10} & 40 < t < 50 \\ 0 & 50 < t \leq 70 \end{cases} \quad y_d(t) = \begin{cases} 0 & 0 \leq t < 10 \\ 1 & 10 < t < 20 \\ 1 - \frac{t-20}{5} & 20 < t < 30 \\ -1 & 30 < t < 40 \\ \frac{t-40}{5} - 1 & 40 < t < 50 \\ 0 & 50 < t \leq 70 \end{cases} \quad z_d(t) = \begin{cases} 2 & 0 \leq t < 30 \\ 2 - \frac{t-30}{10} & 30 < t < 40 \\ 1 & 40 < t < 60 \\ 0 & 60 < t \leq 70 \end{cases} \quad (6.84)$$

where  $x_d(t)$ ,  $y_d(t)$  and  $z_d(t)$  denote the corresponding references and are given in meters [m], and  $t \geq 0$  stands for the time given in seconds [s].

The study was conducted within the MATLAB/Simulink<sup>®</sup> 2018b environment, running on an equipment with an 8GB RAM and an Inter<sup>®</sup> Core™ i5-8250 CPU @ 1.60 GHz & 1.80 GHz processor.

Finally, the simulations for both vehicles took into consideration a time-delay  $\tau$  of 0.1 [s]. Further details concerning the controllers' gains and the behavior of each system are provided in the upcoming subsections.

### 6.6.1 Simulation results: The Typical Quadrotor Case

With base on Proposition 6.4.2 and establishing  $\tau = 0.1$  [s], the controller of the altitude ( $z$ ) was tuned, and the rightmost root was found to be  $s_{0_z} \approx -5.85786437$ . On the other hand, for the  $x$  and  $y$  controllers, Proposition 6.4.3 was used such that  $s_{0_x} = s_{0_y} = -2$ . The results of the tuning criteria led to the control gains summarized in Table 6.15. In this matter, it is worth highlighting that with the given control gains  $s_{\phi,1} = s_{\theta,1} \approx -9.515844632$  and  $s_{\phi,2} = s_{\theta,2} \approx -1.135739338$  such that  $s_{\theta,1} < s_{0_x} < s_{\theta,2}$  (respectively  $s_{\phi,1} < s_{0_y} < s_{\phi,2}$ ) thus, the overall dynamics of the system can be considered to be slightly faster than that of the inner loop but still bounded. The results of the numerical simulation depicted throughout Fig. 6.5 suggest that such difference is acceptable since the UAV achieves and successfully tracks the desired references.

In Figs. 6.5, the left-column results correspond to the vehicle's translational motion, while the right-column plots exhibit the UAV's rotational behavior. In this matter, black color stands for the reference values, blue noisy signals correspond to the response of the non-linear system and orange signals describe the behavior of the linear system.

As it can be appreciated in Fig. 6.5, the vehicle reaches the desired translational references, moreover, the performance of the non-linear system matches that of the vehicle whose dynamics is provided by the linear model. Nevertheless, one may pay special attention to the  $z$  motion as the behavior of the vehicle differs; in this sense, the vehicle with non-linear dynamics experiences some disturbances related to the real couplings existing due to the inherent nature of the UAV, however, the vehicle converges to the reference value in a relatively short time. Regarding the rotational motion of the quadrotor, depicted in Fig. 6.5, it comes to be evident to relate the corresponding peaks on the signals to the corresponding translation DOFs at which they are coupled, such that a change in the desired orientation occurs as the translational desired behavior changes.

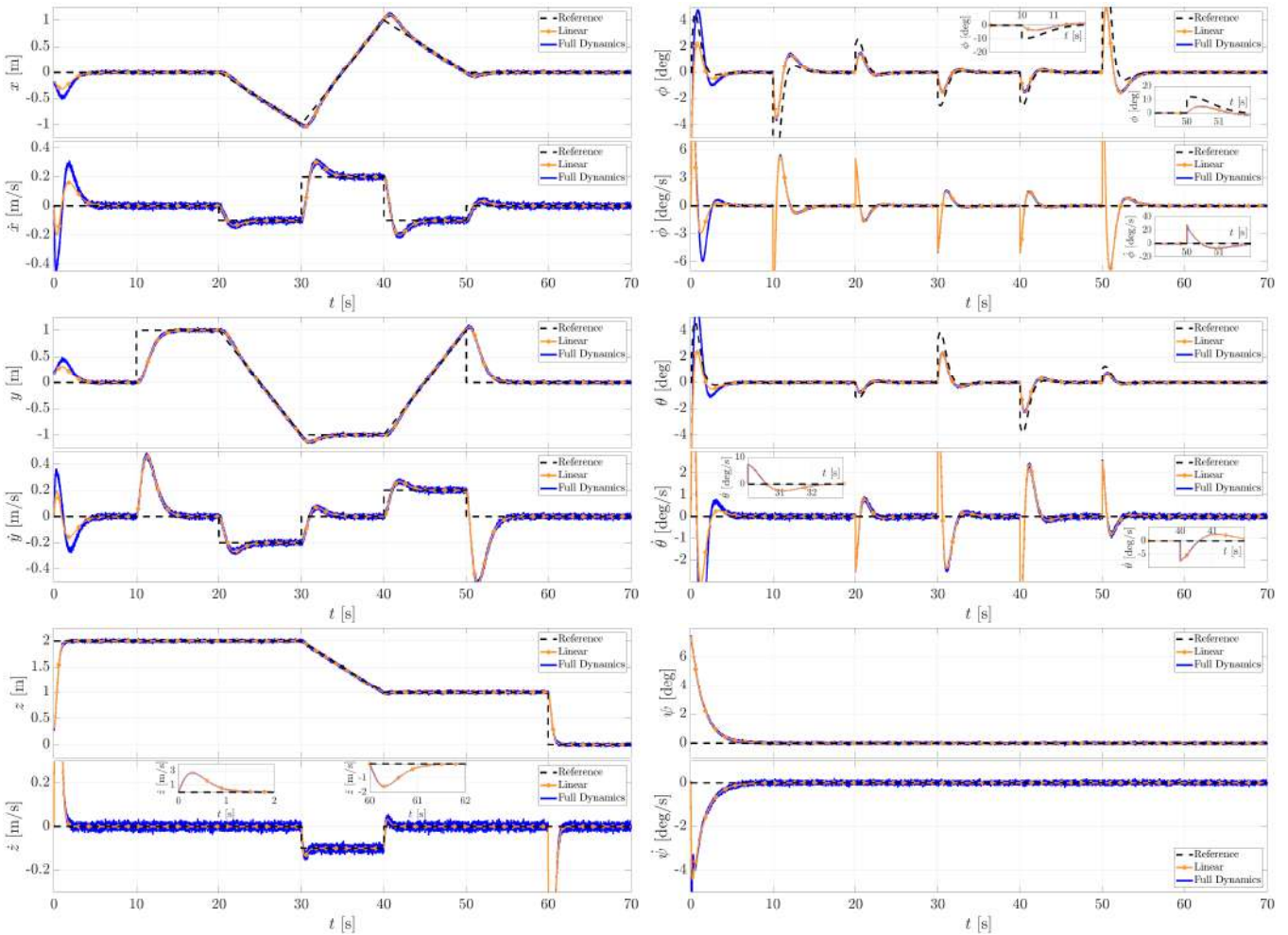


Figure 6.5: Motion of the typical quadrotor vehicle: Left) Translational states. Right) Rotational states.

### 6.6.2 Simulation results: The Tilting-Rotors Case

As discussed in [Section 6.5](#), to tune the controllers regarding the quadrotor vehicle endowed with tilting-rotors, [Proposition 6.4.2](#) was applied to the controller of each translation DOF since the rotational and translational motions of the vehicle are decoupled as previously discussed. Thus, recalling that  $\tau = 0.1$  [s], the control gains in [Table 6.1c](#) were computed.

The results of the simulation are depicted throughout [Figs. 6.6](#) such that the translational motion is described by the plots at the left, and the plots at the right column depicts the rotational the rotational states of the corresponding vehicle. Notice that the response of the servomotors is also depicted in the aforementioned figures.

In comparison with the typical quadrotor vehicle, the translational states of the system seem to follow the similar behavior, nevertheless, [Fig. 6.6](#) shows, that in the case where the non-linear dynamic model was considered, there exists a coupling between the three DOFs, in this sense, one may recall the considerations assumed during the linearization and controllers conception such that the couplings are given by the tilting-rotors.

Regarding the rotational motion of the system, depicted in [Fig. 6.6](#) it can be appreciated that the states of the system remain near to 0 [deg] as the servomotors' action permits to decouple the rotational and transnational motions. Nonetheless, the yaw angle seems to present a large deviation from the desired value due to the influence of the servomotors actuation which was

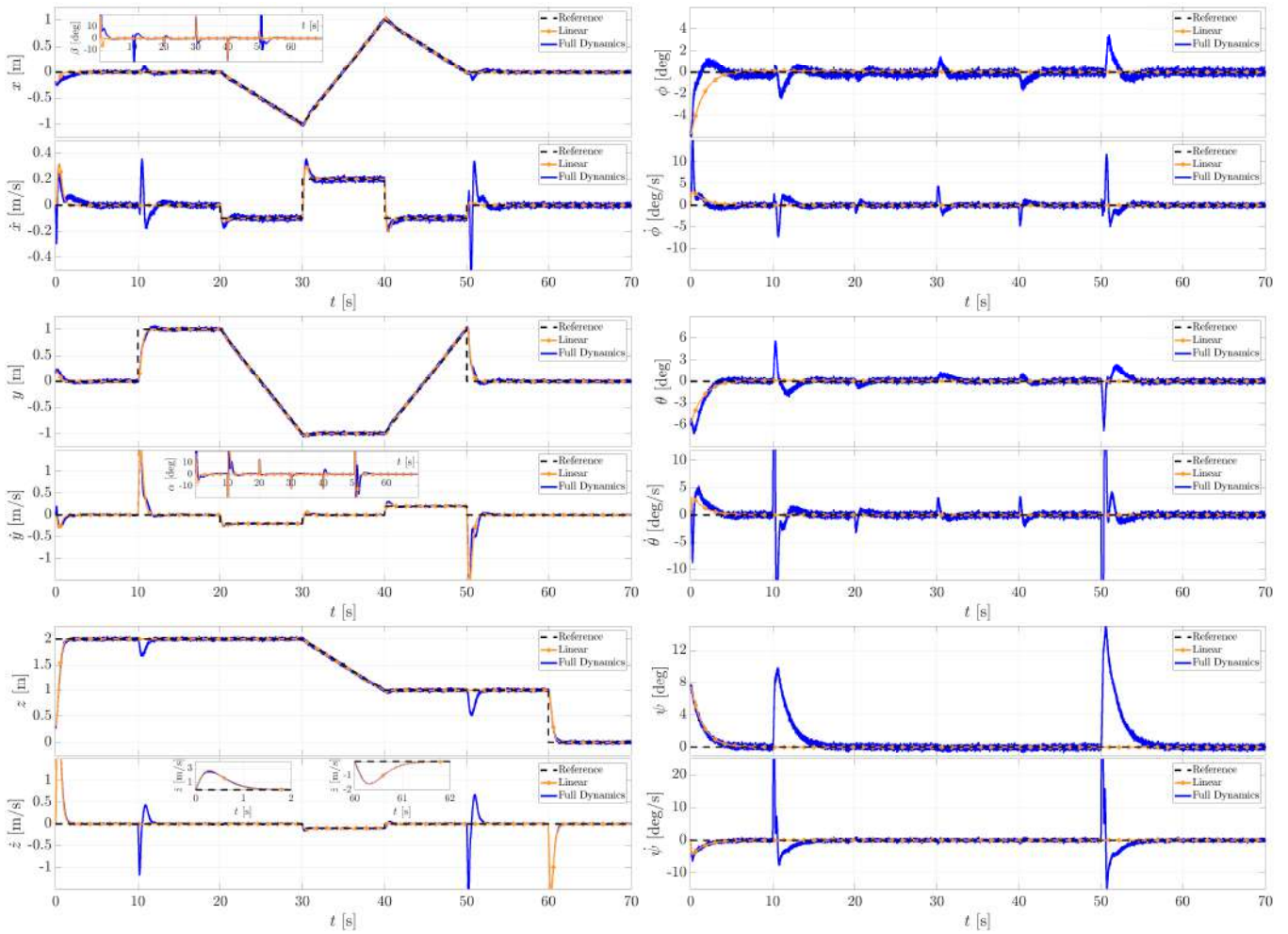


Figure 6.6: Motion of the quadrotor vehicle endowed with tilting-rotors: Left) Translational states. Right) Rotational states.

neglected during the conception of the controllers yet, the orientation tends to be stabilized with no considerable consequence.

## Chapter 7

# Time-delay Control of a VTOL Multi-Agent System

As a matter of fact, it must be highlighted that the current chapter is a product of a research collaboration. In this sense, the main contributions of mine correspond to the redaction of the introductory section as well as the review of the literature in the corresponding regard, the verification of the theoretical prerequisites and the dynamics of the vehicle and the modeling of the multi agent system. Thus, the redaction style may differ from the rest of the thesis. With this being said, the sequel of the chapter is structured as follows, A brief introduction to the problematic and the corresponding state of the art is provided in [Section 7.1](#). In [Section 7.2](#), some useful mathematical preliminaries are presented. [Section 7.3](#) is devoted to the mathematical modeling of the VTOL-mUAV system. [Section 7.4](#) presents the attitude control law for each robot, the formulation of the time-delay tolerant control law and the consensus strategy for the set of aerial vehicles. The simulation scenario and numerical results are presented in [Section 7.5](#). The conclusions and future work are presented in [Subsection 8.2.3](#).

### 7.1 Introduction

The surge in multi-agent systems (MAS) has motivated the scientific community due to the technological advances in autonomous robotics thus, impacting directly in control theory. Swarm control of autonomous systems feature multiple applications in different sectors where an agreement between the agents to recognize the states of each individual of the system, or *consensus* [\[72, 164\]](#), is required. In this regard, prior works as the ones exposed in [\[105, 19, 165\]](#) give evidence of the long-time-inverted effort to overcome the aforementioned problem.

Novel control methods for multiple vehicles are rapidly emerging in recent years due to the wide variety of challenges involved in the large-scale of multi-agent systems development [\[45\]](#). On this subject, [\[100\]](#) exposes experimental verification of the asymptotic stability of a distributed formation algorithm in addition with a model predictive control for a group of Unmanned Aerial Vehicles (UAVs) which brings the aircrafts simultaneously to a prescribed formation shape in a 3 dimensional space. The development of a collaborative event-based control applied to the formation problem of a group of VTOL-UAVs is proposed in [\[62\]](#).

Each VTOL-UAV decides, based on the difference of its current state and its latest broadcast state, when it has to send a new value to its neighbors. [44] presents simulation and experimental results of a time-varying formation tracking for a second-order multi-agent system with switching interaction topologies applied to a set of quadrotors. Stability analysis in the sense of Lyapunov proves the stability of the proposed approach. Similarly, [41] shows the implementation of a distributed movement coordinate algorithm for UAVs swarms in exploratory area surveillance missions.

The influence of time delays in communication protocols has become a difficulty widely studied in the literature [137, 4]. The preceding issue was analyzed by the authors of [160] and has been adopted and adapted to the most recent control techniques in [157]. To cite an example on this regard, the work in [76] presents a robust sliding mode with time delay estimation method for controlling the attitude of a tri-rotor UAV in presence of disturbances and uncertainties.

The effects of delays on output feedback control of dynamical systems have been detailed in [127], which simultaneously has served to develop new approaches, as the ones exposed in [20, 21, 68], to improve the performance of the systems constrained by such adversities, leading to combine robust control techniques, time delay control theory and multi-agent control strategies.

The research in [167] analyzes the consensus problem caused by the communication protocol in networks of agents constituted by single and double integrator systems. An estimator of the states allows increasing the time-delay magnitude. In [135], a consensus control is designed based on a graph-based approach and an input-output linearization scheme is implemented to a three-robot system whose control commands are affected by time delays. Similarly, the work performed in [12] introduces a delayed consensus algorithm as a model for interacting agents where the information provided by each neighbor is used to improve the general convergence. The consensus control problem is transformed into a stability problem of the error system in [173] where the system is subjected by time delays and the error is computed based on the network reference provided by the consensus protocol. Else ways, [85] exposes a single-delay Proportional-Retarded protocol to achieve fast consensus in a multi-agent system with double-integrator agent dynamics.

The actual chapter presents a proposal regarding the coordinating control of a set of mini VTOL rotorcrafts. In addition to the works cited above, it is included the problem of the trajectory tracking of the VTOL MAS considering time-delay in the communication and in the sensors while aiming to perform a simple collective interaction (transport). Thus, time-delay controller is synthesized to fulfill the stabilization objective considering the aerial collective interaction during the simulated transport operation. Explicit stability charts whose gain value are used to carry out a detailed simulation study.

## 7.2 Theoretical Prerequisites

The current section presents the mathematical concepts of graph theory and quaternion representation used throughout the chapter.

### 7.2.1 Graph Theory

A multi-agent system (MAS) can be modeled as a set of dynamic systems (or agents) in which an information exchange occurs. Such information flow is mathematically represented by means of graph theory. In this regard, let  $G = \{V, \xi\}$  be defined by the sets  $V = 1, \dots, N$  and  $\xi$  which represent the vertices (or nodes) and edges of the graph, respectively. *Adjacency* between two

nodes,  $i$  and  $j$ , exists if there is an edge  $(i, j)$  that connects both nodes. In this sense, such nodes are said to be *adjacent* and the aforementioned relation is formally represented as

$$\xi = (i, j) \in V \times V : i, j \quad (7.1)$$

An *undirected graph* is described as a graph where the node  $i$  can obtain information about the node  $j$  and vice versa, i.e.

$$(i, j) \in \xi \Leftrightarrow (j, i) \in \xi \quad (7.2)$$

The matrix  $A$  is called the *adjacency matrix* and its elements  $a_{ij}$  describe the adjacency between nodes  $i$  and  $j$  such that

$$a_{ij} = \begin{cases} 1 & i \text{ and } j \text{ are adjacent} \\ 0 & \text{otherwise} \end{cases} \quad (7.3)$$

If all pairs of nodes in  $G$  are connected, then  $G$  is called connected. The distance  $d(i, j)$  is defined by the shortest path between nodes  $i$  and  $j$  and it is equal to the number of edges that conform the path. The *degree matrix*  $D$  of  $G$  is the diagonal matrix with elements  $d_i$  equal to the cardinality of node  $i$ 's neighbor set  $N_i = \{j \in V : (i, j) \in \xi\}$ . The *Laplacian matrix*  $\mathcal{L}$  of  $G$  is defined as  $\mathcal{L} = D - A$ . For undirected graphs,  $\mathcal{L}$  is symmetric and positive semi-definite, i.e.,  $\mathcal{L} = \mathcal{L}^T \geq 0$ . Moreover, the row sums of  $\mathcal{L}$  are zero. For connected graphs,  $\mathcal{L}$  has exactly one zero eigenvalue, and the eigenvalues can be listed in increasing order  $0 = \lambda_1(G) < \lambda_2(G) \leq \dots \leq \lambda_N(G)$ . The second eigenvalue  $\lambda_2(G)$  is called the *algebraic connectivity*.

## 7.2.2 Unit Quaternion and Attitude Kinematics

Consider two orthogonal right-handed coordinate frames: the body coordinate frame,  $B(x_b, y_b, z_b)$ , located at the center of mass of a rigid body and the inertial coordinate frame,  $N(x_n, y_n, z_n)$ , located at some point in the space (for instance, the earth NED frame). The rotation of the body frame  $B$  with respect to the fixed frame  $N$  is represented by the attitude matrix  $R \in SO(3) = \{R \in \mathbb{R}^{3 \times 3} : R^T R = I, \det R = 1\}$ .

The cross product between two vectors  $\xi, \rho \in \mathbb{R}^3$  is represented by a matrix multiplication  $[\xi^\times] \rho = \xi \times \rho$ , where  $[\xi^\times]$  is the well known skew-symmetric matrix. The  $n$ -dimensional unit sphere embedded in  $\mathbb{R}^{n+1}$  is denoted as  $\mathbb{S}^n = \{x \in \mathbb{R}^{n+1} : x^T x = 1\}$ . Members of  $SO(3)$  are often parameterized in terms of a rotation  $\beta \in \mathbb{R}$  about a fixed axis  $e_v \in \mathbb{S}^2$  by the map  $\mathcal{U} : \mathbb{R} \times \mathbb{S}^2 \rightarrow SO(3)$  defined as

$$\mathcal{U}(\beta, e_v) := I_3 + \sin(\beta)[e_v^\times] + (1 - \cos(\beta))[e_v^\times]^2 \quad (7.4)$$

Hence, a unit quaternion,  $q \in \mathbb{S}^3$ , is defined as

$$q := \begin{bmatrix} \cos \frac{\beta}{2} \\ e_v \sin \frac{\beta}{2} \end{bmatrix} = \begin{bmatrix} q_0 \\ q_v \end{bmatrix} \in \mathbb{S}^3 \quad (7.5)$$

where  $q_v = (q_1 \ q_2 \ q_3)^T \in \mathbb{R}^3$  and  $q_0 \in \mathbb{R}$  are known as the vector and scalar parts of the quaternion respectively. The quaternion  $q$  represents an element of  $SO(3)$  through the map  $R : \mathbb{S}^3 \rightarrow SO(3)$  defined as

$$R := I_3 + 2q_0[q_v^\times] + 2[q_v^\times]^2 \quad (7.6)$$

$R = R(q) = R(-q)$  for each  $q \in \mathbb{S}^3$ , i.e. even quaternions  $q$  and  $-q$  represent the same physical attitude.

Denoting by  $\vec{\omega} = (\omega_1 \ \omega_2 \ \omega_3)^T$  the angular velocity vector of the body coordinate frame,  $B$  relative to the inertial coordinate frame  $N$  expressed in  $B$ , the kinematics equation is given by

$$\begin{bmatrix} \dot{q}_0 \\ \dot{q}_v \end{bmatrix} = \frac{1}{2} \begin{bmatrix} -q_v^T \\ I_3 q_0 + [q_v^\times] \end{bmatrix} \vec{\omega} = \frac{1}{2} \Xi(q) \vec{\omega} \quad (7.7)$$

The attitude error is used to quantify mismatch between two attitudes. If  $q$  defines the current attitude quaternion and  $q_d$  the desired quaternion, i.e. the desired orientation, then the error quaternion that represents the attitude error between the current orientation and the desired one is given by

$$q_e := q_d^{-1} \otimes q = (q_{e0} \ q_{ev}^T)^T \quad (7.8)$$

where  $q^{-1}$  is the complementary rotation of the quaternion  $q$  which is given by  $q^{-1} := (q_0 \ -q_v^T)^T$  and  $\otimes$  denotes the quaternion multiplication.

### 7.3 Attitude and Position Dynamics of the VTOL Multi-Agent System

If a group of  $N$ -VTOL vehicles is considered and each aerial system is modeled as a rigid body, as in Fig. 7.1. Then, according to [61], the six degrees of freedom model (position and orientation) of the system can be separated into translational and rotational motions, represented respectively by  $\Sigma_{T_i}$  and  $\Sigma_{R_i}$  in Eqn. 7.9.

$$\Sigma_{T_i} : \begin{cases} \dot{\mathbf{p}}_i = \mathbf{v}_i \\ m_i \dot{\mathbf{v}}_i = -m_i \mathbf{g} + R \begin{bmatrix} 0 \\ 0 \\ u_i \end{bmatrix} \end{cases} ; \quad \Sigma_{R_i} : \begin{cases} \dot{q}_i = \frac{1}{2} \Xi(q_i) \boldsymbol{\omega}_i \\ J_i \dot{\boldsymbol{\omega}}_i = -\boldsymbol{\omega}_i^\times J_i \boldsymbol{\omega}_i + \boldsymbol{\Gamma}_i \end{cases} \quad (7.9)$$

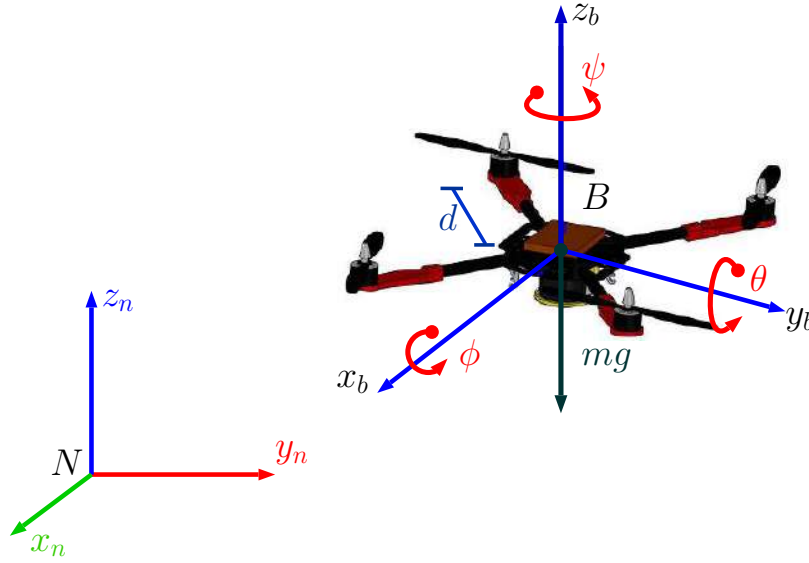


Figure 7.1: Schematic configuration of a VTOL vehicle in the 3d space.

where  $i = 1, \dots, N$ .  $\mathbf{p}_i$  and  $\mathbf{v}_i$  are linear positions and velocities vectors,  $m_i$  is the mass of each aerial system,  $\mathbf{g}$  is the gravity,  $R$  is the rotation matrix, given in Eqn. (7.6). Besides,  $J_i \in \mathbb{R}^{3 \times 3}$  is the inertia matrix of the rigid bodies expressed in the body frame  $B$  and  $\mathbf{\Gamma}_i \in \mathbb{R}^3$  is the vector of applied torques.  $\mathbf{\Gamma}_i$  depends on the (control) couples generated by the actuators and the aerodynamics, such as gyroscopic couples or the gravity gradient.

Note that the rotation matrix  $R$  can also be defined according to the Euler angles as:

$$R(\phi, \theta, \psi) = \begin{bmatrix} C_\theta C_\psi & S_\phi S_\theta C_\psi - C_\phi S_\psi & C_\phi S_\theta C_\psi + S_\phi S_\psi \\ C_\theta S_\psi & S_\phi S_\theta S_\psi + C_\phi C_\psi & C_\phi S_\theta S_\psi - S_\phi C_\psi \\ -S_\theta & C_\theta S_\phi & C_\theta C_\phi \end{bmatrix} \quad (7.10)$$

where  $S \cdot$  and  $C \cdot$  stand for  $\sin(\cdot)$  and  $\cos(\cdot)$  respectively. The roll, pitch and yaw angles are given by  $\phi$ ,  $\theta$ ,  $\psi$  respectively.

## 7.4 Attitude and Position Control for the VTOL MAS

The current section is divided in three parts. First, the attitude control law to stabilize the  $i$ -th agent's attitude is introduced and followed by the position control strategy and finally the multi-agent formation control.

### 7.4.1 Attitude Stabilization Method

The aim of this subsection is to present the design procedure of an attitude control which drives the aerial vehicles to attitude stabilization, i.e. given the following asymptotic conditions

$$q \rightarrow [\pm 1 \ 0 \ 0 \ 0]^T, \ \boldsymbol{\omega} \rightarrow 0 \text{ as } t \rightarrow \infty \quad (7.11)$$

Besides, it is also known that the actuator saturation leads to unfeasible control signals, reducing the benefits of the feedback. The present control law takes into account the physical constraints of the systems in order to apply appropriate control signals.

Given a positive constant  $M$ , a continuous, non-decreasing function  $\sigma_M : \mathbb{R} \rightarrow \mathbb{R}$  is defined by

1.  $\sigma_M = s$  if  $|s| < M$ ;
2.  $\sigma_M = \text{sign}(s)M$  otherwise.

The following result, reported previously in [61] is used for the attitude stabilization of rigid bodies.

Consider a rigid body rotational dynamics described by Eqn. (7.9) with the following bounded control inputs  $\boldsymbol{\Gamma} = (\Gamma_i^1 \ \Gamma_i^2 \ \Gamma_i^3)^T$  such that

$$\boldsymbol{\Gamma}_i^k = -\sigma_{M_i^k} \left( \lambda_i^k [\boldsymbol{\omega}_i^k + \rho_i^k \boldsymbol{q}_i^k] \right) \quad i = 1, \dots, N \quad (7.12)$$

with  $k \in \{1, 2, 3\}$  and where  $\sigma_{M_i^k}$  are saturation functions while  $\lambda_i$  and  $\rho_i$  are positive parameters. Then the inputs in Eqn. (7.12) asymptotically stabilize the rigid body to the origin  $(1 \ 0^T \ 0^T)^T$  (i.e.  $q_0 = 1, q_v = 0$  and  $\vec{\omega} = 0$ ) with a domain of attraction equal to  $\mathbb{S}^3 \times \mathbb{R}^3 \setminus (-1 \ 0^T \ 0^T)^T$ .

The proof is not presented here, but it can be obtained in a similar way to that in [108].

## 7.4.2 Position Control Strategy for the VTOL Multi-Agent System

Assuming that the yaw dynamics can be stabilized by the control law of Eqn. (7.12) at  $\psi = \psi_d$ , then the system in Eqn. (7.9) becomes:

$$\begin{bmatrix} \dot{p}_{x_i} \\ \dot{p}_{y_i} \\ \dot{p}_{z_i} \end{bmatrix} = \begin{bmatrix} v_{x_i} \\ v_{y_i} \\ v_{z_i} \end{bmatrix} \quad (7.13)$$

$$\begin{bmatrix} \dot{v}_{x_i} \\ \dot{v}_{y_i} \\ \dot{v}_{z_i} \end{bmatrix} = \begin{bmatrix} -\frac{u_i}{m_i} (\cos \psi_i \sin \theta_i \cos \phi_i + \sin \psi_i \sin \theta_i) \\ \frac{u_i}{m_i} (\sin \psi_i \sin \theta_i \cos \phi_i - \cos \phi_i \sin \psi_i) \\ \frac{u_i}{m_i} \cos \phi_i \cos \theta_i - g \end{bmatrix} \quad (7.14)$$

With an appropriate choice of the target configuration, it is possible to transform Eqns. (7.13) and (7.14) into three independent linear triple integrators. For this instance, we define

$$\phi_{d_i} := \arctan\left(\frac{r_{2_i}}{r_{3_i} + g}\right), \quad \theta_{d_i} := \arcsin\left(\frac{-r_{1_i}}{\sqrt{r_{1_i}^2 + r_{2_i}^2 + (r_{3_i} + g)^2}}\right) \quad (7.15)$$

where  $r_1$ ,  $r_2$  and  $r_3$  will be described in the following sections. The input control is chosen as positive thrust, such that

$$u_i = m_i \sqrt{r_{1_i}^2 + r_{2_i}^2 + (r_{3_i} + g)^2} \quad (7.16)$$

Let the translational state vector  $\mathbf{p} \in \mathbb{R}^9$  be defined as  $\mathbf{p} = (p_1, p_2, p_3, p_4, p_5, p_6, p_7, p_8, p_9) = (\int p_x, p_x, v_x, \int p_y, p_y, v_y, \int p_z, p_z, v_z)$ , therefore Eqns. (7.13) and (7.14) become:

$$\Sigma_{x_i} : \begin{cases} \dot{p}_{1_i} = p_{2_i} \\ \dot{p}_{2_i} = p_{3_i} \\ \dot{p}_{3_i} = r_{1_i} \end{cases} ; \quad \Sigma_{y_i} : \begin{cases} \dot{p}_{4_i} = p_{5_i} \\ \dot{p}_{5_i} = p_{6_i} \\ \dot{p}_{6_i} = r_{2_i} \end{cases} ; \quad \Sigma_{z_i} : \begin{cases} \dot{p}_{7_i} = p_{8_i} \\ \dot{p}_{8_i} = p_{9_i} \\ \dot{p}_{9_i} = r_{3_i} \end{cases} \quad (7.17)$$

The control strategy proposed inhere is intended to deal with a multi agent system composed by a set of VTOL vehicles; such strategy must lead all the agents states to converge to the average of their initial conditions.

Each VTOL vehicle consists of a position control input which is described by the following consensus protocol:

$$r_{s_i} = - \sum_{j=1}^m \alpha_{ij} (p_{s_i} - p_{s_j}) - \sum_{j=1}^m \beta_{ij} (\dot{p}_{s_i} - \dot{p}_{s_j}) - \sum_{j=1}^m \gamma_{ij} \int (p_{s_i} - p_{s_j}) + r_{s_j} \quad (7.18)$$

with  $s \in \{x, y, z\}$ ,  $\alpha$ ,  $\beta$  and  $\gamma$  constants parameters computed in the forthcoming paragraphs. Also, let us define the next measurement errors for the linear position, velocity and integral of the position

$$E_{(ij)} = p_{s_i} - p_{s_j} ; \quad \dot{E}_{(ij)} = \dot{p}_{s_i} - \dot{p}_{s_j} ; \quad \int E_{(ij)} = \int (p_{s_i} - p_{s_j}) \quad (7.19)$$

The interconnection dynamics in Eqn. (7.18) features a communication delay  $\tau_{1ij} > 0$  between the nodes  $i$  and  $j$ . It is also considered that every VTOL-system owns another sensor-based system, which implies another delay  $\tau_{2ij} = 2\tau_{1ij}$ . Thus, the time-delayed consensus protocol is written as

$$r_{s_i}(t) = - \sum_{j=1}^m \alpha_{ij} (p_{s_i}(t - \tau_{1ij}) - p_{s_j}(t - \tau_{2ij})) - \sum_{j=1}^m \beta_{ij} (\dot{p}_{s_i}(t - \tau_{1ij}) - \dot{p}_{s_j}(t - \tau_{2ij})) - \sum_{j=1}^m \gamma_{ij} \int (p_{s_i}(t - \tau_{1ij}) - p_{s_j}(t - \tau_{2ij})) + r_{s_j}(t) \quad (7.20)$$

It has been demonstrated that a delayed proportional controller (with a single delay) is not able to stabilize a double integrator.

To accomplish this task, a proportional plus a derivative delayed controller [22], can be used to explore the stabilizing effect. However, if the system is under constant disturbances causing stability issues, the design of a robust controller is necessary. Thus, the objective is to have a proportional-integral-derivative term in order to guarantee stability even under the disturbances produced by different phenomena. Moreover, since the system subjected to the current study presents a double time delay for position and velocity data, a first order estimation predictor [12], is used to obtain a new system with a single time delay  $\tau_{1ij}$ . This prediction can be done by a linear extrapolation from past values, namely

$$\hat{p}_j(t - \tau) = p_j(t - 2\tau) + \frac{p_j(t - 2\tau) - p_j(t - 3\tau)}{3\tau} 3\tau = 2p_j(t - 2\tau) - p_j(t - 3\tau) \quad (7.21)$$

Using Eqn. (7.21) for position and velocity in Eqn. (7.20), the model for the multi-agent system considering the time delay is given by

$$r_{s_i}(t) = - \sum_{j=1}^m \alpha_{ij} (p_{s_i}(t - \tau_{1ij}) - p_{s_j}(t - \tau_{1ij})) - \sum_{j=1}^m \beta_{ij} (\dot{p}_{s_i}(t - \tau_{1ij}) - \dot{p}_{s_j}(t - \tau_{1ij})) - \sum_{j=1}^m \gamma_{ij} \int (p_{s_i}(t - \tau_{1ij}) - p_{s_j}(t - \tau_{1ij})) + r_{s_j}(t) \quad (7.22)$$

From Eqn. (7.22) the error dynamics is obtained,

$$\dot{E}_{(ij)}(t) = - \sum_{j=1}^m \alpha_{ij} E_{(ij)}(t - \tau_{1ij}) - \sum_{j=1}^m \beta_{ij} (\dot{E}_{(ij)}(t - \tau_{1ij})) - \sum_{j=1}^m \gamma_{ij} \int (E_{(ij)}(t - \tau_{1ij})) \quad (7.23)$$

Whose Laplace transform corresponds to

$$s^2 E(s) + \sum_{j=1}^m \alpha_{ij} e^{-\tau_{1ij}s} E(s) + \sum_{j=1}^m \beta_{ij} s e^{-\tau_{1ij}s} E(s) + \sum_{j=1}^m \frac{\gamma_{ij}}{s} e^{-\tau_{1ij}s} E(s) = 0 \quad (7.24)$$

which conducts to the definition of the quasipolynomial function as:

$$\Delta(s, \tau) = s^3 + e^{-\tau_{1ij}s} \sum_{j=1}^m (\alpha_{ij}s + \beta_{ij}s^2 + \gamma_{ij}) \quad (7.25)$$

The following assertions hold for Eqn. (7.25):

- i) The multiplicity of any given root of the quasipolynomial function is bounded by 4, it can be attained only on the real axis.
- ii) The quasipolynomial admits a real spectral value with algebraic multiplicity 4 if, and only if (7.29), where  $\alpha := \sum_{j=1}^m \alpha_{ij}$ ,  $\beta := \sum_{j=1}^m \beta_{ij}$  and  $\gamma := \sum_{j=1}^m \gamma_{ij}$ .

The degree of the quasipolynomial function is 4. First, the vanishing of the quasipolynomial  $\Delta$  yields the elimination of the exponential term as a rational function in  $s$ . The substitution of the obtained equality in the set of derivatives gives a system of algebraic equations. Solving the derivatives yields to the solution given by Eqn. (7.29).

$$\alpha = \frac{3e^{2\sqrt{3}\sin(\frac{1}{3}\arctan(\sqrt{2})+\frac{1}{6}\pi)-3}(-58+44\sqrt{3}\sin(\frac{1}{3}\arctan(\sqrt{2})+\frac{1}{6}\pi)+7(2\sqrt{3}\sin(\frac{1}{3}\arctan(\sqrt{2})+\frac{1}{6}\pi)-3)^2)}{\tau^2} \quad (7.26)$$

$$\beta = \frac{3e^{2\sqrt{3}\sin(\frac{1}{3}\arctan(\sqrt{2})+\frac{1}{6}\pi)-3}(-10+8\sqrt{3}\sin(\frac{1}{3}\arctan(\sqrt{2})+\frac{1}{6}\pi)+(2\sqrt{3}\sin(\frac{1}{3}\arctan(\sqrt{2})+\frac{1}{6}\pi)-3)^2)}{\tau} \quad (7.27)$$

$$\gamma = \frac{3e^{2\sqrt{3}\sin(\frac{1}{3}\arctan(\sqrt{2})+\frac{1}{6}\pi)-3}(-434+328\sqrt{3}\sin(\frac{1}{3}\arctan(\sqrt{2})+\frac{1}{6}\pi)+59(2\sqrt{3}\sin(\frac{1}{3}\arctan(\sqrt{2})+\frac{1}{6}\pi)-3)^2)}{\tau^3} \quad (7.28)$$

$$s = \frac{2\sqrt{3}\sin(\frac{1}{3}\arctan(\sqrt{2})+\frac{1}{6}\pi)-3}{\tau} \quad (7.29)$$

The rest of the proof is not presented here, but it can be obtained from the seminal work of [22].

### 7.4.3 VTOL Multi-agent Formation Control

For object transportation operations, the set of air vehicles must be able to perform a stable flight and, in addition, each aircraft must broadcast its angular ( $\psi_i$ ) and linear positions states information to their neighbors. Therefore, the aim is to adapt the control law such that all the robots states converge to the average desired yaw angle and linear positions, which are given by the contact points of the object. Each agent consists of an attitude ( $\psi$ ) and position controllers.

Let us define the states  $\Sigma_i = (p_{x_i}, \dot{p}_{x_i}, p_{y_i}, \dot{p}_{y_i}, p_{z_i}, \dot{p}_{z_i}, \psi_i, \dot{\psi}_i)$  where  $i \in N = \{1, \dots, N\}$ , and the average angular position and velocity as  $\psi_C, \dot{\psi}_C$ , respectively. The average linear positions and velocities  $p_{CM_{x,y,z}}, \dot{p}_{CM_{x,y,z}}$  for all the agents are described by

$$p_{CM_{x,y,z}} = \frac{1}{N} \sum_{i=1}^N p_{i_{x,y,z}} ; \dot{p}_{CM_{x,y,z}} = \frac{1}{N} \sum_{i=1}^N \dot{p}_{i_{x,y,z}} \quad (7.30)$$

$$\psi_C = \frac{1}{N} \sum_{i=1}^N \psi_i ; \dot{\psi}_C = \frac{1}{N} \sum_{i=1}^N \dot{\psi}_i \quad (7.31)$$

Let  $\psi_C^d, \dot{\psi}_C^d$  be the desired yaw angular position and velocity and  $p_{CM_{x,y,z}}^d, \dot{p}_{CM_{x,y,z}}^d$  be the desired average linear positions and velocities for the group of robots.

Eqn. (7.20) allows the multi-agent system to reach its geometrical flock's center of mass. However, the objective of the multi-MAV system is to perform an orientation and position formation linked to the attitude and linear position of the object. In this regard, let  $\Lambda$  be a set of relative, desired inter-agent distances, such that

$$\Lambda = [\mu_{ij} \in \mathbb{R} \mid \mu_{ij} > 0; i, j = 1, \dots, N, i \neq j] \quad (7.32)$$

with  $\mu_{ij} = \mu_{ji}$ , and where it is assumed that  $\Lambda$  is a feasible formation, that is, there are points  $\chi_1, \dots, \chi_N \in \mathbb{R}^3$  such that

$$\|\chi_i - \chi_j\| = \mu_{ij} \quad (7.33)$$

It is possible to extend the consensus algorithms to formation control if the formation is represented by vectors of relative

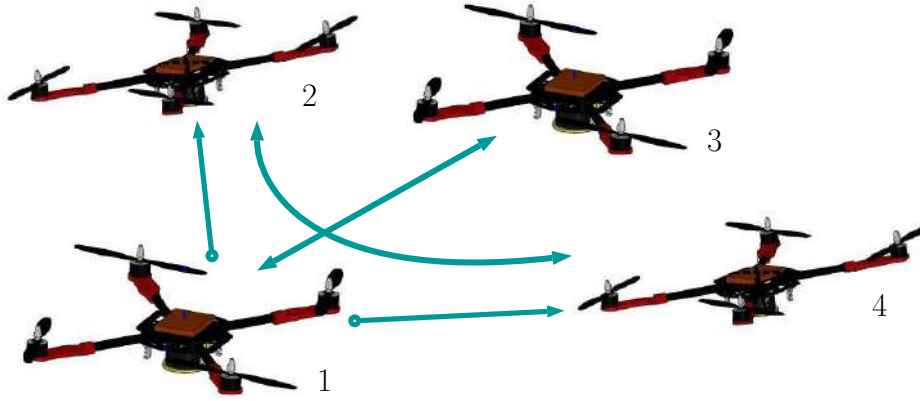


Figure 7.2: Multi-VTOL system and the communication flow.

attitudes or linear positions of neighboring agents, thus, Eqn. (7.18) becomes

$$\mathbf{r}_{s_i} = - \sum_{j=1}^m \alpha_{ij} (\mathbf{p}_{s_i} - \mathbf{p}_{s_j} - \boldsymbol{\mu}_{ij}) - \sum_{j=1}^m \beta_{ij} (\dot{\mathbf{p}}_{s_i} - \dot{\mathbf{p}}_{s_j}) - \sum_{j=1}^m \gamma_{ij} \int (\mathbf{p}_{s_i} - \mathbf{p}_{s_j} - \boldsymbol{\mu}_{ij}) + \mathbf{r}_{s_j} \quad (7.34)$$

## 7.5 Numerical Simulations and Results

This section is devoted to the presentation of numerical simulation results to validate the proposed consensus-delay control strategy of a group of four VTOL aerial vehicles for the grasping and transporting of a generic object.

A simulation was carried out in order to prove the effectiveness of the proposed control strategy. The simulation model features the parameters provided by Table 7.1 for each VTOL vehicle.

Besides, for the case of study presented in this work, four aerial vehicles are considered ( $N = 4$ ), where the agent  $N = 1$  is considered as the leader as depicted in Fig. 7.2

The corresponding adjacency matrix for graph  $G$  is given as:

Table 7.1: Physical parameters for the VTOL vehicle

System	Description	Value	Units
Quadcopter	Mass (m)	400	g
	Distance (d)	20	cm
	Inertial moment $x$ ( $J_\phi$ )	0.0039	$Kg \cdot m^2$
	Inertial moment $y$ ( $J_\theta$ )	0.0039	$Kg \cdot m^2$
	Inertial moment $z$ ( $J_\psi$ )	0.0073	$Kg \cdot m^2$

$$\mathcal{A} = [a_{ij}] = \begin{bmatrix} 0 & 1 & 1 & 1 \\ 0 & 0 & 0 & 1 \\ 1 & 0 & 0 & 0 \\ 0 & 1 & 0 & 0 \end{bmatrix} \quad (7.35)$$

First, it is considered that every robot features a 100ms sensor-based algorithm and the communication between neighbors takes 50ms. To deal with such problem, the predictor given by Eqn. (7.21) is applied to the time-delay originated by the sensor-based algorithm. Afterwards, the time-delay tolerant control Eqn. (7.22) is applied, where the parameters  $\alpha$  and  $\beta$  are computed according to Eqn. (7.29).

It is considered that the control input of the leader agent 1, consisting also of a delayed PID controller with parameters  $\alpha$ ,  $\beta$  and  $\gamma$  given by Eqn. (7.29) is nonzero as well as continuous.

The simulation consisted of four stages described as follows.

- The multi-robot system is initialized at the orientation and 3D position given by the Table 7.2. Then, it is sent to a desired position given by the object center of mass, located at  $p_o = [0.5 \ 1 \ 0.5]^T m$ . The object geometry consists of a square whose borders measure 20cm and its orientation is  $\psi_o = 45^\circ$  related to that of the plane. The VTOL multi-agent system takes off and performs formation control for position at  $p_1^d = [0.43 \ 0.93 \ 1]^T m$ ,  $p_2^d = [0.57 \ 0.93 \ 1]^T m$ ,  $p_3^d = [0.57 \ 1.07 \ 1]^T m$ ,  $p_4^d = [0.43 \ 1.07 \ 1]^T m$ . Then, the set of robots performs formation control for the orientation ( $\psi_i$ ) at  $\psi_i^d = (45^\circ \ 135^\circ \ -135^\circ \ -45^\circ)$ , while they descend at  $p_{z_o} = 0.5m$ . These desired attitudes and positions correspond to the desired contact points on the object, such that the robots attitudes are perpendicular to the contact points of the object.

Table 7.2: Initial conditions for the system

VTOL MAS	$\psi_i$	$p_{x_i}$	$p_{y_i}$	$p_{z_i}$
1	$1^\circ$	0.3m	0.8m	0.01m
2	$3^\circ$	0.7m	0.9m	0m
3	$2^\circ$	0.6m	1.15m	0.02m
4	$-1^\circ$	0.4m	1.1m	0.01m

- Once the robots reach the desired attitudes and positions linked to the object, they grab it by exerting an equal force on the object between 11s and 15s.
- In order to transport and to position the object, a trajectory tracking taking into account the position of the center of mass of the object is executed between the lapse time of 15s and 55s and it is given by  $\xi_{CM_x}^d = 1 + 0.5 \sin(0.08t + \pi)$ ,  $\xi_{CM_y}^d = 1.2 + 0.25 \sin(0.08t + \pi)$  and  $\xi_{CM_z}^d = 0.75 + 0.25 \sin(0.09t + \pi)$ . In order to simulate such task, different disturbances are considered to affect each robot during this stage.
- Finally, when the object center of mass reaches the desired position  $p_{od} = [1.5 \ 1.5 \ 1]^T m$ , the VTOL multi-agent system drops the object and the simulation finishes, accomplishing a 60s operation.

Fig. 7.3 shows the behavior of the set of VTOL vehicles on the 3d space during the simulation with communication and sensor-based delay.

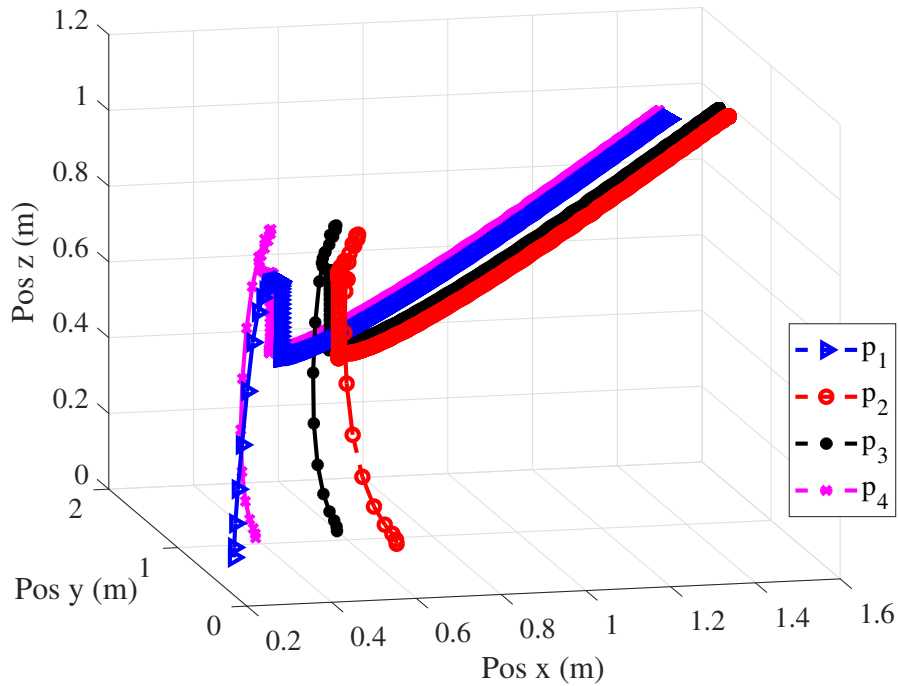


Figure 7.3: Behavior of the multi-agent VTOL system in the 3d space.

Fig. 7.4 presents from top to bottom, the angular and linear positions of the multi-agent system. The different stages of the simulation are represented in the figures: the green area stands for the position and orientation formation stage; the first area in white corresponds to the object grasping stage; the yellow area represents the transportation stage, i.e. where the tracking positions and velocity are achieved; and, lastly, the second white area shows the moment in which the aerial robots arrive to the desired area and drop the object.

Fig. 7.5 presents, from top to bottom, the angles  $\phi$  and  $\theta$  for every VTOL system during the simulation. In this case, it is easily appreciated how the forces exerted on the object act as a disturbance during the trajectory tracking.

The behavior of the system depicted in the figures suggests that even when the system is subjected to time delay communication, it is possible to reach consensus and, in consequence, to perform formation control for linear position and orientation.

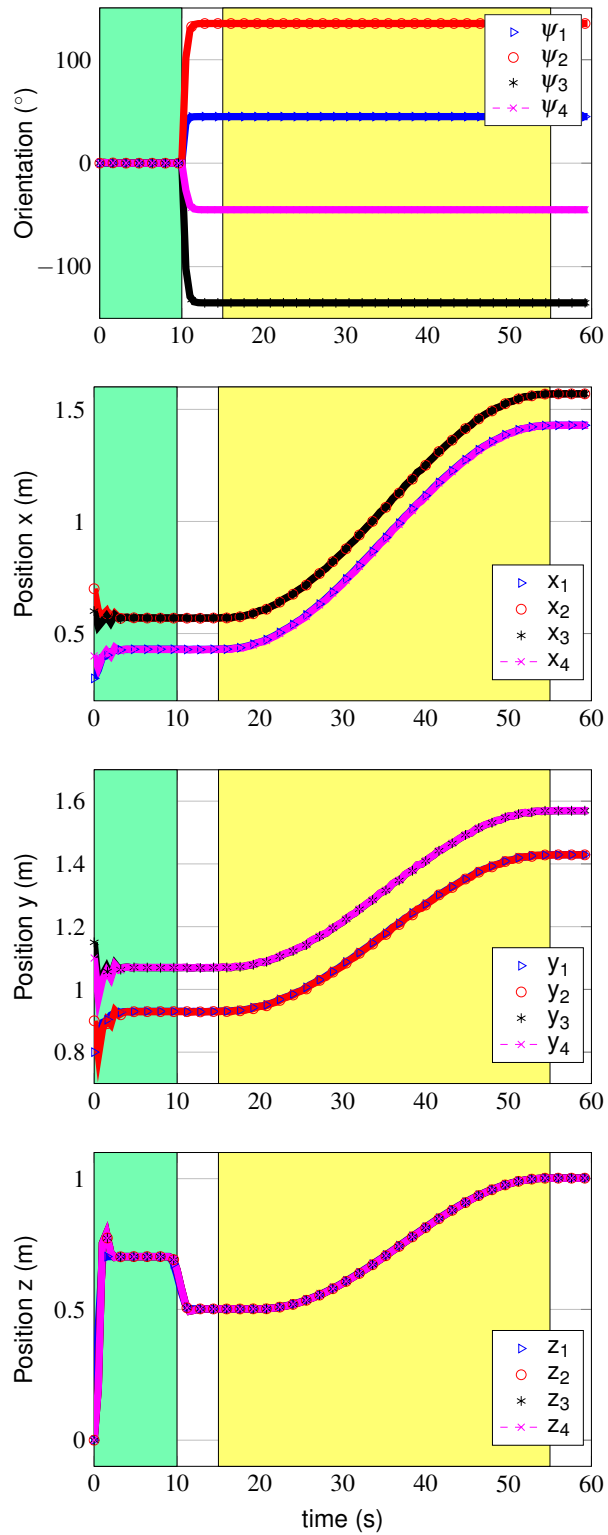
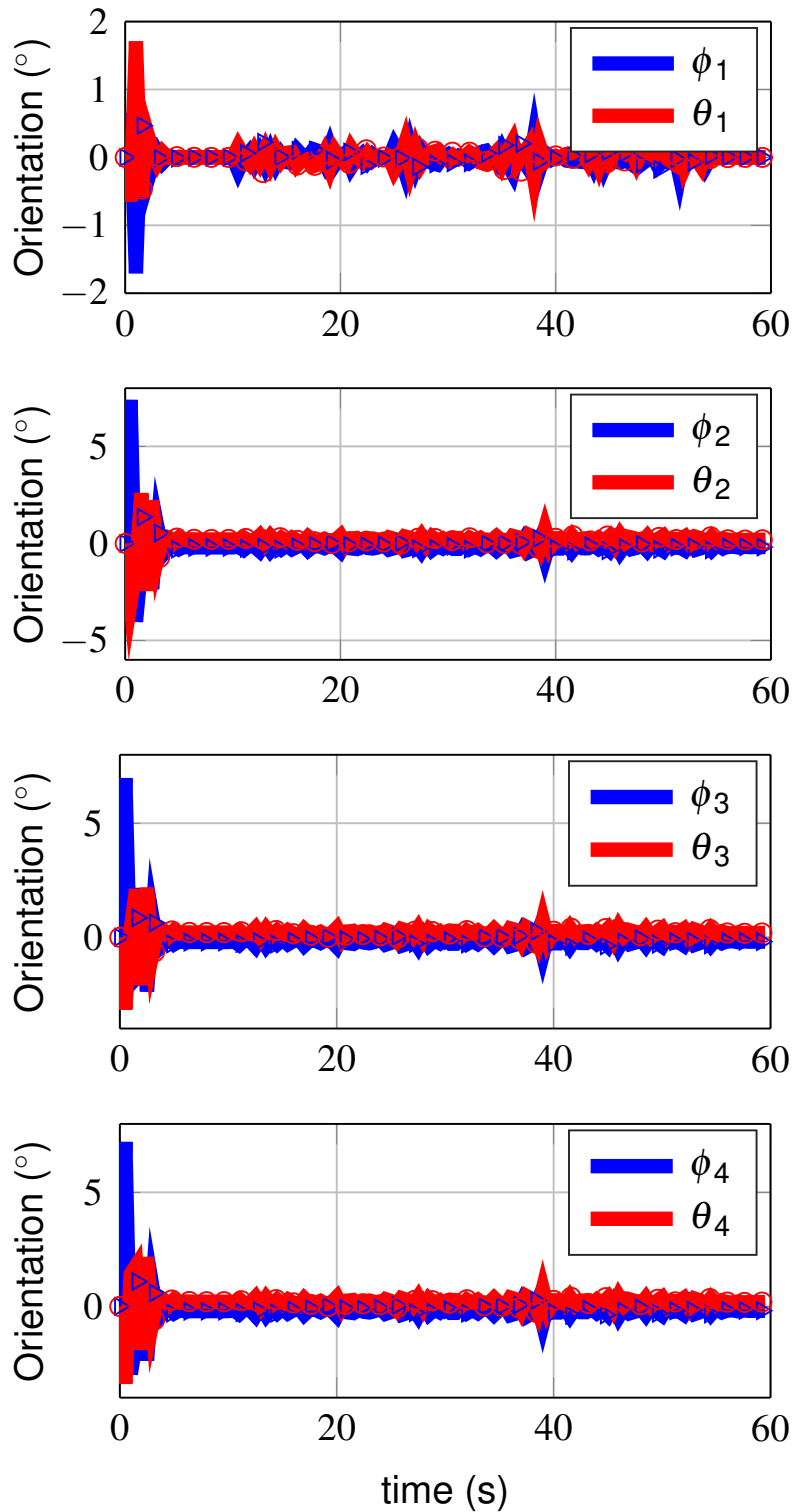


Figure 7.4: Angular ( $\psi_i$ ) and linear positions for the multi-agent system featuring communication and sensor delay

Figure 7.5: Attitude ( $\phi_i, \theta_i$ ) behavior of the different aerial vehicles during the simulation

# Chapter 8

## Concluding Remarks

This last chapter of the thesis gathers the concluding remarks as well as the consideration on forthcoming research. In this vein, [Section 8.1](#) is devoted to the conclusions of the first part of the manuscript, i.e. the study of the Multi-Link Unmanned Aerial System. On the other hand, [Section 8.2](#) exposes the concluding remarks concerning the study of aerial vehicles subjected to time-delay effects. Finally, the general discussion about the overall thesis results is provided in [Section 8.3](#).

### 8.1 Part I: Multi-Link Unmanned Aerial System

In strict order, the concluding remarks of each chapter contained in [Part I](#) are exposed next.

#### 8.1.1 Chapter 2: Modeling and Control: Robust Acquiring and Transport Operations

The dynamic model of a novel flying kinematic chain has been provided, besides, a robust controller based on sliding mode control and adaptive parameters was conceived. Based on the results obtained from the simulations and the Lyapunov stability analysis, the AISM controller guarantees the stability to the system and the tolerance of disturbances in order to accomplish the picking and transport operations. An improvement of the picking strategy shall be proposed with base on a moving objective, in addition the motion of the payloads and the velocity of the operation will be analyzed to design a strategy for smooth links transition. The dynamics of the actuators play an important roll in the performance of the system which suggest the implementation of a robust control law to the aircrafts. The extension to a three dimensional space and the experiments concerning the proposal are left for future works.

#### 8.1.2 Chapter 3: Disturbances and Coupling Compensation for Trajectory Tracking

In this chapter, the dynamical model of a Multi Link Aerial System, based on the Euler-Lagrange formalism, was introduced. Even when the number of links and the aerial vehicles was restricted to 2 and 3 respectively, as future work the study of the system with  $n$  links and  $n + 1$  aircrafts will be addressed.

The linear representation of the system and the addition of the corresponding couplings into the disturbance terms allowed one to design an Augmented State Linear Kalman Filter to estimate such perturbations. This one was proved to have an acceptable performance according to the results obtained during numerical simulations.

The implementation of an Extended Kalman Filter, the design of a robust control law as well as the addition of wind disturbances are left to be included in an extended version of the current work. In addition, the study of the system in a three dimensional space using different aircraft structures as actuators is considered for future projects.

### 8.1.3 Chapter 4: Nonlinear Control and ASEKF-Based Disturbances Compensation

The dynamics of an unconventional ML-UAS configuration was obtained via the Euler-Lagrange formalism yet one did not only succeed to regroup the equations of motion into a well-known compact structure but also useful model's properties regarding control design purposes were verified. It is worth highlighting that the latter enables multiple possibilities of potential controllers to stabilize these kind of aerial robots.

The performance of the system is degraded due to the nonlinear highly-coupled dynamics as well as the presence of parametric uncertainties and unmodeled external disturbances. A joint control-observer strategy, using an ASEKF in cascade with a Lyapunov-based non-linear control, was implemented, showing an enhanced effectiveness regarding the overall performance.

In the control vein, a Lyapunov-based controller guaranteeing global asymptotic stability was implemented to fulfill the trajectory-tracking objective. The controller success relies on the ASEKF estimation effectiveness. Regarding the estimation layer, deducing an ad-hoc ASEKF's process covariance matrix considering the actual structure of uncertain parameters was validated, since the states estimation is accurate enough to overcome parasitic issues and thus stabilizing the system. In this matter, and witnessed by the tracking performance, the overall external disturbance is accurately estimated. Moreover, when sensory anomalies occur, the estimated states maintain acceptable operational performance remaining in the vicinity of the target trajectory.

Forthcoming research entails: (i) the experimental development of the aerial robot, (ii) resilient 3D navigation strategies to encompass highly degraded scenarios, e.g. frequency/amplitude-variable disturbances (wind gusts) as well as (iii) time-delay tolerant controllers/observers.

## 8.2 Part II: Time-Delays on Unmanned Aerial Systems

The conclusions of the chapters conforming Part II are given in the upcoming subsections.

### 8.2.1 Chapter 5: Parametric Analysis of PID Delay-Based Controllers for Quadrotor UAVs

Along this chapter, a preliminary parametric study, concerning the stability regions of PID controllers for quadrotor vehicles subjected to feedback time-delays, was exposed. In this sense, a set of stability charts was provided allowing a suitable selection of the controllers' gains as a function of the parameters  $\tau$ ,  $k_i$  and/or  $\sigma$ . The results of the conducted simulations verify that for the gains inside the stability regions, the stability of the system holds and, additionally, justify the implementation of PID controllers in the presence of external and unmodeled disturbances affecting the translational behavior of the vehicle.

In a general overview, future works consider the formal and strict definition of the parametric dependency of the stability regions and a fully detail study on the fragility of the system to provide a tool to measure the robustness of the control approach. Additionally, the extension of this chapter takes into account the stability of the aircraft when rotational disturbances influence its dynamics. The comparison between this linear approach and the non-linear treatment of the issue is also suggested as an upcoming work. Further efforts will be devoted to validate and complement these results by means of real experimentation.

### 8.2.2 Chapter 6: Time-Delay Control of Quadrotor UAVs: a MID-based Approach

In this chapter, the MID property has been exploited regarding the controllers tuning for two classes, classical quadrotor and its tilting-rotor version, of aerial systems. It has been shown that time-delayed feedback critically degrades the translational motion of the vehicles, for this case, the MID property permits to assign the rightmost root of the characteristic function in such a manner that system's convergence rate or the exponential behavior are guaranteed while providing fast non-oscillatory response. Specific conditions and corresponding proofs were introduced and detailed, leading to the definitions of the control gains with respect to the time delay amount. The latter could equally serve as a tuning methodology proposal whether a time-delay can be induced in the feedback loop.

To the best of my knowledge, similar analytical and numerical method to accurately determine the gains of the controllers for quadrotors, under the conditions herein considered, is not available in current related literature.

The results of the detailed simulations, including the linearized dynamics of the vehicles and the non-linear model representations, verify the proper functioning of the proposal yet, the forthcoming research extension entails (i) the study of PID delay-based controllers by means of the MID approach, (ii) the application of the MID approach to the trajectory tracking case, (iii) a detail comparative analysis of the quadrotors vehicle when manipulated by MID-based linear controllers and non-linear approaches as well as (iv) the validation of the proposals in real conditioned environments.

### 8.2.3 Chapter 7: Time-Delay Control of a VTOL Multi-Agent System Towards Transport Operations

A control methodology to stabilize the collective motion (consensus) of a group of VTOL vehicles, featuring different kinds of time-delays, in order to perform grasping and transport operations, was described. Such control strategy consists of a time-delay tolerant PID controller, which guarantees both attitude and position stability of an individual aerial robot and the trajectory tracking under different disturbances allowing the consensability of the multi-robot system. Simulation results validate the effectiveness of the proposed multi-agent control methodology for an object transportation scenario, which induces different disturbances on every robot conforming the quartet. The simulation also highlights that, even when the effects of the time-delay are present on the system, consensability, formation and trajectory tracking are achievable using the proposed control methodology.

As future work, explicit presentation and explanation of the object contact points and computation of the forces exerted by the robots on the object will be considered and studied.

### 8.3 General Conclusions

During the development of this thesis two different concepts were addressed: (i) the conception, modeling and control of a Multi-Link Unmanned Aerial System and (ii) the control of aerial systems subjected to time-delays.

For the case of the ML-UAS, the results allow one to think of a promising platform to study and use in a vast variety of circumstances and operations. In this vein, even when the dynamical analysis has been successfully accomplished, there still exists an incomplete task to perform which is the corresponding modelling a 3 dimensional space yet, the results of this work may ease the upcoming research approach.

Another concern to be addressed in the continuity of this work is referred to the construction of the flying kinematic chain and the corresponding validation of the analysis conducted. In this sense, it is recommended to consider a full-time student devoted to the mechanical conception and construction of the system. As a matter of personal opinion, it should be firstly tackled the proper functioning of the proposal by using quadrotors vehicles before proceeding to implement different UAV configurations. The main issue faced that did not allow one to execute the real experimentation was the unfortunate sanitary situation which impacts the development of the thesis in a sense that the pandemic came right at the moment when the experimental setup was supposed to be performed, nevertheless, a complementary solution was conceived: the introduction of time-delays to aerial vehicles and the respective theoretical study.

As previously mentioned, addressing the effects of time-delays over unmanned aerial vehicles came as an option to take advantage of the sanitary situation and the expertise of the thesis' advisors. In this matter, one could potentially establish that the MID property was exploited to tune the controllers of aerial vehicles, which stands as the main result of the thesis part concerned. As in the case of the ML-UAS, the experimental validation is still missing thus, the general remarks on this vein are oriented to perform such studies.

The latter may allow future students to focus their research efforts on combining the versatility and novelty of unmanned aerial vehicles and translation of the theoretical results regarding time-delay systems to real conditions, since, according to the literature, the synergy of both seems to increasingly draw the attention of scientist around the globe.

# Appendix A

## Properties of the Multi-Link Unmanned Aerial System

In general terms, a mechanical system whose dynamics can be expressed as:

$$M(\mathbf{q})\ddot{\mathbf{q}} + C(\mathbf{q}, \dot{\mathbf{q}})\dot{\mathbf{q}} + \mathbf{G}(\mathbf{q}) = \boldsymbol{\tau} \quad (\text{A.1})$$

satisfies the properties cited in the current appendix, nonetheless, it is worth recalling the definition of each term on the above equation. In this regard, the matrix  $M(\mathbf{q}) \in \mathbb{R}^{n \times n}$  stands for the inertia matrix,  $C(\mathbf{q}, \dot{\mathbf{q}}) \in \mathbb{R}^{n \times n}$  corresponds to the centripetal effects and Coriolis terms matrix,  $\mathbf{G}(\mathbf{q}) \in \mathbb{R}^n$  is known as the gravitational terms vector and, lastly  $\mathbf{q} \in \mathbb{R}^n$  and  $\boldsymbol{\tau} \in \mathbb{R}^n$  are, respectively, the state and the external forces (and/or torques) vectors.

As it has been shown throughout Part I, the dynamics of the Multi-Link Unmanned Aerial System fits the form of Eqn. (A.1) thus, the properties exposed herein have been proved to be satisfied by this aforementioned system dynamics.

The elements that compose the dynamical model introduced in Eqn. (A.1) possess a set of properties which is listed as follows.

1. The **inertia matrix**  $M(\mathbf{q})$  is a symmetric positive definite matrix that satisfies:

- (a)  $M(\mathbf{q}) \geq \vartheta \mathbf{I} \forall \mathbf{q} \in \mathbb{R}^n$  with  $\vartheta \in \mathbb{R}^+$  and  $\mathbf{I} \in \mathbb{R}^{n \times n}$  the identity matrix.
- (b)  $\lambda_{\max}[M(\mathbf{q})] \leq \zeta \forall \mathbf{q} \in \mathbb{R}^n$  with  $\zeta \in \mathbb{R}^+$ .
- (c)  $\|M(\mathbf{x})\mathbf{z} - M(\mathbf{y})\mathbf{z}\| \leq k_M \|\mathbf{x} - \mathbf{y}\| \|\mathbf{z}\| \forall \mathbf{x}, \mathbf{y}, \mathbf{z} \in \mathbb{R}^n$  and  $k_M \in \mathbb{R}^+$ .
- (d)  $\|M(\mathbf{x})\mathbf{y}\| \leq k'_M \|\mathbf{y}\| \forall \mathbf{x}, \mathbf{y} \in \mathbb{R}^n$  and  $k'_M \in \mathbb{R}^+$ .

2. The **centripetal effects and Coriolis terms matrix**  $C(\mathbf{q}, \dot{\mathbf{q}})$  can be non-unique nevertheless, the vector  $C(\mathbf{q}, \dot{\mathbf{q}})\dot{\mathbf{q}}$  is unique. Additionally, this matrix satisfies the following properties:

- (a)  $C(\mathbf{q}, \mathbf{0}^*) = \mathbf{0} \forall \mathbf{q} \in \mathbb{R}^n$  with  $\mathbf{0} \in \mathbb{R}^{n \times n}$  being the zero matrix.
- (b)  $\forall \mathbf{q}, \mathbf{x}, \mathbf{y} \in \mathbb{R}^n, \|C(\mathbf{q}, \mathbf{x})\mathbf{y}\| \leq k_{C_1} \|\mathbf{x}\| \|\mathbf{y}\|$  where  $k_{C_1} \in \mathbb{R}^+$ .

(c)  $\forall \mathbf{v}, \mathbf{w}, \mathbf{x}, \mathbf{y}, \mathbf{z} \in \mathbb{R}^n$  and  $k_{C_1}, k_{C_2} \in \mathbb{R}^+$ , it holds that  $\|C(\mathbf{x}, \mathbf{z})\mathbf{w} - C(\mathbf{y}, \mathbf{v})\mathbf{w}\| \leq k_{C_1} \|\mathbf{z} - \mathbf{v}\| \|\mathbf{w}\| + k_{C_2} \|\mathbf{x} - \mathbf{y}\| \|\mathbf{w}\| \|\mathbf{z}\|$

(d)  $C(\mathbf{q}, \dot{\mathbf{q}}) + C(\mathbf{q}, \dot{\mathbf{q}})^T = \dot{M}(\mathbf{q})$

3. For the **gravitational terms vector**  $\mathbf{G}(\mathbf{q})$ , it holds that:

(a)  $\forall \tau_i \in \mathbb{R}^+$ ,  $\int_0^{\tau_i} \mathbf{G}(\mathbf{q})^T \dot{\mathbf{q}} dt = \mathcal{U}(\mathbf{q}(\tau_i)) - \mathcal{U}(\mathbf{q}(0))$  where  $\mathbf{q}(\tau_i)$  is the vector  $\mathbf{q}$  measured  $t = \tau_i$  and the vector  $\mathbf{q}(0)$  refers to the initial condition.

(b)  $\forall \tau_i \in \mathbb{R}^+$  and  $k_U = \min_{\mathbf{q}} [\mathcal{U}(\mathbf{q})] \in \mathbb{R}^+$ ,  $\int_0^{\tau_i} \mathbf{G}(\mathbf{q})^T \dot{\mathbf{q}} dt + \mathcal{U}(\mathbf{q}(0)) \geq k_U$ .

(c)  $\forall \mathbf{x}, \mathbf{y} \in \mathbb{R}^6$ ,  $\|\mathbf{G}(\mathbf{x}) - \mathbf{G}(\mathbf{y})\| \leq k_g \|\mathbf{x} - \mathbf{y}\|$  with

$$k_g \geq \left\| \frac{\partial \mathbf{G}(\mathbf{q})}{\partial \mathbf{q}} \right\| \geq \lambda_{\text{Max}} \left[ \frac{\partial \mathbf{G}(\mathbf{q})}{\partial \mathbf{q}} \right] \in \mathbb{R}^+ \quad (\text{A.2})$$

(d)  $\|\mathbf{G}(\mathbf{q})\| \leq k' \forall \mathbf{q}$  with  $k' \in \mathbb{R}^+$ .

4. The **residual dynamics**  $\mathbf{h}(\mathbf{e}, \dot{\mathbf{e}}) \in \mathbb{R}^n$  is a vector, most commonly associated to the dynamics of a robot and the position and velocity errors, and it is defined as:

$$\mathbf{h}(\mathbf{e}, \dot{\mathbf{e}}) = [M(\mathbf{q}_d) - M(\mathbf{q}_d - \mathbf{e})] \ddot{\mathbf{q}}_d + \mathbf{G}(\mathbf{q}_d) - \mathbf{G}(\mathbf{q}_d - \mathbf{e}) + [C(\mathbf{q}_d, \dot{\mathbf{q}}_d) - C(\mathbf{q}_d - \mathbf{e}, \dot{\mathbf{q}}_d - \dot{\mathbf{e}})] \dot{\mathbf{q}}_d \quad (\text{A.3})$$

Such vector satisfies that  $\forall \mathbf{e}, \dot{\mathbf{e}} \in \mathbb{R}^6$  and  $k_{h_1}, k_{h_2} \in \mathbb{R}^+$ ,  $\|\mathbf{h}(\mathbf{e}, \dot{\mathbf{e}})\| \leq k_{h_1} \|\dot{\mathbf{e}}\| + k_{h_2} \|\mathbf{f}_{th}(\mathbf{e})\|$  where

$$\mathbf{f}_{th}(\mathbf{e}) = \left[ \tanh(e_x) \quad \dots \quad \tanh(e_{\beta_2}) \right]^T \in \mathbb{R}^n \quad (\text{A.4})$$

is the hyperbolic tangent function which has the following properties for  $\forall \mathbf{e}, \dot{\mathbf{e}}$ :

$$\|\mathbf{f}_{th}(\mathbf{e})\| \leq \|\mathbf{e}\| \quad (\text{A.5})$$

$$\|\mathbf{f}_{th}(\mathbf{e})\| \leq \sqrt{n} \quad (\text{A.6})$$

$$\|\mathbf{f}_{th}(\mathbf{e})\|^2 \leq \mathbf{f}_{th}(\mathbf{e})^T \mathbf{e} \quad (\text{A.7})$$

$$\|\dot{\mathbf{f}}_{th}(\mathbf{e})\| \leq \|\dot{\mathbf{e}}\| \quad (\text{A.8})$$

## Appendix B

# ML-UAS Linearization for Observability

Due to the nonlinear and coupled dynamics of the ML-UAS, a linearization of Eqn. (4.20) is used to prove local observability at a given operational point  $\boldsymbol{\chi}_*^e, \mathbf{U}_*$ . The observation equation (Eqn. (4.36)) is already linear. In this sense, considering a Taylor series approximation and neglecting the high-order terms, the linearization of Eqn. (4.20) corresponds to:

$$\Delta \dot{\boldsymbol{\chi}}^e = A_l^e \Delta \boldsymbol{\chi}^e + B_l^e \Delta \mathbf{U} \quad (\text{B.1})$$

such that  $\Delta \dot{\boldsymbol{\chi}}^e = \dot{\boldsymbol{\chi}}^e - \mathbf{F}(\boldsymbol{\chi}_*^e, \mathbf{U}_*) \in \mathbb{R}^{18}$ ,  $\Delta \boldsymbol{\chi}^e = \boldsymbol{\chi}^e - \boldsymbol{\chi}_*^e \in \mathbb{R}^{18}$ ,  $\Delta \mathbf{U} = \mathbf{U} - \mathbf{U}_* \in \mathbb{R}^6$  and

$$A_l^e = \left. \frac{\partial \mathbf{F}(\boldsymbol{\chi}^e, \mathbf{U})}{\partial \boldsymbol{\chi}^e} \right|_{\boldsymbol{\chi}_*^e, \mathbf{U}_*} ; \quad B_l^e = \left. \frac{\partial \mathbf{F}(\boldsymbol{\chi}^e, \mathbf{U})}{\partial \mathbf{U}} \right|_{\boldsymbol{\chi}_*^e, \mathbf{U}_*} \quad (\text{B.2})$$

where  $\boldsymbol{\chi}_*^e \in \mathbb{R}^{18}$  and  $\mathbf{U}_* \in \mathbb{R}^6$  represent the operational point at which the linearization is made and  $A_l^e \in \mathbb{R}^{18 \times 18}$ ,  $B_l^e \in \mathbb{R}^{18 \times 6}$ .

Since the observability proof implies only the knowledge of  $A_l^e$  and  $C_k^e$ , we exclusively present the expression that describes  $A_l^e$  for its ulterior evaluation. Following the same procedure introduced in Section 4.2.1 to redefine  $Z$  as in Eqn. (4.34). From the dynamics of  $\mathbf{q}$  given in Eqn. (4.20), one finds that:

$$\frac{\partial \dot{\mathbf{q}}}{\partial \boldsymbol{\chi}^e} = \begin{bmatrix} \frac{\partial \dot{\mathbf{q}}}{\partial \mathbf{q}} & \frac{\partial \dot{\mathbf{q}}}{\partial \dot{\mathbf{q}}} & \frac{\partial \dot{\mathbf{q}}}{\partial \boldsymbol{\rho}} \end{bmatrix} = \begin{bmatrix} \mathbf{0} & \mathbf{I} & \mathbf{0} \end{bmatrix} \in \mathbb{R}^{6 \times 18} \quad (\text{B.3})$$

$$\frac{\partial \ddot{\mathbf{q}}}{\partial \boldsymbol{\chi}^e} = \begin{bmatrix} \frac{\partial \ddot{\mathbf{q}}}{\partial \mathbf{q}} & \frac{\partial \ddot{\mathbf{q}}}{\partial \dot{\mathbf{q}}} & \frac{\partial \ddot{\mathbf{q}}}{\partial \boldsymbol{\rho}} \end{bmatrix} \in \mathbb{R}^{6 \times 18} \quad (\text{B.4})$$

$$\frac{\partial \dot{\boldsymbol{\rho}}}{\partial \boldsymbol{\chi}^e} = \begin{bmatrix} \frac{\partial \dot{\boldsymbol{\rho}}}{\partial \mathbf{q}} & \frac{\partial \dot{\boldsymbol{\rho}}}{\partial \dot{\mathbf{q}}} & \frac{\partial \dot{\boldsymbol{\rho}}}{\partial \boldsymbol{\rho}} \end{bmatrix} = \begin{bmatrix} \mathbf{0} & \mathbf{0} & \mathbf{0} \end{bmatrix} \in \mathbb{R}^{6 \times 18} \quad (\text{B.5})$$

To extend the definition of the partial derivative in Eqn. (B.4), let one recall  $\ddot{\mathbf{q}}$  given in Eqn. (4.27), such that the partial derivatives can be rewritten as:

$$\frac{\partial \ddot{\mathbf{q}}}{\partial \dot{\mathbf{q}}} = -M(\mathbf{q})^{-1} C_{\dot{q}} \quad \frac{\partial \ddot{\mathbf{q}}}{\partial \mathbf{q}} = \ddot{Q}_q \quad \frac{\partial \ddot{\mathbf{q}}}{\partial \mathbf{p}} = M(\mathbf{q})^{-1} \quad (\text{B.6})$$

where

$$C_{\dot{q}} = \begin{bmatrix} \frac{\partial C(\mathbf{q}, \dot{\mathbf{q}}) \dot{\mathbf{q}}}{\partial \dot{x}} & \frac{\partial C(\mathbf{q}, \dot{\mathbf{q}}) \dot{\mathbf{q}}}{\partial \dot{z}} & \dots & \frac{\partial C(\mathbf{q}, \dot{\mathbf{q}}) \dot{\mathbf{q}}}{\partial \beta_2} \end{bmatrix} \in \mathbb{R}^{6 \times 6} \quad (\text{B.7})$$

$$\ddot{Q}_q = \frac{1}{d_M} (A_{M_q} - \ddot{\mathbf{q}} \mathbf{d}_{M_q}) + M(\mathbf{q})^{-1} \mathbf{v}_q \in \mathbb{R}^{6 \times 6} \quad (\text{B.8})$$

$$A_{M_q} = \begin{bmatrix} \frac{\partial A_M^T \mathbf{v}}{\partial x} & \frac{\partial A_M^T \mathbf{v}}{\partial z} & \dots & \frac{\partial A_M^T \mathbf{v}}{\partial \beta_1} & \frac{\partial A_M^T \mathbf{v}}{\partial \beta_2} \end{bmatrix} \in \mathbb{R}^{6 \times 6} \quad (\text{B.9})$$

$$\mathbf{d}_{M_q} = \begin{bmatrix} \frac{\partial d_M}{\partial x} & \frac{\partial d_M}{\partial z} & \dots & \frac{\partial d_M}{\partial \beta_1} & \frac{\partial d_M}{\partial \beta_2} \end{bmatrix} \in \mathbb{R}^{1 \times 6} \quad (\text{B.10})$$

$$\mathbf{v}_q = \begin{bmatrix} \frac{\partial \mathbf{v}}{\partial x} & \frac{\partial \mathbf{v}}{\partial z} & \dots & \frac{\partial \mathbf{v}}{\partial \beta_1} & \frac{\partial \mathbf{v}}{\partial \beta_2} \end{bmatrix} \in \mathbb{R}^{6 \times 6} \quad (\text{B.11})$$

Such that  $A_l^e$  evaluated at  $\boldsymbol{\chi}_{*}^e, \mathbf{U}_{*}$  is defined as:

$$A_l^e = \left[ \begin{array}{ccc} \mathbf{0} & \mathbf{I} & \mathbf{0} \\ \ddot{Q}_q & -M(\mathbf{q})^{-1} C_{\dot{q}} & M(\mathbf{q})^{-1} \\ \mathbf{0} & \mathbf{0} & \mathbf{0} \end{array} \right] \Bigg|_{\boldsymbol{\chi}_{*}^e, \mathbf{U}_{*}} \quad (\text{B.12})$$

## Appendix C

# A Pedagogical Approach to Data Fusion and Kalman Filter

The methodology used in the appendix consists on a full pedagogical discussion and representation about the Kalman filter for data fusion followed by the sensors characterization and the dynamics modelling of the systems to be studied in the examples. Simulations were carried out to illustrate the behavior of the systems with and without the Kalman filter. The conclusions obtained are lastly exposed.

### C.1 Introduction

The current chapter is addressed to under graduated students interested in sensors and data fusion techniques. This work is written in an easy scientific language in order to be understood by the students. It is proposed the usage of the Kalman Filter as a first approach to data fusion as it is widely used in different research fields and applications as cited by [146, 52].

In this matter, [97] define Data fusion as the combination of the data from multiple sensors to achieve specific inferences that could not be achieved by the usage of one single sensor. Different techniques can be applied to carry out the aforementioned task, nevertheless Kalman Filtering is one of the most significant due to the robustness of the approach, the easy-reasoning-and-understanding of the filtering principle, among other benefits and advantages discussed by [146, 51] who also mention several variations of this filter which improve the performance of the data fusion operation and/or estimation.

The literature offers a wide amount of papers and research concerning the application of Kalman Filtering techniques in data fusion, to mention some, [146] used the Kalman Filter to improve the performance of autonomous robots to accomplish the navigation and trajectory-tracking tasks. [179] compute the dynamic displacement of a given structure based on on-line multi-rate data fusion of high-sampling rate acceleration with time-varying bias and low-sampling rate displacement measurements. In addition, a linear Kalman Filter is implemented by [36] to meet the trajectory tracking specifications of a multi-link unmanned aerial system described in detail by [37].

## C.2 Methodology

To understand the Kalman filtering algorithm, let one consider a linear system to be described in a discrete domain by the expressions:

$$x_k = Ax_{k-1} + Bu_k + w_k \quad (\text{C.1})$$

$$y_k = Hx_k + v_k \quad (\text{C.2})$$

Eqn. (C.1) establishes that the current state of the system  $x_k \in \mathbb{R}^n$  is given in some proportion ( $A \in \mathbb{R}^{n \times n}$  and  $B \in \mathbb{R}^{n \times m}$ ) by the previous state  $x_{k-1} \in \mathbb{R}^n$  and the control input  $u_k \in \mathbb{R}^m$ . The term  $w_k \in \mathbb{R}^n$  is called process noise and represents the influence of unmodeled phenomena. Eqn. (C.2) defines the measurement value  $y_k \in \mathbb{R}^p$  as a linear combination of the current state (in some proportion  $H \in \mathbb{R}^{p \times n}$ ) and the measurement noise  $v_k \in \mathbb{R}^p$  which is normal distributed, i.e. Gaussian. One should notice that the better the noise parameters are defined, the better estimates one gets.

Based on Eqns. (C.1) and (C.2), the Kalman Filter equations are conceived such that these are divided in two sets: Time Update (prediction) and Measurement Update (correction). The first set is formed by the expressions:

$$\hat{x}_k^- = A\hat{x}_{k-1} + Bu_k \quad (\text{C.3})$$

$$P_k^- = AP_{k-1}A^T + Q \quad (\text{C.4})$$

$$K_k = P_k^- H^T (HP_k^- H^T + R)^{-1} \quad (\text{C.5})$$

While the correction set is defined by:

$$y_k = \text{sensor measurement} \quad (\text{C.6})$$

$$\hat{x}_k = \hat{x}_k^- + K_k (y_k - H\hat{x}_k^-) \quad (\text{C.7})$$

$$P_k = (I - K_k H) P_k^- \quad (\text{C.8})$$

Both sets are applied at each step or iteration in strict order, moreover,  $I \in \mathbb{R}^{n \times n}$  stands for the identity matrix,  $P_k \in \mathbb{R}^{n \times n}$  is the error covariance matrix and,  $R \in \mathbb{R}^{p \times p}$  and  $Q \in \mathbb{R}^{n \times n}$  are the covariance matrices of the environment noise and the process noise, respectively. Often, these ones result difficult to compute.

To start the process, one needs to know the estimate of  $x$  and  $P$  at the beginning of the process, these values are called initial conditions and are represented as  $\hat{x}_0$  and  $P_0$ , respectively.

The Filter explained above in Eqns. (C.3)-(C.8) is often used for estimation tasks, in order to implement it as a data fusion technique some modifications and assumptions need to be taken into account.

Let one consider a mechanical system whose states are the position and velocity, i.e.  $x$  and  $\dot{x}$ , and a pair of sensors at one's disposal for knowing the position and acceleration, an ultrasonic sensor and an accelerometer, for instance.

The position captured by the ultrasonic sensor is written as  $x_u \in \mathbb{R}$  that can be derived with respect to time to obtain the velocity  $\dot{x}_u \in \mathbb{R}$  and the acceleration  $\ddot{x}_u \in \mathbb{R}$ . By integrating the acceleration signal coming out from the accelerometer  $\ddot{x}_a \in \mathbb{R}$ , also the velocity  $\dot{x}_a \in \mathbb{R}$  and the position  $x_a \in \mathbb{R}$  can be known.

To estimate the states of the system with more accuracy,  $\ddot{x}_a$  is used at the Prediction stage of the Kalman Filter and  $x_u$  is used in the correction stage, as shown next.

By simple kinematics, the position and the velocity of the system can be obtained [32], i.e.

$$x = x_0 + \dot{x}t + \frac{\ddot{x}t^2}{2} \quad (\text{C.9})$$

$$\dot{x} = \dot{x}_0 + \ddot{x}t \quad (\text{C.10})$$

Where  $x_0 \in \mathbb{R}$  and  $\dot{x}_0 \in \mathbb{R}$  are the initial position and velocity of the system,  $t \in \mathbb{R}^+$  stands for the time. The discrete representation of Eqns. (C.9) and (C.10) is given as:

$$x_k = x_{k-1} + \dot{x}_{k-1}dt + \frac{\ddot{x}_k dt^2}{2} \quad (\text{C.11})$$

$$\dot{x}_k = \dot{x}_{k-1} + \ddot{x}_k dt \quad (\text{C.12})$$

Such that  $dt \in \mathbb{R}^+$  is the sample time. The latter Eqns. (C.11) and (C.12) can be comprised in a matrix form as follows

$$X_k = A_X X_{k-1} + B_X U_k \quad (\text{C.13})$$

With

$$X_k = \begin{bmatrix} x_k \\ \dot{x}_k \end{bmatrix}; A_X = \begin{bmatrix} 1 & dt \\ 0 & 1 \end{bmatrix}; B_X = \begin{bmatrix} \frac{dt^2}{2} \\ dt \end{bmatrix}; U_k = \ddot{x}_k \quad (\text{C.14})$$

In this case, the vector  $U_k$  will contain  $\ddot{x}_a$  measured at the instant  $k$ . The fact that we can observe the position by means of the ultrasonic sensor implies an observation equation as follows:

$$Y_k = H_X X_k; H_X = \begin{bmatrix} 1 & 0 \end{bmatrix} \quad (\text{C.15})$$

The information provided by Eqns. (C.13) - (C.15) allows us to rewrite the Kalman filter Eqns. (C.3) - (C.8) as shown below.

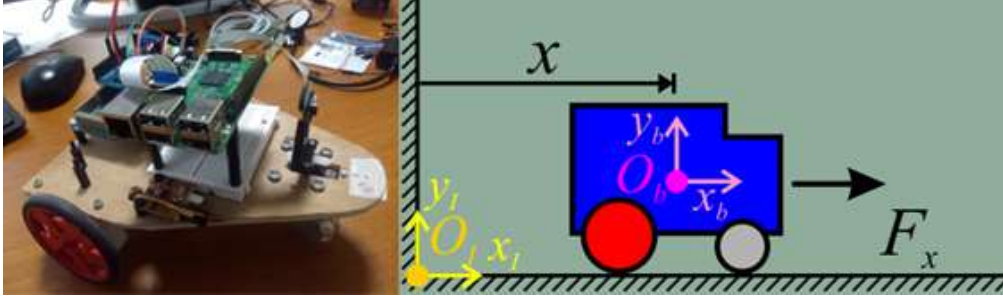


Figure C.1: The mini car robot: Left) Real mini car robot. Right) Mini car free body diagram

$$\hat{X}_k^- = A_X \hat{X}_{k-1} + B_X \ddot{x}_{a_k} \quad (\text{C.16})$$

$$P_{X_k}^- = A_X P_{X_{k-1}} A_X^T + Q_X \quad (\text{C.17})$$

$$K_{X_k} = P_{X_k}^- H_X^T (H_X P_{X_k}^- H_X^T + R_X)^{-1} \quad (\text{C.18})$$

$$Y_k = x_{u_k} \quad (\text{C.19})$$

$$\hat{X}_k = \hat{X}_k^- + K_{X_k} (Y_k - H_X \hat{X}_k^-) \quad (\text{C.20})$$

$$P_{X_k} = (I - K_{X_k} H_X) P_{X_k}^- \quad (\text{C.21})$$

Notice that now, the signals of the ultrasonic sensor and the accelerometer take part of the Kalman filter equations also it is worth to mention that at the output of the filter, the vector  $\hat{X}_k$  contains the states of the system computed from the measurement of both sensors thus it is used to close the control loop as explained later. Further and detailed information about the Kalman Filter theory is available in the references cited.

## C.3 Pedagogical Examples

### C.3.1 Mini Car Robot

Fig. C.1 shows the Mini car robot used in this example. The real platform can be observed at the left, meanwhile the free body diagram is depicted at the right. This vehicle features an Arduino Due board, a Raspberry Pi 3 connected to a camera, an IMU (Inertial Measurement Unit), an ultrasonic sensor and an Arduino Motor shield. The actuators of the system are two continuous servo motors. In the front of the robot a free-to-rotate wheel is placed to balance the system.

For sake of simplicity, one may be interested only in the translational linear movement of the car. Notice that in Fig. C.1, two different frames have been defined: the inertial reference frame ( $O_I$  defined by the axis  $x_I$  and  $y_I$ ) which is fixed to some point in the space and the body-fixed reference frame ( $O_b$  with the axis  $x_b$  and  $y_b$ ) which is located at the center of gravity of the vehicle. The position of the vehicle is described by  $x \in \mathbb{R}$  and measured as shown, additionally, the velocity and the acceleration of the car are represented as  $\dot{x} \in \mathbb{R}$  and  $\ddot{x} \in \mathbb{R}$ , respectively defined by the first and second time derivatives.

In order to control the vehicle, it is important to have the mathematical description of it. The dynamic model can then be

obtained by the Newton Euler formalism or by the Euler Lagrange formalism [32]. For the simplest case of our robot, by both procedures, the dynamics is found to be:

$$m_c \ddot{x} = F_x \quad (\text{C.22})$$

Notice that the friction force between the wheels of the car and the floor has been omitted.  $F_x \in \mathbb{R}$  represents the force applied over the vehicle along the  $x_I$ . The mass of the vehicle is expressed as  $m_c > 0$ .

Let us assume that the force  $F_x$  can be easily manipulated, this allows us to define such force as the control input  $u_x \in \mathbb{R}$ , i.e.:

$$F_x = u_x \quad (\text{C.23})$$

The main goal of the controller in this example is to make the vehicle go to a desired specific point in the space located at a distance  $x_d \in \mathbb{R}$  in the  $x_I$  axis. To do so, one can apply different control techniques however, a PD controller is applied [35]:

$$u_x = K_{p_x} e_x + K_{v_x} \dot{e}_x \quad (\text{C.24})$$

where  $K_{p_x}$  and  $K_{v_x}$  (both  $\in \mathbb{R}^+$ ) are the proportional and derivative gains of the controller, meanwhile  $e_x = x_d - x \in \mathbb{R}$  is the position error and  $\dot{e}_x = \dot{x}_d - \dot{x} = -\dot{x} \in \mathbb{R}$  is the velocity error. Notice that as the desired position is a fixed point in the space, i.e. it is a constant, its time derivative is always 0.

Based on Eqns. (C.23) and (C.24), Eqn. (C.22) can be rewritten such that:

$$m_c \ddot{x} = K_{p_x} e_x - K_{v_x} \dot{x} \quad (\text{C.25})$$

Eqn. (C.25) will be used at the simulation stage to implement the data fusion for merging the information of the sensors.

### C.3.2 Mini Bi-rotor Platform

Analogously to the analysis of the mini car robot, the modelling and control of the bi rotor shown in Fig. C.2 are conceived in this subsection. The main features of the platform are the Arduino Nano board, a PDB or Power Distribution Board to power up the electronics as well as one IMU that measures the acceleration of the vehicle, an ultrasonic sensor to know the distance  $z \in \mathbb{R}$  from the ground and two ESCs (Electronic Speed Controllers) to manipulate the brushless motors velocity.

One may be interested only in the vertical linear movement of the vehicle. For sake of simplicity, Fig. C.2 depicts, at the right, a free body diagram of the system. Two different frames are established: the inertial reference frame ( $O_I$  defined by the axis  $y_I$  and  $z_I$ ) which is a fixed point in the space and the body-fixed reference frame ( $O_b$  with the axis  $y_b$  and  $z_b$ ) which is located at the center of gravity of the vehicle. The velocity and the acceleration of the vehicle are represented as  $\dot{z} \in \mathbb{R}$  and  $\ddot{z} \in \mathbb{R}$ , respectively defined by the first and second time derivative.

The mass of the aircraft is represented by  $m_v > 0$  and the gravity acceleration  $g = 9.81 \text{ m/s}^2$  acts over the vehicle as depicted, defining the equation of motion, according to the Newton Euler formalism, to be:

$$m_v \ddot{z} + m_v g = f_1 + f_2 \quad (\text{C.26})$$

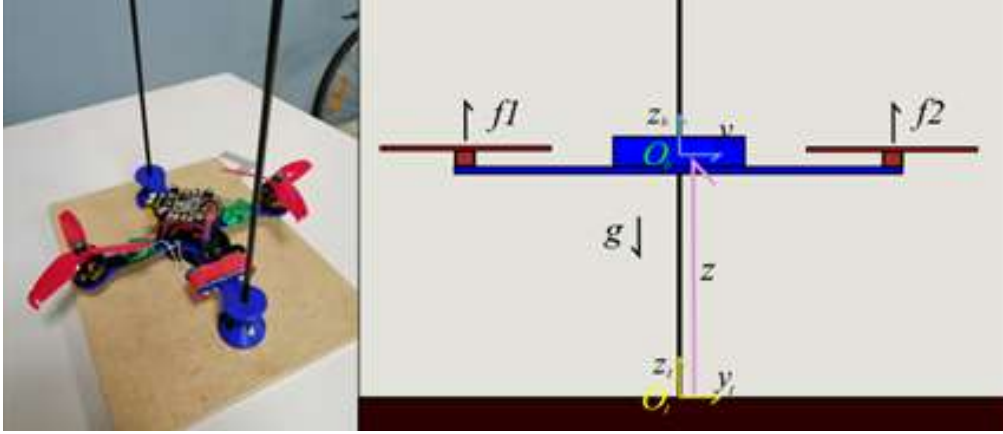


Figure C.2: The bi-rotor platform: Left) Real Bi-rotor platform. Right) Bi-rotor free body diagram

In this case, the sum of the forces acts as the control, i.e.

$$f_1 + f_2 = u_z \quad (\text{C.27})$$

Once more, the objective of the controller is to stabilize the vehicle at certain constant altitude  $z_d \in \mathbb{R}$  above the ground. As in the previous example, a PD controller is used to accomplish such goal nevertheless one may add the gravitational terms to the equation as follows:

$$u_z = K_{p_z} e_z - K_{v_z} \dot{z} + m_v g \quad (\text{C.28})$$

with  $K_{p_z}$  and  $K_{v_z}$  (both  $\in \mathbb{R}^+$ ) are the proportional and derivative gains of the controller, meanwhile  $e_z = z_d - z \in \mathbb{R}$  is the position error. The definitions in Eqns. (C.27) and (C.28) allow one to rewrite the dynamics of the closed loop system in Eqn. (C.26) such that:

$$m_v \ddot{z} + m_v g = K_{p_z} e_z - K_{v_z} \dot{z} + m_v g \quad (\text{C.29})$$

Further information about the dynamics of the vehicle and its control, as well as other models for pedagogical implementation can be found in [33, 32, 49, 35].

### C.3.3 Sensors Characterization

In order to study the proposed data fusion algorithm, the characterization and correct simulation of the sensors are a most. In this regard, the accelerometer can be simulated as a signal with an addition of some white noise (Gaussian) and a given offset, this because the accelerometer measures also the gravity acceleration and, depending on its attitude, the sensor gives back some acceleration value even when the vehicle is not in motion [14] thus, the total acceleration measurement coming from the sensor is composed by the sum of three components: the real acceleration of the vehicle, the Bias acceleration (or Offset) and the Gaussian distributed noise. One should be warned that obtaining the velocity and position from the integration of the accelerometer information can produce significant errors due to the (almost) constant which becomes a linear function when

integrated the first time and a quadratic function after the second integration.

The ultrasonic sensor, in simulation, has the advantage of not carrying a derivation accumulative error for both, velocity and acceleration, computations but presents the disadvantage of amplification of the velocity and accelerations as well as not considering the initial positions and velocities of the system as when using the accelerometer. In addition, the sensing process with this kind of sensors is slow compared with that of the accelerometer [30]. For short, in Matlab/Simulink, this sensor signal will be composed by the real position of the vehicle and a Gaussian distributed noise with slower sampling time than that of the acceleration sensor previously described.

One should have in mind that most of the times, control simulations are carried out considering ideal elements (actuators and plants) that can provide the desired control command to the system which, in fact, does not happen in reality. Moreover, one must think of which kind of control signals one needs, e.g. for translational mechanical systems the signal control is given (typically) in Newtons yet sometimes the actuators provide actions or signals that are related to displacements (meters or radians) and torques (Newton-meters) which implies that a conversion is needed, leading to more errors and less accuracy in the prediction of the response. In these examples, one may consider only a saturation of the control input and assume that one can directly provide such command in the corresponding units.

## C.4 Simulation Results

The proposed fusion data technique can be proved to be valid via numerical simulations, in order to do so, Matlab and Simulink provide the most appropriate tools and environment.

Before giving the detail information about the development of the simulation environment, let one introduce the Table C.1 which contains all the parameters used in simulation as well as the corresponding value or magnitude.

Table C.1: Simulation parameters and conditions

<b>Simulation parameters</b>			
Total simulation time		30 s	
Sampling time $dt$		0.001 s	
Gravity acceleration ( $g$ )		9.81 m/s <sup>2</sup>	
<b>Sensors parameters</b>			
Accelerometer variance		0.0001	
Mean Bias value		-0.97 m/s <sup>2</sup>	
Bias variance		0.001	
Ultrasonic sensor variance		0.0001	
Ultrasonic sensor sampling time		30 $dt$	
<b>Mini car properties and parameters</b>		<b>Bi-rotor properties and parameters</b>	
$m_c$	1 kg	$m_v$	0.5 kg
$x_0$	0 m	$z_0$	2 m
$\dot{x}_0$	0 m/s	$\dot{z}_0$	0 m/s
$K_{p_x}$	1	$K_{p_z}$	1
$K_{v_x}$	1	$K_{v_z}$	1
$x_d$	2 m	$z_d$	0.75 m

```

5      %% Mini Car Simulation Time and Step Time Size
6      tsimc=30; % Simulation time [s]
7      dtc=0.001; % Time step [s]
8      %% Bi-Rotor Simulation Time and Step Time Size
9      tsimr=30; % Simulation time [s]
10     dtr=0.001; % Time step [s]
11     %% Parameters of the Mini Car
12     mc=1; % Mass [kg]
13     xp0=0; % Initial position [m]
14     xv0=0; % Initial velocity [m/s]
15     xd=2; % Desired position [m]
16     %% Parameters of the Bi-Rotor
17     mr=0.5; % Mass [kg]
18     zp0=2; % Initial position [m]
19     zv0=0; % Initial velocity [m/s]
20     zd=0.75; % Desired altitude [m]
21     g=9.81; % Constant of gravity acceleration [m/s^2]
22     %% Mini Car Control Gains
23     Kpc=1; % Proportional gain
24     Kvc=1; % Derivative gain
25     %% Bi-Rotor Control Gains
26     Kpr=1; % Proportional gain
27     Kvr=1; % Derivative gain
28     %% Sensors Characterization
29     Var_a=0.0001; % Accelerometer white noise variance
30     Var_abias=0.001; % Accelerometer bias (offset) variance
31     bias=-0.97; % Mean value of the accelerometer bias
32     Bias_dta=30*dtc; % Bias and Ultrasonic sensor sampling time
33     Var_u=0.0001; % Ultrasonic sensor white noise variance

```

Figure C.3: Matlab code: Systems properties and conditions

```

35     %% Mini Car Kalman Filter Parameters
36     Ac=[1 dtc;0 1]; % Matrix A for Kalman filter
37     Bc=[dtc^2/2;dtc]; % Matrix B for Kalman filter
38     Hc=[1 0]; % Matrix H for Kalman filter
39     Qc=[0 0;0 0.001]; % Covariance matrix of the process noise
40     Rc=Var_u; % Noise variance of the ultrasonic sensor
41     Pc0=[2 0;0 2]; % Initial value of covariance matrix P
42
43     %% Bi-Rotor Kalman Filter Parameters
44     Ar=[1 dtr;0 1]; % Matrix A for Kalman filter
45     Br=[dtr^2/2;dtr]; % Matrix B for Kalman filter
46     Hr=[1 0]; % Matrix H for Kalman filter
47     Qr=[0 0;0 0.001]; % Covariance matrix of the process noise
48     Rr=Var_u; % Noise variance of the ultrasonic sensor
49     Pr0=[2 0;0 2]; % Initial value of covariance matrix P
50
51     %% Running the Simulations in Simulink
52     sim('SimCar',tsimc);
53     sim('SimBirotor',tsimr);

```

Figure C.4: Matlab code: Kalman filter elements

For both systems, the total simulation was set to 30 s with a sampling time of 0.001 s in order to perform a fixed time step simulation. In the case of the Bi rotor platform the gravity acceleration is also established in the program according to Table C.1. In addition, it was assumed that the accelerometer and the ultrasonic sensor installed on the robots have the characteristics exposed in Table C.1. In this regard, Fig. C.3 shows the Matlab code defining what has been commented in this paragraph.

Eqns. (C.16) – (C.21) were used in the simulation to make the data fusion, nevertheless the covariance matrices and those of the system were defined in the Matlab code as exposed by Fig. C.4. In this matter, the covariance matrix of the process noise is most of the times defined as the zero matrix because it is difficult to be defined in reality yet sometimes it is used to indicate parameters variation and or errors in the mathematical modelling process. In this case, one used this matrix to define an error in the computation of the velocity as it comes from an integration of the accelerometer data which has an offset as explained before. In this sense, in this important to keep in mind that the greater the matrix Q, the slower response of the filter [36].

Fig. C.4 also gives evidence of the instructions used to launch the simulation in Simulink. Two different files were used to

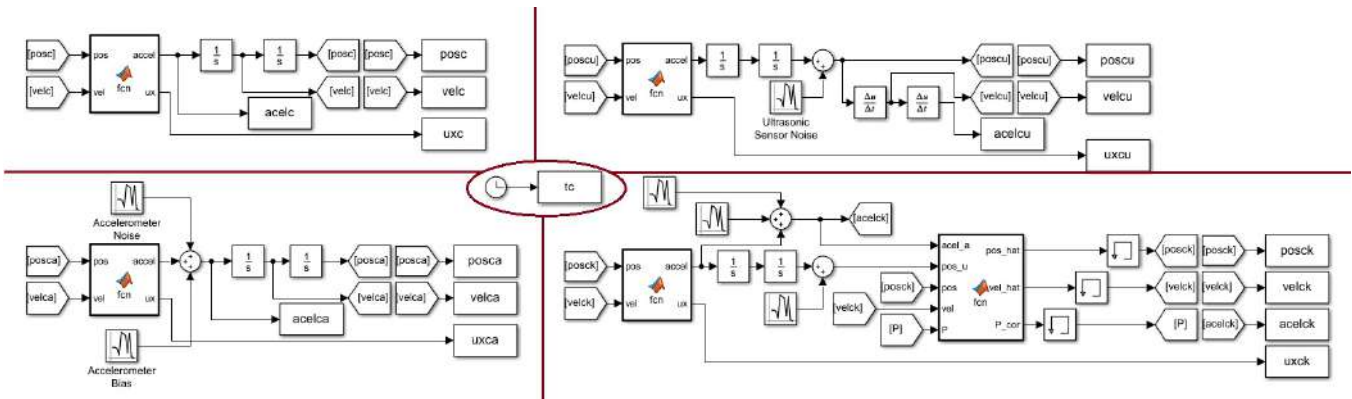


Figure C.5: Simulink environment: up left corner: ideal performance of the sensors; up right corner: usage of the ultrasonic sensor only; bottom left corner: usage of the accelerometer only, and, bottom right corner: data fusion by the Kalman Filter

complete the simulation nevertheless the structure of both files is exactly the same, the only thing that changes is the properties of the systems according to Table C.1 and the equations provided in the subsections of each pedagogical platform. For such reason only the Simulink file of the mini car simulation will be explained and shown next.

Before going any further in the Simulink environment, in the “Model Parameters Configuration” option the simulation time is changed as well as the simulation type which in our case it corresponds to the fixed step time with the given sampling time in Table C.1.

Four different scenarios were simulated for the same system: The first one corresponded to the ideal performance of the sensors, the second one considered only the accelerometer, the third one was defined in order to use only the ultrasonic sensor and lastly, the last one merged the data coming from both sensors by means of the Kalman filter. In the four scenarios, the saturation of the motors was taken into consideration. Fig. C.5 depicts what is discussed in this paragraph.

In the middle of the Fig. C.5, surrounded by a circle, you find the clock connected to a “To Workspace block” which allows us to store the time. All the blocks of the file have a sampling time  $dt$  given in Table C.1. Notice that we have used the “From” and “Goto” blocks to avoid having too many connections which would make more difficult the interpretation of the block diagram below.

The initial conditions of the system took part on the two in-chain integral blocks connected at the output of the Matlab function block. The first integrator (the one connected to the output port of the Matlab function blocks) computes the velocity and the second one does the proper for the position, correspondingly the initial conditions were assigned.

The Matlab function block that appears in the four scenarios has as inputs the position and the velocity of the system. Inside this block, one can find the control equation with the saturation and the dynamics equation at the end to finally send the acceleration and the saturated control signal to the Simulink space. The code lines and the structure are exposed in Fig. C.6 where one may observe that, in reality, the function have several additional inputs. These four additional variables were considered as parameters of the block and not inputs, it was done by clicking over the “Edit data” option in the Matlab editor and changing the Scope option from input to parameter for  $xd$ ,  $Kpv$ ,  $Kvc$  and  $mc$ .

With this being said, the simulation concerning the ideal performance of the sensors can be run. For a better presentation the results are sent to Matlab where they are plotted once the simulation has finished with better quality than in Simulink.

The other 3 scenarios are simulated with base on the simulation at the up left corner block diagram in Fig. C.5. The block

```

function [accel,ux]= fcn(pos,vel,xd, Kpc, Kvc, mc) % Function

ux=Kpc*(xd-pos)+Kvc*(0-vel); % PD Control
ux= min(1,max(-1,ux)); % Saturation of the control signal

accel=ux/mc; % Dynamics of teh system

```

Figure C.6: Mini car simulation results

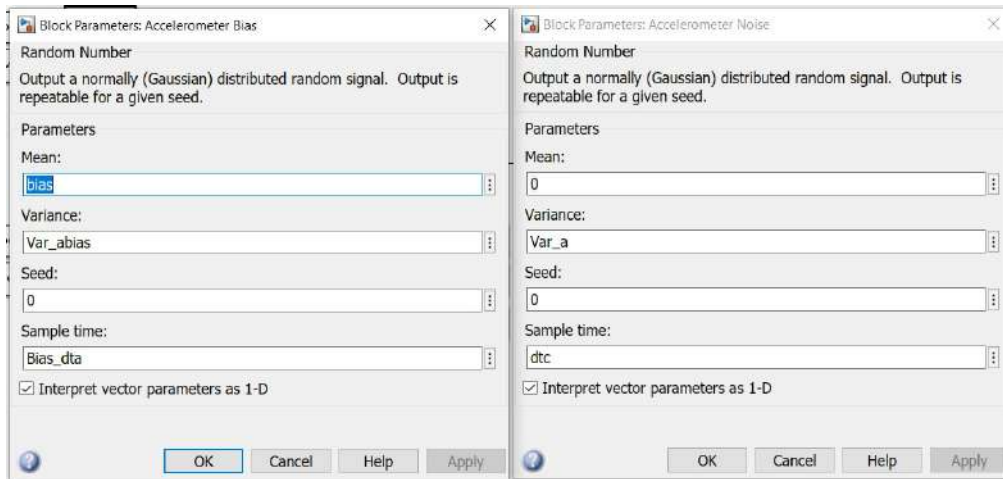


Figure C.7: Accelerometer noise and offset blocks

diagram located at the bottom left corner of Fig. C.5 differs from the ideal case by the addition of the accelerometer noise and the corresponding offset as described in Section C.3. Once these two components are added to the acceleration given by the Matlab function block, it is integrated to compute the velocity and then integrated once more to obtain the position. These two computations were sent back to close the loop. The block parameters are shown in Fig. C.7. By defining two different sample times, we established that one part varies in time faster than other one.

Similarly, the blocks diagram of the up right corner, which corresponds to the system when using only the ultrasonic sensor, differs from the ideal case by the addition of the ultrasonic sensor noise at the output of the integrator that computes the position. Once the position is obtained by a double integration process and the noise had been added to it, the results is derived with respect to time once to get the velocity and twice to compute the acceleration. The noise of this sensor is characterized as depicted in Fig. C.8.

The noisy position and velocity were used as feedback to close the system as can be appreciated in Fig. C.5.

To implement the Kalman filter for data fusion, it has been considered the accelerometer and the ultrasonic sensor as described for the previous scenarios. The signals are given as inputs to the Kalman filter Matlab function block alongside the covariance matrix as shown in Fig. C.5. “Memory” blocks were used to avoid the algebraic loop problem and also to initialize the filter as they contained the corresponding initial values of the position, velocity and covariance matrix. The code written inside the Kalman function block is given in Fig. C.9.

Once the Simulink environment was ready, the file was saved with the name “SimCar” and the simulation was run from the Matlab main file previously explained. It is worth to mention that the files should be located in the same folder.

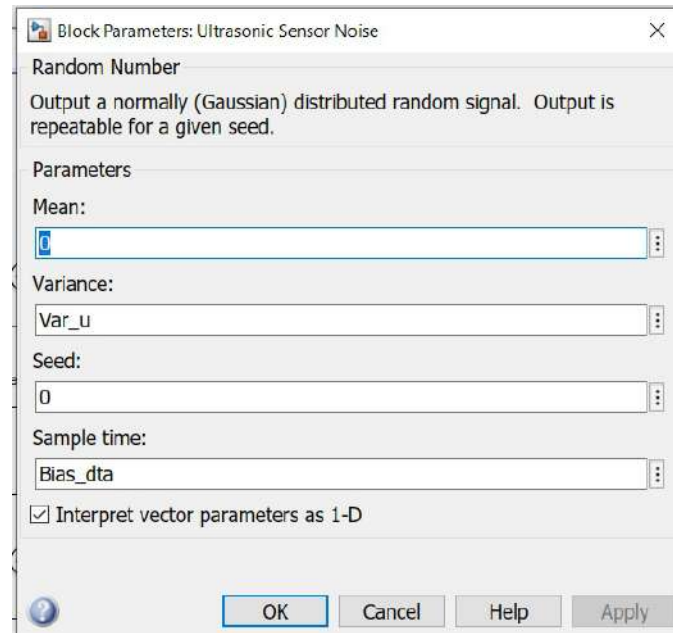


Figure C.8: Ultrasonic sensor noise block

```

1 function [pos_hat, vel_hat, P_cor] = fcn(accel_a, pos_u, pos, vel, P, Ac, Bc, Hc, Qc, Rc)
2
3 xpred=Ac*[pos; vel]+Bc*accel_a; % Equation 16
4 Ppred=Ac*P*Ac'+Qc; % Equation 17
5 K=Ppred*Hc'*inv(Hc*Ppred*Hc'+Rc); % Equation 18
6
7 y=pos_u; % Equation 19
8 xhat=xpred+K*(y-Hc*xpred); % Equation 20
9 P_cor=(eye(2)-K*Hc)*Ppred; % Equation 21
10
11 pos_hat=xhat(1); % Selecting the estimated position
12 vel_hat=xhat(2); % Selecting the estimated velocity

```

Figure C.9: Mini car simulation results

The results of the mini car robot and the bi-rotor platform simulations are depicted in Figs. C.10 and C.11, respectively. In both cases the position of the vehicle, the velocity and the accelerations as well as the control inputs are depicted.

Similar conclusions can be made for both systems. One can observe, in the position plots, that when using only the accelerometer for closing the control loop, it exists a steady state error which is caused by the offset of the sensor and the saturation of the actuators in addition to the accumulative error in the integration process. To use only the ultrasonic sensor seems to work in terms of position and, as expected, the system in which the Kalman filter was implemented accomplishes the goal.

The velocity plots show the disadvantage of using only the ultrasonic sensor as the computed velocity becomes noise and its magnitude is big in comparison with the velocity in the ideal scenario. The Kalman filter provides a noisy velocity that tracks the desired behavior. The velocity obtained only by the integration of the accelerometer signal behaves far from the desired response. In this sense, the Kalman Filter provides a better velocity estimation.

The acceleration plots show a magnification of the acceleration in the case where only the ultrasonic sensor is used. On the other hand, the acceleration given by the accelerometer is clearly affected by the offset and the noise. For the case of the Kalman Filter implementation, one can conclude that even when the acceleration provided by the accelerometer is not the real one, the

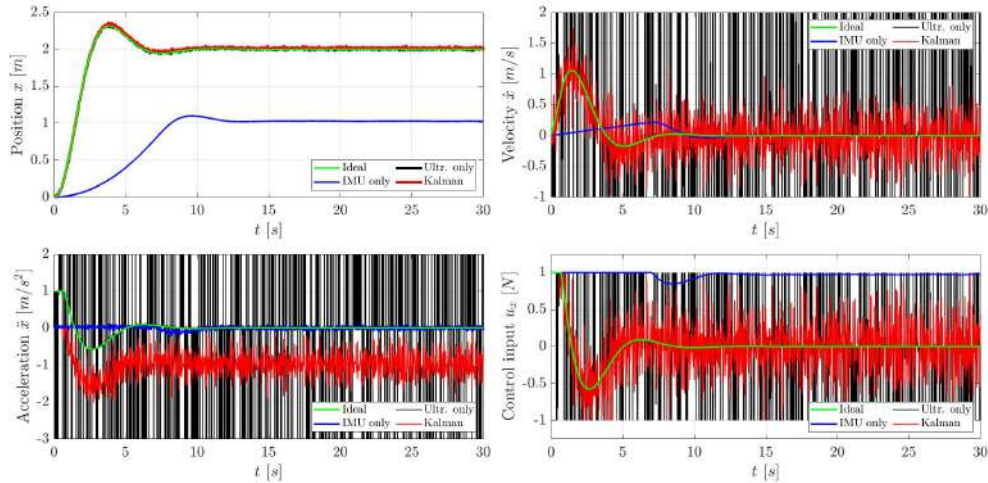


Figure C.10: Mini car simulation results

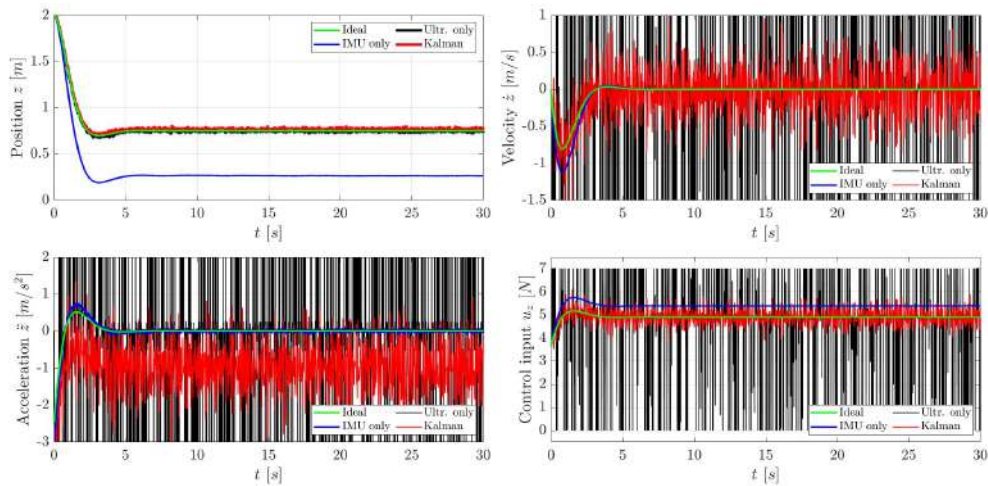


Figure C.11: Bi-rotor simulation results

data fusion technique does a correct estimation of the position and the velocity, making the system reach the desired position even with wrong acceleration measurements. The influence saturation of the actuators is more evident in the case of the mini car robot as depicted by the corresponding plots, however the system is able to overcome such issue when implementing the data fusion by means of the Kalman Filter.

## C.5 Conclusions

After a further and detailed results discussion given in the previous section, one can establish that a pedagogical approach to Kalman Filtering was given and explained considering two examples where such technique was used to illustrate the data fusion algorithm. In addition, the characterization of an ultrasonic sensor and an accelerometer was established and can be considered in future simulations for students. It is expected the usage of the in-here studied technique to improve the results of academic projects in engineering formation.

# Appendix D

## Teaching Activities

### D.1 IPSA Courses

According to the PhD contract, during the PhD studies, 64 hours per scholar year are demanded by the funding institution, i.e. l'IPSA. In this regard, the [Table D.1](#) shows, in a compact format, the courses and the corresponding hours covered until this moment.

Table D.1: Courses list

Course Name	Level Year	Course Responsible	Hours (Cs/TD/TP)
Commandes Intelligentes	M2 2018-2019	Assia BELBACHIR	28 (4/0/24)
Drones et Asservisement visuel	M2 2018-2019	Jonatan ALVAREZ	24 (0/8/16)
Principes de guidage des systemes autonomes	M1 2018-2019	Jonatan ALVAREZ	24 (0/0/24)
Commandes Intelligentes	M2 2019-2020	Assia BELBACHIR	16 (4/0/12)
Drones et Asservisement visuel	M2 2019-2020	Jamy CHAHAL	8 (2/2/4)
Projet CURSUS	M2 2019-2020	Assia BELBACHIR	24 (4/0/20)
Principes de guidage des systemes autonomes	M1 2019-2020	Jamy CHAHAL	24 (0/0/24)
Commandes Intelligentes	M2 2020-2021	Assia BELBACHIR	20 (4/0/16)
Drones et Asservisement visuel	M2 2020-2021	Jamy CHAHAL	8 (2/2/4)
Projet CURSUS	M2 2020-2021	Assia BELBACHIR	24 (4/0/20)
Principes de guidage des systemes autonomes	M1 2020-2021	Jamy CHAHAL	16 (0/0/16)

I collaborated at the **2019 IPSA International Summer School** as the responsible of the Practical Aspects (**18 hours**).

## D.2 Pedagogical Platforms

In addition to the teaching activity, I have worked in the development of pedagogical platforms in order to improve the comprehension of the courses and to facilitate the translation of the theory to the practical application field. In this sense, I may introduce them as follows:

### ▷ Edu-copter rehabilitation

This already existing platform was not in operation in the laboratory, it was re-built and re-programmed to perform the basic stabilization tasks concerning different propulsion operational profiles as fixed or tilting motors configurations. Due to confidentiality declarations, early stages of the prototype are shown in the figure below.

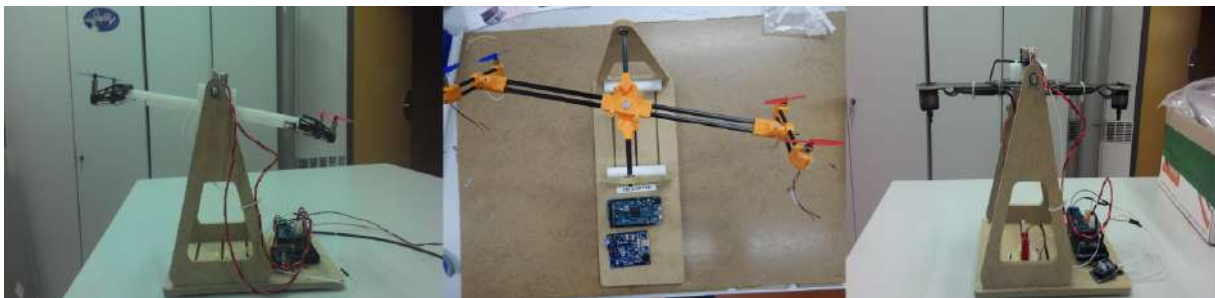


Figure D.1: Edu-copter pedagogical platform

### ▷ Mini-car vehicle

The vehicle was re-designed in order to enhance the space and material distribution over the platform in order to provide to the student a strong platform easy to manipulate, with a simple design and a small structure. Figure 2 shows the re-designed vehicle at the left and the vehicle at the right corresponds to a bought pedagogical model also used in the laboratory.

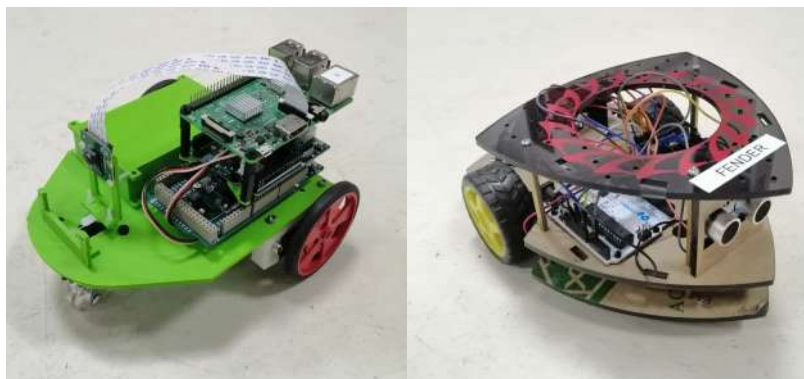


Figure D.2: Mini-car vehicle platforms

### ▷ 1(2)-DOF(s) Bi-rotor platform

This platform was conceived for the IPSA international summer school and the introductory courses on control of aerial vehicles. The platform provides two different control scenarios: altitude stabilization and altitude/orientation stability.

### ▷ Home-made visual tracking system

In order to perform basic experimental tests at the IPSA laboratory concerning the vision courses, a visual tracking system



Figure D.3: 1(2)-DOF(s) Bi-rotor platform

based on ROS, Aruko markers and a Web-cam available at the workplace was conceived.



Figure D.4: Home-made visual tracking system

▷ **Edu-wing conception**

This platform is devoted to the control and stability analysis, in terms of a 1-DOF rotational motion, of mini aerial fixed-wing vehicles through 2 different locomotion configuration: a tilting propeller or an aerodynamic control surface.

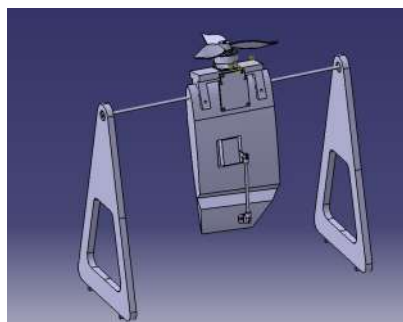


Figure D.5: Edu-wing conception

▷ **Aerial mechanical gripper**

In the regard of aerial vehicles applications, the design and conception of efficient mechanical grippers for perching and grasping operations are being studied at the laboratory. Figure 6 provides the evidence of some built grippers.



Figure D.6: Aerial mechanical gripper

▷ **Quadrotor tuning platform**

Using the structure of the Edu-copter test-bed, a home-built quadrotor is adapted to it in order to allow it to rotate freely about its  $x$  (or  $y$ ) axis to tune the controllers gain to ensure the rotational dynamics stability at first (Figure 7).

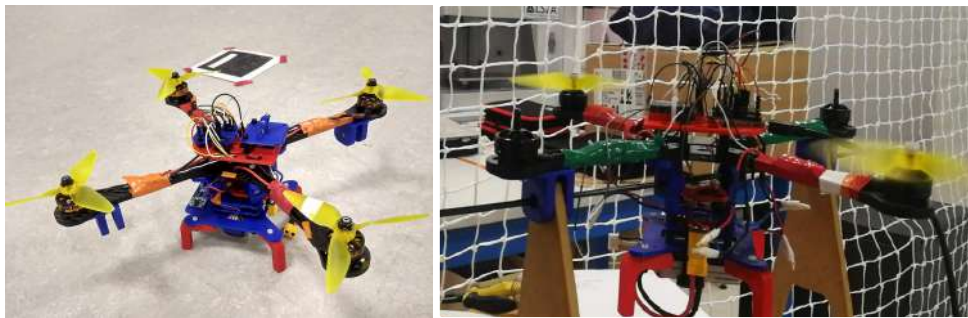


Figure D.7: Quadrotor tuning platform

## D.3 Internships Mentoring

The content of this section is devoted to present a list of the corresponding internships supervised during the development of the thesis. All of the projects took place at the laboratory of autonomous aerial systems of the Institut Polytechnique des Sciences Avancées, located at Ivry-sur-Seine.

- **4th-year stage: [Co-Advisor]**

**Pauline GIL** (Polytech Sorbonne, Sorbonne Université), *Mechanical Design of a 2-DOF Docking Mechanism*, @ Laboratoire des Systemes Aeriens Autonomes (LS2A) IPSA, Ivry-sur-Seine, Île de France, France. (2018).

- **3th-year final project : [Co-Advisor]**

**Lucas KLEPIC** (Institut Polytechnique des Sciences Avancées), *Aero - pendulum position control with Reinforcement Learning*, @ Laboratoire des Systemes Aeriens Autonomes (LS2A) IPSA, Ivry-sur-Seine, Île de France, France. (2018).

- **1-month international master visit : [Advisor]**

**Jean Karlo GOMEZ REYES** (Autonomous University of Queretaro), *ROS control of a Bee-bop quadrotor*, @ Laboratoire des Systemes Aeriens Autonomes (LS2A) IPSA, Ivry-sur-Seine, Île de France, France. (2018).

- **PMI (Project Master IPSA): [Co-Advisor]**

**Jordan MARQUES, Kévin BOYER**, (Institut Polytechnique des Sciences Avancées), *3D design of a quadrotor frame*, @ Laboratoire des Systemes Aeriens Autonomes (LS2A) IPSA, Ivry-sur-Seine, Île de France, France. (2018).

- **PMI (Project Master IPSA): [Advisor]**

**Marvin DESTOUR, Antoine MERVANT, Bryan TROVATI CHAVES**, (Institut Polytechnique des Sciences Avancées), *Design and modeling of a platform for aerodynamics control tests: EDU-wing*, @ Laboratoire des Systemes Aeriens Autonomes (LS2A) IPSA, Ivry-sur-Seine, Île de France, France. (2018).

- **PMI (Project Master IPSA): [Advisor]**

**Heitor Adalberto SILVA, Venira Sofia CARDOSO DE PINA**, (Institut Polytechnique des Sciences Avancées), *Mechanical conception of a testing platform for aerodynamics characterization of propeller-motor systems*, @ Laboratoire des Systemes Aeriens Autonomes (LS2A) IPSA, Ivry-sur-Seine, Île de France, France. (2018).

- **4th-year stage: [Advisor]**

**Chéryne AREF** (Institut Polytechnique des Sciences Avancées), *Design Improvement of the pedagogical platform EDU-Wing*, @ Laboratoire des Systemes Aeriens Autonomes (LS2A) IPSA, Ivry-sur-Seine, Île de France, France. (2019).

- **4th-year stage: [Advisor]**

**Briac GRAUBY** (Polytech Sorbonne, Sorbonne Université), *Conception of a mechanical claw for perching drone maneuvers*, @ Laboratoire des Systemes Aeriens Autonomes (LS2A) IPSA, Ivry-sur-Seine, Île de France, France. (2019).

- **2-months international master visit : [Co-Advisor]**

**Suphanut PLENGKHAM** (Faculty of Engineering Kasetsart University Bangkok), *Mechanical conception of a mini-car robot and a mini bi-rotor vehicle structures*, @ Laboratoire des Systemes Aeriens Autonomes (LS2A) IPSA, Ivry-sur-Seine, Île de France, France. (2019).

- **5th-year stage: [Advisor]**

**Mauricio Franklin VERA VERA** (Ecole Nationale Supérieure de Mécanique et des Microtechniques), *Construction and Control of UAV Pedagogical Platforms*, @ Laboratoire des Systèmes Aériens Autonomes (LS2A) IPSA, Ivry-sur-Seine, Île de France, France. (2019).

- **5th-year stage: [Advisor]**

**Johvany GUSTAVE** (Polytech Sorbonne, Sorbonne Université), *Control and tracking of vehicles using Robot Operating System*, @ Laboratoire des Systèmes Aériens Autonomes (LS2A) IPSA, Ivry-sur-Seine, Île de France, France. (2019).

- **PMI (Project Master IPSA) Anticipé: [Advisor]**

**Nicolas BOJIKIAN, Valentin LEGRIS, Lucas KLEPIC, Luc PARMENTIER** (Institut Polytechnique des Sciences Avancées), *Martial Rover* @ Laboratoire des Systèmes Aériens Autonomes (LS2A) IPSA, Ivry-sur-Seine, Île de France, France. (2020).

# Bibliography

- [1] W. Aburime, H. Schwartz, and S. Givigi. Compensation for time delays in the navigation of unmanned aerial vehicles. In *2019 IEEE International Systems Conference (SysCon)*, pages 1–8. IEEE, 2019.
- [2] I. Al-Ali, Y. Zweiri, N. AMoosa, T. Taha, J. Dias, and L. Senevirtane. State of the art in tilt-quadrotors, modelling, control and fault recovery. *Proceedings of the Institution of Mechanical Engineers, Part C: Journal of Mechanical Engineering Science*, 234(2):474–486, 2020.
- [3] J. Alvarez-Muñoz, J. Escareno, N. Marchand, J. Guerrero-Castellanos, T. Raharijaona, and M. Rakotondrabe. Quaternion modeling and observer-based torque compensation of an aerial manipulator. *IFAC-PapersOnLine*, 51(13):543–548, 2018.
- [4] J. Alvarez-Munoz, J. Escareno, F. Mendez-Barrios, I. Boussaada, S. Niculescu, and D. Nieto-Hernández. Time-delay tolerant control of an omnidirectional multi-agent system for transport operations. In *2018 22nd International Conference on System Theory, Control and Computing (ICSTCC)*, pages 111–116. IEEE, 2018.
- [5] J. Alvarez-Munoz, N. Marchand, J. Guerrero-Castellanos, J. Tellez-Guzman, J. Escareno, and M. Rakotondrabe. Rotorcraft with a 3dof rigid manipulator: quaternion-based modeling and real-time control tolerant to multi-body couplings. *International Journal of Automation and Computing*, 15(5):547–558, 2018.
- [6] J. Alvarez-Muñoz, J. Castillo-Zamora, J. Escareno, I. Boussaada, F. Méndez-Barrios, and O. Labbani-Igbida. Time-delay control of a multi-rotor vtol multi-agent system towards transport operations. In *2019 International Conference on Unmanned Aircraft Systems (ICUAS)*, pages 276–283. IEEE, 2019.
- [7] J. D. Anderson Jr. *Fundamentals of aerodynamics*. Tata McGraw-Hill Education, 2010.
- [8] L. Angel and J. Viola. Fractional order pid for tracking control of a parallel robotic manipulator type delta. *ISA transactions*, 79:172–188, 2018.
- [9] T. Anzai, M. Zhao, X. Chen, F. Shi, K. Kawasaki, K. Okada, and M. Inaba. Multilinked multirotor with internal communication system for multiple objects transportation based on form optimization method. In *Intelligent Robots and Systems (IROS), 2017 IEEE/RSJ International Conference on*, pages 5977–5984. IEEE, 2017.
- [10] S. Aoi, Y. Egi, and K. Tsuchiya. Instability-based mechanism for body undulations in centipede locomotion. *Physical Review E*, 87(1):012717, 2013.

- [11] S. K. Armah and S. Yi. Analysis of time delays in quadrotor systems and design of control. In *Time delay systems*, pages 299–313. Springer, 2017.
- [12] F. M. Atay and D. Irofti. A delayed consensus algorithm in networks of anticipatory agents. In *2016 European Control Conference (ECC)*, pages 1880–1885. IEEE, 2016.
- [13] R. Aucoin, S. A. Chee, and J. R. Forbes. Linear-and linear-matrix-inequality-constrained state estimation for nonlinear systems. *IEEE Transactions on Aerospace and Electronic Systems*, 55(6):3153–3167, 2019.
- [14] S. Awasthi and A. Joshi. Mems accelerometer based system for motion analysis. In *2015 2nd International Conference on Electronics and Communication Systems (ICECS)*, pages 762–767. IEEE, 2015.
- [15] T. Balogh, T. Insperger, I. Boussaada, and S.-I. Niculescu. Towards an mid-based delayed design for arbitrary-order dynamical systems with a mechanical application. In *21st IFAC World Congress*, 2020.
- [16] T. Balogh, I. Boussaada, T. Insperger, and S.-I. Niculescu. Conditions for stabilizability of time-delay systems with real-rooted plant. *International Journal of Robust and Nonlinear Control*, pages 1–19, 2021. doi: <https://doi.org/10.1002/rnc.5698>.
- [17] S. Barawkar, M. Radmanesh, M. Kumar, and K. Cohen. Fuzzy logic based variable damping admittance control for multi-uav collaborative transportation. In *2018 Annual American Control Conference (ACC)*, pages 2084–2089. IEEE, 2018.
- [18] A. Benarab, I. Boussaada, K. Trabelsi, G. Mazanti, and C. Bonnet. The mid property for a second-order neutral time-delay differential equation. In *2020 24th International Conference on System Theory, Control and Computing (ICSTCC)*, pages 7–12. IEEE, 2020.
- [19] V. Borkar and P. Varaiya. Asymptotic agreement in distributed estimation. *IEEE Transactions on Automatic Control*, 27(3): 650–655, 1982.
- [20] I. Boussaada and S.-I. Niculescu. Tracking the algebraic multiplicity of crossing imaginary roots for generic quasipolynomials: A vandermonde-based approach. *IEEE Transactions on Automatic Control*, 61(6):1601–1606, 2015.
- [21] I. Boussaada and S.-I. Niculescu. Characterizing the codimension of zero singularities for time-delay systems. *Acta Applicandae Mathematicae*, 145(1):47–88, 2016.
- [22] I. Boussaada and S.-I. Niculescu. On the dominance of multiple spectral values for time-delay systems with applications. *IFAC-PapersOnLine*, 51(14):55–60, 2018.
- [23] I. Boussaada, H. U. Unal, and S.-I. Niculescu. Multiplicity and stable varieties of time-delay systems: A missing link. In *22nd International Symposium on Mathematical Theory of Networks and Systems (MTNS)*, pages –, 2016.
- [24] I. Boussaada, S. Tliba, S.-I. Niculescu, H. U. Ünal, and T. Vyhlídal. Further remarks on the effect of multiple spectral values on the dynamics of time-delay systems. application to the control of a mechanical system. *Linear Algebra and its Applications*, 542:589–604, 2018.

- [25] I. Boussaada, S.-I. Niculescu, A. El Ati, R. Pérez-Ramos, and K. L. Trabelsi. Multiplicity-induced-dominancy in parametric second-order delay differential equations: Analysis and application in control design. *ESAIM: Control, Optimisation and Calculus of Variations*, 2019.
- [26] I. Boussaada, G. Mazanti, S.-I. Niculescu, J. Huynh, F. Sim, and M. Thomas. Partial pole placement via delay action: A python software for delayed feedback stabilizing design. In *2020 24th International Conference on System Theory, Control and Computing (ICSTCC)*, pages 196–201. IEEE, 2020.
- [27] K. M. Cabral, S. R. B. dos Santos, S. N. Givigi, and C. L. Nascimento. Design of model predictive control via learning automata for a single uav load transportation. In *Systems Conference (SysCon), 2017 Annual IEEE International*, pages 1–7. IEEE, 2017.
- [28] T. Cabreira, L. Brisolará, and P. R. Ferreira. Survey on coverage path planning with unmanned aerial vehicles. *Drones*, 3(1):4, 2019.
- [29] G. Cai, J. Dias, and L. Seneviratne. A survey of small-scale unmanned aerial vehicles: Recent advances and future development trends. *Unmanned Systems*, 2(02):175–199, 2014.
- [30] A. Carullo and M. Parvis. An ultrasonic sensor for distance measurement in automotive applications. *IEEE Sensors journal*, 1(2):143, 2001.
- [31] V. Casas and A. Mitschele-Thiel. On the impact of communication delays on uavs flocking behavior. In *2018 IEEE Wireless Communications and Networking Conference Workshops (WCNCW)*, pages 67–72. IEEE, 2018.
- [32] J. Castillo-Zamora. *Analysis and Comparison of Dynamics and Control Simulations of a V-tail Quadcopter and a Mini AUV*. PhD thesis, Master Thesis, Tecnológico Nacional de México en Celaya, 2016.
- [33] J. Castillo-Zamora, K. Camarillo-Gómez, and G. Pérez-Soto. Diseño de un control pid de posición para un cuadricoptero v-tail basado en la teoría de control de robots manipuladores. In *XVII Congreso Mexicano de Robótica (COMRoB)*, 2015.
- [34] J. Castillo-Zamora, J. Hernandez-Diez, I. Boussaada, J. Escareno, and J. Álvarez-Munoz. A preliminary parametric analysis of pid-delay-controllers for quadrotor uavs. In *Submitted to 2021 International Conference on Unmanned Aircraft Systems (ICUAS)*, pages 1–1. IEEE, 2021.
- [35] J. J. Castillo-Zamora, K. A. Camarillo-Gómez, G. I. Pérez-Soto, and J. Rodríguez-Reséndiz. Comparison of pd, pid and sliding-mode position controllers for v-tail quadcopter stability. *IEEE Access*, 6:38086–38096, 2018. ISSN 2169-3536. doi: 10.1109/ACCESS.2018.2851223.
- [36] J. J. Castillo-Zamora, J. Escareno, J. Alvarez, J. Stéphant, and I. Boussaada. Disturbances and coupling compensation for trajectory tracking of a multi-link aerial robot. In *2019 6th International Conference on Control, Decision and Information Technologies (CoDIT)*, pages 738–743, 2019. doi: 10.1109/CoDIT.2019.8820513.
- [37] J. J. Castillo-Zamora, J. Escareno, I. Boussaada, O. Labbani, and K. Camarillo. Modeling and control of an aerial multi-cargo system: Robust acquiring and transport operations. In *2019 18th European Control Conference (ECC)*, pages 1708–1713, 2019. doi: 10.23919/ECC.2019.8796045.

- [38] J. J. Castillo Zamora, J. Escareno, I. Boussaada, J. Stephant, and O. Labbani-Igbida. Nonlinear control of a multilink aerial system and asekf-based disturbances compensation. *IEEE Transactions on Aerospace and Electronic Systems*, 57(2): 907–918, 2021. doi: 10.1109/TAES.2020.3034010.
- [39] I. Chakraborty, S. S. Mehta, J. W. Curtis, and W. E. Dixon. Compensating for time-varying input and state delays inherent to image-based control systems. In *2016 American Control Conference (ACC)*, pages 78–83. IEEE, 2016.
- [40] W. Cui, J. Tian, X. Xia, and S. Wu. An approach for parameter estimation of maneuvering targets with nonlinear motions. *IEEE Transactions on Aerospace and Electronic Systems*, 56(1):67–83, 2020.
- [41] R. S. de Moraes and E. P. de Freitas. Distributed control for groups of unmanned aerial vehicles performing surveillance missions and providing relay communication network services. *Journal of Intelligent & Robotic Systems*, 92(3-4):645–656, 2018.
- [42] R. S. Dimitrova, M. Gehrig, D. Brescianini, and D. Scaramuzza. Towards low-latency high-bandwidth control of quadrotors using event cameras. In *2020 IEEE International Conference on Robotics and Automation (ICRA)*, pages 4294–4300. IEEE, 2020.
- [43] Y. Ding, Y. Wang, and B. Chen. A practical time-delay control scheme for aerial manipulators. *Proceedings of the Institution of Mechanical Engineers, Part I: Journal of Systems and Control Engineering*, page 0959651820946511, 2020.
- [44] X. Dong, Y. Zhou, Z. Ren, and Y. Zhong. Time-varying formation tracking for second-order multi-agent systems subjected to switching topologies with application to quadrotor formation flying. *IEEE Transactions on Industrial Electronics*, 64(6): 5014–5024, 2016.
- [45] X. Dong, Y. Hua, Y. Zhou, Z. Ren, and Y. Zhong. Theory and experiment on formation-containment control of multiple multirotor unmanned aerial vehicle systems. *IEEE Transactions on Automation Science and Engineering*, 16(1):229–240, 2018.
- [46] S. Driessen, N. Janssen, L. Wang, J. Palmer, and H. Nijmeijer. Experimentally validated extended kalman filter for uav state estimation using low-cost sensors. *IFAC-PapersOnLine*, 51(15):43–48, 2018.
- [47] A. Dzul, T. Hamel, and R. Lozano. Nonlinear control for a tandem rotor helicopter. *IFAC Proceedings Volumes*, 35(1): 229–234, 2002.
- [48] J. Escareno, A. Belbachir, T. Raharijaona, and S. Bouchafa. Generalized disturbance estimation via eslkf for the motion control of rotorcraft having a rod-suspended load. In *Proceedings of the 13th International Conference on Informatics in Control, Automation and Robotics*, pages 526–533. SCITEPRESS-Science and Technology Publications, Lda, 2016.
- [49] J. Escareño, J. Castillo, W. Abassi, G. Flores, and K. Camarillo. Navigation strategy in-flight retrieving and transportation operations for a rotorcraft mav. In *4th Workshop on Research, Education and Development of Unmanned Aerial Systems (RED-UAS 2017)*, pages elec–proc, 2017.
- [50] J.-A. Escareno-Castro. *Conception, modélisation et commande d'un drone convertible*. PhD thesis, Compiègne, 2008.

- [51] Q. Gan and C. J. Harris. Comparison of two measurement fusion methods for kalman-filter-based multisensor data fusion. *IEEE Transactions on Aerospace and Electronic systems*, 37(1):273–279, 2001.
- [52] J. Gao and C. J. Harris. Some remarks on kalman filters for the multisensor fusion. *Information Fusion*, 3(3):191–201, 2002.
- [53] E. Gauterin, P. Kammerer, M. Kühn, and H. Schulte. Effective wind speed estimation: Comparison between kalman filter and takagi–sugeno observer techniques. *ISA transactions*, 62:60–72, 2016.
- [54] M. J. Gerber and T.-C. Tsao. Twisting and tilting rotors for high-efficiency, thrust-vectoring quadrotors. *Journal of Mechanisms and Robotics*, 10(6), 2018.
- [55] J. Gerhard, D. J. Jeffrey, and G. Moroz. A package for solving parametric polynomial systems. *ACM Communications in Computer Algebra*, 43(3/4):61–72, 2010.
- [56] M. Ghanai, A. Medjghou, and K. Chafaa. Extended kalman filter based states estimation of unmanned quadrotors for altitude-attitude tracking control. *Advances in Electrical and Electronic Engineering*, 2018.
- [57] F. A. Goodarzi and T. Lee. Global formulation of an extended kalman filter on se (3) for geometric control of a quadrotor uav. *Journal of Intelligent & Robotic Systems*, 88(2-4):395–413, 2017.
- [58] K. Gu and S.-I. Niculescu. Survey on recent results in the stability and control of time-delay systems. *J. Dyn. Sys., Meas., Control*, 125(2):158–165, 2003.
- [59] K. Gu, J. Chen, and V. L. Kharitonov. *Stability of time-delay systems*. Springer Science & Business Media, 2003.
- [60] J. Guerci, R. Goetz, and J. Dimodica. A method for improving extended kalman filter performance for angle-only passive ranging. *IEEE Transactions on Aerospace and Electronic systems*, 30(4):1090–1093, 1994.
- [61] J. Guerrero-Castellanos, N. Marchand, A. Hably, S. Lesecq, and J. Delamare. Bounded attitude control of rigid bodies: Real-time experimentation to a quadrotor mini-helicopter. *Control Engineering Practice*, 19(8):790–797, 2011.
- [62] J.-F. Guerrero-Castellanos, A. Vega-Alonzo, N. Marchand, S. Durand, J. Linares-Flores, and G. Mino-Aguilar. Real-time event-based formation control of a group of vtol-uavs. In *2017 3rd International Conference on Event-Based Control, Communication and Signal Processing (EBCCSP)*, pages 1–8. IEEE, 2017.
- [63] I. Hadjipaschalis, A. Poullikkas, and V. Efthimiou. Overview of current and future energy storage technologies for electric power applications. *Renewable and sustainable energy reviews*, 13(6-7):1513–1522, 2009.
- [64] Y. S. Hagh, R. M. Asl, and V. Cocquempot. A hybrid robust fault tolerant control based on adaptive joint unscented kalman filter. *ISA transactions*, 66:262–274, 2017.
- [65] J. K. Hale and S. M. V. Lunel. *Introduction to functional differential equations*, volume 99. Springer Science & Business Media, 2013.
- [66] N. D. Hayes. Roots of the transcendental equation associated with a certain difference-differential equation. *Journal of the London Mathematical Society*, s1-25(3):226–232, 1950. ISSN 1469-7750.

- [67] M. Hehn and R. D'Andrea. A flying inverted pendulum. In *2011 IEEE International Conference on Robotics and Automation*, pages 763–770. IEEE, 2011.
- [68] J.-E. Hernández-Díez, C.-F. Méndez-Barrios, S. Mondié, S.-I. Niculescu, and E. J. González-Galván. Proportional-delayed controllers design for lti-systems: a geometric approach. *International Journal of Control*, 91(4):907–925, 2018.
- [69] K. L. Hoffman and R. J. Wood. Turning gaits and optimal undulatory gaits for a modular centipede-inspired millirobot. In *Biomedical Robotics and Biomechatronics (BioRob), 2012 4th IEEE RAS & EMBS International Conference on*, pages 1052–1059. IEEE, 2012.
- [70] K. L. Hoffman and R. J. Wood. Robustness of centipede-inspired millirobot locomotion to leg failures. In *Intelligent Robots and Systems (IROS), 2013 IEEE/RSJ International Conference on*, pages 1472–1479. IEEE, 2013.
- [71] Z. Hou, W. Wang, G. Zhang, and C. Han. A survey on the formation control of multiple quadrotors. In *Ubiquitous Robots and Ambient Intelligence (URAI), 2017 14th International Conference on*, pages 219–225. IEEE, 2017.
- [72] W. Huang, Y. Huang, and S. Chen. Robust consensus control for a class of second-order multi-agent systems with uncertain topology and disturbances. *Neurocomputing*, 313:426–435, 2018.
- [73] Y.-J. Huang, T.-C. Kuo, and S.-H. Chang. Adaptive sliding-mode control for nonlinear systems with uncertain parameters. *Ieee Transactions On Systems, Man And Cybernetics Part B Cybernetics*, 38(2):534, 2008.
- [74] A. Jafar, S. Fasih-UR-Rehman, S. Fazal-UR-Rehman, and N. Ahmed. H infinity controller for unmanned aerial vehicle against atmospheric turbulence. *American-Eurasian Journal of Scientific Research*, 11(4):305–312, 2016.
- [75] R. Jiao, W. Chou, Y. Rong, and M. Dong. Anti-disturbance attitude control for quadrotor unmanned aerial vehicle manipulator via fuzzy adaptive sigmoid generalized super-twisting sliding mode observer. *Journal of Vibration and Control*, 0(0):–, 2021. doi: 10.1177/1077546321989495.
- [76] Y. Kali, J. Rodas, R. Gregor, M. Saad, and K. Benjelloun. Attitude tracking of a tri-rotor uav based on robust sliding mode with time delay estimation. In *2018 International Conference on Unmanned Aircraft Systems (ICUAS)*, pages 346–351. IEEE, 2018.
- [77] Y. Kartal, K. Subbarao, N. R. Gans, A. Dogan, and F. Lewis. Distributed backstepping based control of multiple uav formation flight subject to time delays. *IET Control Theory & Applications*, 14(12):1628–1638, 2020.
- [78] K. Karydis and V. Kumar. Energetics in robotic flight at small scales. *Interface focus*, 7(1):20160088, 2017.
- [79] E. Kaufman, K. Caldwell, D. Lee, and T. Lee. Design and development of a free-floating hexrotor uav for 6-dof maneuvers. In *2014 IEEE Aerospace Conference*, pages 1–10. IEEE, 2014.
- [80] A. Kazharov and V. Kureichik. Ant colony optimization algorithms for solving transportation problems. *Journal of Computer and Systems Sciences International*, 49(1):30–43, 2010.

- [81] R. Kelly and C. Monroy. On robustness of pd control with gravity compensation of torque-driven robot manipulators. In *2019 International Conference on Control, Automation and Diagnosis (ICCAD)*, pages 1–5. IEEE, 2019.
- [82] R. Kelly, V. S. Davila, and J. A. L. Perez. *Control of robot manipulators in joint space*. Springer Science & Business Media, 2006.
- [83] N. Ko, W. Youn, I. Choi, G. Song, and T. Kim. Features of invariant extended kalman filter applied to unmanned aerial vehicle navigation. *Sensors*, 18(9):2855, 2018.
- [84] D. Koh, J. Yang, and S. Kim. Centipede robot for uneven terrain exploration: Design and experiment of the flexible biomimetic robot mechanism. In *Biomedical Robotics and Biomechanics (BioRob), 2010 3rd IEEE RAS and EMBS International Conference on*, pages 877–881. IEEE, 2010.
- [85] M. Koh, A. Ramírez, and R. Sipahi. Single-delay proportional-retarded (pr) protocols for fast consensus in a multi-agent system. *IFAC-PapersOnLine*, 51(14):31–36, 2018.
- [86] P. Kolar, N. Gamez, and M. Jamshidi. Impact of time delays on networked control of autonomous systems. In *Beyond Traditional Probabilistic Data Processing Techniques: Interval, Fuzzy etc. Methods and Their Applications*, pages 151–178. Springer, 2020.
- [87] V. B. Kolmanovskii, S.-I. Niculescu, and K. Gu. Delay effects on stability: A survey. In *Proceedings of the 38th IEEE Conference on Decision and Control (Cat. No. 99CH36304)*, volume 2, pages 1993–1998. IEEE, 1999.
- [88] A. L’Afflitto. *A mathematical perspective on flight dynamics and control*. Springer, 2017.
- [89] D. Lazard. Computing with parameterized varieties. In *Algebraic geometry and geometric modeling*, pages 53–69. Springer, 2006.
- [90] D. Lazard and F. Rouillier. Solving parametric polynomial systems. *Journal of Symbolic Computation*, 42(6):636–667, 2007.
- [91] V. Lertpiriyasuwat, M. C. Berg, and K. W. Buffinton. Extended kalman filtering applied to a two-axis robotic arm with flexible links. *The International Journal of Robotics Research*, 19(3):254–270, 2000.
- [92] J. Li and P. Li. Stability regions analysis of pid controllers for time-delay systems. In *2006 6th World Congress on Intelligent Control and Automation*, volume 1, pages 2219–2223. IEEE, 2006.
- [93] L. Li, M. Wang, K. Xue, Q. Cheng, D. Wang, W. Chen, M. Pan, and Z. Han. Delay optimization in multi-uav edge caching networks: A robust mean field game. *IEEE Transactions on Vehicular Technology*, 2020.
- [94] S. Li, N. Duan, Z. Xu, and X. Liu. Tracking control of quadrotor uav with input delay. In *2020 39th Chinese Control Conference (CCC)*, pages 646–649. IEEE, 2020.
- [95] X.-G. Li, S.-I. Niculescu, A. Cela, L. Zhang, and X. Li. A frequency-sweeping framework for stability analysis of time-delay systems. *IEEE Transactions on Automatic Control*, 62(8):3701–3716, 2016.
- [96] S. Liang, J. Gerhard, and D. Jeffrey. A new maple package for solving parametric polynomial systems, 2007.

- [97] M. Liggins II, D. Hall, and J. Llinas. *Handbook of multisensor data fusion: theory and practice*. CRC press, 2017.
- [98] H. Liu, W. Zhao, Z. Zuo, and Y. Zhong. Robust control for quadrotors with multiple time-varying uncertainties and delays. *IEEE Transactions on Industrial Electronics*, 64(2):1303–1312, 2016.
- [99] H. Liu, D. Li, Z. Zuo, and Y. Zhong. Robust attitude control for quadrotors with input time delays. *Control Engineering Practice*, 58:142–149, 2017.
- [100] Y. Liu, J. M. Montenbruck, D. Zelazo, M. Odelga, S. Rajappa, H. H. Bühlhoff, F. Allgöwer, and A. Zell. A distributed control approach to formation balancing and maneuvering of multiple multirotor uavs. *IEEE Transactions on Robotics*, 34(4): 870–882, 2018.
- [101] P. Londhe, Y. Singh, M. Santhakumar, B. Patre, and L. Waghmare. Robust nonlinear pid-like fuzzy logic control of a planar parallel (2prp-ppr) manipulator. *ISA transactions*, 63:218–232, 2016.
- [102] J. López-Hernández, J. Escareno, C.-F. Méndez-Barríos, O. Labbani, V. Ramírez-Rivera, J. Coronado, and H. Méndez-Azúa. A comparative stability analysis of underactuated versus fully-actuated rotorcrafts having time-delay feedback. In *2019 6th International Conference on Control, Decision and Information Technologies (CoDIT)*, pages 1640–1645. IEEE, 2019.
- [103] K. Low, T. Hu, S. Mohammed, J. Tangorra, and M. Kovac. Perspectives on biologically inspired hybrid and multi-modal locomotion. *Bioinspiration & biomimetics*, 10(2):020301, 2015.
- [104] S. Lupashin, A. Schöllig, M. Sherback, and R. D’Andrea. A simple learning strategy for high-speed quadcopter multi-flips. In *2010 IEEE international conference on robotics and automation*, pages 1642–1648. IEEE, 2010.
- [105] N. A. Lynch. *Distributed algorithms*. Elsevier, 1996.
- [106] D. H. Lyon. A military perspective on small unmanned aerial vehicles. *IEEE Instrumentation & Measurement Magazine*, 7(3):27–31, 2004.
- [107] D. Ma, I. Boussaada, C. Bonnet, S.-I. Niculescu, and J. Chen. Multiplicity-induced-dominancy extended to neutral delay equations: Towards a systematic pid tuning based on rightmost root assignment. In *2020 American Control Conference (ACC)*, pages 1690–1695. IEEE, 2020.
- [108] N. Marchand, F. Guerrero-Castellanos, D. Syl-vain, A. Lopez-Luna, et al. Improving control of quadrotors carrying a manipulator arm. In *XVI Congreso Latinoamericano de Control Automtico*, pages 6–p, 2014.
- [109] C. Masone, H. H. Bulthoff, and P. Stegagno. Cooperative transportation of a payload using quadrotors: A reconfigurable cable-driven parallel robot. In *2016 IEEE/RSJ International Conference on Intelligent Robots and Systems (IROS)*, pages 1623–1630. IEEE, 2016.
- [110] G. Mazanti, I. Boussaada, and S.-I. Niculescu. On qualitative properties of single-delay linear retarded differential equations: Characteristic roots of maximal multiplicity are necessarily dominant. *arXiv preprint arXiv:2002.06146*, 2020.

- [111] G. Mazanti, I. Boussaada, and S.-I. Niculescu. Multiplicity-induced-dominancy for delay-differential equations of retarded type. *Journal of Differential Equations*, 286:84–118, 2021.
- [112] D. Mellinger, M. Shomin, N. Michael, and V. Kumar. Cooperative grasping and transport using multiple quadrotors. In *Distributed autonomous robotic systems*, pages 545–558. Springer, 2013.
- [113] J. Mendoza-Mendoza, G. Sepulveda-Cervantes, C. Aguilar-Ibanez, M. Mendez, M. Reyes-Larios, P. Matabuena, and J. Gonzalez-Avila. Air-arm: A new kind of flying manipulator. In *2015 Workshop on Research, Education and Development of Unmanned Aerial Systems (RED-UAS)*, pages 278–287. IEEE, 2015.
- [114] J. Mendoza-Mendoza, V. J. Gonzalez-Villela, C. Aguilar-Ibañez, M. S. Suarez-Castañón, and L. Fonseca-Ruiz. Snake aerial manipulators: A review. *IEEE Access*, 8:28222–28241, 2020.
- [115] W. Michiels and S.-I. Niculescu. *Stability, control, and computation for time-delay systems: an eigenvalue-based approach*. SIAM, 2014.
- [116] S. Mie, Y. Okuyama, Y. Sato, Y. Chan, N. K. Dang, and B. A. Abderazek. Real-time uav attitude heading reference system using extended kalman filter for programmable soc. In *Embedded Multicore/Many-core Systems-on-Chip (MCSoc), 2017 IEEE 11th International Symposium on*, pages 136–142. IEEE, 2017.
- [117] S. Mobayen and F. Tchier. Nonsingular fast terminal sliding-mode stabilizer for a class of uncertain nonlinear systems based on disturbance observer. *Scientia Iranica*, 24(3):1410–1418, 2017.
- [118] O. Mofid and S. Mobayen. Adaptive sliding mode control for finite-time stability of quad-rotor uavs with parametric uncertainties. *ISA transactions*, 72:1–14, 2018.
- [119] C. A. Molnar, T. Balogh, I. Boussaada, and T. Insperger. Calculation of the critical delay for the double inverted pendulum. *Journal of Vibration and Control*, page 1077546320926909, 2020.
- [120] J. Morales, G. Rodriguez, G. Huang, and D. Akopian. Toward uav control via cellular networks: Delay profiles, delay modeling, and a case study within the 5-mile range. *IEEE Transactions on Aerospace and Electronic Systems*, 56(5): 4132–4151, 2020.
- [121] G. Moroz. *Sur la décomposition réelle et algébrique des systemes dépendant de parametres*. PhD thesis, Université Pierre et Marie Curie-Paris VI, 2008.
- [122] H. A. Museum. Hiller aviation museum. url<https://www.hiller.org/>, 2021.
- [123] L. R. Newcome. *Unmanned aviation: a brief history of unmanned aerial vehicles*. American Institute of Aeronautics and Astronautics, 2004.
- [124] A. Nez, L. Fradet, F. Marin, T. Monnet, and P. Lacouture. Identification of noise covariance matrices to improve orientation estimation by kalman filter. *Sensors*, 18(10):3490, 2018.

- [125] H.-N. Nguyen, S. Park, and D. Lee. Aerial tool operation system using quadrotors as rotating thrust generators. In *2015 IEEE/RSJ International Conference on Intelligent Robots and Systems (IROS)*, pages 1285–1291. IEEE, 2015.
- [126] S.-I. Niculescu and W. Michiels. Stabilizing a chain of integrators using multiple delays. *IEEE Transactions on Automatic Control*, 49(5):802–807, 2004.
- [127] S.-I. Niculescu, W. Michiels, K. Gu, and C. T. Abdallah. Delay effects on output feedback control of dynamical systems. In *Complex time-delay systems*, pages 63–84. Springer, 2009.
- [128] N. S. Nise. *Control systems engineering*. John Wiley & Sons, 2020.
- [129] I. Palunko, P. Cruz, and R. Fierro. Agile load transportation: Safe and efficient load manipulation with aerial robots. *IEEE robotics & automation magazine*, 19(3):69–79, 2012.
- [130] Y. Pan, C. Yang, L. Pan, and H. Yu. Integral sliding mode control: performance, modification and improvement. *IEEE Transactions on Industrial Informatics*, 2017.
- [131] S. Park, J. Her, J. Kim, and D. Lee. Design, modeling and control of omni-directional aerial robot. In *2016 IEEE/RSJ International Conference on Intelligent Robots and Systems (IROS)*, pages 1570–1575. IEEE, 2016.
- [132] S. Park, J. Lee, J. Ahn, M. Kim, J. Her, G.-H. Yang, and D. Lee. Odar: Aerial manipulation platform enabling omnidirectional wrench generation. *IEEE/ASME Transactions on mechatronics*, 23(4):1907–1918, 2018.
- [133] S. Park, Y. Lee, J. Heo, and D. Lee. Pose and posture estimation of aerial skeleton systems for outdoor flying. In *2019 International Conference on Robotics and Automation (ICRA)*, pages 704–710. IEEE, 2019.
- [134] H. A. Pointon, B. J. McLoughlin, C. Matthews, and F. A. Bezombes. Towards a model based sensor measurement variance input for extended kalman filter state estimation. *Drones*, 3(1):19, 2019.
- [135] W. Qiao and R. Sipahi. Consensus control under communication delay in a three-robot system: Design and experiments. *IEEE Transactions on Control Systems Technology*, 24(2):687–694, 2015.
- [136] G. V. Raffo and M. M. d. Almeida. A load transportation nonlinear control strategy using a tilt-rotor uav. *Journal of Advanced Transportation*, 2018, 2018.
- [137] A. Ramírez and R. Sipahi. Single-delay and multiple-delay proportional-retarded (pr) protocols for fast consensus in a large-scale network. *IEEE Transactions on Automatic Control*, 64(5):2142–2149, 2018.
- [138] S. Refoufi and K. Benmahammed. Control of a manipulator robot by neuro-fuzzy subsets form approach control optimized by the genetic algorithms. *ISA transactions*, 77:133–145, 2018.
- [139] G. Reina and A. Messina. Vehicle dynamics estimation via augmented extended kalman filtering. *Measurement*, 133:383–395, 2019.
- [140] R. Ritz and R. D’Andrea. A global strategy for tailsitter hover control. In *Robotics Research*, pages 21–37. Springer, 2018.

- [141] T. Robertazzi and S. Schwartz. On applying the extended kalman filter to nonlinear regression models. *IEEE transactions on aerospace and electronic systems*, 25(3):433–438, 1989.
- [142] F. Rouillier. Solving zero-dimensional systems through the rational univariate representation. *Applicable Algebra in Engineering, Communication and Computing*, 9(5):433–461, 1999.
- [143] F. Ruggiero, V. Lippiello, and A. Ollero. Aerial manipulation: A literature review. *IEEE Robotics and Automation Letters*, 3(3):1957–1964, 2018.
- [144] M. Ryll, H. H. Bühlhoff, and P. R. Giordano. A novel overactuated quadrotor unmanned aerial vehicle: Modeling, control, and experimental validation. *IEEE Transactions on Control Systems Technology*, 23(2):540–556, 2014.
- [145] A.-W. A. Saif, A. Aliyu, M. Al Dhaifallah, and M. Elshafei. Decentralized backstepping control of a quadrotor with tilted-rotor under wind gusts. *International Journal of Control, Automation and Systems*, 16(5):2458–2472, 2018.
- [146] J. Sasiadek and P. Hartana. Sensor data fusion using kalman filter. In *Proceedings of the Third International Conference on Information Fusion*, volume 2, pages WED5–19. IEEE, 2000.
- [147] M. S. Schlosser and K. Kroschel. Limits in tracking with extended kalman filters. *IEEE Transactions on Aerospace and Electronic Systems*, 40(4):1351–1359, 2004.
- [148] M. H. Shaheed, A. Abidali, J. Ahmed, S. Ahmed, I. Burba, P. J. Fani, G. Kwofie, K. Wojewoda, and A. Munjiza. Flying by the sun only: The solarcopter prototype. *Aerospace Science and Technology*, 45:209–214, 2015.
- [149] H. Shakhatreh, A. H. Sawalmeh, A. Al-Fuqaha, Z. Dou, E. Almaita, I. Khalil, N. S. Othman, A. Khreishah, and M. Guizani. Unmanned aerial vehicles (uavs): A survey on civil applications and key research challenges. *IEEE Access*, 7:48572–48634, 2019.
- [150] F. Shi, M. Zhao, T. Anzai, X. Chen, K. Okada, and M. Inaba. External wrench estimation for multilink aerial robot by center of mass estimator based on distributed imu system. In *2019 International Conference on Robotics and Automation (ICRA)*, pages 1891–1897. IEEE, 2019.
- [151] J. Shirai, T. Yamaguchi, and K. Takaba. Remote visual servo tracking control of drone taking account of time delays. In *2017 56th Annual Conference of the Society of Instrument and Control Engineers of Japan (SICE)*, pages 1589–1594. IEEE, 2017.
- [152] R. Shokirov, N. Abdujabarov, T. Jonibek, K. Saytov, and S. Bobomurodov. Prospects of the development of unmanned aerial vehicles (uavs). *Technical science and innovation*, 2020(3):4–8, 2020.
- [153] H. Shraim, A. Awada, and R. Youness. A survey on quadrotors: Configurations, modeling and identification, control, collision avoidance, fault diagnosis and tolerant control. *IEEE Aerospace and Electronic Systems Magazine*, 33(7):14–33, 2018.
- [154] J. Simpson, E. S. Weiner, et al. Oxford english dictionary online. *Oxford: Clarendon Press. Retrieved March*, 6:2008, 1989.

- [155] R. Sipahi, S.-I. Niculescu, C. T. Abdallah, W. Michiels, and K. Gu. Stability and stabilization of systems with time delay. *IEEE Control Systems Magazine*, 31(1):38–65, 2011.
- [156] D. Six, S. Briot, A. Chriette, and P. Martinet. The kinematics, dynamics and control of a flying parallel robot with three quadrotors. *IEEE Robotics and Automation Letters*, 3(1):559–566, 2018.
- [157] J.-J. E. Slotine, W. Li, et al. *Applied nonlinear control*. Prentice hall Englewood Cliffs, NJ, 1991.
- [158] E. Small, E. Fresk, G. Andrikopoulos, and G. Nikolakopoulos. Modelling and control of a tilt-wing unmanned aerial vehicle. In *2016 24th Mediterranean Conference on Control and Automation (MED)*, pages 1254–1259. IEEE, 2016.
- [159] E. Steed, E. Quesada, L. Rodolfo, G. Carrillo, A. N. Ramirez, and S. Mondie. Algebraic dominant pole placement methodology for unmanned aircraft systems with time delay. *IEEE Transactions on Aerospace and Electronic Systems*, 52(3):1108–1119, 2016.
- [160] I. Suh and Z. Bien. Proportional minus delay controller. *IEEE Transactions on Automatic Control*, 24(2):370–372, 1979.
- [161] J. Tang, B. Li, Z. Li, and J. Chang. A novel underwater snake-like robot with gliding gait. In *2017 IEEE 7th Annual International Conference on CYBER Technology in Automation, Control, and Intelligent Systems (CYBER)*, pages 1113–1118. IEEE, 2017.
- [162] D. Teodorovic and M. Dell’Orco. Bee colony optimization—a cooperative learning approach to complex transportation problems. *Advanced OR and AI methods in transportation*, 51:60, 2005.
- [163] M. Tognon and A. Franchi. Dynamics, control, and estimation for aerial robots tethered by cables or bars. *IEEE Transactions on Robotics*, 33(4):834–845, 2017.
- [164] V. P. Tran, M. Garratt, and I. R. Petersen. Time-varying formation control of a collaborative multi-agent system using negative-imaginary systems theory. *arXiv preprint arXiv:1811.06206*, 2018.
- [165] J. N. Tsitsiklis. Problems in decentralized decision making and computation. Technical report, Massachusetts Inst of Tech Cambridge Lab for Information and Decision Systems, 1984.
- [166] K. P. Valavanis. *Advances in unmanned aerial vehicles: state of the art and the road to autonomy*, volume 33. Springer Science & Business Media, 2008.
- [167] M. Velasco-Villa, J. Heras-Godínez, J. A. Vázquez-Santacruz, and V. Fragoso-Rubio. Delayed consensus problem for single and double integrator systems. *Mathematical Problems in Engineering*, 2015, 2015.
- [168] D. Verstraete, K. Lehmkuehler, A. Gong, J. R. Harvey, G. Brian, and J. L. Palmer. Characterisation of a hybrid, fuel-cell-based propulsion system for small unmanned aircraft. *Journal of power sources*, 250:204–211, 2014.
- [169] W. Wang, K. Nonami, M. Hirata, and O. Miyazawa. Autonomous control of micro flying robot. *Journal of Vibration and Control*, 16(4):555–570, 2010. doi: 10.1177/1077546309106149. URL <https://doi.org/10.1177/1077546309106149>.

- [170] Y. Wang, Z. Cheng, and M. Xiao. Uavs' formation keeping control based on multi-agent system consensus. *IEEE Access*, 8:49000–49012, 2020.
- [171] G. Wu and K. Sreenath. Geometric control of multiple quadrotors transporting a rigid-body load. In *Decision and Control (CDC), 2014 IEEE 53rd Annual Conference on*, pages 6141–6148. IEEE, 2014.
- [172] S. Xu and J. Lam. A survey of linear matrix inequality techniques in stability analysis of delay systems. *International Journal of Systems Science*, 39(12):1095–1113, 2008.
- [173] A. M. Yunhong, S. Zhang, B. G. Jie, et al. Consensus control of multi-agent system with stochastic time-varying delay. In *2018 IEEE 14th International Conference on Control and Automation (ICCA)*, pages 612–617. IEEE, 2018.
- [174] J. Zhang, D. Gu, Z. Ren, and B. Wen. Robust trajectory tracking controller for quadrotor helicopter based on a novel composite control scheme. *Aerospace Science and Technology*, 85:199–215, 2019.
- [175] M. Zhao, K. Kawasaki, K. Okada, and M. Inaba. Transformable multirotor with two-dimensional multilinks: modeling, control, and motion planning for aerial transformation. *Advanced Robotics*, 30(13):825–845, 2016.
- [176] M. Zhao, T. Anzai, F. Shi, X. Chen, K. Okada, and M. Inaba. Design, modeling, and control of an aerial robot dragon: A dual-rotor-embedded multilink robot with the ability of multi-degree-of-freedom aerial transformation. *IEEE Robotics and Automation Letters*, 3(2):1176–1183, 2018.
- [177] M. Zhao, F. Shi, T. Anzai, K. Chaudhary, X. Chen, K. Okada, and M. Inaba. Flight motion of passing through small opening by dragon: Transformable multilinked aerial robot. In *2018 IEEE/RSJ International Conference on Intelligent Robots and Systems (IROS)*, pages 4735–4742. IEEE, 2018.
- [178] Y. Zheng, L. Dong, and Q. Wang. Multi-rotor uav attitude calculation based on extended kalman filter. In *2018 Chinese Control And Decision Conference (CCDC)*, pages 478–483. IEEE, 2018.
- [179] Z. Zheng, H. Qiu, Z. Wang, S. Luo, and Y. Lei. Data fusion based multi-rate kalman filtering with unknown input for on-line estimation of dynamic displacements. *Measurement*, 131:211–218, 2019.

**Titre :** Conception, Modélisation et Contrôle d'un Système Multi-Drone pour la Manipulation Aérienne

**Mots clés :** Contrôle non Linéaire, Modélisation de Systèmes Dynamiques, Manipulation de Plusieurs Drones, Systèmes Retardés

**Résumé :** Un sujet passionnant dans le domaine des véhicules aériens autonomes est l'interaction avec l'environnement par la manipulation en vol, y compris la récupération, le transport et le déploiement, qui dévoile un énorme potentiel vis-à-vis des applications industrielles et de service. À cet égard, cette thèse doctoral se concentre sur la conception et l'étude dynamique basé sur l'énergie d'un système aérien sans pilote à liaisons multiples capable d'effectuer des tâches de manipulation.

L'étude de ce système aérien comprend le contrôle du véhicule volant à liaisons multiples par la théorie du contrôle en mode glissant, la conception de contrôleurs basés sur le principe de Lyapunov et, parallèlement, à l'application de filtres de Kalman pour l'estimation de l'état et des perturbations. La dernière partie de la thèse est consacrée à l'examen des effets des retards sur les drones. Des résultats de simulation sont fournis pour prouver l'efficacité de la proposition globale de la thèse.

**Title :** Design, Modeling and Control of a Multi-Drone System for Aerial Manipulation

**Keywords :** Nonlinear Control, Dynamic System Modelling, Multi-Drone Manipulation, Time-Delayed Systems

**Abstract :** A recent and exciting topic within the field of autonomous aerial vehicles is the interaction with the surrounding environment via in-flight manipulation, including retrieving, transport and deployment, which unveils an enormous potential vis-a-vis industrial and service applications. In this regard, the actual thesis focuses on the conception and energy-based dynamical study of a multi-link unmanned aerial system able to perform manipulation tasks.

The study of the aforementioned robotic aerial system includes the control of the flying multi-link vehicle by the sliding mode control theory and the conception of Lyapunov-based controllers alongside the application of Kalman Filters for state and disturbances estimation. The last part of the thesis is devoted to the examination of time-delays effects on unmanned aerial systems. Detailed simulation results are provided to prove the effectiveness of the overall thesis proposal.